Tribological and Structural Characterisation of Ceramic on Metal Hip Replacements

SARAH REBECCA WILLIAMS

Tribological and Structural Characterisation of Ceramic on Metal Hip Replacements

Sarah Rebecca Williams

A Thesis presented for the degree of
Doctor of Philosophy

School of Engineering
University of Durham
England

October 2010

Tribological and Structural Characterisation of Ceramic on Metal Hip Replacements

Sarah Rebecca Williams

Submitted for the degree of Doctor of Philosophy
2010

Abstract

A tribological investigation of ceramic on metal hip replacements was carried out using *in vitro* wear testing methods. Two ceramic materials, pure alumina and an alumina matrix compound (zirconia toughened alumina (ZTA)), were articulated against as-cast CoCrMo alloy cups. The diameter was changed from 38 mm to 60 mm to explore the effect of diameter on the tribological performance. Three distinct wear tests were undertaken to allow a direct comparison between materials and sizes. These were; wear testing using standard loading and motion profiles, microseparation (edge loading) in which the loading and motion profiles were modified to allow medial-lateral and inferior-superior displacement of the head, and third body particle tests which incorporated 0.5 g of <1 μm alumina particle in the lubricant.

The Durham Mark I Hip Wear Simulator was used to simulate the standard walking cycle, and was further modified to incorporate microseparation during the swing phase of the walking cycle. All simulator tests were gravimetrically analysed and linear regression analysis was used to determine running in and steady state wear rates. In addition, surface analytical techniques including non contacting profilometery, atomic force, scanning electron and optical microscopy were used to identify changes in surface topography throughout the wear tests. Parameters such as the root mean squared roughness and skewness were monitored to provide quantitative changes in the surface features. The roughness was also used to calculate the

ratio of minimum film thickness to equivalent roughness known as the lambda ratio. This provided an theoretical indication of the lubrication regime. Dynamic friction measurements were undertaken on the Durham Friction Simulator, using water based bovine serum based lubricants, which allowed the lubrication mechanism to be identified through the generation of a Stribeck Curve.

The results showed low wear rates for all materials and sizes tested, compared with standard metal on polyethylene and metal on metal components. The wear of the ceramic heads was unmeasurable using the gravimetric method, as the volume change of the heads fluctuated with a similar trend and magnitude to the control head which did not experience wear. Wear was detected for the softer metallic cups in all tests.

The standard wear test produced the lowest cup wear rates, compared with microseparation and third body tests which showed increased wear rates through extensive abrasive and adhesive wear mechanisms. After microseparation testing, characteristic stripe wear patterns were found on the ceramic heads and a flattened lip on the metallic cups. Metal transfer was also identified, which was thought to be due to impact during dislocation of the head during the swing phase of the walking cycle. Third body tests resulted in significant grain loss from the ceramic components compared with both standard or microseparation testing. Low friction factors were recorded for all ceramic on metal components, generally showing the joints to be working close to full fluid film lubrication during the high load stance phase of the walking cycle.

Declaration

The work in this thesis is based on research carried out in the School of Engineering at the University of Durham. No part of this thesis has been submitted elsewhere for any other degree or qualification and it is all my own work unless referenced to the contrary in the text.

Acknowledgements

I would like to express my thanks to the people who have made this thesis possible. I acknowledge the principle supervisor, Dr Junjie Wu, the industrial partner, Biomet and EPSRC for providing the funding and opportunity to undertake this PhD. The time I spent at Biomet provided me with an industrial perspective and I would especially like to thank Dr Imran Kahn, Dr Siu Yan Mak, Dr Elise Pegg and Mary Matthews for the valuable experience I had whilst working at the company. I would especially like to thank Professor Tony Unsworth for his continued support and encouragement throughout the project, without which I feel this thesis would not have been completed!

In addition, there are many people who significantly helped me along the way... Mr Arthur Newman and the mechanical workshop in the School of Engineering for making and fixing things that I broke! To my office mates, Neal Wade, Janette Tourney, Zak Jarvis and my virtual officemate, Tim Marriott, for putting up with my complaints and the daily encouragement to complete the work. To the members of the Biogroup, Susan Scholes, Martin Stanley, QianQian Wang and Daniel Giddings for help when the simulators would just not work!

I would also like to thank my family for their continued support and help when times were tough! And finally, to Rich for fixing everything that I could not! Thank you.

Contents

List of Figures

List of Tables

Nomenclature

SYMBOLS

E'	effective elastic modulus	l	sliding distance
E_c	elastic modulus of the cup	Q	total volume of wear data
E_h	elastic modulus of the head	R_c	radius of cup
f	frequency	R_h	radius of head
ff	friction factor	T	measured torque
H	hardness	U	dimensionless speed
h_{min}	minimum film thickness	u	velocity
i	encoder position	W	load
K	wear coefficient	Z	Sommerfeld number

GREEK SYMBOLS

α	angle
λ	ratio of minimum film thickness to surface roughness
η	viscosity
υ	Poissons ratio

ABBREVIATIONS

AFM	atomic force microscopy
ALVAL	aseptic lymphocytic vasculitis-associated lesions
BHR	Birmingham Hip Resurfacing
CD	circular dichroism
CMC	carboxymethylcellulose
CoC	ceramic on ceramic
CoM	ceramic on metal
CoP	ceramic on polyethylene
EDTA	ethylenediaminetetraacetic acid
ESEM	environmental scanning electron microscope
FCC	face centered cubic
FIB	focused ion beam
HA	hydroxyapatite
HCP	hexagonal close packed
LVDT	linear variable displacement transformer
MoM	metal on metal
MXS	microseparation
OCP	open circuit potential
PMMA	polymethylmethacrylate
PTFE	polytetrafluroethylene
PV	peak to valley
RI	running-in
RMS	root mean squared
SEM	scanning electron microscope
SKW	skewness
SS	steady state
UHMWPE	ultra high molecular weight polyethylene
XPS	x-ray photoelectron microscopy
ZTA	zirconia toughened alumina

Chapter 1

Introduction

The replacement of human joints as a result of disease, trauma or aging has become common place and then improvement of their design of great interest to bioengineers. Joints such as the hip, knee and shoulder have been widely studied in the quest to create replacements which function as well as a healthy natural joint. At the present time joints are being designed which reduce the pain and increase the mobility of patients, however the perfect design has not yet been achieved.

This thesis aims to add to the vast research area surrounding hip replacements, in particular exploring hard on hard bearings, through joints composed of a ceramic femoral head articulating against a metallic acetabular cup. The use of differential hardness bearing materials for joint replacements is not new, as even today the Charnley metal on polyethylene implant is considered the gold standard of hip replacements. The decision to use a metallic bearing against a ceramic surface was first introduced in 2001 by Firkins *et al.* [1]. The results looked promising, showing wear rates comparable to the low wear found with ceramic on ceramic replacements, leading to an resurgence of work exploring ceramic on metal couples [2–9].

The majority of work within this thesis investigates alumina based ceramics articulating against CoCrMo alloys. Three main rationales for using ceramic on metal replacements are:

- Reduction in metal particles and ions compared with MoM replacements,
- A reduced chance of fracturing the ceramic component compared with CoC

replacements,

- A reduction in the adhesive wear between different bearing materials.

Metal on metal replacements were found to be highly successful [10] with results at least as good as metal on polymer implants [11], however a number of authors have reported concerns over metal ion release from these bearings [12–14]. *In vitro* experiments have reported cobalt and chrome levels to be toxic to cells in higher concentrations. However, it is yet unclear whether the large number of particles released during each walking cycle are detrimental to the patient. Metal sensitivity has also been shown in a number of patients [15, 16], which could lead to increased complications if the joint were to be retrieved and a second metal bearing implanted. A small number of reports have shown so called 'pseudo tumours' around the joint during retrieval operations which has increased the concerns of some surgeons when using metal on metal replacements [17]. With this in mind, it was thought that by using only one metal component, the number of metal particles would decrease compared with fully metal bearings. In addition, the use of smoother ceramic counterparts will result in reduced wear rate and therefore a lower number of metal particles will be released.

Ceramic on ceramic replacements have also shown high clinical success rates [18] [19], and with such low wear rates ceramic on ceramic replacements are regularly implanted in younger more active patients. However, the concerns with ceramic materials remain their brittle nature, which can lead to catastrophic failure if the bearing were to fracture [20]. It is therefore hypothesised that by pairing a ceramic head with a softer metallic component, the chances of fracture of the ceramic would reduced [1].

Adhesive wear is often found when contact between the asperities of two similar surfaces occurs. In identical material combinations, cold welding of the surfaces results in wear as the surfaces slide over one another. However by using two different materials it is thought that the difference in atomic structure on the surfaces will reduce the occurrence of adhesive wear [1]

The second part of the work described within this thesis, involved further wear tests to establish the effect on the wear rates of joints under more severe wear testing

conditions. Work published by Komistek and Dennis in 2000 [21–24] initiated an area of research which looked at 'microseparation' motion between the head and cup. The authors suggested that during the swing phase of the walking cycle the head and cup separated, resulting in edge contact when the head relocated back into the cup. Fluoroscopy and computer models were used to determine the degree of separation between the components. These results were then used to provide an explanation for the wear marks found on explanted ceramic on ceramic replacements, which showed an area of stripe wear on the head and wear on the rim of the cup. The microseparation mechanism was therefore thought to be a possible explanation for the wear found on retrieved implants.

The 3 main areas of investigation within this thesis are:

- The effect of changing the ceramic material from pure alumina to an alumina matrix composite, zirconia toughened alumina,
- The effect of changing the diameter of the bearing from 38 mm to 60 mm,
- The effect of changing the wear testing conditions from the standard walking cycle loading pattern, to a more severe 'microseparation' loading pattern. In addition, a second severe test which included the addition of alumina particles into the lubricant, was investigated.

Standard wear testing was carried out on the Mark II Durham Hip Wear Simulator which incorporated two axes of motion, namely flexion/extension and internal/external rotation. A simplified square wave loading pattern of approximately 300N-2500N was implemented, which had previously been shown to give similar wear results to simulators which carry out a physiological loading pattern including a double peak [25]. For the severe wear testing, a unique mechanism was designed and built which modified the standard wear simulator resulting in medial lateral displacement of the head compared with the cup. As a result of this, edge impact occurred during the swing phase of the walking cycle. The loading pattern was adjusted to a square wave of 0-2500 N, to provide inferior detraction of the head from the cup and allow medial lateral displacement.

In addition to the microseparation test, a severe third body wear test was carried out using 0.5g of $<1\mu$m alumina particles. Particles were incorporated in the lubricant to simulate conditions which may arise *in vivo* if higher wear of the ceramic component occurred, and a greater number of alumina particles were present in the fluid surrounding the bearing. The components used had undergone standard wear testing (up to 6 million cycles) prior to the third body tests which allowed a direct comparison of wear rates with and without particles in the lubricant. Following the 2 million cycles of particle testing, a further 1/1.5 (alumina test/ZTA test) million cycles was carried out to investigate the recovery wear rates of the materials. Both 38 mm alumina and zirconia toughened alumina were tested under these conditions.

This thesis discusses research on the topic of ceramic on metal hip replacements and presents a thorough investigation including the wear, friction and surface analysis of 38 mm and 60 mm alumina and zirconia toughened alumina heads against CoCrMo alloy cups.

Chapter 2

Theory

2.1 Synovial Joints

Diarthrodial joints such as the hip are composed of bones where the ends are covered in a thin layer of cartilage, to provide a low friction freely articulating joint. The hip joint is a multi-axis ball and socket which is designed for stability and weight bearing. A healthy joint can undergo 4 movements namely, flexion/extension, abduction/adduction, internal/external rotation and circumduction. The joint is enclosed in a fibrous capsule lined with a synovial membrane. The capsule attaches to the margins of the acetabular surfaces of the femur, and the acetabulum, and forms a tubular covering around the ligaments of the head. The synovial membrane contains the cells which produce the natural lubricant, synovial fluid. The hip joint consists of a bony femoral head which sits within the acetabulum of the pelvis.

Bone is composed of 65% hydroxyapatite, 35% collagen, cells and water [26]. The collagen provides the tensile strength of bone and compressive strength is provided by the crystals of hydroxyapitite. On the macroscopic scale, bone can be divided into cortical bone, a hard compact structure, and cancellous bone which is porous and spongy. The ends of long bones (such as the femur) generally consist of cancellous bone with a thin layer of cortical bone which is lined with a thin layer of articular cartilage.

The main function of the cartilage is to transfer load from one bone to the next by spreading the load over a large surface area, therefore preventing damage to

the underlying cells whilst exhibiting low friction. Cartilage is a porous permeable composite composed of an organic solid matrix which is saturated with water. In addition it contains type II collagen fibres and proteoglycans which primarily carry the load. The proteoglycans can absorb water up to 50 times their weight [26]. Mature cartilage does not have a blood supply, neural network or lymphatic drainage system, therefore it lacks the capacity fully to repair structural damage from injury or disease [27]. Ligaments and muscles are responsible for the stability and movement of the hip joint. The three ligaments which stabilise the joint are the iliofemoral, pubofemoral and ischiofemoral ligaments, which are put into tension when the bone moves. The muscles of the hip abduct and adduct, extend and flex and medially and laterally rotate the femur relative to the pelvic bone [28]. The abductor and adductor muscles include the gluteus maximus, minimus and adductor magus. Muscles which mainly extend and flex include the psoas and semiteninous and the external and internal rotators include the deep piriformis muscle and tensor fascia latae. Many of the important nerves are situated between the two muscle groups [28]. The hip is partly held together by the congruency of the ball and socket which is not found in many other joints within the human body.

Hip replacements are often undertaken in order to alleviate pain and restore mobility to the patient. The majority of replacements that occur, are as a result of arthritis which is a painful condition of the joints and bones, although replacements may also be required as a result of trauma to the hip. Osteoarthritis is the most common form of arthritis with an estimated 8.5 million people affected in the UK [29]. It is characterised by damage to the cartilage and can result in bony growths around the edge of the joint (osteophytes), resulting in mild inflammation of the tissues (synovitis). Rheumatoid arthritis (also known as inflammatory arthritis) is another common form of arthritis which is more severe and results from the body's immune system attacking and destroying the joint. Initial enzyme attack in rheumatoid arthritis can lead to secondary osteoarthritis as a result of additional wear mechanisms. In addition to the damage of the joints, a decrease in viscosity of the synovial fluid is found with arthritis. This further hinders effective lubrication causing pain and damage.

2.2 Lubrication

The tribologist, Ernest Rabinowicz, described a lubricant as 'a substance which is capable of altering the nature of the surface interactions between contacting solids' [30] and has more recently been defined as 'any substance interposed between two surfaces in relative motion for the purpose of reducing the friction and/or wear between them' [31]. A lubricant can be in the form of a solid, liquid or gas, and has functions such as reducing the frictional force and lowering the wear between two surfaces. Lubricants may also act as coolants in situations where heat may cause damage to the material surfaces.

In the case of replacement joints, lubrication is used both to lower the friction and wear of the components, and also, to a lesser extent, maintain a low temperature suitable for *in vivo* applications. Lubricants, including water [5], silicone fluids [32, 33], bovine serum [33–36] and synovial fluid [33, 37] have been used as test media for joint replacement materials. The results of which have been shown to be greatly affected by the composition of the lubricant, indicating that the choice of lubricant and any additives must be carefully considered before commencing *in vitro* testing.

2.2.1 Theory

There are 4 principal lubrication mechanisms that can be applied to joint replacements, which depend on the nature of the relative motion and the type of lubricant and material under investigation. These are hydrodynamic, elastohydrodynamic, mixed and boundary lubrication.

Hydrodynamic lubrication is a form of full fluid film lubrication which occurs when a film of gas or liquid, completely separates the two surfaces, resulting in no contact. As a result, the fluid film completely separates the surfaces therefore the friction generated is solely due to shearing of the lubricant, and so depends on its dynamic viscosity. Hydrodynamic lubrication usually occurs as a result of a converging wedge resulting from the geometry and motion of the two surfaces. A fluid film can also form as a result of an external pump increasing the lubricant pressure which is therefore known as externally pressurised, or hydrostatic lubrication.

Elastohydrodynamic lubrication (EHL) occurs when the pressure in the film is sufficient to cause deformation of the surfaces, which changes the geometry and so increases the contact area. The lubrication in soft elastic bodies can be described by soft EHL where only the elastic deformation of the surfaces is considered as the loads are low and there is no effect of increased pressure on the viscosity of the lubricant. In hard EHL where the pressures in the film are high, the increase in viscosity of the pressure dependent lubricant and the deformation of the surfaces must both be considered. However water based lubricants do not normally exhibit pressure dependence of viscosity. The stress is not uniform over the contact area with a maximum at the centre of the contact, falling to zero at the edge. If the load is transient, pressure will be generated in the absence of an external source or a converging wedge using a method called squeeze film lubrication. The pressure is caused by the finite time taken for the fluid (which was present between the surfaces before loading) to flow out and the gap to be closed, during this time the surfaces are protected.

Boundary lubrication results when very thin films which adsorb to the surfaces, modifying the surface properties. Wear occurs through asperity contact which are protected (to a certain degree) by the adsorbed lubrication film. Boundary lubricants, either solid or liquid must interact with the surface resulting in a solid boundary layer. Contact occurs between surfaces as a result of the asperities breaking through the fluid film, increasing in friction and wear. A good boundary lubricant adheres strongly to the bearing surface, therefore avoiding intimate contact between the surfaces, protecting them from damage.

Between full fluid film lubrication and boundary lubrication is **mixed lubrication**. This is present when both mechanisms are occurring simultaneously, with part of the load being carried by the fluid film, and part of the load being carried by asperity contact. As a generality mixed lubrication results in less wear than boundary lubrication, but more wear than full fluid film lubrication.

2.2.2 Minimum Film Thickness Calculations

A model was developed, which used the root mean squared roughness of the bearing surfaces and other material dependent factors, to indicate whether a bearing couple was working within boundary, mixed or full fluid film lubrication. For elliptical contacts, the theoretical film thickness calculations were derived by Hamrock and Dowson in 1978 [38]. The model used a ball on plate configuration and assumed that the fluids were isoviscous and the bearing materials were linear elastic. In addition for hard on hard bearing components, the bearing surfaces were assumed to be semi-infinite and therefore the equation in the form shown in Equation 2.1 could be used.

The original equation [38] for film thickness included ellipticity, speed and load parameters. If a ball on plate configuration is assumed, the ellipticity parameter, k, is equal to 1. Therefore, the minimum film thickness (h_{min}) equation calculated from EHL elliptical contact theory was defined as:

$$\frac{h_{min}}{R_x} = 2.80\left(U^{0.65}W^{-0.21}\right) \tag{2.1}$$

The dimensionless speed, U, and the load parameter, W, are calculated as follows:

$$U = \frac{u\eta}{E'R_x} \tag{2.2}$$

And

$$W = \frac{L}{E'R_x^2} \tag{2.3}$$

Where u is the entraining velocity, η is the lubricant viscosity, L is the applied load, E' is the effective elastic modulus and R_x is the equivalent radius. The effective elastic modulus, E', and the equivalent radius, R_x, are shown below:

$$\frac{1}{R_x} = \frac{1}{R_h} - \frac{1}{R_c} \tag{2.4}$$

And

$$\frac{1}{E'} = 0.5\left\{\left(\frac{1-\upsilon_h^2}{E_h}\right) + \left(\frac{1-\upsilon_c^2}{E_c}\right)\right\} \tag{2.5}$$

Where R_h, υ_h, and E_h are the radius, Poisson's ratio and elastic modulus of the femoral head, and R_c, υ_c, and E_c are the radius, Poisson's ratio and elastic modulus of the acetabular cup respectively.

The ratio of the minimum film thickness to the combined surface roughness allowed the dimensionless parameter λ to be calculated which indicated, under which lubrication regime the joints would operate. The λ value is given in equation 2.6.

$$\lambda = \frac{h_{min}}{\sqrt{(rms_h^2 + rms_c^2)}} \tag{2.6}$$

Where rms_h and rms_c are the root mean squared roughness of the head and cup respectively (or the two mating surfaces).

The lambda value provides an indication of asperity contact between the bearing surfaces. If a standard normal distribution of data is assumed, and the ratio of film thickness to combined roughness (λ) is >3 only 1% of the asperities will contact the opposing surface and low wear occurs. This is because 3 standard deviations away from the mean is close to 99% confidence interval, in which a full fluid film may be assumed. If the roughness is greater, then the λ will decrease (between $1 < \lambda < 3$), and a mixed lubrication regime is found. As the value of roughness increases to more than the film thickness the ratio becomes less than one, and total asperity contact known as boundary lubrication, occurs. Many previous researchers have used this equation to determine theoretical lubrication regimes for metal on metal and ceramic on ceramic hip replacements [33, 39–41]

2.3 Lubrication of the Natural Joint

The mechanisms of lubrication have been widely debated historically. After Osborne Reynolds brief mention of animal joint lubrication in 1886, little interest was shown until MacConaill in 1932. MacConaill [42] (reference details from [43]) concluded, using knee joints, that hydrodynamic lubrication was the principal mechanism in biological bearings. Following this Jones, in 1936, carried out experiments using interphalangeal joints as the fulcrum of a pendulum, finding an exponential decay in amplitude, which he attributed to full fluid film lubrication[44]. In 1959 [45],

McCutchen proposed a novel type lubrication known as 'weeping lubrication', in which a porous deformable material that was soaked with liquid carried the majority of the load. When loaded, the fluid 'weeps' out of the matrix into the bearing space, resulting in a pressurised fluid between the surfaces, forced from the interstices of the cartilage. Little *et al.* [46] carried out experiments on a cadaveric hip which proved to give a linear decay in amplitude of the pendulum with time, therefore boundary lubrication was predicted. Dintenfass (1963)[47], Tanner(1966) and Dowson(1966-1967) proposed elastohydrodynamic lubrication as the mechanism for joint lubrication within the body. It was hypothesised that since the cartilage would deform substantially under load, this would allow a fluid film to be established between the surfaces. In 1968 a modified form of squeeze film was suggested by Walker *et al.*[48], where it was thought that the molecular structure of the synovial fluid and the elasticity, porosity and surface topography of the articular cartilage contributed to increasing the life of the lubricating films. This was known as 'boosted lubrication'. In contrast to this, in 1959 Charnley predicted boundary lubrication and suggested that the exponential decay found by Jones (1932) was due to the effects of the soft tissue surrounding the joint which resisted the motion of the pendulum. Charnley's own experiments showed that the decay in amplitude of a cadaveric ankle was linear and as a result boundary lubrications predominated. Barnett and Cobbold [49] confirmed this with friction tests using a dog's ankle in which the surrounding tissue and tendons were cut away. However results also showed a linear decrease in amplitude when a hydrostatic bearing was tested, which was well known to undergo full fluid film lubrication, therefore the theory that linear decay as an indication of boundary lubrication was questioned.

In 1963 Dintenfass stated that "neither the hydrodynamic theory nor the boundary theory permits an adequate description and explanation of lubrication in synovial joints". In the late 1970's Linn and Radin [50] carried out a series of experiments in which hyaluronic acid (an important constituent in synovial fluid) was digested with hyaluronidase to break down the molecule into smaller pieces. This had little effect on the friction, however digesting the proteins with trypsin resulted in an increase in friction even though the viscosity of the lubricant had not changed. It

was therefore suggested that proteins were an important factor and boundary lubrication occurred. However the experiments were carried out under heavy constant load and were therefore pre-disposed to boundary conditions

In 1972, Radin and Paul [51] wrote that the low coefficient of animal joints was a combination of lubricating mechanisms, namely a specialised boundary lubrication phenomenon and fluid lubrication. Lubricant molecules were thought to remain on the cartilage surfaces during low loads which reduced the friction by decreasing the interaction of asperities, and at high loads the molecules were squeezed out of the way protecting the surfaces. Finally in 1975 Unsworth *et al.* [44] discussed that the predicted lubrication regime appeared to depend on the type of equipment used to measure the friction between the joints, as pendulum devices tended to indicate boundary lubrication, whereas reciprocating machines had concluded that fluid film lubrication was important in human joints. Unsworth [37] showed analytically that in a pendulum, if the viscous frictional term and coulomb frictional term were both zero, then simple harmonic motion would result. However if only Coulomb frictional resistance were present, then boundary lubrication; a linear decay with time would be observed, and if only viscous frictional resistance (fluid film lubrication) were present exponential decay would be observed. Following this, Unsworth described how if typical values for radius of the head and pendulum, fluid viscosity, mass and film thickness were entered into the resulting equations, then the exponential component would be very small, and would be very difficult to detect. In addition, as more than one mechanism is likely to be occurring in the natural joint, the exponential component may be lost [37].

Following this, Unsworth and co-workers designed a new pendulum device to overcome the limitations found with the earlier pieces of equipment [37]. Unsworth showed that extremely sensitive equipment would be required to detect the exponential decay which was required to indicate full fluid film lubrication. Therefore instead of measuring amplitude of motion and converting the results to frictional torque, the torque produced by the head was directly measured using a transducer.

Healthy joints with their own synovial fluid were used to provide evidence of squeeze film lubrication[37]. The unlubricated joints showed a constant value of

friction over a range of sliding times, therefore predicting boundary lubrication. Pre-loaded joints showed no period of squeeze film (i.e. increased friction) as would be expected. Unsworth *et al.*[37] showed that a self generating fluid film could be created at low loads, however asperity contact would occur at high loads when the film thickness becomes too small to support the load. In agreement with earlier researchers, Unsworth *et al.*[37] suggested that the friction increased with time because the cartilage was effectively "wrung out" which increased the contact area, increasing the friction. The lack of an increase in friction as the pendulum came to rest was thought to be due to the cartilages' elastic resistance to imposed shear forces, therefore friction was no longer being recorded, but elastic deformation of the cartilage.

In 1982 [32], the pendulum design was modified to incorporate a hydraulic mechanism to apply dynamic loading to the joint while an oscillating motion representing flexion and extension was included. The angle of swing and the speed of oscillation could be varied. Animal joints were tested using various lubricants including: silicone fluids; sodium carboxymethylecellulose (SCMC); synovial fluid with the addition of hyaluronic acid; hyaluronidase digested bovine serum and trypsin digested synovial fluid. At low loads, silicone fluids resulted in fluid film lubrication with a transfer to mixed lubrication at very low viscosities. At high loads, squeeze film effect was found in addition to the hydrodynamic mechanism, which led to a thicker film and constant values of friction factor for all viscosities. SCMC fluids produced similar results to silicone fluids at the high loads, showing a constant value of friction, and at lower loads mixed lubrication operated. Friction testing for digested hyaluronic acid resulted in similar results to the synthetic lubricants with full fluid film at high loads, with a transition to mixed lubrication at lower loads. The results of the trypsin digested serum were not found to be significantly different from those before digestion, with some tests showing increased friction and some showing decreased friction. Overall the results showed at low loads, the viscosity of the fluid is important in reducing the friction, however at higher loads, the friction factor remained constant as a result of the squeeze film effect, which resulted in full fluid film lubrication, even at low viscosities.

2.4 Wear

Wear occurs when two surfaces come into contact and slide over each other. This contact can be dry, or lubricated in some way which acts to reduce the wear. The wear rate and the friction between two surfaces are dependent on the sliding conditions such as the lubricant, temperature, load, velocity and distance. In 1953 Archard [52] devised a wear equation which related the total volume of wear debris (Q) to the normal load (W), the sliding distance (l) and the hardness of the softer surface (H).

$$Q = \frac{KWl}{H} \tag{2.7}$$

where K is a dimensionless constant known as the wear coefficient which allowed the severity of the wear of different processes to be compared. Therefore to reduce the wear (without changing the sliding distance), either the hardness, H, must be increased, or K, must be reduced. However, the Archard equation cannot be used to understand the mechanism responsible for material removal such as adhesion, abrasion, erosion, fatigue and corrosion.

2.4.1 Adhesion

Adhesive wear occurs when adhesion between contacting surfaces leads to the removal of material from one or both surfaces [30]. It is characterised by high wear rates and coefficients of friction. Adhesion will occur between most solids, in the absence of a contaminant layer and is decreased by increased hardness or a high surface roughness. In metal on metal contacts, adhesion is often prevented by an oxide layer (a passivation layer), however if two clean surfaces (metal or ceramic) are brought into contact adhesion will readily occur [53]. Numerous free electrons can exchange between the two solids and establish bonds, even if the two surfaces in contact have different atomic structures (e.g. a metal and a ceramic). The metal with the higher electron affinity will donate its electrons to the opposite material.

Metal Adhesive wear

'Asperity junction growth' can be used to explain adhesive wear [54]. Contact occurs between the asperities of the two opposing materials. If the normal load on the asperities is high enough to cause plastic deformation, the introduction of tangential stress can result in the asperity plastically yielding. This increases the surface area and reduces the pressure at the contact. The tangential force which can now be sustained is increased, and the surface area will continue to grow until the maximum shear stress of the material is reached and a wear particle is formed. This increases the friction between the surfaces. The plastic deformation is usually associated with work hardening of the asperity, therefore yielding occurs in the lower shear stress material resulting in particle transfer. A ductile material is more likely to wear by this mechanism than a brittle material. Lubricants reduce adhesive wear by preventing intimate contact between surfaces [54].

If an asperity is formed on the opposite surface (due to particle adhesion), further sliding can lead to particles adhering to the new asperity until a large agglomerate of particles break away as a loose piece of wear debris. The shape of this particle will depend on whether plastic deformation of the asperity occurs, thus leading to a flattened plate like particle. Flat particles can also be formed by shear fracture of layers of an asperity or the formation of subsurface cracks which propagate parallel to the surface leading to a plate like wear particle [55]. Particles which detach from metallic materials may contain or be solely consisting of the oxide of the metal which can then lead to further abrasive wear due to the hard nature of the oxide material. Adhesion and friction have been found to be dependent on the ductility of the material with the hardness of the material being of great importance [53].

Ceramic Adhesive Wear

Adhesive wear of ceramics differs from metals due to the nature of the bonding and reduced plastic deformation which can occur within ceramic structures. The crystal structure has a significant effect on adhesive wear. Hexagonal closed packed (HCP) structures, such as alumina, show less adhesion than other crystal structures such as face centered cubic (FCC), body centered cubic (BCC) and tetragonal structures,

due to the reduced number of slip planes in HCP structures preventing plastic deformation [54].

Strong adhesion can form between metals and ceramics. As metals have a lower cohesive strength than ceramics, rupture of the adhesive bond results in metal transfer to the ceramic surface. The mechanism of metal adhesion to a ceramic with the formation of metal transfer is shown in Figure 2.1.

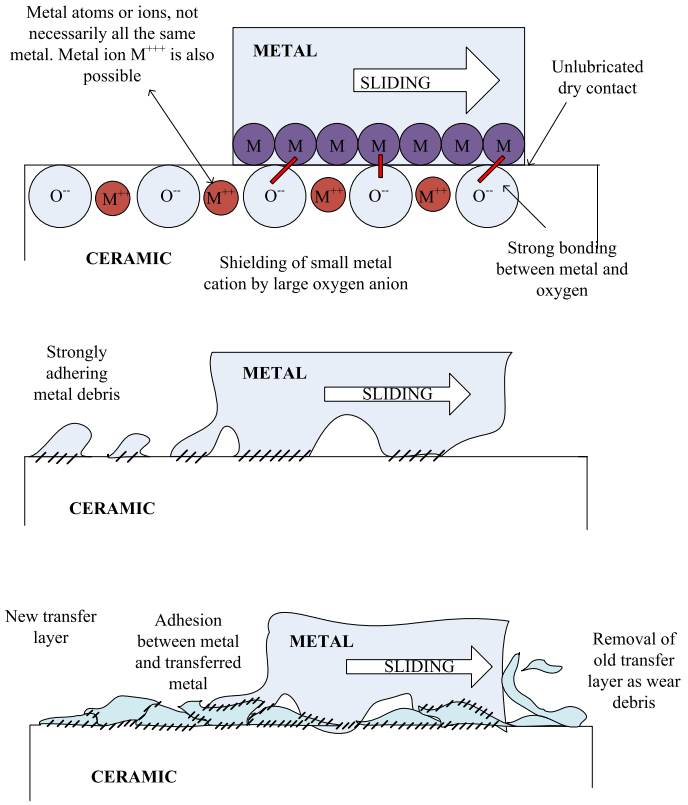

Figure 2.1: *Mechanism of metal adhesion to ceramic surface with the formation of metallic transfer layers (from [54])*

Environmental factors such as the presence of water can alter the mobility of the near surface dislocations, affecting the limited amount of plastic flow that can occur within ceramics. Brittle fracture of ceramics typically takes place along grain boundaries leading to individual grain removal. Crystal orientation plays an important role in the extent of plastic flow or brittle fracture which occurs. Ceramic materials also follow the Archard wear equation showing a linear dependency of wear on sliding distance and load and the wear coefficient K can be used to compare the severity of different situations [55].

2.4.2 Abrasive Wear

> "Abrasive wear is the loss of material by the passage of hard particles over a surface" [54]

Abrasive wear occurs when a harder substance displaces material from an opposing surface [56]. This can be in the form of two-body wear when the harder material ploughs through a softer material or third-body wear when harder particles are able to move freely between the surfaces subsequently leading to wear by embedding of the particle into one of the softer surfaces. If the stress placed on a third-body particle causes the particle to break up, smaller particles with an increased surface area are formed and increased wear can result. The mechanisms of abrasive wear can involve both plastic flow and brittle fracture [55]. Adhesive wear as described in section 2.4.1 can result from a work hardened particle transferred to one of the bearing surfaces, which can then lead to abrasive wear of the corresponding surface.

Abrasive wear can occur by four different methods,

1. **Cutting** - when hard or sharp particles cut through the softer surface material, and shearing of the material creates a wear particle.

2. **Fracture** - when a brittle material such as ceramic is abraded, limited plastic deformation can occur and wear particles are formed as a result of crack convergence.

3. **Fatigue** by repeated ploughing - when the abraded material and the particle are ductile, cutting is unlikely, and repeated deformation results in particles released via a fatigue mechanism.

4. **Grain pull-out** - which results in entire grain removal, usually as a result of weak grain boundaries or large grains in ceramics.

In general, the greater number of sharp edges on the cutting particle the more wear occurs. Strain hardening can occur beneath the surface which can result in a reduction of abrasive wear. Third-body wear is found to be a slower wear method compared with two-body wear as the particles spend most of the time rolling rather

than sliding therefore competing with other wear mechanisms such as adhesion. Two-body wear results in a series of scratches, whereas third-body worn surfaces show a random topography, as a result of successive contact of the third body particle [54]. The brittleness of the abrasive particles can have a large effect on the wear. If the particle is brittle, it is likely to break up possibly reducing the wear. If the particle is tough, and does not fracture, new cutting faces do not occur, and the resulting rounded smooth particle produces reduced wear [54].

Generally, the wear predicted for brittle fracture is greater than the wear predicted for plastic deformation mechanisms. In plastic deformation mechanisms the wear is dominated by the hardness of the material surface, however with brittle mechanisms the wear is dominated by the fracture toughness. Adding a lubricant may not significantly reduce the wear by abrasive mechanism as the particles can be larger than the fluid film generated to separate the surfaces [54].

2.4.3 Fatigue

If the film thickness between two surfaces is too small, contact may occur between asperities leading to very high contact stresses. If these are repeated a number of times as with sliding or rolling, wear particles can occur as a result of fatigue propagated cracks [30]. Fatigue failure is controlled by the mechanisms of crack formation, growth and fracture.

Material imperfections such as inclusion, weak grain boundaries, and zones of high residual stress are good initial sites for crack development and therefore should be avoided if possible. In a lubricated rolling contact of a metal surface under high load, pits can form with the removal of a wear particle due to hydraulic pressure crack propagation [54] (see Figure 2.2).

A crack can open due to traction forces ahead of the moving body. If lubricant fills the crack, subsequent pressurisation and stresses cause the crack to close and forces it to extend. Repeated fluctuations in stress can eventually result in a wear particle being produced leaving a pit in the metal surface. The particles from a fatigue wear process are characteristically much larger than particles from abrasive or adhesive wear [57].

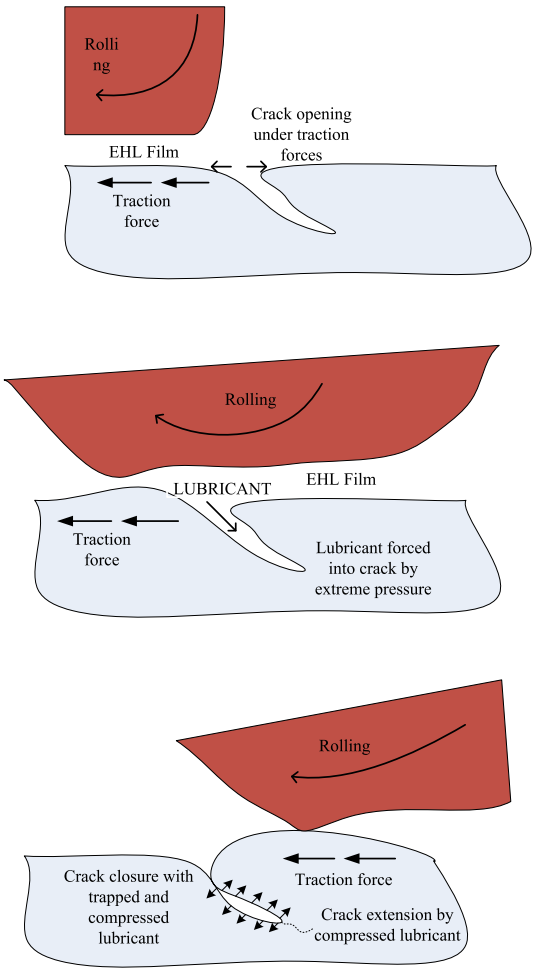

Figure 2.2: *Mechanism of fatigue as a result of hydraulic pressure crack propagation (copied from [54])*

2.4.4 Corrosion

Corrosion is a chemical attack on metals, which although in the majority of cases results in visual damage to the material, can also leave no visible signs, and has been described as:

> "a group of processes that produce compounds and free ions from bulk metals" [58]

There are various forms of corrosion including uniform attack, crevice corrosion, pitting corrosion, intergranular corrosion, and stress corrosion [58, 59]. Corrosion occurs due to potential differences between two areas of a metal surface or two different metals, resulting in preferential degradation of a particular area. This

results in metal ion release and breakdown of the metal surface.

Uniform corrosion is the most common form, and occurs as a result of small local variations in structure and environment over the surface which allows electrons to flow across the surface and results in small pits.

Crevice corrosion is one of the more severe forms of attack which primarily occurs between different components, however can also form within incomplete fatigue cracks which are narrow and deep. Oxygen depletion within the crevice leads to anodic corrosion along the crevice face, and cathodic protection of the bulk material surface.

Pitting corrosion is similar to crevice corrosion but is more isolated and often occurs along scratches and as a result of inclusions on the surface.

Intergranular corrosion is found to occur along disordered regions such as grain boundaries. The material within the grain boundary often differs from that of the adjacent grain, therefore the grain boundary inclusions act as cathodes, and the surface as an anode therefore corrosion of the grain surface is found.

Stress corrosion is a result of tensile stresses and areas of high stress which increases the chemical activity of the metal. The tensile or high stress areas become anodic compared with the adjacent areas and are preferentially attacked. Cracks can form leading to corrosion similar to intergranular attack however the cracks are often smaller and more isolated.

Metals which form oxides with the surrounding medium form a protective layer called the passivation layer, which is often disrupted leading to corrosion of the underlying metal. The oxide layer can then form third-body abrasive particles which are trapped between the surfaces, accelerating the damage of the passivation layer, and therefore the corrosion which occurs. Between two surfaces, depassivation and repassivation can only occur if the material can repassivate quickly. The passivation layer can have a detrimental effect if disrupted as it may become cathodic compared to the bulk material, therefore increasing the corrosion of the metal surface [60].

Chapter 3

Literature Survey

This literature review examines the research and topics related to the wear and topography of ceramic on metal hip replacements. Initially a brief history is provided of the development of early hip replacements to the more recent metal on metal resurfacing and hybrid ceramic on metal implants. A review of the *in vivo* and *in vitro* response to particles is also included with discussions regarding the sizes and morphologies resulting from retrieval implants and particles produced using *in vitro* methods. A comprehensive review of lubricants, and protein deposition is provided to examine the effect of lubricant composition and protein deposition onto metal and ceramic surfaces. Following this metal on metal, ceramic on ceramic and ceramic on metal implants are discussed with respect to the changes in design over time and the respective wear rates found. Finally the microseparation and third body wear particles are reviewed in relation to the literature and knowledge available to date.

3.1 Brief History of Hip Replacements

Impairment of the natural hip joint is commonly caused by damage to the cartilage surfaces. The Swedish Hip Arthroplasty register published in 2006 showed an increase in hip replacement operations from 6 in 1967 to 13,822 in 2005 [61]. The UK joint register reported 74,752 (NHS and independent) hip operations in 2009 [62]. In 2001 over 20% of the United Kingdom's population was aged 60 years or older [63], which inevitably increases the demand on the health service. The Swedish hip regis-

ter reported that over 80% of replacements carried out in 2005 were due to primary osteoarthritis [61] which has generally been accepted as the main reason for requirement of a replacement. The second most common reason was stated as fracture, where numbers were found to increase with age.

In the mid 1900's experimental materials such as acrylic and ivory were used as replacement for the natural hip joint. The main aim was to restore the integrity of the joint and relieve pain, rather than restore complete mobility. The majority of implants covered only the head of the femur, leaving the acetabulum intact. Additional materials tried include glass, celluloid (a compound made of nitrocellulose), and cobalt chrome alloy, which resulted in the fracture of the glass components, and a foreign body reaction to the celluloid [64]. However, the cobalt chrome alloy was found to be relatively successful. In addition, Perspex was tried but failed due to its high wear rate [64].

In 1961 Charnley [65] published a paper in which he discussed that the materials previously used were not suitable to be lubricated by synovial fluid or any other tissue fluid. Consequently the low friction material polytetrafluroethylene (PTFE) was introduced for use in hip replacements [65]. Initially, Charnley reported failures due to the operative technique, which resulted in a necrotic femoral head [66]. Knowing this, cemented prostheses were introduced, and a reduction in femoral head size from just over 40 mm down to 22 mm. This reduced the wear due to the lower sliding distance, and resulted in a reduced frictional torque. By keeping a reasonably large external diameter of the cup, the high friction between the cup and bony acetabulum was used to maintain a stationary component. This technique was observed from January 1960 and the early results, up to 1.5 years, were encouraging. Unfortunately the PTFE joint had to be abandoned after three years due to a higher wear rate than expected, and a severe foreign-body reaction, as a result of the particles released from the surface [66]. These particles resulted in loosening of the socket, and caused motion between the cup and acetabulum resulting in pain [67].

In 1961 John Charnley said 'Neither surgeons nor engineers will ever make an artificial hip joint which will last thirty years and at some time in this period enable the patient to play football' [65]. The inaccuracy of this statement has been shown

through the thousands of successful implants which are still surviving today, allowing the patient to return to an active lifestyle free of pain.

Following the poor success of the PTFE replacement, Charnley introduced a high density polyethylene (HDPE) cup in November 1962 which articulated against a stainless steel head. He reported a 92.7% success rate for 379 hips between 4 and 7 years [68]. In a later study [69] a 92% success rate of 106 implants was found for a 9-10 year follow up which reported no evidence of deterioration. From this work, Charnley set a standard that the total average linear wear must be less than 1 mm in 5 years, of which 75% of the implants met. No correlation with clinical factors could be made for the 25% which showed approximately 3 times the standard wear. A small amount of bone resportion was noted in the region of the calcar femorale in a minority of cases. More recently a paper publishing the results of 228 Charnley implants implanted between 1972 and 1976, showed success rates of 93% at 10 years and 73% after 30 years documenting the success of the Charnley prosthesis which remain the gold standard for hip replacements [70].

Although the majority of the early metallic 'cups' used to cover the femoral head were found to fail, the limited success led to the conception of fully metallic implants. At a similar time to the Charnley low friction arthroplasty, the McKee-Farrar replacements were introduced which were manufactured totally from cobalt chrome alloys. However the limited tribological knowledge within the replacement joint community meant that parameters such as surface finish, sphericity and clearance of the joint were neglected resulting in a high failure rate due to high wear and equatorial contact causing seizing [71, 72]. However, some long term cases of successful McKee Farrar replacements have been reported, lasting as long as 30 years without loosening or failure [73]. The success of the small number of the McKee Farrar joints was due to the good fortune of two biomechanical compatible components being implanted together. Mid term success (10 years) of McKee Farrar joints was low compared with the Charnley prosthesis which resulted in surgeons abandoning the metal on metal prosthesis, in favour of the metal on polyethylene combination. In 1972, Patterson *et al.* [74] published short term data on McKee-Farrar implants with a mean follow up time of 1.4 years of 368 components implanted in 5 hospi-

tals. The results showed 85% improvement in pain relief, however 5% felt the post operative pain was worse. Improvement in motion was felt by 76% and improved ability to walk expressed by 69% of patients. However many complications were found, including 5 deaths and numerous cases of loosening or infection.

The long term success (15-20 years) of the McKee Farrar and Charnley implant were found to be similar. Clarke *et al.* [73] reported a case of a patient who had both a McKee Farrar and a Charnley implant, both of which survived to 30 years. Although significant polyethylene wear was seen 23 years after implantation the cast CoCr alloy implant was unscratched and no loosening was found, with neither joint favoured over the other.

Follow ups of the early hip arthoplasties revealed that failures tended to depend on the length of time of implantation. Once the initial problems of infection were overcome through improved operating theatre procedures and the use of antibiotics [75], it was discovered that early failures were often caused by femoral stem fracture. In response to this, Charnley increased the cross sectional area of the implant, and reduced this form of failure [76]. Implants which survived to 7-8 years were then found to fail due to femoral component loosening and implants which had survived to 10-15 years were found to be failing from acetabular component loosening, followed by bearing surface failure.

Improved design and cementing techniques resolved many of these problems, consequently a new mode of failure was emerging called "cement disease". Reports started to appear in which implants had failed and localised loss of endosteal bone of the femur at the cement interface was noticed [77]. Initial reports concluded that the bone loss was as a result of using polymethylmethacrylate (PMMA) cement, which therefore led to the use of cementless prostheses. However the bone loss was still found, in the absence of PMMA, and the problem was renamed "particle disease". Lysis due to particles had been prevalent for many decades, and was a contributing factor to failure of the Charnley PTFE implant in 1962, which was assumed to be due to deep sepsis even though bacteria could not be grown from the lesions. In the early 1970's, the link between particles and macrophage activation was established [78].

3.2 Lubricants

3.2.1 *In vivo* lubricants

In the natural joint, the bearing surfaces are lubricated with synovial fluid which provides a film of fluid, preventing contact between the cartilage. Synovial fluid is a non Newtonian fluid which is a dialysate of blood plasma containing long chain molecules called hyaluronic acid. The protein content of synovial fluid is less than that of serum with very large proteins such as β-lipoprotein and fibrinogen, and smaller proteins such as haptoglobulin, missing from synovial fluid. However synovial fluid found in diseased joints differs in composition. Inflammatory diseases such as rheumatoid arthritis result in synovial fluid with increased protein concentration and plasma proteins such as fibrinogen (which are not found in healthy synovial fluid). Degenerative joint diseases also show an increase in protein however the composition differs from that of inflammatory diseases, which suggests that the proteins originate from cells and surrounding tissues [79].

Synovial fluid is viscoelastic in nature, due to its hyaluronic acid (HA) content. At low strain frequencies, the chains of HA slip past each other resulting in viscous flow of the lubricant. At high strain frequencies the molecules deform and store the mechanical energy, which is released elastically. The transition between viscous fluid and elastic behaviour is a rapid reversible transition with no deteriorating effects. This transformation allows the fluid to flow between the cartilage surfaces under low strain frequencies when the joint moves, however under high shear frequencies the fluid viscosity increases and is unable to flow quickly out of the joint space, effectively protecting the cartilage surfaces from touching. This mechanism allows sensitive elements such as cells to be protected when stress is imposed [79]. The viscosity and elasticity of diseased synovial fluid (within osteoarthritic and rheumatoid arthritic joints) is less than that of normal synovial fluid[80]. Albumin is the most abundant protein in synovial fluid, which occupies approximately 56% of the composition of normal synovial fluid, which is reduced to 42% in rheumatoid arthritic patients [81].

3.2.2 *In vitro* lubricants

The most commonly used lubricant today for *in vitro* testing is newborn calf serum [82–88], due to its similarities to synovial fluid. Other lubricants including water have also been used as the lubrication medium [5, 89] however water has been shown to produce significantly different results to *in vivo* situation. The quantities of natural synovial fluid which would be required for *in vitro* testing is far beyond attainable quantities. In addition the differences in composition between patients could become a problem for comparison between tests, therefore a standard substitute (ISO 14242-2 [90]) lubricant was determined as a suitable medium for testing and comparing replacement joints. The majority of researchers use a diluted form of bovine serum, generally with a protein content of >17g/l.

Many researchers have investigated the effect of protein concentration on the wear rate and particle morphology of UHMWPE [36, 91]. An increase in protein concentration has been shown to produce lower wear rates [36]. The addition of phospholipids has shown a significant decrease in wear between UHMWPE cups and CoCr heads [92]. The morphology of particles produced in a pin on plate test revealed large thin flakes when water was used as the lubricant, whereas with the bovine serum submicron sized equiaxed or elongated particles were produced [91]. This indicated the importance of lubricant composition on the wear mechanisms occurring.

Friction testing, using both water based CMC lubricants and bovine serum based lubricants, has been used to investigate the effect of proteins on the friction coefficient of different bearing surfaces [34, 93]. Results showed that the addition of proteins to MoM implants led to a reduction in friction due to protein against protein contact in addition to metal on metal contact. As proteins have a lower shear modulus, a reduction in friction factor was found. The addition of proteins to CoC implants increases the friction as large protein molecules are introduced into fluid film, increasing the friction compared with water based CMC fluids [34, 93].

The lubricant used often contains additional elements such as ethylenediaminetetraacetic acid (EDTA) and sodium azide (NaN_3). EDTA has been added to prevent calcium phosphate deposition particularly onto ceramic heads [94], however it has

been suggested that EDTA may initiate micro-corrosion on metal on metal surfaces. EDTA has been shown to have no effect on the wear of UHMWPE cups against zirconia heads [88]. In addition sodium azide is used to prevent bacterial growth during testing.

3.3 Protein

The most abundant protein in bovine serum is albumin; a multifunctional non glycosylated, negatively charged, plasma protein [81] which is able to bind to a wide range of ligands such as drugs, amino acids and hydrophobic molecules [95]. The secondary structure of albumin contains α-helixes, however no β-sheets are present. Wear testing can lead to increased temperatures, which may affect the protein within the lubricant.

3.3.1 Conformational changes to albumin

Circular dichroism (CD) spectroscopy has been used to detect conformation changes to albumin during thermal processing [81, 96]. The decrease in number of α-helixes structures found with increasing temperature, suggested the secondary structure of albumin was altered, thus decreasing in intramolecular hydrophobic interactions and increasing the exposure of hydrophobic accessible surface areas. The altered structure of thermally treated albumin resulted in a compact layer forming on the material surfaces [81].

Heuberger *et al.* [96] investigated the change in α-helix conformation between 20-100 ^{o}C and found that a decrease in α-helixies occurred between 20-50 ^{o}C followed by a clear increase in unfolding of the protein. Before 70 ^{o}C refolding was apparent upon cooling, however irreversible denatured albumin was detected above 70 ^{o}C which was found to aggregate upon cooling. Studies have shown that thermally treated human serum albumin can increase the friction coefficient compared with untreated albumin [81]. However changes in the concentration of albumin (4-60 mg/ml) [97] with UHMWPE pins and metallic plates showed negligible effect. Further techniques used to investigate protein include X-ray photoelectron spectroscopy (XPS) and I-

BSA radiolabeling which showed a higher driving force for adsorption of albumin on metallic surfaces compared with ceramic surfaces. Results indicated that monolayers of albumin formed on ceramic surfaces, however multi-layer albumin layers formed on metallic counterfaces. The authors suggested that the driving force for protein adsorption was greater on hydrophobic surfaces compared with hydrophilic surfaces and that the difference between monolayers and multi-layer formation was due to differences in molecular conformation on the adsorbed surfaces. As alumina is a hydrophilic surface, denaturation of the albumin molecules directly bonded to the surface may occur, which as a result would be less likely to attract further albumin molecules to the surface [97] [98].

In contrast to the previous studies, Heuberger *et al.* [96] measured the quantity of native and denatured albumin on plasma treated (more hydrophilic) and non treated (more hydrophobic) surfaces. They concluded that more hydrophobic surfaces adsorb denatured albumin to a greater extent than hydrophilic materials which can act as a passivation layer and effectively prevented adsorption of further molecules from solution. A higher adsorbed mass was found on the hydrophilised polymer surface which preferentially adsorbed a loosely deposited layer of native albumin. It was suggested that the natively adsorbed albumin maintained the more hydrophilic moieties at their surface which meant they were more hydrated therefore providing better lubrication. The preferential denatured layer on the hydrophobic surface gave higher friction as the proteins were less efficiently hydrated, therefore functioned less well as low shear-modulus boundary lubricants. Temperature ramp experiments showed that a decrease in α-helixies, and therefore native structure, was found between 20 ^{o}C and 50 ^{o}C which was completely lost by 90 ^{o}C. SDS-PAGE has been used to show that the tribological process did not break down the albumin structure and only thermal denaturing of the protein structure occurred [99].

3.3.2 Thermal denaturation of albumin - effect on friction

A study by Yang *et al.* [100] reported that thermally denatured albumin (95 ^{0}C for 30mins.) had a similar structure to friction induced denatured albumin with a decrease in α-helixies. The report [100] compared the coefficient of friction of

UHMWPE against steel and cartilage against steel. When fresh albumin was used as the lubricant with the UHMWPE pin (against steel), a decrease in coefficient of friction was found with increasing compressive displacement due to more concentrated native albumin between the surfaces. When thermally treated albumin was used as the lubricant, a higher friction coefficient was found with increasing compressive displacement. It was hypothesised that native albumin revealed the hydrophilic side chains on the outermost structure however unfolding during denaturation increases the exposure of the hydrophobic side chains of the amino acids within the albumin. This therefore resulted in a greater number of hydrophobic interactions between the albumin and UHMWPE resulting in a compacted layer of denatured albumin. However when the UHMWPE was replaced with the more hydrophilic cartilage, a lower coefficient of friction was found due to the lubricating abilities of native albumin. Hydrophilic interactions occurred between the cartilage and protein surface. The enhanced lubrication was thought to be due to a rolling effect of the heart-shaped native albumin on the sliding surface which is thought to contribute to better lubrication. When denatured albumin was used, a decrease in coefficient of friction was also found with compressive displacement, as the denatured albumin did not form interactions therefore was able to leave the articulating surfaces easily and did not adsorb to the surface [100].

Bovine serum albumin has been shown to be a less effective boundary than other glycoproteins [101]. Under frictional measurements on a hydrophobic material, adsorbed albumin revealed the hydrophobic core, therefore adsorbing via hydrophobic interactions. The resulting high shear strength layer with strong hydrophobic interactions leads to increased friction. However the other glycoproteins resulted in lower friction, generally leading to lower friction than PBS (used as a control).

3.3.3 *In vitro* simulator temperatures

It has been suggested that elevated temperatures during hip simulation may cause precipitation or degradation of proteins which may therefore have adverse effects on the lubrication and perhaps lead to non-physiological wear mechanisms within the simulator [88, 96]. In a study which recorded the protein precipitation and deposi-

tion, using UHMWPE as the acetabular cup, the steady state serum temperature was found to be highest with zirconia, due to its lower thermal conductivity. As a consequence precipitation of proteins occurred, which were suspended in the lubricant resulting in a more opaque solution. The protein collected between the bearing surfaces of the joints which was more prevalent with the zirconia heads, but was also observed when the alumina or CoCr heads were tested. A lower wear rate was found for the zirconia heads, and it was suggested that this was an artificially low wear rate due to a protective layer of precipitated proteins [88]. It was suggested that decreasing the serum concentration to 25% may 'increase the danger of defeating its lubricating properties' [88]. During friction tests with pin on disc apparatus, white precipitates were found for UHMWPE discs against CoCr and alumina pins [99]. CoCr pins articulating on CoCr discs produced a brown precipitate which was considered to be a mixture of wear particles and denatured albumin. The temperature at which albumin was thought to thermally denature was between 50-55 ^{o}C, which was determined as a result of an increase in viscosity around this temperature [99].

Temperatures within UHMWPE cups have been recorded using thermocouples incorporated into the head/cup holders in wear simulators [94]. UHMWPE cup subsurface temperatures, 0.5 mm below the surface, have been reported to be 51.3 $\pm$ 5.2 ^{o}C , 40.4 $\pm$ 1.8 ^{o}C, and 35.6 $\pm$ 3.8 ^{o}C for corresponding zirconia, cobalt chrome and alumina heads respectively all of which were higher than the ambient lubricant temperatures. Finite element analysis was used to predict the surface temperatures assuming that the heat dissipated primarily in a radial direction and were found to be 90 ^{o}C, 60 ^{o}C and 45 ^{o}C respectively (zirconia, CoCr and alumina). The temperature measurements taken within alumina and CoCr heads were found to be greater than the temperatures taken below the corresponding UHWMPE cup surfaces. This was attributed to the greater thermal conductivity of the heads compared with UHMWPE. The authors also commented that the head was fixed on the load axis, therefore the apex of the head was constantly contacting the cup and therefore continuously heated. The protein precipitation was found to be consistent with the temperature within the balls, in that the highest temperature produced the greatest protein precipitation. A study by Liao *et al.* [88] predicted that protein

precipitation was initiated above 60 ^{o}C. However, the predicted surface temperatures within the CoCr and alumina couples was 60 ^{o}C and 45 ^{o}C and precipitation of proteins was found to occur for both materials. The authors speculated that the additional agitation due to motion within the simulator may have allowed precipitation of the proteins to occur at these lower temperatures. Considerable discussion has been undertaken with regards to the lubricant bath temperature used in reported studies. Lu *et al.* [94] discussed that maintaining the bath at 37 ^{o}C because that is body temperature, may lead to overheating of the lubricant chamber, causing protein precipitation which affects the wear mechanism of the assembly. It was also noticed that the maximum temperatures were not reached until 5-6 hours of continuous simulation, which is not a typical walking time of a patient with a hip replacement [94].

3.4 Metal on Metal Hip Replacements

As mentioned in section 3.1, many first generation metal on metal replacement implanted in the 1960's, were found to fail due to high frictional torque, thought to be caused by equatorial contact. However, a number of devices survived for many years resulting in revived interest in fully metal implants. A long term follow-up of 38 McKee Farrar hips [72] revealed 10/38 were functioning well (after a mean follow up of 21.8 years) 11/38 had to be replaced (mean follow up 10.2 years) and 17/38 of the patients had died or discontinued follow up (mean follow up of 5.7 years). The still surviving implants had the lowest mean age at operation, (52.0 years, 57.8 years and 60.3 years for surviving, replaced or died/discontinued follow up respectively). In the concluding remarks the authors suggested that metal on metal may be suitable for use in younger patients.

Changes in manufacture such as improvements to sphericity, clearance and surface finish, led to second generation metal on metal implants in the late 1980's, such as the Metasul articulation in 1988. In spite of these improvements many second generation implants were failing as a result of poor design which resulted in dislocations or impingements. The small diameters initially used did not promote full fluid

film lubrication and many reports were failing to show superiority of metal on metal bearings over metal on polyethylene, despite problems with osteolysis. A study by Dorr in 2000 [11] reported on 53 patients who were implanted with Metasul metal on metal devices between 1991-1994, indicated similar results to metal on polyethylene however a lower rate of acetabular loosening and osteolysis was found. However, the metal on metal joints were not found to be superior to metal on polyethylene articulations. Nineteen patients who had bilateral replacements, one with metal on metal and one with metal against polyethylene, did not favour one hip over the other.

3.4.1 Metal on Metal Resurfacings

Metal on metal resurfacing implants were introduced in the 1990's, the rationale of which was to reduce bone destruction, allow normal femoral loading, avoid stress shielding and restore normal anatomy. In addition the large diameter implants such as the Birmingham hip resurfacing (BHR) device had advantages of a reduction in the risk of dislocation, and easier revision should it be required [102]. Early clinical and radiological results of 310 BHRs showed very satisfactory results using the Harris hip score with no dislocations found [102].

The relationship between diametral clearance and lubrication was shown to have a significant effect on wear of metal on metal joints. Dowson *et al.* [103] reported an increase in running in wear rate with an increase in clearance for both 36 and 54 mm bearings. However, as Tipper *et al.* discussed [12], a minimum clearances is reached, below which a substantial increase in wear occurred, thought to be due to errors in sphericity. Hernandez-Rodriguez *et al.* [104] reported an increase in wear with increases in radial clearance for a severe test (constant 2 kN load) using hemisphere femoral components. In contrast, Scholes *et al.* [105] tested low carbon 28 mm diameter joints with two radial clearances (22 and 40 μm) in a hip simulator and showed that similar wear was found for both clearances but agreed that slightly less wear was seen for the smaller clearance.

Although CoCrMo alloys have generally been accepted as the material of choice for metal on metal prosthesis, factors such as the carbon content and method of

production are still under question. As-cast CoCrMo alloys exhibit blocky $M_{23}C_6$ carbides which have an average size of 10-30 μm. Whereas complete solution microstructures exhibited relatively small globular carbides with an average size of 2-10 μm as a result of the transformation from $M_{23}C_6$ to M_6C carbides. Reports have shown that wear is inversely proportional to the carbide volume fraction in the microstructure [104], and it has been shown that high carbon CoCrMo alloys produce lower wear than low carbon CoCrMo alloys[85, 106].

3.4.2 Concerns with metal particles *in vivo*

The improvements in the wear rates found for metal on metal components with the introduction of large diameter bearings and improvements in material and device manufacture are still overshadowed by the underlying problem with metal on metal prosthesis, the release of metal particles and ions into the body. Even though the wear of metal on metal prosthesis is low, over 100 times as many particles are released compared with conventional metal on polyethylene [107]. There are concerns that the small metallic particles may provoke biological reactions that have not been previously recognised. Chromium and cobalt ion levels have been shown to be elevated in patients with metal on metal prosthesis, usually monitored in serum, blood or urine levels[14]. A study in 2000[108] looked at post-mortem specimens of 29 patients and 2 biopsy specimens of living patients with failed implants, using scanning electron microscopy. The results showed metal particles in the liver and spleen to be more prevalent in patients who had had failed hip arthroplasties. Recently, surgeons from Oxford have reported cases of 'pseudotumours' which are soft-tissue masses found at the site of a metal on metal replacement [17]. The study of 17 patients, all of which were women with hip resurfacings, presented a soft-tissue mass in the area of the hip resurfacing device. The mean age of the patients was 53 years at the time of operation and the mean time to presentation was 17 months. The most common presenting symptom was discomfort, either in the groin or on the lateral aspect of the hip or in the buttock. Two of the patients had late dislocations and complained of symptoms of instability. The authors stated that this type of pseudotumour was not found with conventional hip replacements and thought it was a

late complication associated with hip resurfacings. An estimate of incidence was calculated at 1%, however as some of the tumours were asymptomatic, there may be a number of unrecognised tumours in other patients. A recent report in 2009 by the Oxford surgeons [109] reported that the outcome of revision of cases associated with pseudotumours was significantly worse than other resurfacing revision cases (i.e. for fracture) and that of matched primary Exeter hip replacements. Complications after revision as a result of pseudotumours were recurrent dislocations, palsy of the femoral nerve, stenosis of the femoral artery and loosening of the component. Cases of recurrent pseudotumours were found, and one case of further revision was required. The authors stated that their results showed a "potentially catastrophic complication" of metal on metal hip resurfacings. Although other cases of soft-tissue masses have not been reported [17], individual case studies of a benign mass [110] and other biological responses have been reported. Davies *et al.* [107] reported incidences of unusual lymphocytic perivascular infiltrations in tissues surrounding contempory metal on metal implants. The response was thought to be similar to that found in association with type-IV-hypersensitivity cases [111]. Unpublished data by Davies *et al.* discussed in their 2005 paper [107] stated that synovial fluid from failed metal on metal implants may be toxic to human fibroblasts, and they suggested that "the cells lining the pseudosynovial neocapsule around the prosthesis may not have the secretory and regulatory capabilities of normal synovial cells and thus may expose the deeper layers of the neocapsule to higher concentrations of these substances". It was also stated however, that it is unknown whether this was responsible for the lymphocytic reactions seen in the tissues surrounding hip replacements. The term aseptic lymphocytic vasculitis-associated lesions (ALVAL) has been applied to metal-sensitive histologic features [15]. It appears from the literature, that although a number of cases of undesirable reactions have been reported in association with metal on metal implants, it is yet unclear whether the metal particles released from metal on metal articulations warrants the disuse of such devices.

3.5 Ceramic on Ceramic Hip Replacements

Concerns about metal ions within the body have increased the popularity of ceramic on ceramic implants. Ceramics were first introduced by Boutin in the 1970's [112], due to the low wear rate and frictional characteristics of the material. At a similar time, Mittelmeier and Heisel developed a ceramic on ceramic bearing comprising a press-fit femoral stem and non cemented acetabular cup. This was known as the Autophor total hip replacement system [19] which was quickly abandoned in the USA due to high rates of aseptic loosening thought to be as a result of poor implant design, minimal osseous integration and material failure. Often early implants suffered from large grain sizes and poor manufacturing techniques which led to unsatisfactory results. In 1994 [112] the result of 67 early ceramic replacements with a mean follow up time of 144 months showed that 59 sockets were radiographically stable, 2 showed early signs of loosening and 4 late signs of loosening. Wear rates for two of the retrieved implants were 2.6 μm in the stable implant and 68μm for a loose implant.

Improvements in manufacturing led to a reduction in grain size from 4.2 μm in the 1980's to 3.2 μm between 1988-1994 [113]. A retrieval study [113] of 307 Mittelmeier total hip arthroplasties implanted over 16 years, (1980-1996) showed 24 revised implants (average time for revision 7.4 yrs). Eleven case studies were investigated and categorised as 4 severe wear, 6 stripe wear and 1 low wear. Grain removal was evident resulting in a negatively skewed surface. Linear penetrations of approximately 0.15 mm were found with the majority of implants exhibiting stripe wear. Of the severe wear group two had become more vertically positioned, however the volumetric wear of the components implanted at 45^o was less than 1 mm^3 with the exception of an old Mittelmeier design with a collared head. It was concluded that a steeper implantation angle was found to lead to an increased wear rate.

A review article [114] discussed the advantages of ceramics such as their hardness, good wettability, low friction and wear, and also the concerns such as the importance of correct clearance, ceramic quality and the need to avoid high contact stresses. Retrieval press-fit fully hydroxyapitite-coated $TiAl_6V_4$ shell with alumina liners articulating against alumina heads showed promising results. No adverse ef-

fects were recorded after a mean follow up of 16 years. No osteolysis, radiolucent lines or subsidence was observed, and the authors stated that the results were encouraging even though the results were too short term for conclusive results [114].

An extensive study by Clarke *et al.* [115] showed the wear of the ceramic components to be significantly less than the metal on metal implants producing a steady state wear of 0.004 mm^3/million cycles. In comparison the steady state wear rate for the zirconia head against alumina cup was 0.014 mm^3/million cycles.

A range of wear rates have been found for simulator studies of alumina on alumina joints. Studies have shown an over 500 fold decrease for ceramic cups compared with UHMWPE cups (0.097 $\pm$0.039 mm^3/mc compared with 50.32 $\pm$7.07 mm^3/mc)[116]. More recently, wear rates of < 0.1 mm^3/mc have been reported for simulator studies over 5 million cycles for 32 mm alumina heads against alumina cups[117] which was significantly lower than the metal on metal and ceramic on cross-linked polyethylene reported in the same study. Running in and steady state wear rates of 0.38 mm^3/mc and 0.011 mm^3/mc respectively, were reported for Biolox Forte implants over 5 million cycles of wear [118].

3.6 Ceramic on Metal

The available literature regarding CoM pairings has covered the range of diameters, 22, 28, 32, 36, 38 and 54 mm components [1–9] with a range of clearances from 29.5-92 μm. The studies investigated the wear, friction and particle size and morphology produced during simulation.

3.6.1 Alumina alloy against metal hip replacements

Firkins *et al.* [1] in 2001 reported on the first simulator study investigating the hybrid CoM combination. A very low wear rate of 0.01 $mm^3/10^6$ cycles for 28 mm diameter alumina against CoCr alloy pairings was found with only a small increase (to 0.04 $mm^3/10^6$ cycles) found for one component for 0.5 million cycles. However difficulties in measuring the wear using a gravimetric technique was found, due to material transfer from the metal to the ceramic, and the very small amount of

volumetric wear which occurred during the test.

Following this in 2002, Smith *et al.*[3] investigated both 22.225 mm and 28 mm diameter zirconia against CoCr alloy bearings, with a range of clearances, finding that 22.225 mm diameter joints with a clearance of 95 μm produced the most wear with a linear wear rate throughout the test. The joints were seen to be acting in a boundary lubrication regime. Reducing the clearance to 54 μm caused a move towards mixed lubrication producing a wear rate less than a quarter of that of the larger diametral clearance which is comparable to other researchers for MoM and CoC. Increasing the diameter of the head to 28 mm with a clearance of approximately 85 μm resulted in a biphasic wear rate, again with a considerable reduction in wear. It was concluded that the larger diameter joint promoted improved lubrication in CoM bearing, and that the 'wearing in' of CoM pairings was more rapid than MoM components therefore leading to a reduced long term wear rate. The authors noted that the wear of the CoM pairings occurred almost entirely on the metallic cups, rather than both the head and cup in the MoM pairing.

Larger diameter, 32 mm and 38 mm CoM pairings (Alumina against CoCr) have been investigated by Ishida *et al.* [2], and the results compared with a 32 mm MoM pairing. 3.5 million cycles were carried out on an orbital simulator, the bearings having an average diametral clearance of 60 μm. A biphasic wear rate was seen for all combinations with the CoM combinations showing lower wear rates compared with the MoM pairing. The 32 mm diameter joint wear rates for running in and steady state phases averaged 1.12 and 0.20 mm^3/million cycles respectively compared with the lower wear of 1.01 and 0.1 mm^3/million cycles respectively for the 38 mm joints. As with Smith *et al.* [3] the majority of the wear was found on the metallic cup and the lowest wear found on the larger diameter components. It was briefly discussed that the overall wear rate of 0.38 mm^3/Mc found for the CoM pairing is only one quarter of the wear of the MoM pairing (1.58 mm^3/Mc). This differs from the results of Firkins *et al.* [1] which showed the wear of CoM to be approximately 1/100 of the wear of the MoM components. The difference was attributed to a biofilm which was found on both CoM and MoM pairings, which may have reduced the detectable wear using the gravimetric technique.

The largest diameter reported in the literature was 54 mm alumina head against cast CoCr alloy cup. A 5 million cycle wear test was conducted using an orbital simulator which compared the CoM components with the same hardness metal on metal and differential hardness metal on metal implants. The CoM components produced the lowest wear, with running in and steady state wear rates of 0.084 and 0.018 mm^3/million cycles.

Haider *et al.* [6] presented six 28 mm and 36 mm diameter pairings with two different clearances (81.7 $\pm$3.7 μm and 29.5 $\pm$4.3 μm), which were tested in a wear simulator to 5 million cycles. The study concluded that a very small amount of wear was found for the CoM pairings, and biphasic wear rates were detected. Again the larger diameters joints were found to be the lowest wearing. The femoral heads were found to increase in weight, thought to be due to metal transfer from the metallic liner. This metal transfer was evident even though a standard walking gait simulator was used.

3.6.2 Alternative ceramics against metal hip replacements

An alternative material combination of silicon nitride cups against CoCr heads was recently investigated Bal *et al.* [8]. In contrast to the majority of studies, the ceramic component was the acetabular cup and the metallic component was the femoral head. Wear tests to 1 million cycles found a wear rate of 0.18 mm^3 for the CoM pairing (compared to 0.2 mm^3 for Si_3N_4- Si_3N_4 pairing). The wear results were extrapolated to 10 million cycles, giving a predicted wear of 0.47 mm^3. However this method was not accurate when attempting to predict wear. As found with many of the previous studies two different wear rates, a running and steady state wear rate, were found. As the authors only took the test to 1 million cycles, it is likely that the predicted wear rate was higher than would be found in true steady state wear. The higher fracture toughness of Si_3N_4 resulted in a material more resistant to the initiation and propagation of microcracks, which is the precursor to brittle failure.

3.6.3 Microseparation of ceramic on metal hip replacements

In addition to the standard walking cycle tests carried out on ceramic on metal combinations, more severe microseparation tests have also been reported.

A microseparation test on 28 mm hip joints consisting of a zirconia platelet toughened alumina material against a CoCrMo alloy was carried out by Williams *et al.* [7]. CoM (ceramic head and metal cup) and MoC (metal head and ceramic cup) combinations were tested to 2 million cycles in a prosim hip simulator, using a twin peak loading cycle with a maximum load of 3 kN. A significantly higher overall wear rate was found for the MoC (overall mean wear rate of 0.71 $\pm$0.30 mm^3/Mc) compared with the CoM pairing (overall mean wear rate of 0.09 $\pm$0.025 mm^3/Mc). Deep stripe wear was seen on the metallic head caused by separation, however only a small amount of metal transfer was seen on the ceramic head.

3.6.4 Pin on plate studies of ceramic on metal materials

In addition, simplified tests such as pin on plate tests have been carried out providing encouraging results. A very short study investigating a CoCr pin articulating against an alumina plate was carried out to 90000 cycles by Figueiredo-Pina *et al.*[119]. Tests were undertaken to compare a MoM combination against the CoM pairing, under open-circuit potential (OCP) and with an applied cathodic protection (CP). The OCP was used to give a qualitative indication of surface corrosion, with a more negative value signifying a higher rate of surface corrosion. During the CP tests the cathodic potential was maintained at a constant value to prevent "anodic dissolution of the metal surface". In the OCP test, less corrosion was seen for the CoM pairing compared with the MoM pairing. Pitting and delamination by fatigue was seen for the metal plate of the MoM pairing, however this was not observed in the CoM pairing. A wear factor ten times larger was found for the MoM pairing compared with the CoM. No metal transfer was found for the MoM pairing and the authors suggested that the higher wear factor was connected with higher corrosion activity. The results of the CP test showed that a higher current was required to protect the MoM pairing before, during and after sliding. Corrosion during wear testing

was found to be ten times more intense for the MoM pairing compared with the CoM pairing. No pitting or corrosion deposits were found during the CP tests. The authors [119] compared the alumina plate roughness with wear rate and confirmed that although corrosion-wear played a role in the wear of the pairings, the tests were affected by the alumina plate's surface roughness, with an increased roughness causing an increase in wear rate. The wear mechanisms contributing to the wear of the CoM pairing were similar to those found in simulator studies revealing alumina grain pull out, abrasion, adhesion and corrosion wear[119].

Pin on plate experiments [120] have been used to show that CoM components have a smaller contribution of wear caused by corrosion compared with MoM, and therefore an overall decrease in wear was found. The ion release tests showed that selective dissolution of Co occurred as the ratio of Co:Cr:Mo was not the same as in the tested material. Ions were also found in the serum of the CP tests where corrosion was eliminated suggesting that ion release from wear particles does occur.

3.6.5 Friction of ceramic on metal hip replacements

Friction of CoM pairings was investigated by Brockett *et al.* [5] who reported that the friction compared favourably with CoC bearings and was significantly lower than that of MoM pairings. CoM friction factors were higher with increasing protein concentration with the lowest friction factor shown when lubricated in water. The trend was the same for CoC, MoP and CoP pairings but not the MoM pairings, where an increase in protein concentration led to a reduction in friction factor. The authors concluded that the higher friction observed for the MoM pairings was due to high shear stresses which were required to break the adhesive junctions formed when MoM asperity contact occurs during lubrication. When the protein content was increased it was thought that proteins adsorb to the surface [93] and reduced the adhesive surface forces between MoM asperity contacts. Thus shearing took place in the lower shear stress material (the protein) resulting in a reduction in friction. Brockett *et al.* [5] discussed that in CoC pairings proteins adsorb to the surface, which effectively increases the surface roughness, resulting in a requirement for a thicker lubricant film in order for the joints to operate in full fluid film lubrication.

Alternative hypotheses suggested that when proteins were present in the lubricant of a CoC pairing, the proteins were physically larger than the fluid film thickness which resulted in the protein being sheared and therefore causing the friction to increase [121].

3.6.6 Retrieved ceramic on metal hip replacements

Two retrieval studies have been published regarding CoM pairings. These were a Metasul cup against a Biolox alumina head [122] and a stainless steel head against an alumina cup [123] both of which were revised due to pain. The stainless steel/alumina combination had an alumina cup and a stainless steel head. Physical examination revealed reduced movement and a "palpable mass on the anterior and lateral side of the proximal third of the thigh". Acetabular loosening and increased tissue density was evident from radiography and macroscopic wear was observed on both bearing surfaces. A granulomatous reaction and metallosis was found. The authors concluded that more research was required concerning CoM pairings before it would be suggested as a suitable bearing combination.

Failure of the Metasul socket against Biolox head [122] was due to pain, and a "strange grinding and noisy mechanical phenomenon" which occurred during walking and hip movement. Revision of the CoM pairing was required which was replaced with a MoP combination. During retrieval a "fair smoky-grey discoloration of the repair-capsule was found with no effusion or massive metallosis debris" [122]. The joint was found to be stable however the beginnings of a granulation tissue reaction were apparent. The retrieved acetabular cup was observed to be smooth with no scratches or matte areas. The femoral head was found to show two separate areas of blackening; one running over the pole in a semilunar shape, and the other 90 degrees perpendicular to the first area. This was a much larger, less easily identified area, situated in the load bearing region. Again the authors concluded that more work was required to decide whether CoM combinations were to be recommended.

They felt that the wear pattern raised suspicions that sphericity and matching of the heads and cups may be more important than in MoM and CoC. They also questioned what would happen to CoM components when an incorrectly orientated

component was implanted and recommended that further research and development of CoM components was undertaken.

3.7 Microseparation

There has been much discussion concerning separation of the head and cup during gait. Stripe wear patterns observed on retrieved joints [124–126] have led to increased interest in quantifying *in vivo* hip kinematics. Fluoroscopic imaging has been used to obtain real-time images of internal structures. X-rays and a fluorescent screen coupled to a camera were used to allow videos to be recorded and replayed. However because of the risk of x-rays, a balance had to be made between the benefits and danger to health. This imaging technique was carried out by Dennis, Komistek and colleagues in the late 1990's, and early 2000's [21–24, 127] which mainly compared metal on metal joints with metal on polyethylene joints. A study to investigate hip separation during gait using MoM and MoP replacements was undertaken to see whether the bearing material had an effect on hip separation [22]. Ten subjects with MoM prostheses and ten subjects with MoP prostheses performed normal gait on a treadmill while under video fluoroscopy surveillance. The 2-dimensional images produced were converted into 3-dimension using a computer automated model-fitting technique. The authors carried out error analysis by comparing separations recorded by their technique, to known separation distances. From this they set a threshold of separation of 0.75 mm, below which they said that separation was not occurring [24]. Their results showed separation for MoP joints as the value recorded was 2 mm, however separation did not occur with MoM joints as the recorded value was 0.4 mm.

In 2000, Lombardi *et al.* [128] carried out a study to determine to what extent hip joint separation occurred during normal gait, and during abduction/adduction leg-lift manoeuvres. Using a method similar to earlier reports, a model-fitting technique was used to convert 2-dimensional fluoroscopic images into 3-dimensional real-time images. There results showed that all 10 joints in their study experienced separation between the head and cup. The average separation was 1.2 mm (range 2.8 mm -

0.8 mm) and 2.4 mm (range 3.0 mm-1.7 mm) for gait and abduction/addiction manoeuvres respectively. It was reported that although the head separates from the cup, contact is maintained at the superior most tip of the cup. They concluded that the results were important for hip simulator studies to produce wear patterns found in retrieval studies.

The controversial paper by Lombardi *et al.* [128] resulted in a discussion through letters to the editor published in the Journal of Arthroplasty in 2001 [129–132]. Lombardi *et al.* [128] incorrectly referenced that a paper by Hodge *et al.* [133] supported their findings that femoral and acetabular components separate during the swing phase of gait. Hodge *et al.* [133] believed that although certain pressure transducers between the cartilage of the natural acetabulum and the metal pseudo-femoral head reach or go slightly below zero pressure, at no time do all transducers register zero. In reply through "letter to the editor" [132], Komistek agreed that all transducers should not simultaneously register zero, since separation between the whole femoral head and cup did not occur, and that 'hip separation' was a misleading term to describe the phenomenon. He described the action as the 'femoral head sliding in and out of the acetabular cup, predominantly on the superior/lateral edge of the polyethylene insert' [132]. It is thought that separation is observed medially while a portion of the femoral head remains in contact with the acetabular component superolaterally, creating conditions where the femoral head pivoted on the superolateral lip of the acetabular liner.

Disagreement between authors over the technique used to measure the separation of the components also occurred. Derbyshire *et al.* [130] criticised the accuracy of the fluoroscopic measurements and the 2-dimensional to 3-dimensional conversion used by Lombardi *et al.* [128], and concluded that the technique was not "sufficiently accurate to reveal separation" [130]. The reply by Komistek *et al.* [132], shows disagreement between the two authors who believed that attempting to test the accuracy of the technique was not possible using scanned images without the clinical data which accompanied the x-ray images. No conclusions were drawn as to which opinion was correct.

3.7.1 Comparisons of simulator and retrieval studies of ceramic on ceramic hip joints incorporating microseparation

The discovery of 'hip separation' or 'hip joint sliding' has led to a number of studies which attempt to replicate the wear scars found on retrieval joints. Retrieval studies have shown various stripe wear patterns. Following a brief communication by Nevelos *et al.* [134] which showed clinically relevant wear rates and patterns of 2 ceramic on ceramic (one modern and one 1st generation alumina on alumina). Stewart *et al.* [135] presented the first long term simulator study which incorporated microseparation motion during simulation. Hot isostatically pressed (HIPed) alumina on alumina joints were tested to 5 million cycles at two microseparation severity levels. Using the Leeds MkII simulator which applied a physiological loading cycle, a small positive swing phase load was applied to ensure the head remained located correctly into the insert. A small lateral to medial force was applied by a spring to the acetabular cup to provide microseparation, the severity of which varied by altering the swing phase load from 50 N for severe to 400 N for mild microseparation conditions. The medial-lateral separation was regularly adjusted to provide a separation of between 200 - 500 μm. Under normal walking gait without microseparation, the wear rates were reported to be 0.11 mm ^{3}/million cycles for bedding-in and 0.05 mm^3/million cycles for steady-state wear. Under mild microseparation these increased to 0.55 mm^3/million cycles and 0.1 mm^3/million cycles for bedding in and steady state respectively, and under severe conditions they increased to 4 mm^3/million cycles and 1.3 mm^3/million cycles respectively. Stripe wear was found on both the severe and mild microseparation after the initial 1 million cycles. The stripe area was seen to increase in average roughness (R_a) from < 0.01 μm to between 0.14 μm and 0.3 μm, with inter-granular fracture seen on the ceramic heads under scanning electron microscopy (SEM). Comparing the stripe wear to retrieved implants, Stewart *et al.* [135] reported that the simulator implants had narrower wear scars compared with the first generation non-HIPed Mittelmeier replacements, however had similar stripe patterns compared with the early retrieved HIPed alu-

mina retrievals[134]. It was reported that wear debris found from this *in vitro* study was comparable to particles found in retrieval studies, with a mean particle size of 42 nm. A characteristic wear stripe was also produced on the femoral head with a corresponding marking on the rim of the acetabular cup.

Manaka *et al.* [126] reported a number of ceramic on ceramic retrieval hip replacements which showed stripe wear. They reported an alumina ball retrieved at 17 years (Mittelmeier case; stem loosening problem) which showed two wear stripes on the superior to inferior-anterior and posterior aspects which were approximately 51x15 mm and 21x4 mm in extent. This was compared to simulator wear studies of alumina-on-alumina hip implants under both microseparation and standard conditions. A 12 station hip simulator was modified with a spring to provide 0.5 mm translation in the horizontal plane, and a negative load during swing phase to produce vertical distraction of 1 mm. The microseparation test mode of Leeds was adopted with the cups mounted in the anatomical position above the head and inclined at 50^o to the horizontal. The results showed 2 wear scars were produced on the femoral head tested under microseparation conditions which had the similar overall shape and position however, they were narrower than scars found on the retrieved sample used in this study (17 years retrievals). The alumina liner did not show any obvious stripe wear.

A paper by Shishido *et al.* [118] compared two types of retrieved hip prosthesis, namely the Biolox (1st generation alumina) and Osteal (2nd generation alumina) hip with the simulator results of the Biolox-forte (3rd generation) hip in standard and microseparation conditions. The simulator joints were analyzed using SEM and gave steady-state wear rates ranging from 0.16 to 0.65 mm^3/million cycles in microseparation mode, compared with 0.011 mm^3/million cycles in standard mode. Differences were seen in the wear scars of the retrieval and simulation joints. Simulation produced two narrow wear scars of dull appearance on the heads, which showed mild wear. One of the stripes appeared near the main worn area around the superior of the head, which is thought to be due to microseparation. The second stripe was thought to be caused by neck-socket impingement rather than microseparation. The simulator implant and the retrieved Osteal implant were found to have

less severe wear compared with that of the retrieved Biolox implant. The difference in the severity of the wear was thought to be due to the alumina quality.

Akagi *et al.* [136] reported severe wear of an alumina-on-alumina implant in the peripheral portion of the alumina inlay and the superolateral portion of the alumina ball. It was thought that this may be due to edge loading as a result of microseparation of the joint, which could cause high contact stress in the hard material producing damage to the surface. It was postulated that the edge loading led to an increase in surface roughness which resulted in high frictional torques, which was thought to be a possible reason for the higher incidence of loosening found in ceramic on ceramic implants compared to the Charnley joint. However, the conclusion drawn in this study came from the work reported by Lombardi *et al.* [128] which as previously mentioned has been questioned by other researchers in this field.

Walter *et al.* [125] in 2004, questioned the frequency at which microseparation occurred by examining 16 retrievals from 1588 cementless hip arthroplasties in the hope of characterising the stripe wear mechanism. All joints were third-generation alumina ceramics , which differ from early alumina bearings in that they were treated by hot isostatic pressing producing smaller grain size and fewer impurities. None of the retrievals were due to bearing failure. The authors believe that edge loading during gait could not produce the stripes found. For the wear patch on the head to match the wear on the liner the hip must be flexed to about 90^o, such as rising from a chair, or climbing a high step. The authors went on to discuss a self-limiting phenomenon. They suggested that when edge loading first occurs, the contact between the non conforming surfaces is small leading to high contact stresses which can lead to grain pull out. With further edge loading, it is thought that the surfaces will begin to conform geometrically, therefore increasing the contact area and reducing the contact stress which would "favour a more benign wear process" [125]. Long term follow-up is required to investigate this phenomenon, since the retrievals in this study had an average of 18.7 months from implantation. Walter *et al.* [125] believed that 1 million cycles of standard hip simulation , do not represent 1 year *in vivo*, and that edge contact must be incorporated into hip simulation.

3.7.2 Simulator studies of metal on metal hip replacements incorporating microseparation

Research into microseparation of MoM combinations has also been carried out. Williams *et al.* [137] compared different swing phase loads, including microseparation, on the wear, friction and wear particles of CoCr hip replacements. Wear tests were carried out using low load (100 N), ISO standard load (280 N) and microseparation conditions (100 N negative load) for swing phase in a 10 station ProSim simulator. Under microseparation conditions the head was displaced inferiorly and laterally by approximately 0.8 mm in swing phase. The results showed that all conditions had higher bedding in wear than steady-state wear with lower wear of the cups compared with the head. It was found that the overall mean wear increased from low swing phase, to ISO standard to microseparation conditions with wear rates of 0.06 $\pm$0.05 mm^3/million cycles, 0.58 $\pm$0.53 mm^3/million cycles and 1.58 $\pm$0.85 mm^3/million cycles respectively. As seen with ceramic joints tested under microseparated conditions [3] the metal joints produced two wear stripes thought to be caused by the inferior cup rim at toe off, however the metal scars are wider and fatter than the scars found on the ceramic joints. In these areas the surface roughness was found to increase (0.01 μm to $<$0.1 μm) compared with a small increase found in the standard conditions (0.01 μm to 0.02 μm). Superior rim contact was also visible. This increase in surface roughness however has not been found in retrieved metal-on-metal joints. The authors of this paper had the opinion that microseparation does not occur during every step of gait, as found in hip simulation, and it is thought the absence of scars from retrieval MoM joints is due to self polishing during normal gait.

3.7.3 Simulator studies of ceramic on polyethylene hip replacements incorporating microseparation

Microseparation conditions have also been applied to wear simulators testing ceramic-on-polyethylene. Williams *et al.* [138] tested an alumina femoral heads against a moderately cross-linked polyethylene cup. A reduction in volume change was found

when microseparation conditions were applied, from 25.6 ±5.3 mm^3/million cycles under standard conditions to 5.6 ±4.2 mm^3/million cycles under microseparation conditions. Due to the softer polyethylene cup there was no damage to the head, however there was local deformation to the rim of the cup and the reduction of scratching within the wear patch which resulted in a decreased wear rate.

3.8 Third Body Wear

Third body ingress into the joint space within hip replacements has been suggested as a contributor to runaway wear seen from some retrieval implants. Studies have shown that 3rd body particles can cause accelerated wear for polyethylene components against both ceramic and metallic heads [86, 139–142]. The majority of studies investigate the effect of polymethylemethacrylate (PMMA) bone cement particles on either conventional or highly cross-linked polyethylene. Results have shown highly cross linked polyethylene to have superior resistance to 3rd body particles. Concentrations have range from 10 g/L [141] down to 0.15mg/cm^3 [140]. Research has shown that reducing the concentration of PMMA particles from 10 g/L to 5 g/L resulted in a 40% reduction in wear [139]. The method of manufacture of the PMMA has also differed with some particle produced by crushing pre-polymerised PMMA bone cement in a cryogenic mill under liquid nitrogen temperatures [141], to using manufactured powders [139]. PMMA particle sizes ranging from 500 μm[141] to 30 μm [140] have been used as the 3rd body particles which reports showing a reduction in wear with smaller particles [139]. PMMA often contains approximately 10% barium sulphate ($BaSo_4$) particles [86] which allows the bone cement to be visible under x-rays [140],[142],[86]. Studies have shown that PMMA particles with and without $BaSo_4$ show similar abrasive scratches, wereas round PMMA bead slurry containing $BaSo_4$ were not found to scratch the CoCrMo alloy surfaces [142].

In addition, bone particles have been added as third body particles to the lubricant of *in vitro* tests. The addition of cortical bone into the lubricant with the presence of head-cup separation was found to produce wear patterns on polyethylene cups with the closest appearance to *in vivo* retrieval cups [143] with trabecular

bone being less effective at scratching the polyethylene cup. A mixture of bone and PMMA slurries has been tested against CoCr disks [142], which revealed scratches and an increases in roughness of the surface. The dominant wear mechanism found was ploughing rather than cutting, which resulted in the 3rd body particles displacing the material rather than removing it from the surface. The presence of carbides protruding from the as-cast CoCr surface was thought to interrupt the third body scratches.

Limited research has investigated the effect of alumina particles on the wear of hip replacements. Affatato *et al.* [86] reported the addition of alumina particles into the lubricant of a test to simulate severe test conditions that may occur when an unstable ceramic hip chips or fractures. Alumina particles with a purity of 99.7% and a size range between 2-8 μm were added to bovine serum with a concentration of 0.1 mg/mL. The test was carried out on 28 mm alumina on alumina implants at three different inclination angles, namely, 23 ^{0}, 45 ^{0} and 63 ^{0}. Increased wear was seen for all inclination angles when particles were included into the lubricant. Squeaking was experienced when third body particles were present.

3.9 Summary

This literature review comprehensively evaluates the available literature surrounding the topics of wear testing and surface analysis of ceramic on metal hip replacements, and the phenomenon of 'microseparation'. With the increased demand for hip replacements, researchers are working towards finding a replacement that can last the lifetime of the patient. The improvements in manufacturing techniques and refinements to the design of the hip replacement have resulted in significant improvements to wear rates and survivorship of implants. As the understanding of lubrication mechanisms and wear has improved, researchers have started to appreciate the need to consider the lubricants and conditions used within a simulator. International standards have been developed to outline the motions, loadings and protocols that should be used in order to allow comparisons between laboratories. Although these are not always used, they provide basic conditions which researchers

can follow. One of the more recent topics with regards to wear testing of hip replacements is the behaviour of protein molecules within the serum. A number of researchers have investigated the impact of varying protein contents on the wear results, mainly under simple pin-on-disc or pin-on-plate configurations. A consensus has not yet been established as to which proteins adsorb onto the surface or whether they are in the native or denatured state, however it has become an important topic of discussion. In addition, the temperature of the lubricant has also been found to be an important factor when considering wear testing as high temperatures can lead to denatured proteins. As a result, these may act as a protective layer on the bearing surfaces reducing the wear.

The results from early metal on metal replacements led to clinicians abandoning the material combination, due to the large number of failures. However a small number of implants survived for many years, resulting in a revival of metal on metal implants. In addition metal on metal resurfacing devices were introduced for younger patients. These allowed preservation of the bone and as a result of the large diameter, a greater range of motion was possible. In recent years the enthusiasm for metal implants has been suppressed due to the concerns with metal ions *in vivo*. Surgeons from Oxford have reported cases of 'pseudotumours' which are soft-tissue masses found at the site of metal on metal resurfacings. The tumours, primarily found in female patients have caused great anxiety amongst the orthopaedic community, a result which may have detrimental effects on the market for metal on metal implants.

Ceramic on metal replacements were introduced in 2001 by Firkins *et al.* [1], who claimed low wear rates for the metallic acetabular component. It was suggested that the reduced levels of metal ions released as a result of wear and corrosion, could be advantageous for the patient, as a consensus has not yet been reached regarding the problems of metal ions *in vivo*. The limited *in vitro* data available for ceramic on metal replacements has shown relatively low wear, however the majority of the wear was found on the softer metallic component. Further research is still required to fully understand the wear of ceramic on metal implants, and the clinical impact of the metal ions to be determined. Altering factors such as the material, clearance and wear conditions may provide additional evidence to support the use of ceramic on

metal replacements. Clinical studies are in very early stages and the only retrieved ceramic on metal combinations were implanted unintentionally. These implants were retrieved because of pain, with the authors suggesting that considerable research is required before ceramic on metal implants can be recommended for implantation.

Wear simulators are mechanical rigs which are used to test a joint replacement, under conditions approximating to those occurring *in vivo*. However they usually test bearing combinations under 'ideal' conditions of standard walking gait. As the design of implants has improved, the wear rates have decreased making it difficult for wear to be detected through volumetric wear under gravimetric conditions. Analysis of retrieved implants has shown wear patches which were not thought to be possible as a result of normal walking gait. Fluoroscopy analysis has shown that the head can separate from the cup during walking and adduction/abduction manoeuvres, a motion which researchers have attempted to replicate in *in vitro* simulators. After much discussion, there seems to be no consensus as to whether the mechanism proposed by these researchers occurs *in vivo* however, the work highlighted the need for a more severe wear simulator to differentiate wear rates between bearing combinations. The initial research led to the development of microseparation simulators which included medio-lateral separation of the head from the cup and edge impact. This provided a more severe mechanism to test the implants. These simulators may differentiate wear found for material combinations which would not be identified under standard wear testing conditions and thus establish the limits of performance of a material. Only one study is available which tests ceramic on metal hip replacements under more severe conditions, therefore microseparation wear of ceramic on metal components may be useful to improve the understanding of how these materials would withstand the harsher conditions within the body.

In addition to microseparation, severe testing of hip replacements has been carried out using third body particles in the lubricant. The majority of studies have investigated bone cement, with and without barium sulphate and have found an increase in wear with the addition of particles. However limited work has investigated the addition of ceramic particles which may be present as a result of ceramic fracture or general wear of the ceramic component. This area of research may be

particularly relevant for a second implant after a ceramic fracture.

With respect to ceramic on metal hip replacements, the questions that need to be answered are:

- In the Durham Wear Simulator, what wear rates are found under standard wear testing conditions?
- Does changing the ceramic femoral head affect the wear rate of the metal component?
- Does changing the size to a larger diameter affect the wear rates?
- Under severe wear testing conditions such as microseparation does the wear of the components increase?
- Does the addition of third body particles affect the wear of the components?

If ceramic on metal components under standard and severe wear conditions are found to show low wear, the results may support the use of this material combination and may provide another option for surgeons, especially in patients where high metal particles may be a problem. The softer metallic component may reduce the chances of fracture of the ceramic head and as a result of the smooth wettable surface provide conditions where full fluid film lubrication can prevail. The result of this would be to increase the life of the components by removing the problems with polyethylene particles and osteolysis, and by reducing the problems associated with metal ion release such as 'pseudotumours' thus improving the quality of life for the patient.

Chapter 4

Apparatus

The Durham Wear Simulator was used to model human gait and simulate the wear which may occur *in vivo*. Gravimetric analysis allowed the weight change of both the head and the cup to be monitored and the wear rates determined. Comparisons of different material couples and radii of joints were undertaken using identical simulator conditions. The loading and motion was also varied and a comparison was made between identical bearings for standard and more severe loading conditions. A variety of instruments were used to obtain and investigate changes in surface topography throughout the wear tests including optical microscopy, non contacting profilometery and atomic force microscopy. Further to this, friction testing allowed the lubrication regime of each bearing couple to be determined before and after wear testing which indicated whether the couple was acting under boundary, mixed or full fluid film lubrication.

4.1 Durham Wear Simulator

Wear simulators are a means by which *in vitro* testing can take place to compare different material combinations and device design, loading and motion parameters and to indicate whether a particular combination is likely to be suitable as a successful replacement *in vivo*.

The Mark II Durham wear simulator was used for all wear tests within this study as descibed by Smith *et. al* [144]. The loading was set to follow a simplified

square wave pattern, with 2 axes of motion. An a.c. motor and gearbox drove a crank and connecting rod to provide flexion/extension which oscillated the femoral component with an approximate sinusoidal motion through $+30^o$ to -15^o, at 1 Hz. Internal/external rotation in the transverse plane was generated by a second crank and connecting rod, which oscillated the acetabular component with an approximate sinusoidal motion of $\pm 10\ ^o$. A phase difference of 90 ^{o} between the two motion cycles was set, to create the correct wear vector over the acetabular surface. Loading was controlled by 3 optical switches and a Norgren (Staffs, WS13 6SB) pneumatic proportional valve which ensured that the load was applied during the stance phase of the walking cycle. The output pressure from the proportional valve was pneumatically amplified using a booster valve. A manifold was used to supply an equal pressure to the Hoerbiger (Gloucester, Gl2 2AL) pneumatic actuator in each of the 6 stations, 5 of which underwent motion and loading, and one control station which underwent loading only. For standard wear testing the load was set to a minimum of 300 N and a maximum of 2500 N $\pm$500 N.

A self-aligning gimble mechanism was used to ensure correct orientation of the head and cup so that the centre of rotation of the acetabular cup was in-line with the centre of the femoral head. To ensure this, a head height setting mechanism was used during simulator set-up as shown in Figure 4.3.

4.2 Durham Microseparation Wear Simulator

Modifications to the Durham hip wear simulator resulted in a machine capable of carrying out a more aggressive test termed 'microseparation wear conditions'. This incorporated medial-lateral displacement of the heading during the swing phase of the walking cycle, in an attempt to simulate motion thought to occur *in vivo*. Gait analysis has shown that separation of the head from the cup [24][21] occurs during the low load swing phase part of the walking cycle. This was thought to be due to joint laxity after replacement surgery or during high flexion of the hip, such as rising from a low chair [125]. By carefully controlling the inlet and back pressure of the pneumatically controlled load cycle, and by using a displacement block, medial-

lateral displacement of the head during the swing phase of the walking cycle was achieved. When the load increased upon heel strike, edge contact occurred followed by relocation of the head within the cup. Figures 4.1 and 4.2 shows the mechanism used for the microseparation set-up.

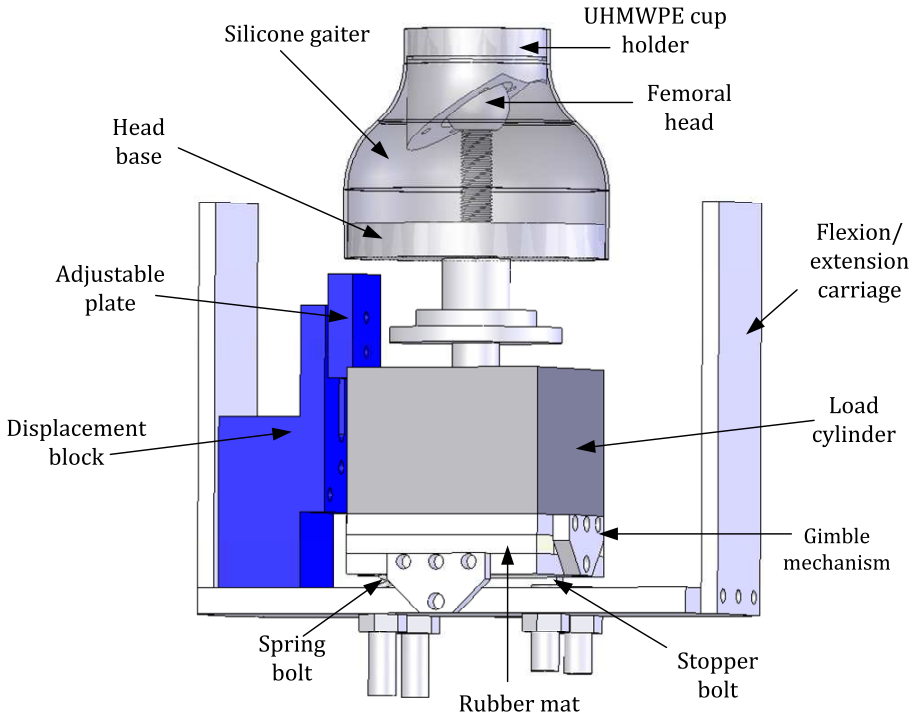

Figure 4.1: *Microseparation displacement mechanism*

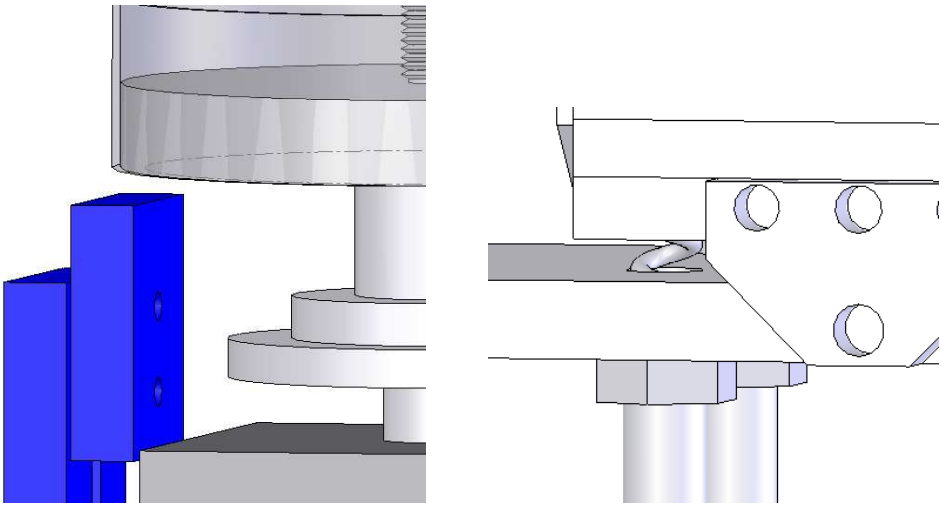

(a) Displacement mechanism ***(b) Spring Bolts***

Figure 4.2: *Close-up images of medial lateral displacement mechanism*

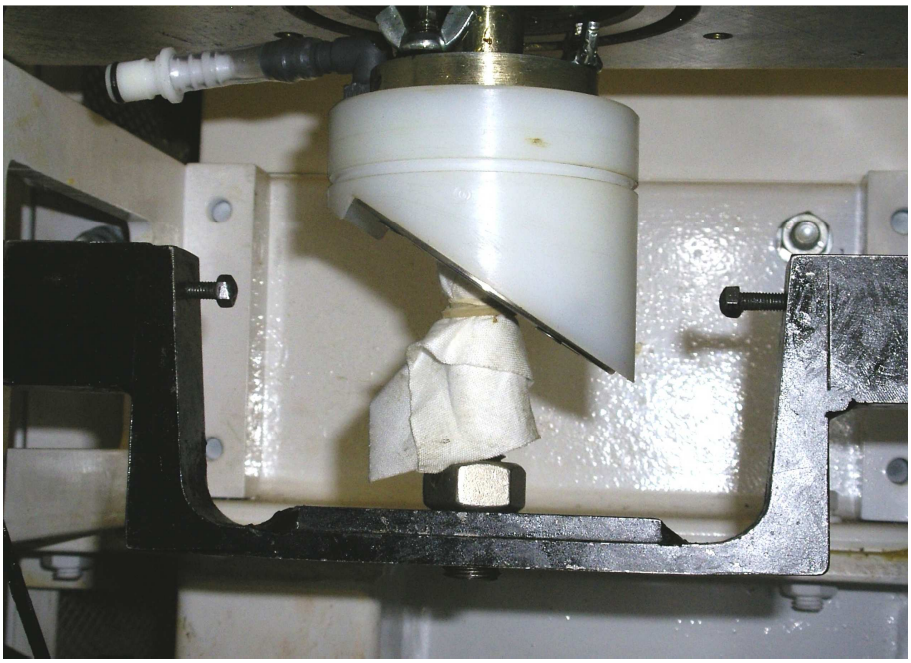

Figure 4.3: *Head height setting jig*

The main control of the displacement was achieved by setting the stroke length of the cylinder and by using a displacement block to tilt the head laterally (see Figure 4.2). The cup was positioned so that when the head was loaded, the centre of rotation of the head was in-line with the centre of the swing bearing. This was achieved by using the same setting jig as for standard wear testing (see Figure 4.3). The position of the head in the inferior-superior direction, in relation to the cup, was set during static loading so that the maximum movement of the head (inferiorly-superiorly) was approximately 1-2 mm. The displacement block was used to tilt the head and produce medial-lateral movement of approximately 0.8 mm-1.2 mm. A 0.4 mm space was set using slip gauges, between the top of the displacement block and the head base plate. To prevent posterior-anterior displacement during the early stages of the swing phase, rubber sheeting was placed between the gimbles. In addition, to ensure the head remained medio-laterally displaced until relocation into the cup at the end of the swing phase, spring loaded bolts were placed through the bottom plate of the frame on the medial side, and stops set with a gap of 0.4 mm on the lateral side. Displacement was measured using a clock gauge attached to a magnetic stand for both the superior-inferior and medial-lateral orientations.

A linear variable displacement transformer (LVDT) was used in an attempt to record inferior superior and medial lateral displacement during microseparation testing. However, 'true' displacements could not be measured due to the space constraints of the simulator and the equipment available. Figure 4.4 shows the position of the LVDT and the jigs used to hold the transducer. The x-axis is labelled 'counts'. Each walking cycle takes 1 second, and each second is represented by 1000 'counts'. Each Figure shows 2.5 seconds therefore 2.5 gait cycles.

The tip of the LVDT was found to slip during measurement and the tilting of the head base plate resulted values which were not strictly inferior-superior or medial-lateral displacements. Therefore the values were only used as an indication of the displacements during motion. Figures 4.5 show two typical graphs of the recorded displacements. Similar motion of head dislocation and relocation were found for all stations, although the magnitudes were found to vary slightly. The results for the alumina test are shown in Figures 4.6 and 4.7 show individual plots for each station.

The results were relatively consistent between stations with inferior-superior displacement between $\approx$ 1.5-2 mm. This resulted in a medial-lateral displacement of $\approx$ 0.6-1.1 mm. The shape of the curves were found to differ slightly between stations which is likely to be caused by the positioning of the LVDT and possibly the movement of the head in and out of the cup. As mentioned previously, the method used had many problems, and therefore the values were used as a guide rather than absolute displacements. The motions were set initially using a clock gauge during static loading, after which the motions were not altered.

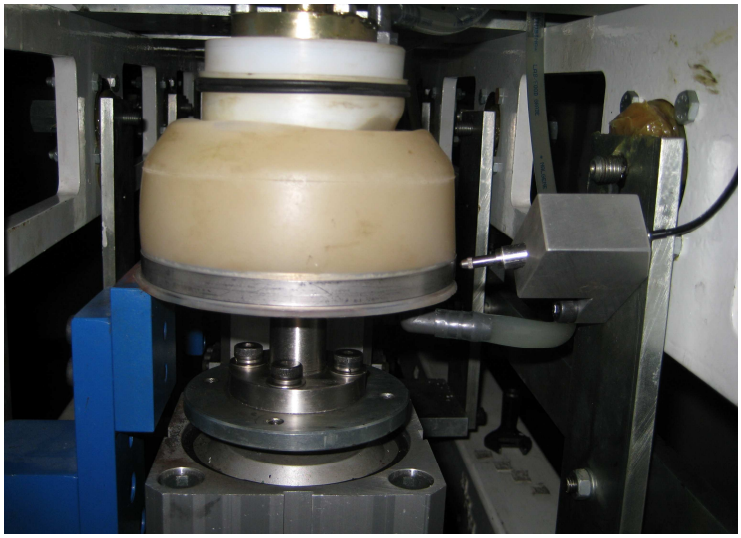

(a) Medial lateral displacement

(b) Superior inferior displacement

Figure 4.4: *Images of LVDT measurement during MXS tests.*

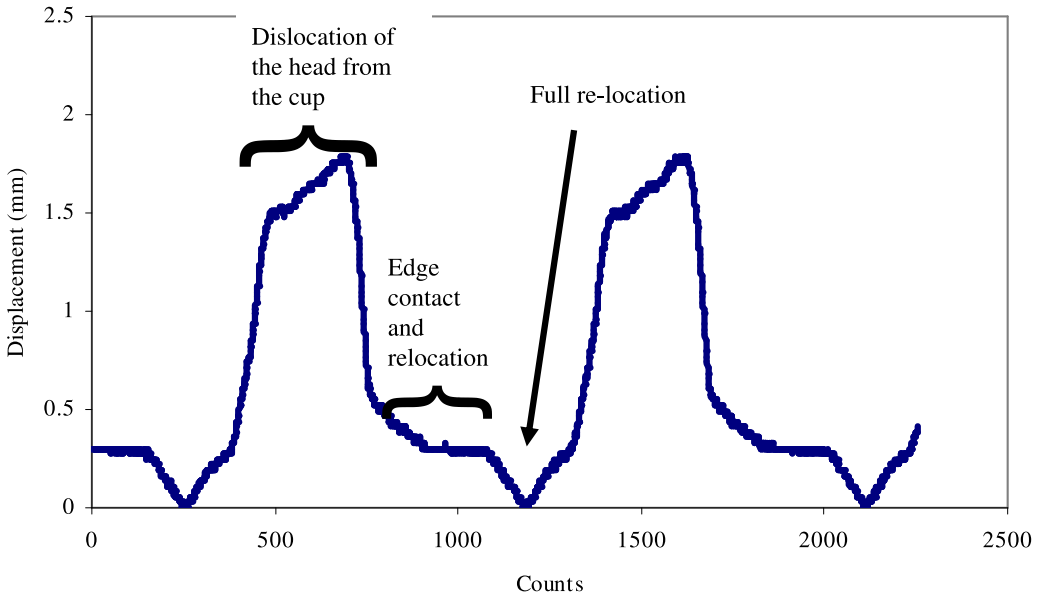

(a) Inferior-superior displacement

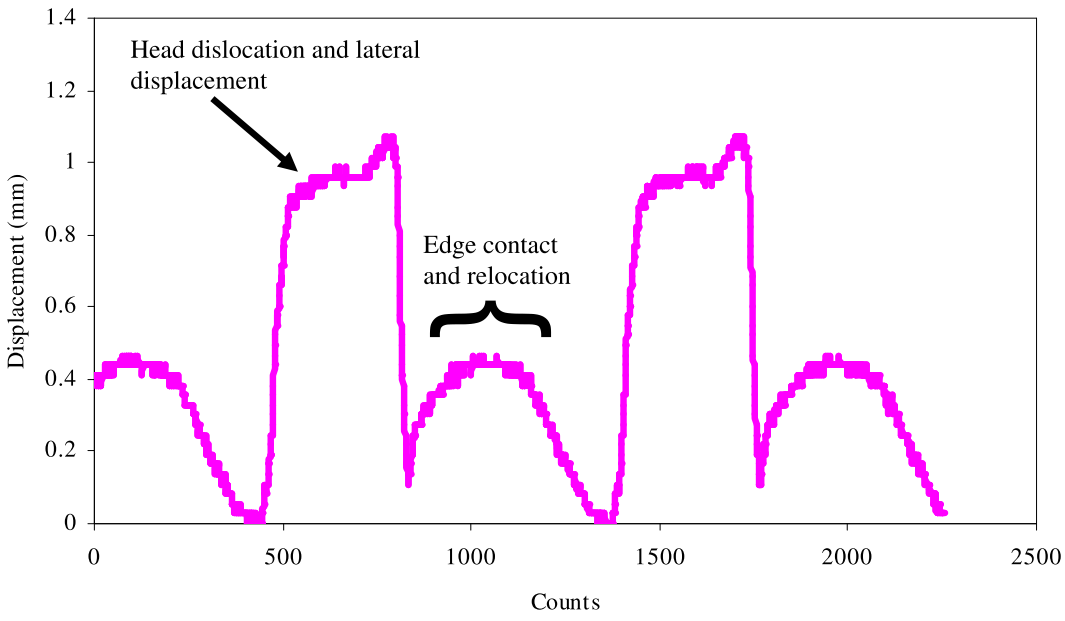

(b) Medial-lateral displacement

Figure 4.5: *'Inferior superior' and 'medial lateral' displacement graphs showing the movement recorded during microseparation motion (1 second = 1000 counts).*

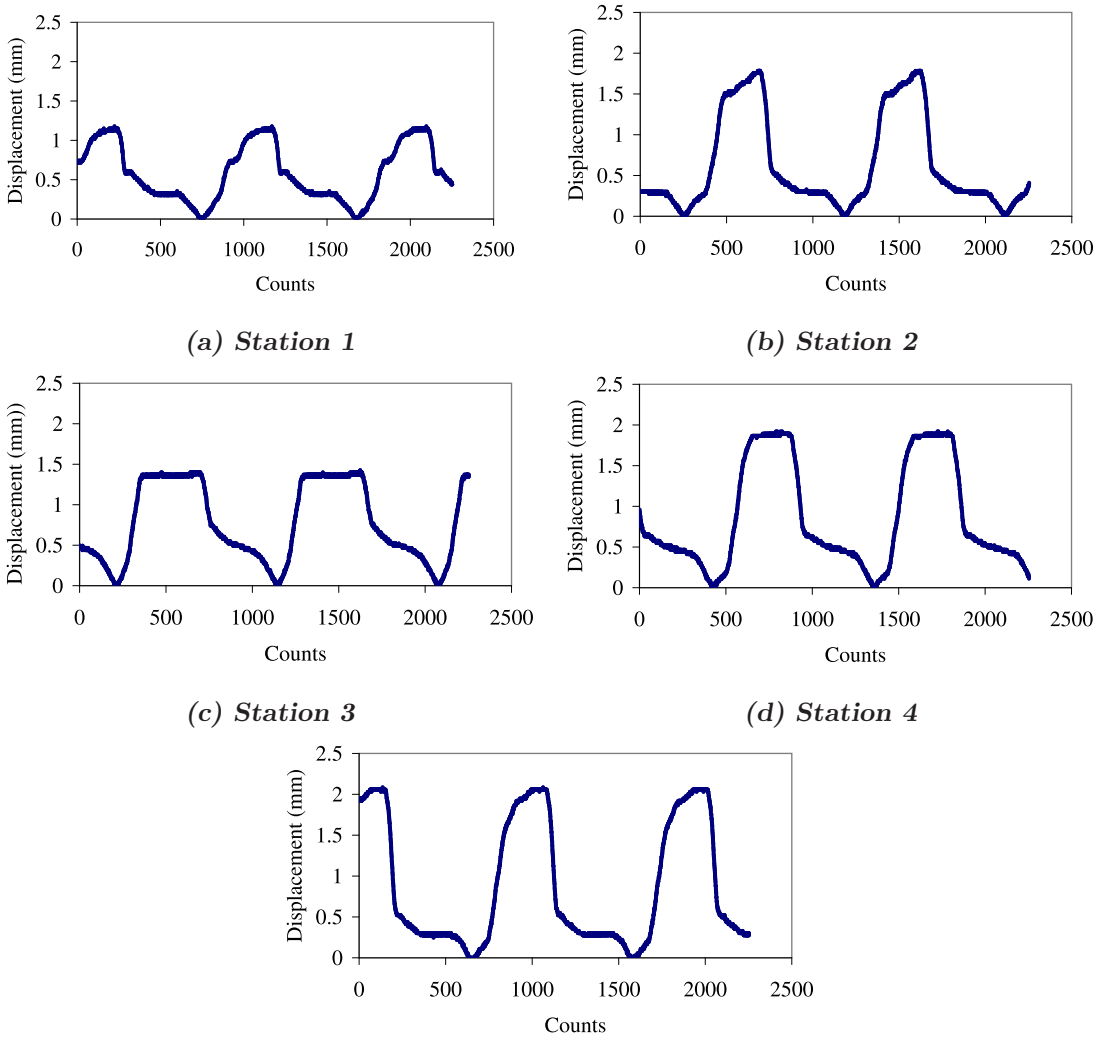

(a) Station 1

(b) Station 2

(c) Station 3

(d) Station 4

(e) Station 5

Figure 4.6: *'Inferior superior' displacement recorded using an LVDT during the alumina mxs test(1 second = 1000 counts).*

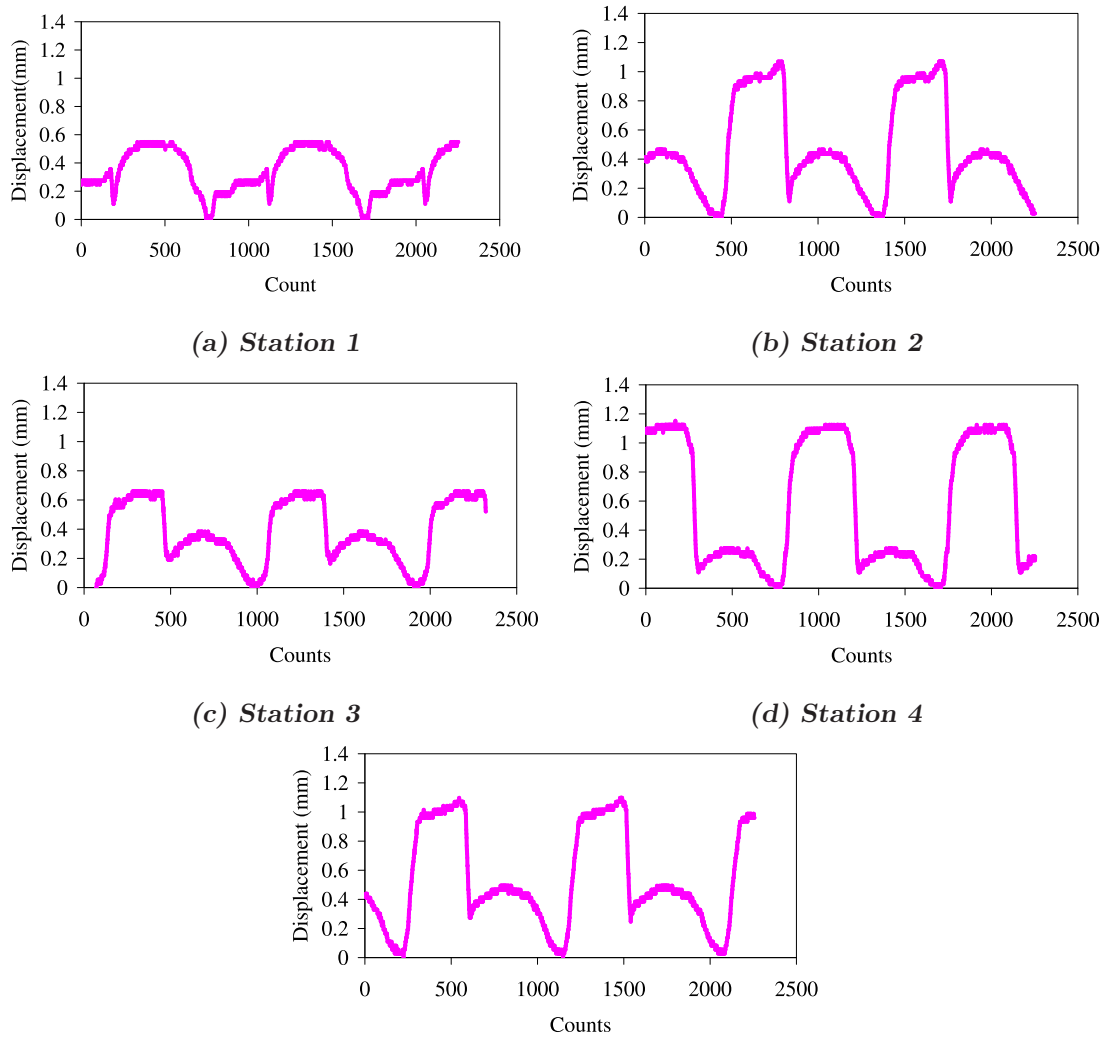

(a) Station 1

(b) Station 2

(c) Station 3

(d) Station 4

(e) Station 5

Figure 4.7: *'Medial lateral' displacement recorded using an LVDT during the alumina mxs test (1 second = 1000 counts).*

4.3 Durham Friction Hip Simulator

Early work investigating the friction of natural and artificial joints used pendulum machines which recorded the decay in amplitude with time, and predicted the type of lubrication under which the joints were operating. A linear decay in amplitude with time was thought to suggest boundary lubrication, while an exponential decay suggested full fluid film lubrication [44]. Following this a modified pendulum design was built which incorporated a load transducer which directly measured the friction between the joints, using a carriage built on hydrostatic bearings[37]. Although this machine was capable of measuring the coefficient of friction, and showed the effect of dynamic loading, the conditions were not very realistic. The load applied was constant and it was not possible to control or vary the speed greatly. Therefore apparatus was designed to incorporate factors such as variable loads, oscillating motion with variable frequency, varying amplitudes and the ability to measure the frictional torque and loads. This would more accurately reproduce the conditions found in the human hip *in vivo*. The simulator could not designed to provide full simulation of the joint and still accurately measure friction, therefore internal-external rotation, and abduction-adduction were not incorporated into the design [145][146]. The simulator as it is today was described by Unsworth *et al.*[147] in 1988 where a computer was added to store the information and act as a feedback signal for the servo mechanism which loaded the joints.

The simulator used within this study was a single station friction simulator, controlled by a microprocessor attached to a P.C. It comprised a fixed main frame and a moving loading frame into which the components of the joint were fixed. The joint was inverted from the natural position with the acetabular component in the lower friction cradle held in the fixed frame and the femoral head bolted into the upper moving frame. Misalignment of the components was accommodated within the cradle arrangement without affecting the measured friction. Using a motor and variable speed drive, motion was transmitted to the upper moving frame in which the femoral head was located. A toothed belt and scotch yoke mechanism were used to provide simple harmonic oscillation through an adjustable amplitude. The lower friction cradle, which supported the acetabular component, sat on externally

pressurised bearings with a coefficient of friction of at least two orders of magnitude lower than that of the joints being tested. The standard testing loaded the components so that the load vector oscillated with the angle of swing of the femoral head with a minimum and maximum value of 100 N and 2000 N respectively. During oscillation, friction generated between the components rotated the cradle on the externally pressurised bearings. This movement was resisted by a piezo-electric force transducer located on the side of the cradle which was calibrated to record the frictional torque during motion. Normal and inverse runs were undertaken for each lubricant viscosity, to take account of misalignment between the head and cup, with any eccentricities adjusted for once the files were merged. During the normal run the load was applied as the head swung through flexion. Conversely during the inverse run the load was applied when the head swung through extension. As a result of merging these files, the true frictional torque was calculated.

Forty one cycles were undertaken during each normal and inverse run. Values were recorded during the high load stance phase of the test, from cycles 1, 21 and 41. The average friction factors and Sommerfeld numbers were calculated from encoder positions 61, 62, 63, 64, 65, and 66 (between approximately $\pm$ 5° with the vertical position representing zero degrees) resulting in one friction factor and Sommerfeld number. Three runs were undertaken for each viscosity and the results averaged to give a mean and standard deviation. Figure 4.8 shows an example of the merged friction factors from the normal and inverse run, plotted against the encoder position which shows a stable reading between encoder positions of approximately 50-70. This corresponds to the high load part of the loading curve (plotted on the secondary axis) on which encoder positions 61-66 have been highlighted. These are the friction factors which are averaged to provide one value per viscosity of fluid and is plotted against the Sommerfeld number in the Stribeck Curve.

The data collected from the microprocessor included the encoder position, i, applied load Li, frictional torque Ti, and swing angle Ai. From this the mean load, frictional torque and angle were calculated. The velocity (u) was calculated using the following equation

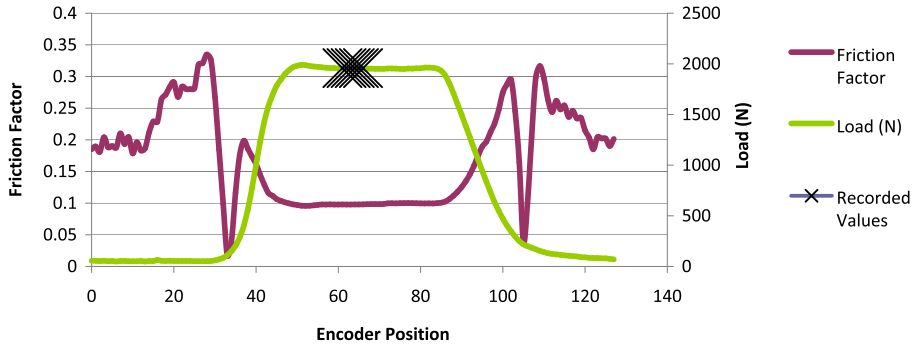

Figure 4.8: *Friction Factor vs encoder position and loading profile from friction simulator*

$$u = \left\{ \frac{\pi^2 \alpha}{180} f cos\left(\frac{2\pi \mathrm{i}}{128} + \frac{2\pi \alpha_0}{360} \right) \right\} R_h \tag{4.1}$$

where α is the angle , α_0 is the zero angle offset, f is the frequency, i is the encoder position and R_h is the radius of the head.

The Stribeck curve was initially described by Gümbel, which plotted the coefficient of friction vs the Sommerfeld number. This was modified by Unsworth to present a Stribeck curve which plotted the friction factor, f, against a modified Sommerfeld parameter, Z [148]. This was called friction factor rather than the coefficient of friction because the two are only equal when the ball and socket are in point contact. However in a replacement joint the load is distributed over an area, and therefore point contact does not occur. The friction factor, *ff*, (see equation 4.2) was defined as the torque measured by the piezoelectric transducers divided by the product of the load and radius of the femoral head.

$$ff = \frac{T}{rL} \tag{4.2}$$

where T is the measured torque, r is the radius of the head and L is the load.

The modified Sommerfeld parameter [149] was defined as:

$$z = \frac{\eta u r}{L} \tag{4.3}$$

Where u is the entraining velocity, η is the viscosity of the lubricant, r, is the

radius of the femoral head and L is the applied load. By changing the viscosity of the lubricant used, an indication of the lubrication regime can be obtained by relating the friction factors to the shape of the curve.

4.4 Surface Analysis

Various surface analysis techniques were used to investigate the topography of the surfaces. The Zygo non contacting profilometer (NewView 100) was used to quantify the surface topography features such as the root mean square roughness and skewness skewness of both the ceramic heads and cups. Skewness is a measure of symmetry of the profile about the mean line. Negative skew indicates a predominance of valleys, while positive skew indicates a 'peaky' surface. Bearing surfaces should have negative skew. In addition, an optical microscope, scanning electron microscope, and environmental scanning electron microscope was used to monitor the surfaces of the metallic cups, and an atomic force microscope was used to image the surface of the ceramic heads.

4.4.1 Topometrix Explorer Atomic Force Microscope (Vecco ltd., Cambridge, CB24 4UQ)

The atomic force microscope (AFM) was used to image the ceramic femoral heads, both before, during, and after wear testing. AFM's use high-resolution scanning-probes to create 3-dimensional maps of surface heights while scanning parallel lines, determining the height for every point measured along the line.

The AFM used a piezoelectric device to scan a tip over the surface of the sample, measuring the deflection that occurs. The tip was mounted onto a cantilever, which together was known as the probe. The deflection of the tip was measured with a laser which was reflected off the probe onto a split photodiode. This allowed both horizontal and vertical measurements during probe deflection. During translation of the probe over the surface, the tip underwent either an attractive or repulsive force which bended the cantilever. A computer controlled feedback mechanism was used to hold the cantilever at a constant force which controlled the piezoelectric

device, determining where the tip should move to maintain a constant force. The distance which the cantilever was adjusted, was recorded and therefore the sample topography determined. The AFM was used in contacting mode for the work carried out within this thesis.

The resolution of the technique was controlled by the sharpness of the tip and typically approached the atomic scale. The majority of the images for this study used a general Au reflective coated probe with a tip radius of 10 nm (max 40 nm) and a tip height of 2.5-3.5 μm. Although atomic force microscopy was an useful technique to reveal the surface of the ceramics, there were a number of drawbacks. These included the small area which could be measured per scan, the maximum for most being 100 μm^2, and then determining whether the image was representative of the surface. In addition, the damage caused to the surface when used in contact mode, including scratching and movement of contamination over the surface could result in false or inaccurate imaging. Measuring surfaces where large differences in height were found, could also be difficult as the tip could lose contact with the surface. A further disadvantage was the time taken to acquire an image as the scanning speed was slow and was affected by thermal drift and changes in the environment.

4.4.2 Zygo NewView 100 Non Contacting Profilometer (Zygo, Middlefield, CT)

Surface topography measurements were taken using the Zygo non contacting profilometer. This technique used white light to create light and dark fringes from the sample surface, resulting from an optical path difference between a reference and sample beam. The light beam was split inside the instrument, one part of the beam going to the internal reference and the other going to the sample. Fringes were created due to beam reflection from the surfaces, which underwent constructive and disconstructive interference. A precision stage and CCD camera created an interferogram of the sample which was transformed into a three-dimensional image.

A x10 lens and a x2 zoom were used for the majority of images within this thesis, which resulted in a measured area of 0.363 mm x 0.272 mm. Both the ceramic heads and metallic cups were measured periodically throughout testing. Measurements

were taken in the area thought to be the wear patch however this was difficult when the wear area was not visible by eye and therefore a through investigation of the surface was required to locate different areas of wear. Measurements on the metallic cups were taken in the wear patch, usually situated at 33^o to the horizontal. In the initial stages of the test, measurements were taken on the ceramic heads at 33^o as with the metal cups. However as the study progressed it was concluded that the measurements should be taken on the pole of the heads which is in-line with the axis of loading, therefore the location where wear occurs under standard wear conditions. Microseparation components required measurements to be taken on the pole and in stripe wear and metal transfer regions which resulted from edge contact between the head and cup.

Parameters recorded included root mean square roughness, (RMS), skewness (SKW) and peak-to-valley height (PV). RMS roughness is defined as the average of the measured height deviations taken within the evaluation length or area and measured from the mean linear surface.

$$RMSroughness = \sqrt{\frac{1}{l_x l_y}\int_0^{l_x}\int_0^{l_y} n^2(x,y)dxdy} \tag{4.4}$$

Skewness is a measure of symmetry of the profile about the mean line. Negative skew indicates a predominance of valleys, while positive skew indicates a "peaky" surface. Bearing surfaces should have negative skew.

$$Skw = \frac{1}{rms^3}\int_{-\infty}^{\infty}\int_{-\infty}^{\infty} n^3(x,y)p(n)dxdy \tag{4.5}$$

Peak-to-valley height is the distance between the tallest peak and lowest valley in the area being measured.

4.4.3 Zeiss Optical Microscopy (Rugby, CV21 1ST)

An optical microscope with a live camera attachment (PixeLINK) was used to record images of the metallic cups at intervals during testing. The shiny, smooth, un-

featured topography of the ceramic heads made imaging difficult and resulted in images of little use. However the metallic cup topography was imaged successfully, showing different mechanisms of wear, and highlighted the contrast between the matrix and carbides. The majority of images were taken using the 10x magnification lenses as higher magnification was difficult due to the curved nature of the samples. The microscope was used to look at both unworn and worn surfaces, including the edge contact area resulting from microseparation wear testing.

4.4.4 Hitachi SU-70 Field Emission Gun Scanning Electron Microscope (Berkshire, SL6 8YA)

Scanning electron microscopy (SEM) was used to investigate the topography of the metal cups, especially looking at the carbide structure and carbide removal. Imaging was carried out by the Experimental Officer for electron and FIB microscopy, Leon Bowen.

SEM's image the surface by scanning high energy beams of electrons in a raster scan pattern. The electrons interact with the atoms of the surface and can provide information about the surface topography and atomic nature of the surfaces. Images result from interaction of the electron beam with the atoms at or near the surface. The electron beam was thermionically emitted from the electron gun, usually fitted with a tungsten filament cathode. The electron beam was focused by condenser lenses to a spot which achieved a large depth of field. The beam passed through final lenses which allow deflection in the x and y direction. Two methods of detection used in this thesis were, secondary electron and back scattered electrons. In secondary electron mode, low energy electrons were ejected from the k-orbital of the specimens, which originated from within a few nanometres of the sample surfaces. The secondary electrons were detected by attracting them to an electrically biased grid, and then further accelerated towards the detector. The accelerated electrons caused emissions of light which were conducted to a photomultiplier and converted to a digital image. Backscattered electrons are high energy electrons which are reflected out of specimen by elastic scattering. Heavy elements (high atomic number) backscattered the electrons more strongly than light elements (low atomic number)

and therefore appeared brighter on the image. A requirement of the technique was that samples were conducting otherwise electrical charge can build up on the surface and distort the images. Samples are often coated in gold to achieve conductivity.

A Environmental Scanning Electron Microscopy (ESEM) was introduced in the late 1980's to overcome the problem of coating samples to achieve the imaging and resolution required. ESEM's allow samples to be observed in low pressure, gaseous environments therefore wet samples can be imaged. The sample was placed in a chamber with relatively high pressure compared with the vacuum required for the electron optical column. Positively charged ions help to neutralise the negative charge on the specimen surface. An ESEM was used to briefly look at the metal cups of the 38 mm alumina standard walking cycle tested samples. Imaging was difficult due to the curved nature of the cup.

Chapter 5

Materials and Methods

Material selection for medical devices is important for the success of the device. Criteria such as low wear, low friction, good biocompatibility and good corrosion resistance are all important factors when considering a suitable material for medical use.

The current study concentrated on ceramic on metal bearing combinations supplied by Biomet UK. The acetabular cups were as-cast cobalt chrome molybdenum (CoCrMo) alloy, whilst the ceramic heads were made from either pure alumina or an alumina matrix composite, zirconia toughened alumina (ZTA). The tests carried out are shown in Table 5.1.

Size (mm)	Head	Cup	Test	Lubricant	No. of cycles (million cycles)
38	Alumina	CoCrMo	Std	Bovine Serum	5
38	Alumina	CoCrMo	Mxs	Bovine Serum	5
38	ZTA	CoCrMo	Std	Bovine Serum	6
38	ZTA	CoCrMo	Mxs	Bovine Serum	5
60	ZTA	CoCrMo	Std	Bovine Serum	5
38	Alumina	CoCrMo	Std	$\leq 1\mu$m alumina particles	3
38	ZTA	CoCrMo	Std	$\leq 1\mu$m alumina particles	3

Table 5.1: *Wear Simulator tests carried out*

The standard ZTA 38 mm test was carried out to 6 million cycles to confirm the steady state wear rate.

The acetabular cups were made from identical as-cast CoCrMo material manufactured to different sizes. Each cup had 4 fins located on the reverse side which ensured correct re-location after each washing cycle. The bearing surfaces were highly polished however the posterior side had a roughened sand blasted finish. The cups had been removed from the manufacturing line before a porous coating was applied, as this coating would trap debris, increasing difficulties when using the gravimetric weighing method.

The properties of CoCrMo alloys are strongly related to the crystallographic structure [150]. The as-cast manufacturing technique resulted in hard carbides dispersed in a softer matrix. The carbides were clearly visible under low magnification techniques. The fine homogeneous grain structure resulted in enhanced mechanical properties, however the abrasive resistance is related to the carbon content, and therefore the percentage of carbides present. The hard ceramic carbides, protruded from the surface and were thought to protect the surrounding softer matrix from wear. CoCrMo was originally chosen because of the high corrosion resistance provided by the formation of a thin passivation film, which acted to protect the surface. The oxide layer consisted of both chromium and cobalt oxides, however it is predominantly Cr_2O_3, [151]. These passive oxide films greatly affect the chemical and mechanical stability of the implant. The disruption of the layer can quickly lead to corrosion, and quick re-passivation of a surface is required to protect the material surface. CoCrMo has been found to be susceptible to work hardening with the processes involved in manufacture resulting in the surface layers undergoing strain induced transformations. The ductility of as-cast CoCrMo used for implants is often low compared with other face centred cubic alloys due to low stacking fault energies resulting in restricted plastic deformation due to dislocation glide [150]. Vidal *et al.* [151] in 2008 presented a brief review of papers which have investigated the electrochemical properties of CoCr alloys under different conditions and showed that a consensus had not been reached as to whether the microstructure affected the corrosion resistance of the alloy. Studies looking at the effect of electrolyte compo-

sition on the corrosion resistance showed that proteins and other components may competitively adsorb on to the surface influencing the electrochemical behaviour of the alloy.

The ceramic femoral heads were composed of either alumina or zirconia toughened alumina (ZTA). The mechanical properties of ceramics are greatly influenced by the manufacturing techniques used. The first generation ceramics were found to fail catastrophically. However with improvements in manufacturing, such as hot isostatic pressing, the porosity and the mechanical integrity of the ceramics has improved considerably. Alumina is a dense polycrystalline ceramic composed of a metal, aluminum, and a non metal, oxygen, which is stable and chemically inert. Alumina has been successful as a material for biomedical applications due to the high hardness, low friction coefficient and good corrosion resistance. In addition it is highly wettable which provides optimal conditions for a lubricated joint [152]. The disadvantage of alumina is the high elastic modulus (approx 380 GPa) [114] resulting in a low fracture toughness and impact resistance which has led to catastrophic failure of the implant in a small number of cases due to the limited plastic deformation which occurs. Wear usually take place by grain fracture and removal.

Zirconia toughened alumina (ZTA) was introduced to improve the fracture resistance of monolithic alumina. ZTA consists of an alumina matrix with embedded stable or unstabilised zirconia particles. The addition of zirconia results in an increase in the flexural strength, fracture toughness and fatigue resistance through a diffusionless phase transformation. At the crack tip a stress-induced phase transformation occurs as the tetragonal phase zirconia transforms into the more stable monoclinic phase. This is accompanied by a volume increase (approx 4%) that results in compressive stresses around the tip of the crack, reducing the propagation through the matrix. In addition the microstructural coarsening caused by the zirconia particles may also increase the fracture toughness of the sample [153]. There is typically between 10% and 20% zirconia in the material. In addition to the increased strength, toughness, and wear resistance, corrosion resistance is found with high temperature stability.

An image was provided by Morgan Ceramics (Rugby, CV23 0WE) of the ZTA

head. This image is shown in Figure 5.1.

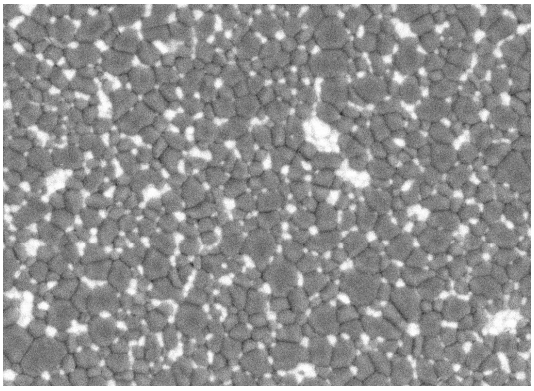

Figure 5.1: *SEM image of ZTA head (provided by Morgan Ceramics)*

The image clearly shows the ZrO_2 particles (white) distributed within the alumina matrix. The ZrO_2 were seen as individual particles or as larger clusters. Although the ZrO_2 particles were included to increase the fracture toughness of the material, it also introduces a weakness between the different structures which may result in easy removal of these particles from the matrix. This image should be kept in mind during AFM analysis of the ceramic.

5.1 Clearances

Heads and cups were matched to give radial clearances of approximately 100 μm. The heads and cups were measured using a co-ordinate measuring machine by Biomet UK, and supplied with the components. The initial components in this study were 38 mm in diameter (see Figure 5.2). Following this, 60 mm diameter joints were tested.

5.2 Lubricant

Ideally synovial fluid would be used as the lubricant for simulator testing in order to replicate the conditions found *in vivo*. However, this is difficult due to the quantities that would be required for testing and the difference in the properties of the fluid found between donors. In addition, there are questions to whether healthy fluid

	Std Test			MXS Test	
Station	38mm Alumina :CoCrMo μm	38mm ZTA :CoCrMo μm	60mm ZTA :CoCrMo μm	38mm Alumina :CoCrMo μm	38mm ZTA :CoCrMo μm
1	100	89	100	96	97
2	98	95	100	102	91
3	99	101	101	102	98
4	98	92	101	96	91
5	97	91	100	100	96
6	97	89	100	101	100

Table 5.2: *Radial clearances of the hip replacements used in this study.*

should be used, or lower viscosity fluid to replicate degenerated lubricant as would be found in an arthritic patient. As discussed in section 3.2.2, many different lubricants have been used in replacement joint research including bovine and human synovial fluid, silicone fluids of different viscosities, Ringer's solution with the addition of hyaluronic acid, and deionised water. An international standard (14242-1) [154] has now been published which dictates that the lubricant should have a "protein mass concentration of not less than 17g/l" [154]. Often bovine serum is used for testing, due to its comparable viscosity and protein content to synovial fluid.

The lubricants used within the current studies were newborn calf serum supplied by Harlan, (Harlan Sera-Lab Ltd., Leicestershire, LE12 9TE. Batches 6031201 and 9030203). The bovine serum was diluted with deionised water, resulting in a solution with a protein content of 18.75 g/l. In addition 8-10 pellets of NaOH, 20 mMol EDTA, and 0.2% w/v of Sodium Azide were added. Sodium hydroxide was required to create the correct pH to dissolve EDTA, which prevents calcium phosphate deposition. Sodium azide is used as a bacterial agent to retard bacterial growth in the lubricant.

5.2.1 Third Body Particle Lubricant

Third body particle tests were carried out on preworn 38 mm alumina:CoCrMo and ZTA:CoCrMo samples worn under standard walking cycle loading conditions. Alumina particles were added to the lubricant to investigate the effect that additional third body ceramic particles may have on the wear.

Preliminary testing was carried out to investigate whether the additional alumina particles in the lubricant would remain in suspension, or the majority would sink to the bottom of the gaiter. Various tests under both static conditions and a with a magnetic stirrer were carried out. Initially tests were undertaken using distilled water. Following this diluted bovine serum was used as the solution. Digital images were taken periodically throughout the test to observe the change in translucency of the solution. It was assumed that the greater the number of particles suspended in the solution, the more opaque the solution appeared.

As expected, many of the alumina particles sank to the bottom when the solution was static. When a magnetic stirrer was introduced a larger proportion of the particles remained suspended in solution, however significantly a large proportion of sample sank to the bottom. Therefore based on these results the particle test was carried out. As the motion in a hip simulator is more vigorous than a magnetic stirrer, it was hoped that the motion would cause more of the particles to stay suspended in the serum rather than sink to the bottom of the gaiter (see Figure 5.3)

Diluted bovine serum with the same additives as the standard test was used as the lubricant. In addition 0.5 g of <1 μm alumina particles were added to the solution. Of the 0.5 g, 0.25 g was placed directly into the cup with 3-4 drops of serum before assembly with the head. The remaining 0.25 g of powder was mixed with 500 ml of lubricant and the gaiter filled as usual. It was important that the lubricant was continuously stirred as it was poured into the gaiter in order that the vast majority of the particles entered the gaiter.

Particles were analysed using an environmental scanning electron microscope (ESEM), which found the majority of the particles to be less than 0.5 μm. An acceleration voltage of 15 kV was used with a spot size of 2.5/3. Samples were prepared by placing approximately 0.1 g of alumina powder into 20 ml of isopropanol

(a) Static for 18 hours ***(b) Stirring for 3 hours***

Figure 5.2: *18 hours of 0.5g of alumina powder in 400ml distilled water*

and the solution sonicated for approximately 30 minutes. A syringe was used to place 1 drop of solution onto a black carbon disk which was left to dry in air to evaporate the isopropanol.

ESEM revealed agglomerated particles (see Figure 5.4) even though the solution had been sonicated. The individual particles, which were $\leq$500 nm in diameter and round in nature, agglomerated into larger particles in the tens of microns range. The alumina powder added to the lubricant for the wear testing was not sonicated, therefore it is thought that the particles may have agglomerated in the lubricant.

5.3 Component Assembly

Polymethylmethacrylate (PMMA) tapers were designed to hold the ceramic heads in the correct position in the assembly. The design, which was first described by Vasilliou *et al.* [155] used a threaded stainless steel taper, coated in a thin shell of PMMA. A slight modification was made to include both horizontal and vertical slots

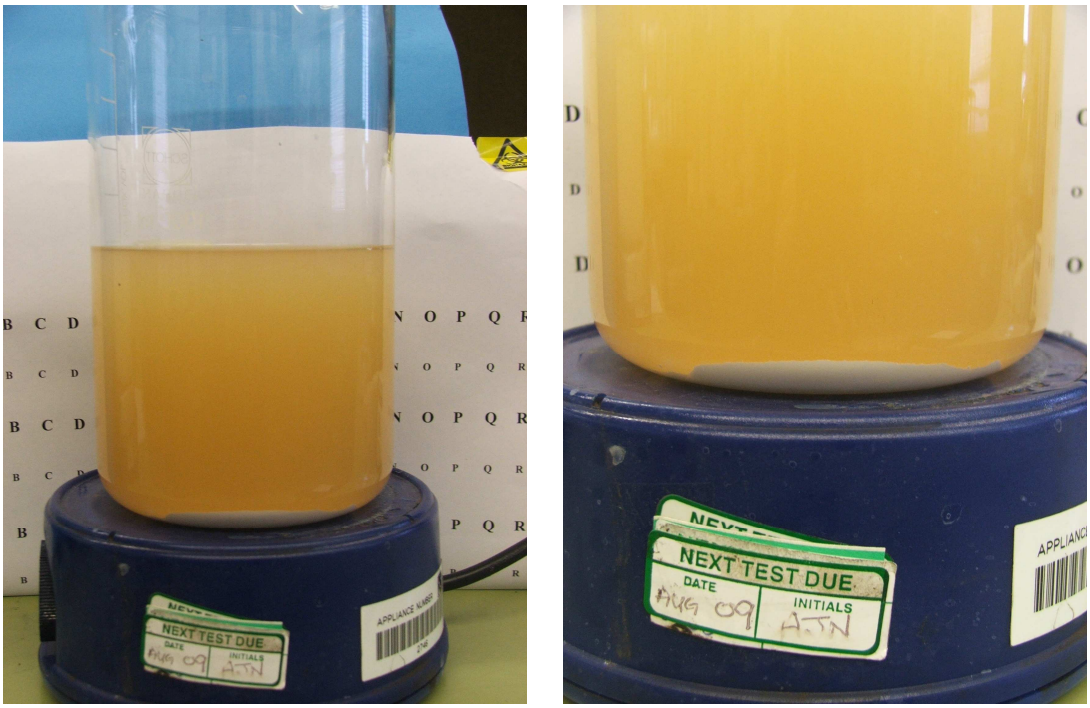

(a) Static ***(b) Stirring***

Figure 5.3: *0.5g of alumina powder in bovine serum stirring for 19 hours.*

in the stainless steel taper to prevent movement of the PMMA coat on the central metal shaft (see Figure 5.5(a)). This design took advantages of the difference in thermal coefficient of expansion of the PMMA and ceramic heads, allowing easy removal of the head for cleaning and weighing. Additionally a hole was drilled and tapped through the stem to aid component disassembly.

The cups were mounted in UHMWPE holders made in the School of Engineering Mechanical Workshop (see Figure 5.7). UHMWPE was chosen for the cup holders as it was the closest practical material to mimic the mechanical properties of bone. The holders were designed so that the cup was positioned at 33^o to the horizontal to mimic the *in vivo* positioning as the acetabulum is positioned at 45^o and the load line for the femoral head at 12^o to the vertical, resulting in a net angle of 33^o. Stainless steel clamping rings were used for the majority of tests to hold the cup firmly in place so that motion of the cup in the holder was limited (see Figure 5.7(b)).The clamping ring was modified to use UHMWPE for the 60 mm heads to avoid metal transfer from the clamping ring as the larger diameter joint increased the chances

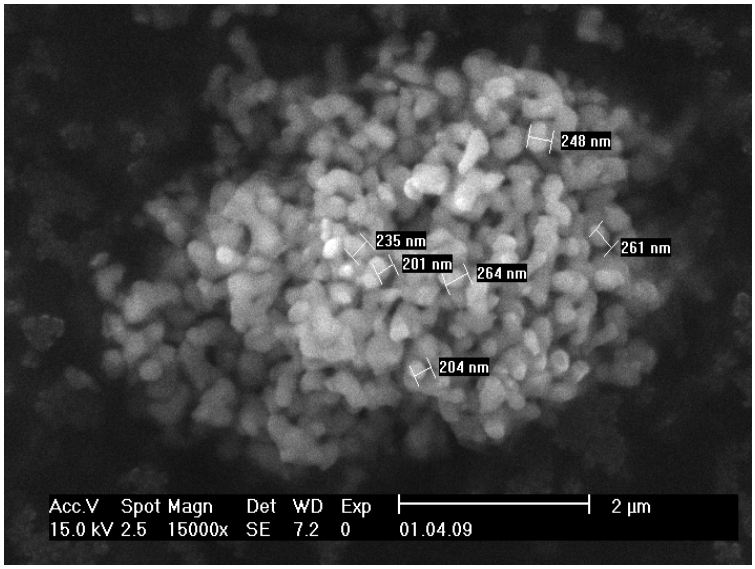

(a)

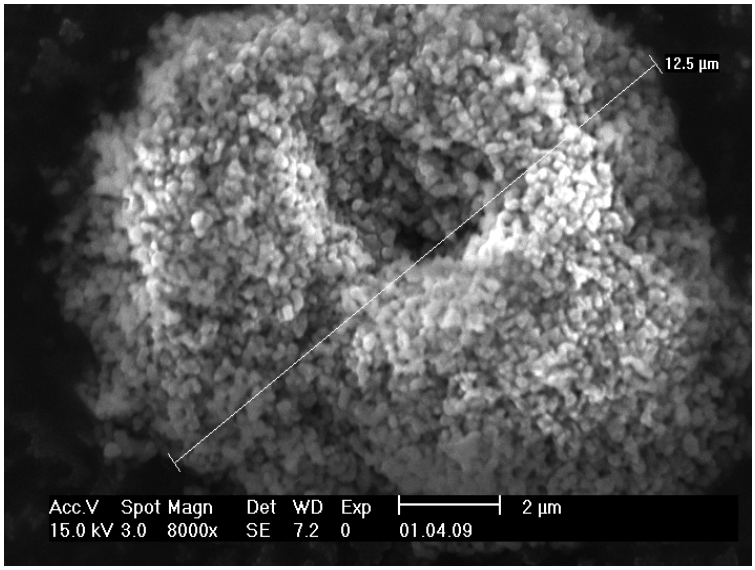

(b)

Figure 5.4: *ESEM images of alumina powder.*

of material transfer due to the limited space in the simulator. The fins on the back of the metallic cups ensured exact positioning of the cups after removal from the holders. Markings on the head were used to ensure exact re-positioning of the head after removal. Positioning of the components was important to align the wear patches on the bearing surfaces after gravimetric or surface analysis. Figures 5.6 and 5.7 show the component and set-up used.

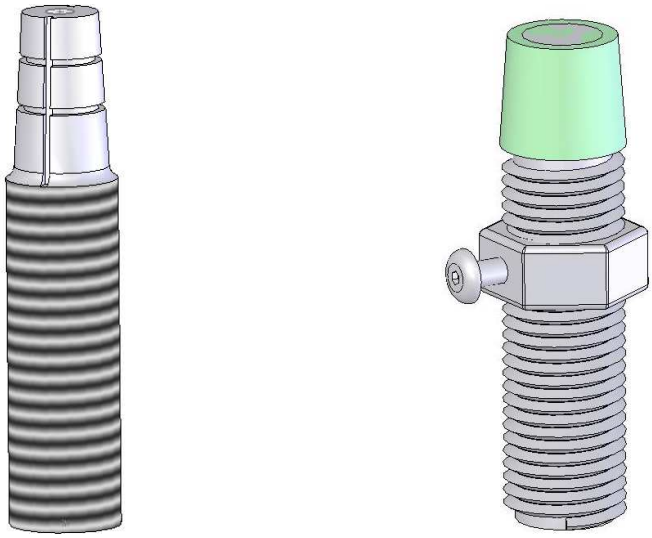

(a) Metal Taper *(b) PMMA coated Metal Taper, with locking nut*

Figure 5.5: *Head tapers for wear simulation*

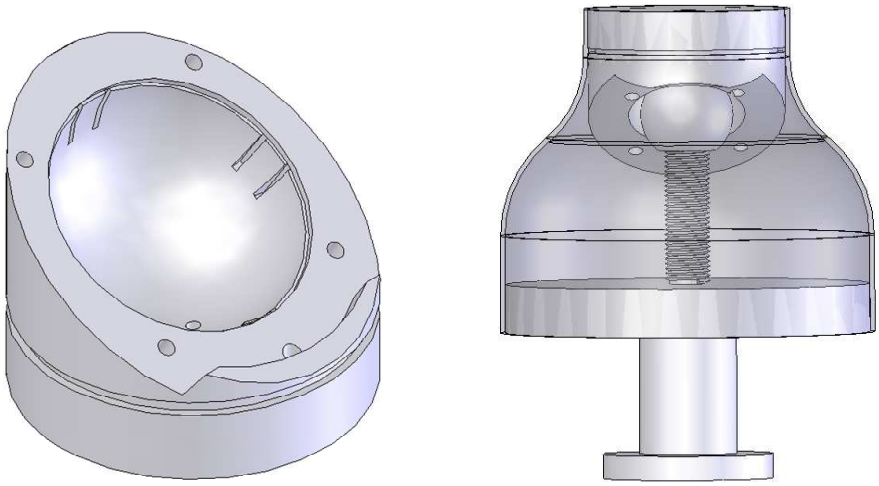

(a) UHMWPE cup holder *(b) Head, Cup and Gaiter arrangement*

Figure 5.6: *Cup holder and gaiter arrangement*

A silicone elastomeric gaiter was used to form the lubricant bath, containing approximately 500 ml of fluid. The gaiter was clamped onto the head base using metal clips, and onto the cup holder using two o-rings. A tube was used, connecting the cup holder to the head base, which allowed removal of trapped air within the gaiter using an in-line needle free release valve. The design of the tubes and gaiter

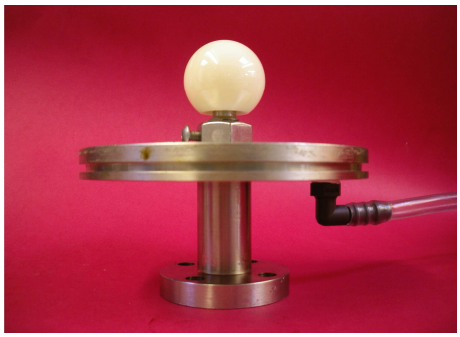

(a) Head base

(b) UHWMPE cup holder with clamping ring

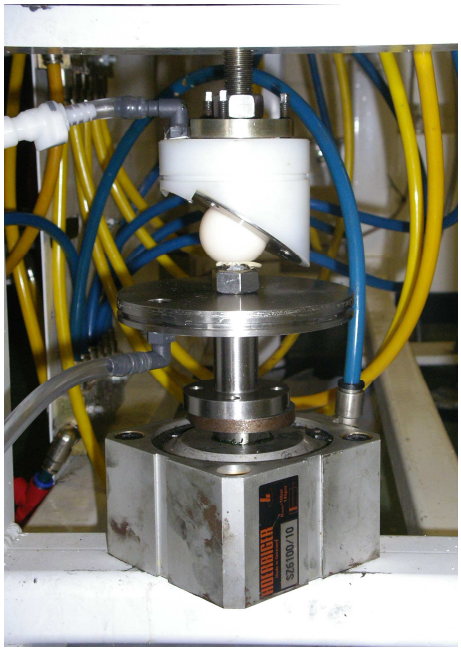

(c) Head and cup simulator set-up without gaiter

Figure 5.7: *Photographs of the head, cup and simulator set-up*

system was modified for the 60 mm and 38 mm ZTA MXS test, where bottles were incorporated into the system to provide a space for the air which forms within the

gaiter to escape from the bearing surface, see Figure 5.8.

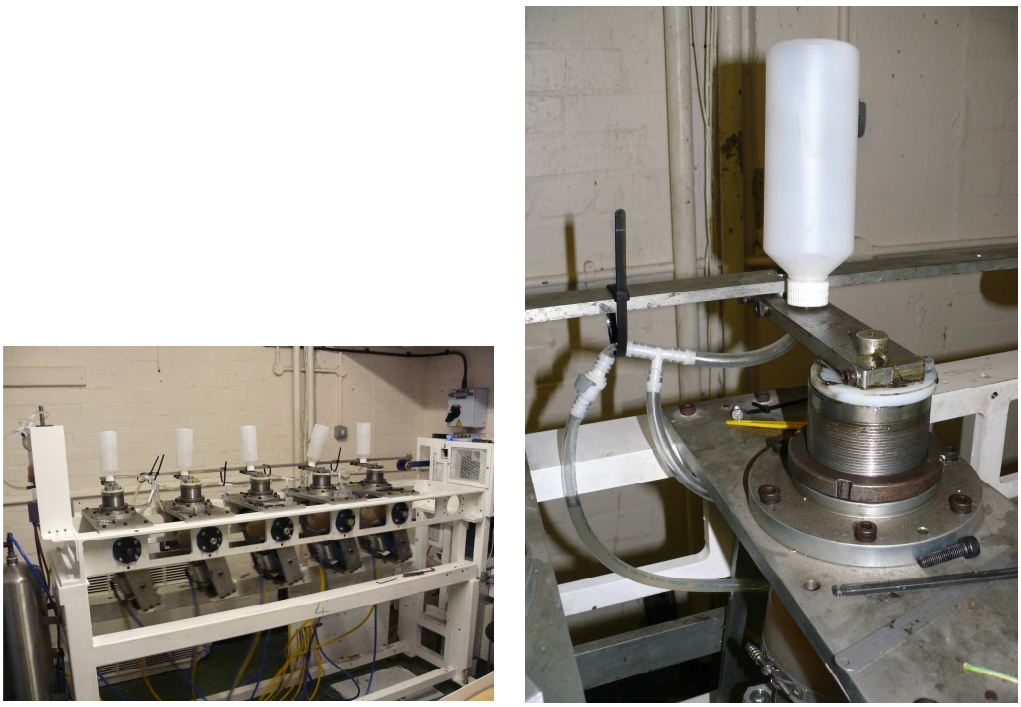

(a) *(b)*

(c)

Figure 5.8: *Bottle configuration on the wear simulators, to provide space for air to escape, and reduce the possibility of dry contact.*

5.4 Cleaning Protocol

Joints were cleaned, dried and weighed every 0.5 million cycles. The cleaning protocol was similar to the ISO standard (ISO14242-2, 2000 [90]) and is shown in Appendix A.

The protocol briefly consisted of cleaning the bearings in deionised water in an ultrasonic cleaning bath for 10 minutes. Following this the components were cleaned for 10 minutes in a solution of deionised water and approximately 2% neutracon (decon laboratories,East Sussex, BN3 3LY) to remove grease, followed by 10 minutes in deionised water. After this the components were sonicated for a further 3 minutes in deionised water. During cleaning, lint free paper and a small soft 'baby' brush were used to remove adsorbed protein from the bearing surfaces (lint free paper) and the roughened back surface of the metallic cups (baby brush), so that the weight change was accurately recorded. The joints were dried using a vacuum oven at approx 37^o and allowed to acclimatise next to the balance for 30 minutes prior to weighing. Initially components were weighed sequentially until three consecutive masses within ± 0.1 mg were recorded. This accuracy could be achieved for the 38mm components, however this was difficult with the 60mm components which fluctuated in mass to a greater extent. For these components 6 masses were recorded and an average calculated.

5.4.1 Control Components

Control components are used to take account of fluid absoprtion, especially for polymers, and take account of the volume changes occurring during the washing, weighing and drying process. Loaded controls go into the simulator however experience loading only and no motion. These components experience the same conditions as the active stations such as simulator assembly and disassembly, washing, drying, weighing. Soak controls are used to investigate whether the washing, drying and weighing process has an effect on the volume change of the components. The components remains in a serum bath at 37 degrees for the duration of the test and are only removed to be washed and dried and weighed with the active stations. In

addition an environmental control can be used which remains next to the balance and is not placed in serum and does not go through the washing protocol. It is used to determine changes in mass due to differences in balance readings over time. Table 5.3 shows the controls used for each test. The third body tests used the same components and controls as the standard 38 mm tests.

Test	Std Test			MXS Test	
Component Size	38 mm	38 mm	60 mm	38 mm	38mm
Head Material	Alumina	ZTA	ZTA	Alumina	ZTA
Controls	Load	Load	Load	Load	Load
			Soak		Soak
			Environmental		

Table 5.3: *Control components used for each test.*

5.5 Wear Detection Techniques

5.5.1 Gravimetric method

Gravimetric analysis was used to determine how much wear volume had been removed during the wear simulations. This involved removing the samples from the simulator every 0.5 million cycles, followed by, washing, drying and weighing the components (to the protocol shown the appendix A) to detect changes in mass. The components were weighed on Mettler Toledo (Mettler-Toledo Ltd., Leicester, LE4 1AW) balances (38 mm components: AX205, max 220 g, and the 60 mm components: XP504, max-520 g) until three consecutive readings to 0.1 mg were achieved. If this could not be determined, as with the 60 mm components, an average of 6 consecutive readings was used. The readability and repeatability of balance AX205 was 0.01 mg and 0.03 mg respectively. The readability and repeatability of balance XP504 was 0.1 mg and 0.04 mg respectively. In addition a loaded soak control was used to take account of fluid absorption and any environmental changes which had an effect on the mass of the components during the washing/drying process. The

true mass change of the components was obtained by subtracting the mass change of the soak control at every weighing interval. An environmental control was also used for the 60 mm ZTA components which remained next to the weighing balance to ensure that any recorded mass changes were genuine wear changes, not fluctuations due to the scales. The volume change was calculated using the density of the material (Alumina=3.980 g/cm^3, ZTA= 4.269 g/cm^3 CoCrMo=8.287 g/cm^3) and a volume change versus number of cycles graph was plotted. Wear rates were determined using linear regression analysis (Microsoft Excel). Each station was treated as an individual data set and a regression equation calculated. This equation (in the form y = mx + c) was then used to normalise each station individually by calculating a specific value y value for each data set by setting x to be the median number of cycles for the wear period being calculated (for example, steady state wear for 2-5 million cycles x would be set to 1.5). The y value then subtracted from each data point in the specific data set to obtain a normalised set of data for each station. The individually normalised data sets were then combined and one regression equation calculated with an associated 95% confidence interval. The coefficient of x gave an average wear rate for all stations.

5.5.2 Deposit Visualisation

During wear testing, a cream/white solid was deposited onto the surface of both the heads and cups. This was found after each 0.5 million cycle testing period. The deposit was visualised at each weighing stage to monitor changes in deposit position. The deposit could be visualised by dipping the head or cup into a non permanent ink solution and rinsing the component with water. This allowed digital images to be taken and comparisons of the location of the deposition between different test conditions. The position revealed the contact area on the components and was helpful in locating wear areas on the heads tested under microseparation conditions. After freezing the components for 30-60 minutes the components were imaged as the resulting condensation dulled the shiny surfaces resulting in more useful images.

Attempts were made to determine the composition of the white deposit. Samples were taken from the surfaces of the components and chromatography was used,

comparing the sample with bovine serum albumin. However too larger quantities of the components were used and the results merged providing no useful information. In addition attempts were made dissolve the deposit in different solvents so that mass spectroscopy could be used to determine the composition, however the sample did not readily form a solution in the solvents used and therefore further investigation was not undertaken.

5.6 Friction

Friction experiments were carried out using a range of viscosities of both bovine serum based fluids and sodium carboxy methyl cellulose (CMC) based fluids. The data was then used to determine Stribeck Curves which plot friction factor versus Sommerfeld Number. The lubricants ranged in viscosity from 0.001 Pa s to 1.0 Pa s and were measured on a Ferranti-Shirley cone-on-plate viscometer MK3 (Manchester, M10 0BE) at a shear rate of 3000 s^{-1}. Even though the physiological shear rate is much greater than this, 3000 s^{-1} was used as the majority of data for natural synovial fluid is measured at this rate, therefore similar result to physiological fluid were obtained. A combination of the friction factors and the shape of the curve provided an indication of which lubrication regime the components were operating under.

The femoral head was mounted on a PMMA coated stainless steel taper (see Figure 5.9), and fastened into the head plate using a screw. Depending on the holder used, copper and stainless steel washers or a threaded stem were used to ensure that the head height was set so that the centre of the head aligned with the centre of rotation of the simulator. The cup was mounted in an UHMWPE holder at 33^o to the horizontal and set with a clearance between the head and cup of approximately 2 mm using a jig made in house. The rotation of the head and cup were set so that the wear patch in the wear simulator matched the wear patch in the friction simulator.

Calibration of the friction involved three parameters, namely the load, the frictional torque and the angle. Calibration was carried out using the 'setup.dat' file

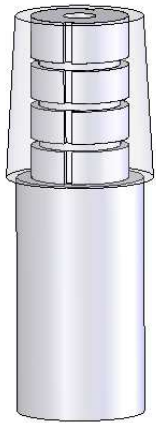

Figure 5.9: *PMMA coated head stem used for friction testing*

which enabled the load, frictional torque and angle to be taken through the full range of values, with the known and recorded values logged. As a result, three curves were plotted, and the equations used to calculate various calibration coefficients which were inputted to the correct calibration files on the PC. For example, the angle calibration relates the encoder position with the head angle resulting in a graph of $\pm\ 20^0$ through 128 encoder positions. The equation of the curve results in 4 calibration coefficients which are then used to calculate the step constant, maximum speed and angle offset. Calibration was carried out periodically.

During testing the head position was fixed, however the flexion/extension motion of the carriage containing the cup free allowing self alignment of the components. Approximately 5 ml of lubricant was placed between the components during testing.

Preliminary testing was carried out to determine the effects of friction (if any) of cleaning with solutions of Neutracon (Decon Laboratories, Sussex BN3 3LY), Gigasept (Schülke and Mayr Uk Ltd., S9 1AT) and Isopropanol between friction runs. The results showed no significant effect on the friction results (Figure 5.10), for the majority of viscosities therefore a cleaning protocol of a weak solution of Neutracon was chosen followed by rinsing with isporopanol. The results of the isoproanol test at the highest viscosity are slightly different to the Neutracon and Gigasept however at such low friction factors, the difference is negligible.

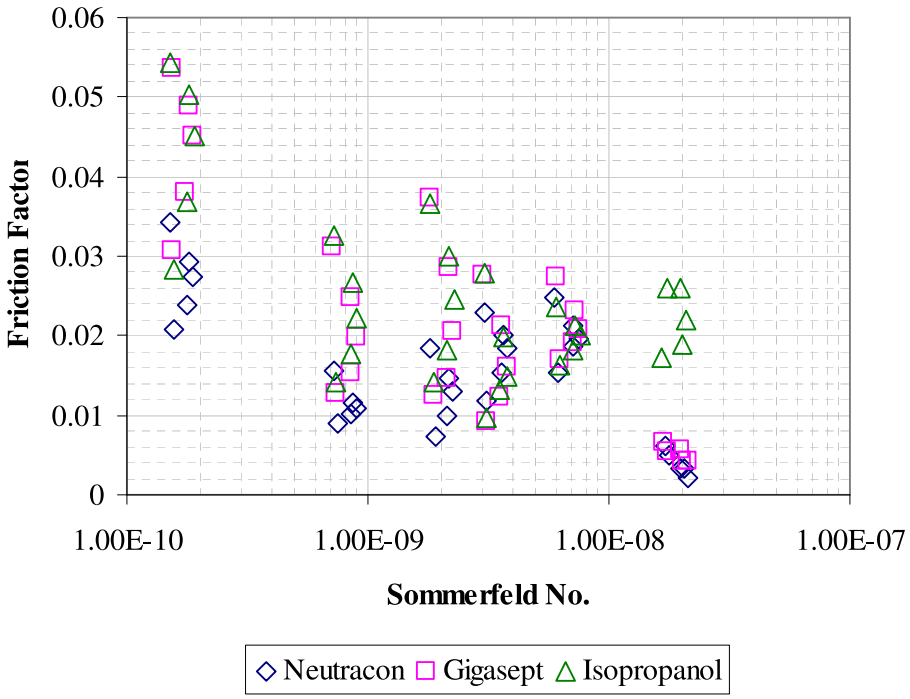

Figure 5.10: *28mm ceramic on ceramic washing protocol investigation (Bovine serum was used as the lubricant)*

5.7 Surface Topography Analysis

Identical cup holders to that used in the simulator were used to record surface topography data from the cups. This positioned the cup at 33 ^{o} to the horizontal with the lens vertically positioned above it. For each cup 10 data points were taken randomly in the wear patch and averages calculated. Measurements for the head were taken on the pole for the standard walking cycle testing, and additionally in metal transfer and at approximately 33^o to the horizontal for the microseparation testing. Again 10 points were taken at each location and average data calculated. At various stages throughout testing, unworn parts of both the head and cup were recorded to ensure that the topography was unchanged compared with the initial results.

AFM images were taken on the heads periodically throughout testing. Heads were cleaned before imaging and often wiped with ethanol or isopropanol and air dusters were also used to remove any loose dust from the surface. For the large diameter heads (60 mm) adjustments had to be made to the head stand which

increased the height between the base and the AFM head and changed the AFM head stand shape from a rectangular to a 2 piece arrangement, to allow the head to fit in the microscope (see Figure 5.11). It was important to ensure that the stand was secure and the sample stable to avoid problems due to sample drifting.

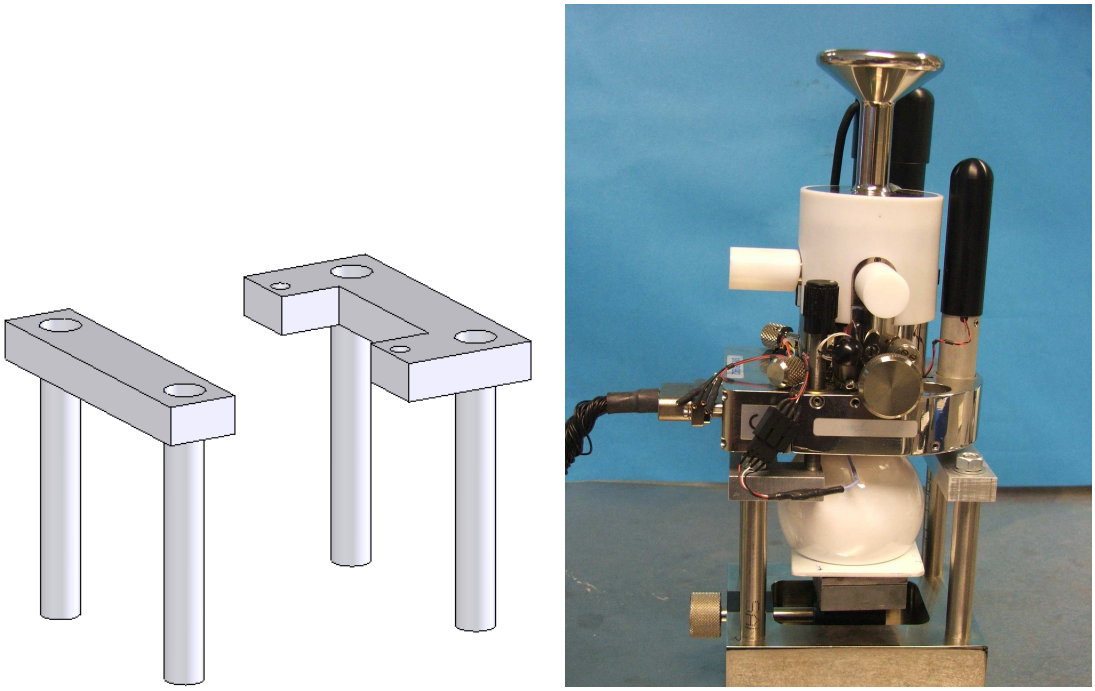

(a) *(b)*

Figure 5.11: *Modified AFM setup which included a taller two-piece arrangement for the top plate which allowed the head to fit in the microscope*

Difficulties were found throughout the work due to thermal drifting of the probe, which resulted in 'smudging' of the image and an inaccurate representation of the surface. Although this was not overcome, the effects were reduced by wiping the surface repeatedly with alcohol and by increasing the scan rate, which reduced the chances of drifting between individual line scans.

Optical microscopy images were taken in the wear patch of the cups for both the standard and microseparation testing. In addition images were taken in the region of edge contact on the head and lip formation on the cups during microseparation testing which allowed a more thorough investigation of the effect of medial lateral displacement. For this a small jig was made to allow the cups to be positioned at required angles for the images to be taken. As with the non contacting interferometry

work, regular images were also taken in the unworn areas of the cup to ensure they remained similar to that of the initial surfaces.

In addition the edge contact lip was measured using a micrometre to monitor the dimensions of the lip as it evolved during testing. The width and breadth were recorded periodically throughout testing.

Chapter 6

Results - Standard 38 mm Alumina

A set of six, 38 mm diameter alumina femoral heads were paired with as-cast CoCrMo acetabular cups, an example of which is shown in Figure 6.1. The components were paired to give radial clearances close to 100 μm. The pairings are shown in Table 6.1.

Figure 6.1: *38mm alumina head and as-cast CoCrMo alloy cup*

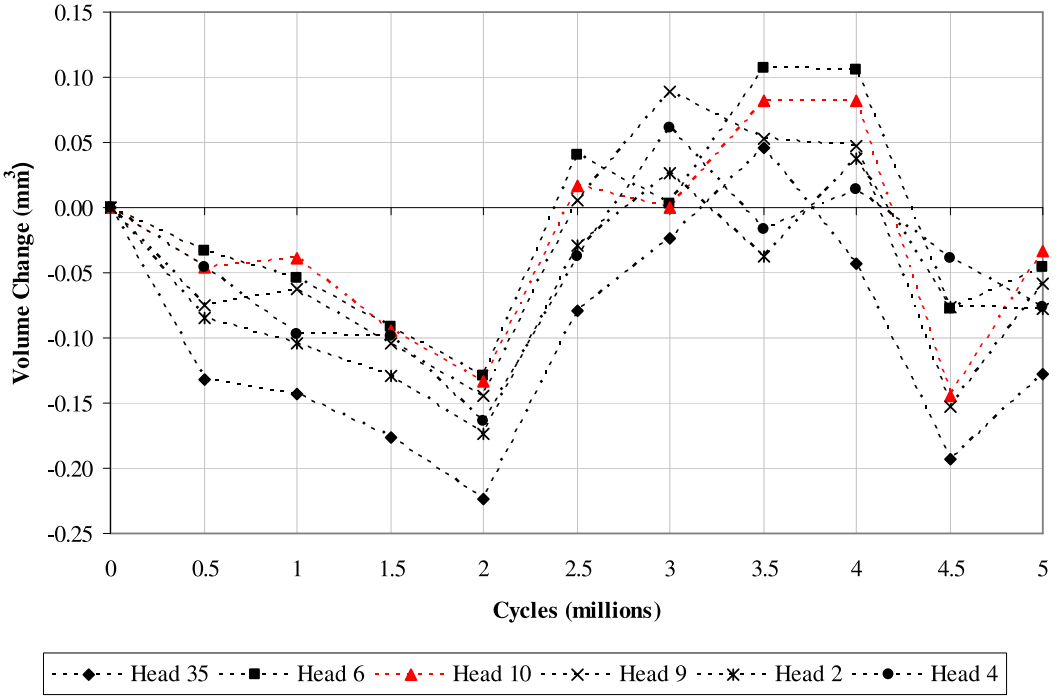

Figure 6.2: *Volume change of 38 mm alumina femoral heads under standard wear conditions (Control = head 10).*

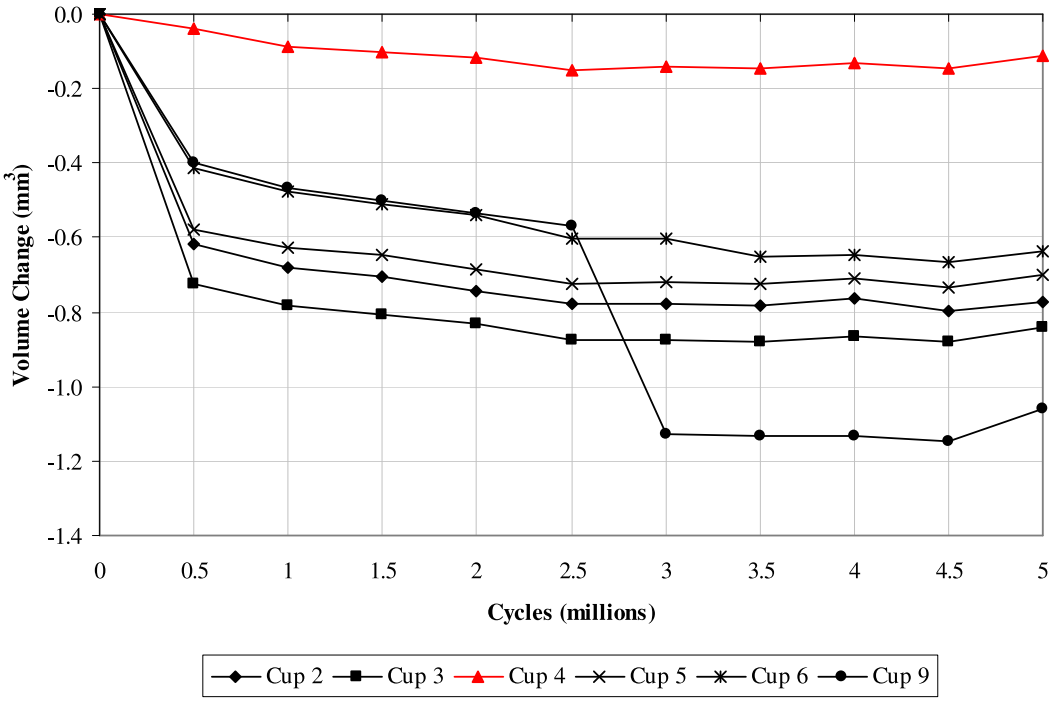

Figure 6.3: *Volume change of 38 mm as-cast CoCrMo acetabular cups (from alumina test) under standard wear conditions (Control = cup 4).*

Station	Head	Dimension (mm)	Cup	Dimension (mm)	Radial Clearance (μm)
1	4	18.970	9	19.070	100
2	2	18.968	6	19.066	98
3	9	18.969	5	19.067	98
4	35	18.970	2	19.067	97
5	6	18.968	3	19.064	96
Control	10	18.963	4	19.061	98

Table 6.1: *38 mm alumina against CoCrMo pairings and radial clearances for the standard wear test.*

6.1 Standard Wear Testing

The test included 5 active stations which experienced both loading and motion. The loaded control underwent loading only, which in this test was cup4/head 10. Figures 6.2 and 6.3 show the volume change versus the number of cycles.

Low wear was found for all heads and cups. As can be seen from Figure 6.2 the volume change of the ceramic heads fluctuated around zero for the entire 5 million cycles. The results of the loaded control, were found to be similar to the 5 active stations, therefore it was concluded that the volume change of the heads was due to external factors during the weighing process and not attributed to the wear of the components during *in vitro* simulation. In order to compensate for this, the volume change of the control component was subtracted from the volume change of the active components for each 0.5 million cycle interval, resulting in the 'true' wear of the components. The adjusted results are shown in Figure 6.4.

In contrast to the alumina heads, the metallic cups showed a significant change in volume, especially during the first 0.5 million cycles, known as the running in wear. Following this a lower wear rate was found between 0.5 and 5 million cycles. The number of cycles considered to be running in and steady state wear are determined by looking at the graph and deciding at which point it appears that the wear of the components is generally constant. This can be difficult if not all of the components

appear to have reached a steady state after the same number of cycles. In this case it is generally decided to measure steady state wear from the number of cycles after which all cups have reached a steady wear rate although more than one wear rate can be calculated if clear differences are found between components. Running in is a period of higher wear as the components 'bed in' and the machining or polishing marks are worn, after which the surfaces become smoother. For smooth surfaces such as ceramics, running in wear is difficult to distinguish and therefore one wear rate is often calculated. For materials such as metals and polymers, running in is more prevalent as the larger asperities are worn in the first few thousand or million cycles before the wear rate decreases to a steady state.

As expected the control cup showed considerably lower volume change (control = cup 4) compared with the active stations therefore it had little effect when subtracted to achieve 'true' wear. The large volume drop experienced by cup 9 between 2.5 and 3 million cycles was thought to be due to trapped air at the top of the gaiter causing an area with no lubricant between the bearing surfaces. It is worth noting that the station returned to the original low wear rate (seen between 0.5 and 2.5 million cycles) after 3 million cycles and followed the same trend as the remaining 4 active stations. The adjusted data is shown in Figure 6.4 which highlights the difference in magnitude of volume change between the heads and cups.

After adjusting the results to take account of the volume change of the control components, the alumina heads were found show little detectable wear using the current gravimetric method. The cups experienced a higher wear rate running in period between 0 and 0.5 million cycles, which decreased to a lower steady state wear rate for the remainder of the test. Due to the undetectable wear for the head, wear rates were calculated for the metallic cups only. Individual running in and steady state wear rates for each station (presented in table 6.2) and average wear rates were calculated.

Running in wear was calculated between 0-0.5 million cycles and steady state wear calculated between 0.5-5 million cycles. The large loss of volume between 2.5-3.0 million cycles was removed for the wear rate calculation.

Considerable variation in wear rates were seen between the components,with cup

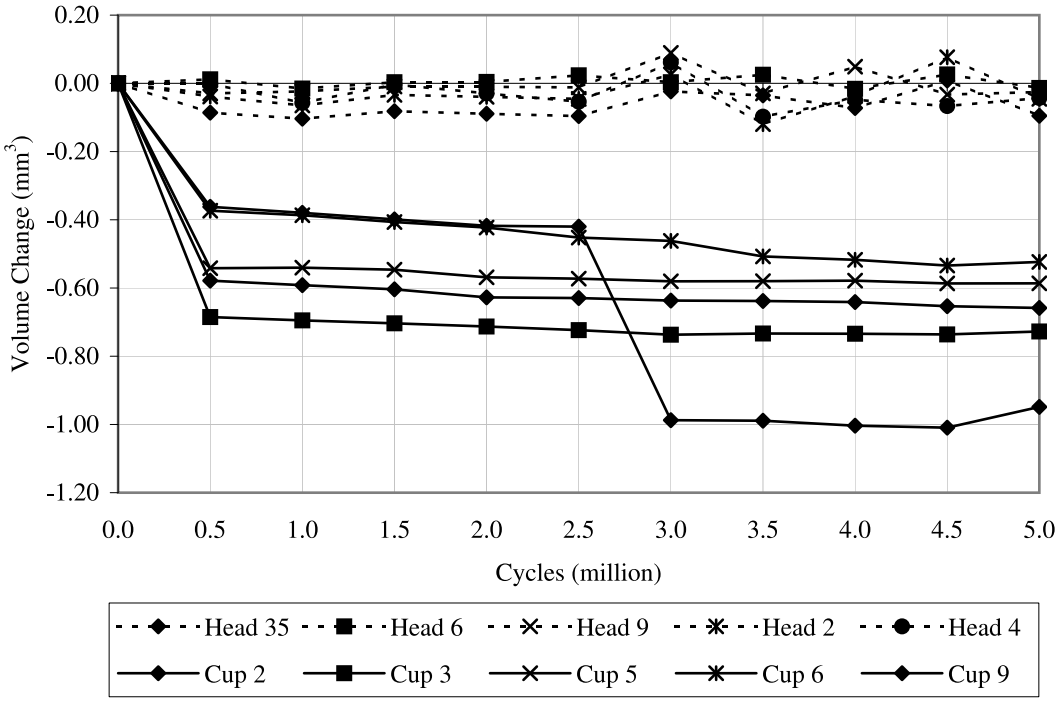

Figure 6.4: *Volume change of 38 mm alumina:CoCrMo under standard wear conditions (adjusted using the loaded soak control).*

Cup	Running in wear rate (mm^3/million cycles)	Steady state wear rate (mm^3/million cycles)
2	1.1866	0.0166
3	1.4054	0.0112
5	1.1118	0.0116
6	0.7659	0.0395
9	0.7425	0.0316

Table 6.2: *Individual wear rates for 38 mm CoCrMo cup under standard wear conditions(alumina test).*

3 showing a wear rate nearly twice that of cup 9. The adjusted data was used to calculate a wear rate using linear regression analysis. The average running in and steady state wear rates were 1.04 ± 0.293 mm^3/million cycles (mean ±95% C.I.) and 0.021 ±0.004 mm^3/million cycles respectively.

6.2 Friction testing

Friction tests were carried out on a new 'unworn' sample and the samples run to 5 million cycles in a standard wear simulator. The results are presented in the form of a Stribeck Plot which indicates the lubrication regime within which the joints are operating.

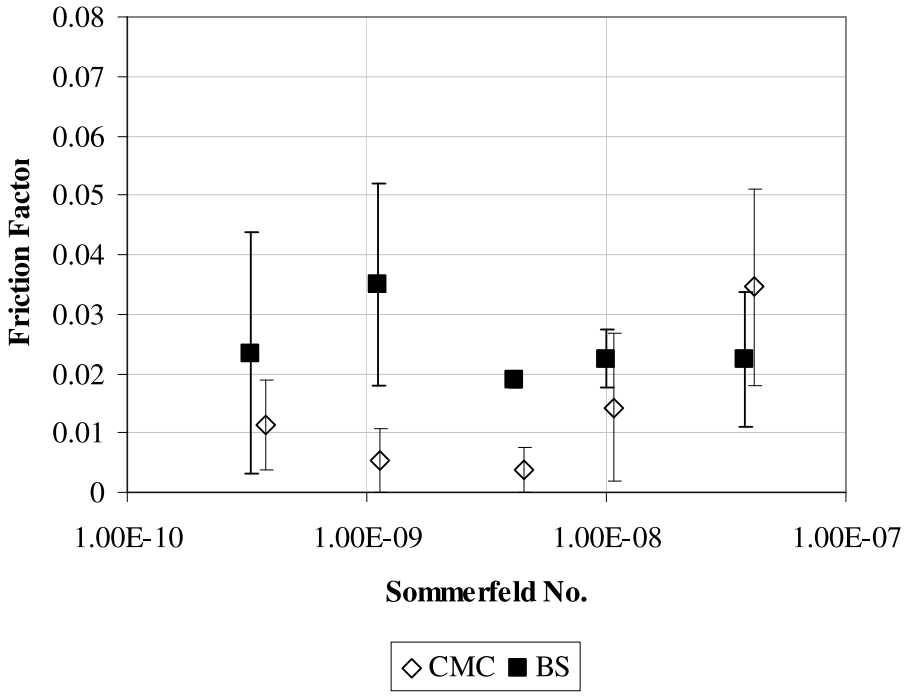

Figure 6.5: *Stribeck plot of unworn 38mm alumina: CoCrMo tested with water based and bovine serum based CMC lubricants.*

Figures 6.5 and 6.6 show the results of the unworn and worn samples which show similar results. Tests were carried out using different viscosities of water based and bovine serum based lubricants. The majority of the mean friction factors were below 0.05.

The unworn sample when tested with water based lubricants resulted in friction factors which gave a curve typical of full fluid film lubrication with a minimum friction factor of 0.004 at a corresponding Sommerfeld No. of $4.57\text{x}10^{-9}$. Results either side of this Sommerfeld number showed higher friction factors, with a maximum mean friction factor of 0.035 corresponding to the highest viscosity of fluid. The bovine serum based lubricants showed similar friction factors for all Sommerfeld

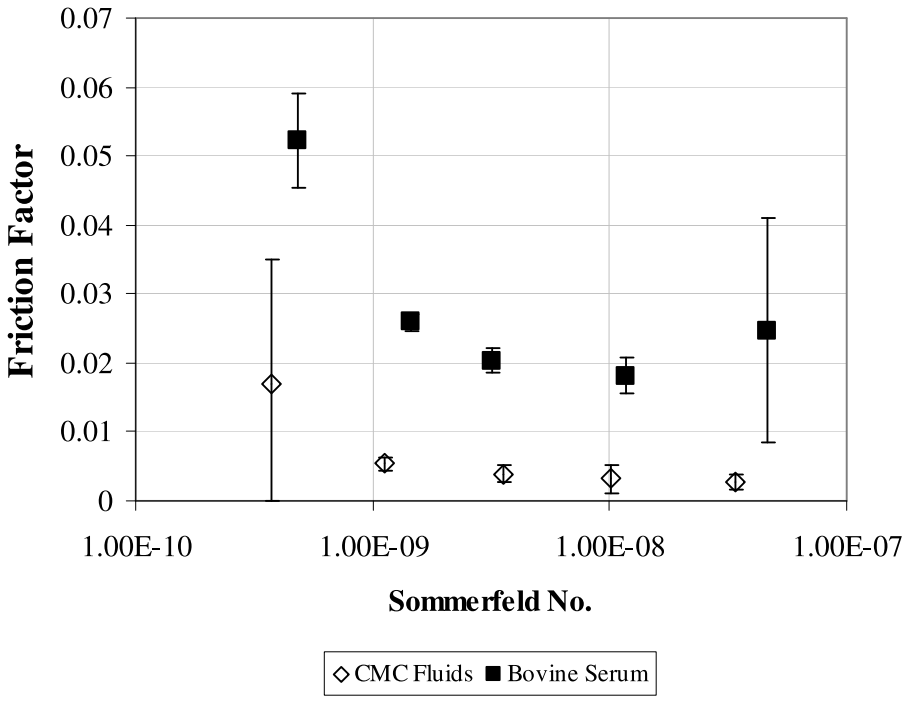

Figure 6.6: *Stribeck plot of 38mm alumina against CoCrMo worn to 5 million cycles in a standard wear simulator tested under water based and bovine serum based CMC fluids.*

numbers the majority of which were higher than the water based lubricants with the exception of the highest Sommerfeld number. The results for the highest viscosity of water based and bovine serum based lubricants were similar with overlapping standard deviation error bars. The low friction factors and shape of the curve suggest that the joints were operating close to full fluid film lubrication.

The worn data shows a similar result producing a curve typical of a bearing which is working in full fluid film lubrication. A decreasing friction factor was seen for the bovine serum based lubricants as the Sommerfeld number increased, to a minimum at a Sommerfeld number of $1.02E^{-8}$, after which the friction factor increased. The highest friction factor (0.052) was found for the lowest viscosity which was 25% bovine serum. The water based CMC fluids showed distinctly lower friction factors at all Sommerfeld numbers compared with the water based lubricants.

Theoretical lubrication calculations were carried out and compared with the experimental data. Root mean squared roughness values taken at various stages throughout testing were used to calculate the minimum film thickness and corre-

Cycles (millions)	Head Rms (μm)	Cup Rms (μm)	H min (μm)	λ	Friction factors CMC*/BS**
0	0.010	0.016	0.07	>3	-
2	0.013	0.017	0.07	>3	-
3	0.009	0.017	0.07	>3	-
5	0.009	0.017	0.07	>3	0.017/0.052

* CMC η=0.001 Pa s^{-1}, **BS η=0.0013 Pa s^{-1}

Table 6.3: *Theoretical minimum film thickness and lambda values for 38mm alumina against CoCrMo*

sponding lambda values. The results are presented in Table 6.3.

The calculations showed that the effective surface roughnesses initially and after 2, 3 and 5 million cycles indicated that the joints were operating within full fluid film lubrication with lambda value >3.

6.3 Surface Analysis

6.3.1 Zygo NewView 100 non contacting interferometry

Wear testing in a standard simulator produced very little change of the surface roughnesses or surface topography or the heads of cups. Non contacting interferometry results were recorded initially, after 2, 3 and 5 million cycles of wear.

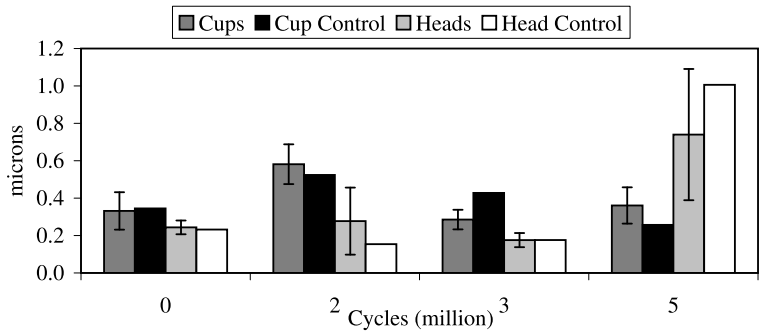

(a) RMS roughness

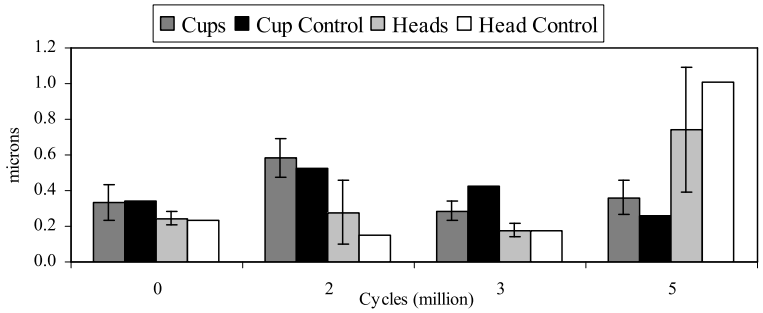

(b) Peak to valley heights

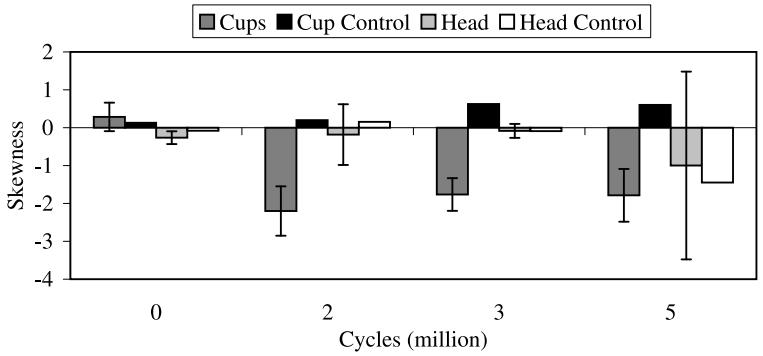

(c) Skewness

Figure 6.7: *Surface topography from the 38 mm alumina heads under standard wear simulator conditions*

The mean rms roughness of the metallic cups decreased between 0 and 2 million cycles (0.23 to 0.17 μm) after which it remained constant. The carbides which were visible under a microscope, at the initial analysis, became less visible as testing progressed as they were worn smooth, fractured or pulled out of the surface. The head rms roughness remained similar throughout testing with the control head staying similar to the active stations.

The peak to valley (pv) heights were recorded for both the head and cup at the same intervals as the roughness. It should be noted that the results should be interpreted with care as one large individual value can significantly bias the mean result giving misleading data. The pv heights of the metallic cup increased slightly between 0 and 2 million cycles which may be as a result of abrasive scratches or carbide removal which results in deeper valleys, thus increasing the pv value. Analysis of the cups after 3 and 5 million cycles showed a mean pv value which was lower compared with 2 million cycles, possibly due to wear of the softer matrix material which surrounded the carbides, and was originally protected by the harder protruding carbides. The pv value of the ceramic heads remained constant until 5 million cycles (from 0.18 $\pm$0.04 μm at 3 million cycles to 0.74 $\pm$0.4 μm at 5 million cycles) where an increase was found. This may have been due to grain removal shown in images in section 6.3.3.

As with the pv height, the skewness can easily be biased by one large hole or peak on the surface and therefore the results must be treated with caution. The skewness value of the unworn surfaces was positive, as a result of the carbides protruding from the surface. However as the test progressed, the carbides were worn smooth, or pulled out which with the addition of abrasive scratching resulted in a negative skewness value as the test progressed. As was expected, the control cup remained positively skewed as the carbides were not altered and the surface unscratched. The head skewness fluctuated around zero up to 3 million cycles, after which a negative skewness was observed. This again may be due to grain removal seen after 5 million cycles of wear.

Figure 6.8 shows the change in surface topography of the CoCrMo cups as the wear testing progressed. Initially the carbides projecting from the surface (Fig-

ure 6.8(a)), however as the test progressed the carbides appeared flattened or sunken within the matrix as if they were worn smooth or pulled out (Figure 6.8(b)). Abrasive scratches were noticeable after wear however it was difficult to draw conclusions regarding the size or number of scratches due to the heterogeneous nature of the wear patch of each cup. As the images are presented on the same scale it is clear that the general undulating nature of the surface decreases as the wear test progressed and the surface was polished.

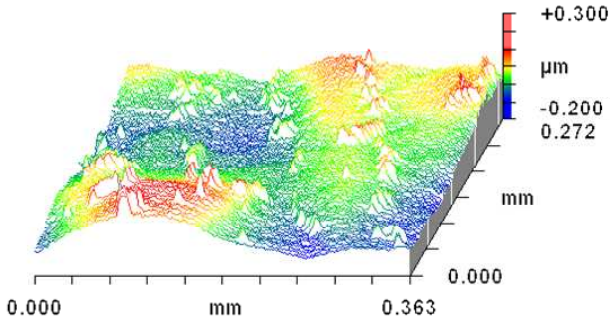

(a) unworn

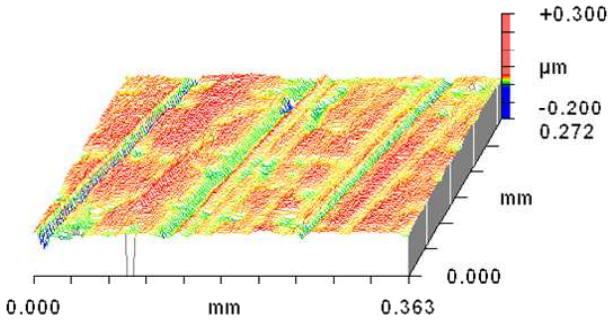

(b) 3mc

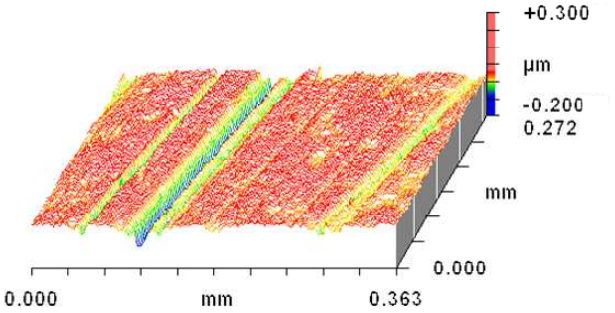

(c) 5mc

Figure 6.8: *Zygo 3D profiles of 38 mm CoCrMo cup (alumina test) over 5 million cycles of wear under standard conditions.*

Zygo images of the ceramic heads (shown in Figure 6.9) showed little change between the unworn and worn surfaces. Individual features were visible on the heads such as occasional large holes, metal transfer or occasional abrasive scratching; however the majority of the surface did not appear to change. As will be evident in the AFM images presented later, grains were removed from the surface which was not visible using non contacting profilometry. Examples of the individual features mentioned are shown in Figures 6.10

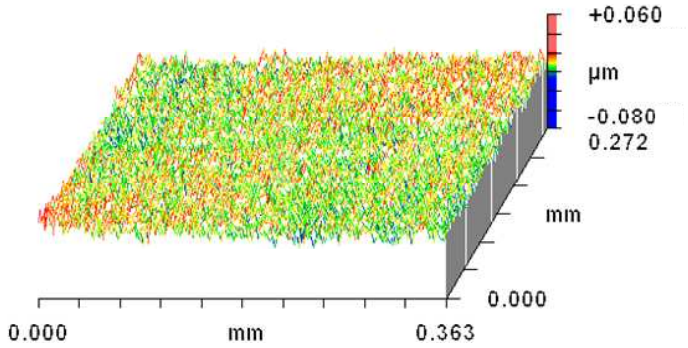

(a) Unworn

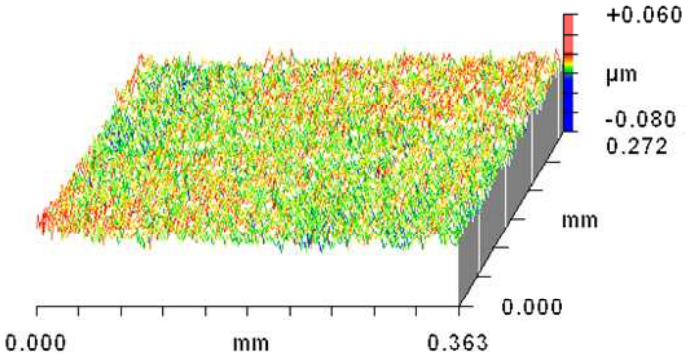

(b) 5mc

Figure 6.9: *Zygo 3D profiles of 38 mm alumina head unworn and 5 million cycles of wear under standard conditions.*

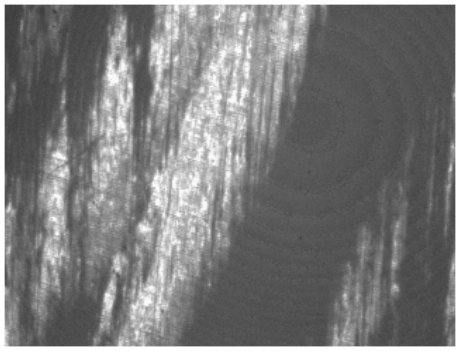

(a) Metal transfer on ceramic head

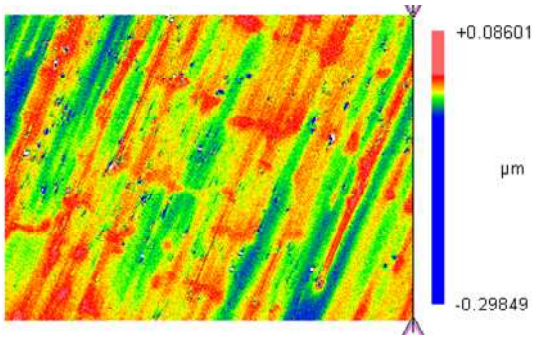

(b) Pulled matrix on metal cup

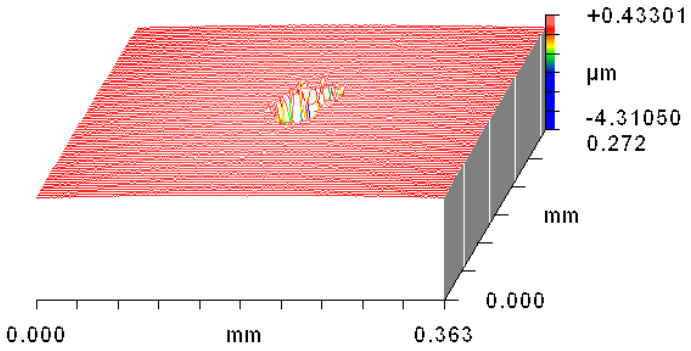

(c) Large hole on ceramic head

Figure 6.10: *Zygo image showing metal transfer, pulled matrix metal cup material, and an unusually large hole in the ceramic head.*

6.3.2 Optical Microscopy

Optical micrographs of the metallic cups were taken during the standard alumina tests, however, it was not possible to take informative images of the ceramic heads due to the pale smooth un-featured surface.

Images of the unworn metal cups showed blocky, irregular shaped carbides resulting from the as-cast manufacturing technique. These were clearly visible within the softer CoCrMo matrix and are shown in Figure 6.11.

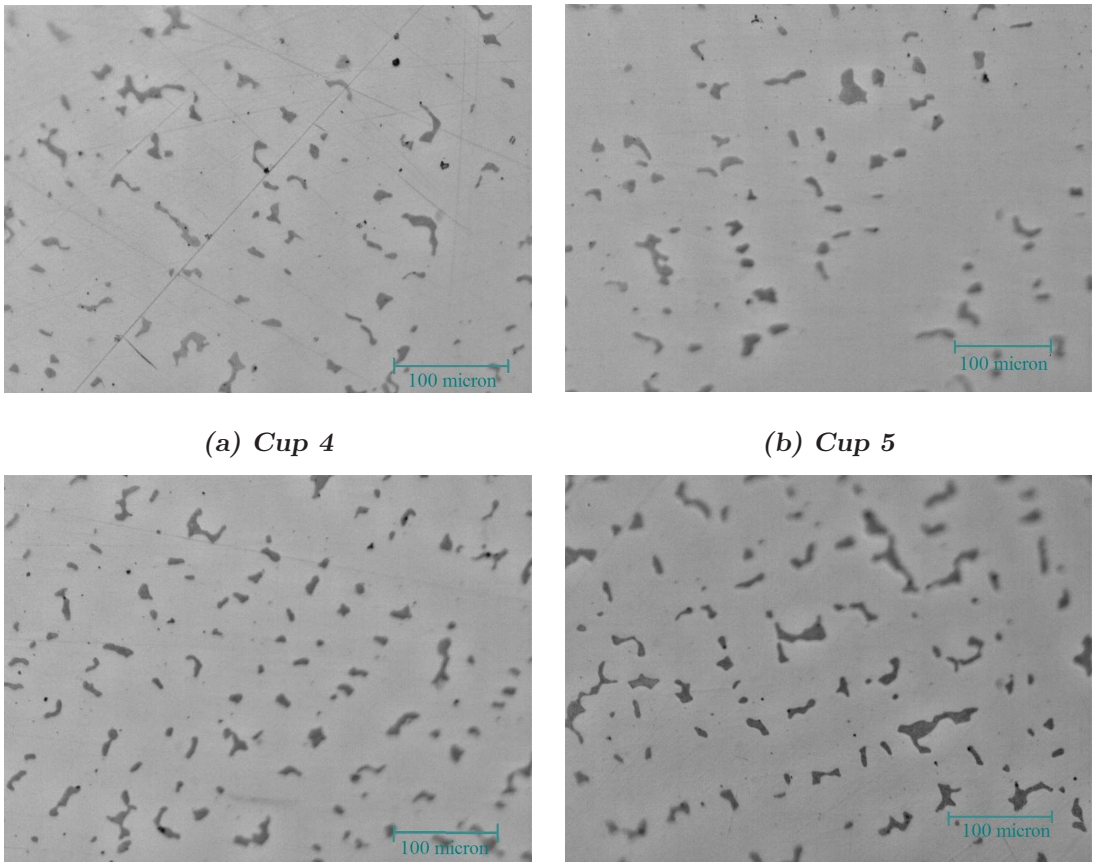

(a) Cup 4 ***(b) Cup 5***

(c) Cup 6 ***(d) Cup 9***

Figure 6.11: *Optical micrographs of the unworn surface of the 38 mm CoCrMo cups (alumina standard test) metallic cup clearly showing the irregularly shaped darker carbides projecting from the surface.*

Images taken after 3 million cycles of wear (see Figure 6.12), showed abrasive scratching, pitting of the matrix material and carbide removal. The carbides within the matrix generally became less visible and smoothed as the test progressed.

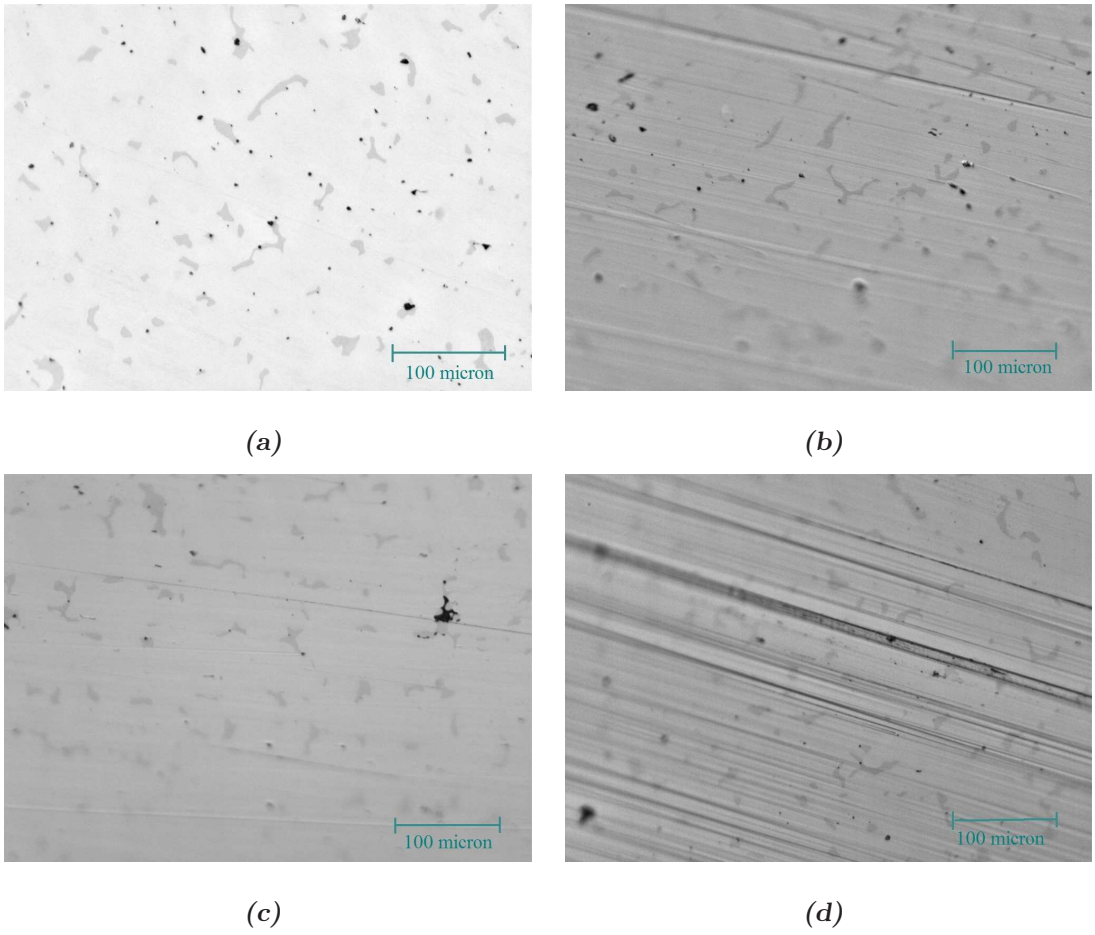

(a) *(b)*

(c) *(d)*

Figure 6.12: *Optical micrographs showing the metallic cups after 3 million cycles of wear; (a) Pitting and partial carbide removal, (b) Pitting and abrasive wear, (c) Removal or smoothing of the carbides shown by the lack of contrast between the carbides and matrix, (d) Abrasive scratches.*

Surfaces imaged after 5 million cycles of wear (see Figure 6.13) were taken using a lower magnification so that a larger area of the surface could be visualised. The images showed significant abrasive scratching and pitting on the surfaces, as seen at 3 million cycles. Adhesive wear was also seen where matrix material was removed and pulled across the surface producing an abrasive comet tail feature. The carbides appeared smooth and less visible.

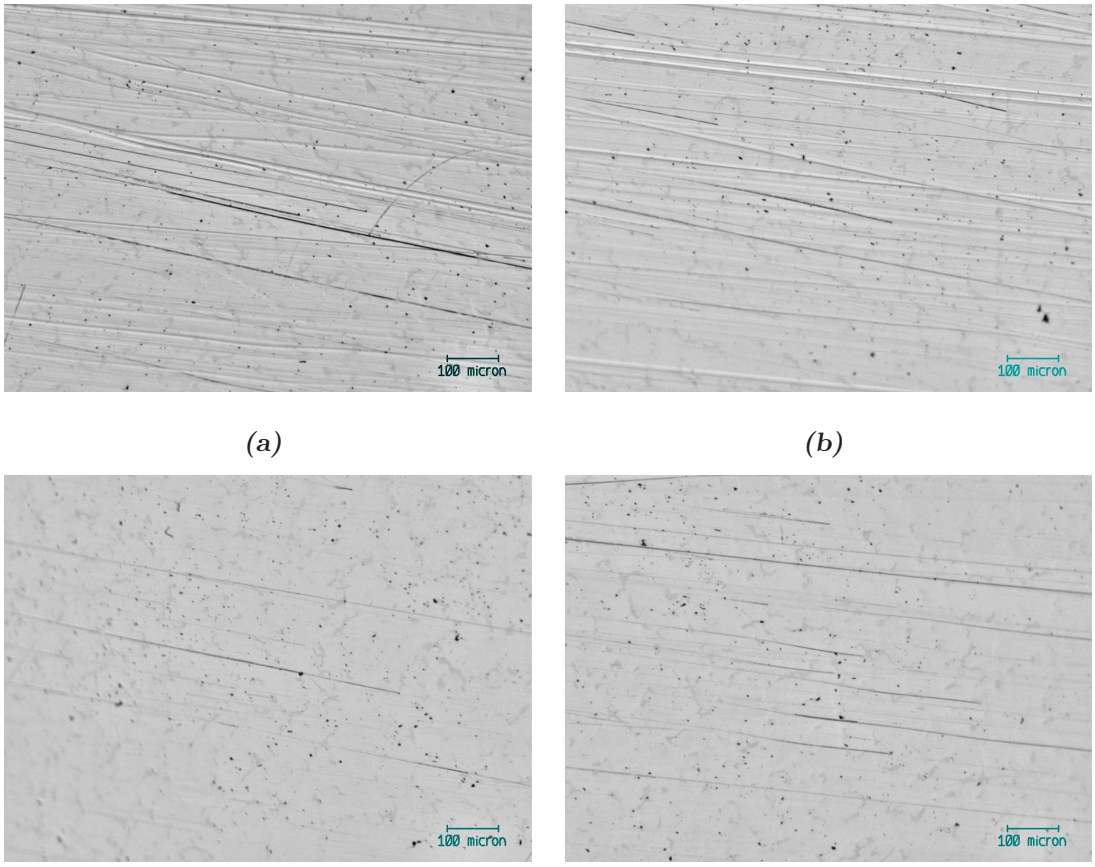

(a) *(b)*

(c) *(d)*

Figure 6.13: *Optical micrographs of the metallic cups after 5 million cycles. (a)-(d) Abrasive scratching, pitting and adhesive wear were evident as shown in all subfigures.*

6.3.3 AFM

AFM analysis of the ceramic heads after 5 million cycles of standard wear differed considerably from the topography of the unworn surfaces. The unworn surface of the head (shown in Figure 6.14(a)) revealed regular perpendicular machining scratches and the grains were not visible. In contrast, images taken on the pole of the ceramic head after 5 million cycles of wear showed contrasting areas which appeared to be removed or fractured and a reduced quantity and regularity of abrasive scratches. The removed grains were shallow and polygonal in shape.

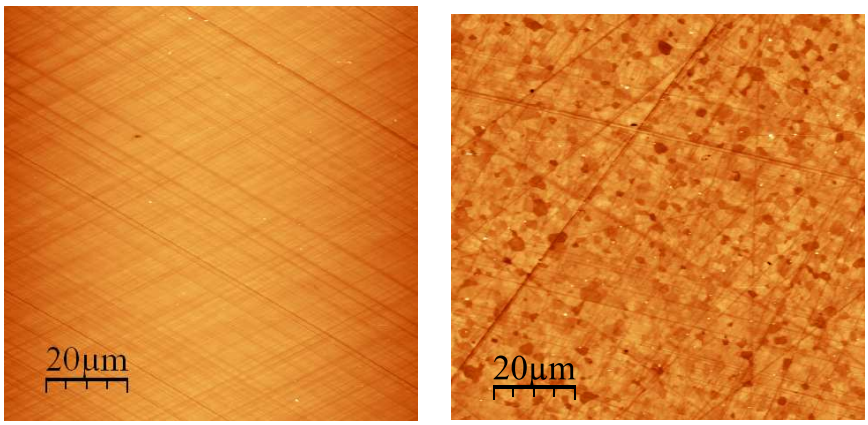

(a) Pole -Unworn ***(b) Pole - Worn to 5mc***

Figure 6.14: *AFM images of the unworn surface and surface worn to 5 million cycles. The unworn surface shows regular polishing scratches. The worn surface shows random scratches, and shallow removed grains.*

Line profiles show the pulled out or fractured grains to be very shallow in the region of 20 nm with occasional deep holes and scratches shown in Figure 6.15

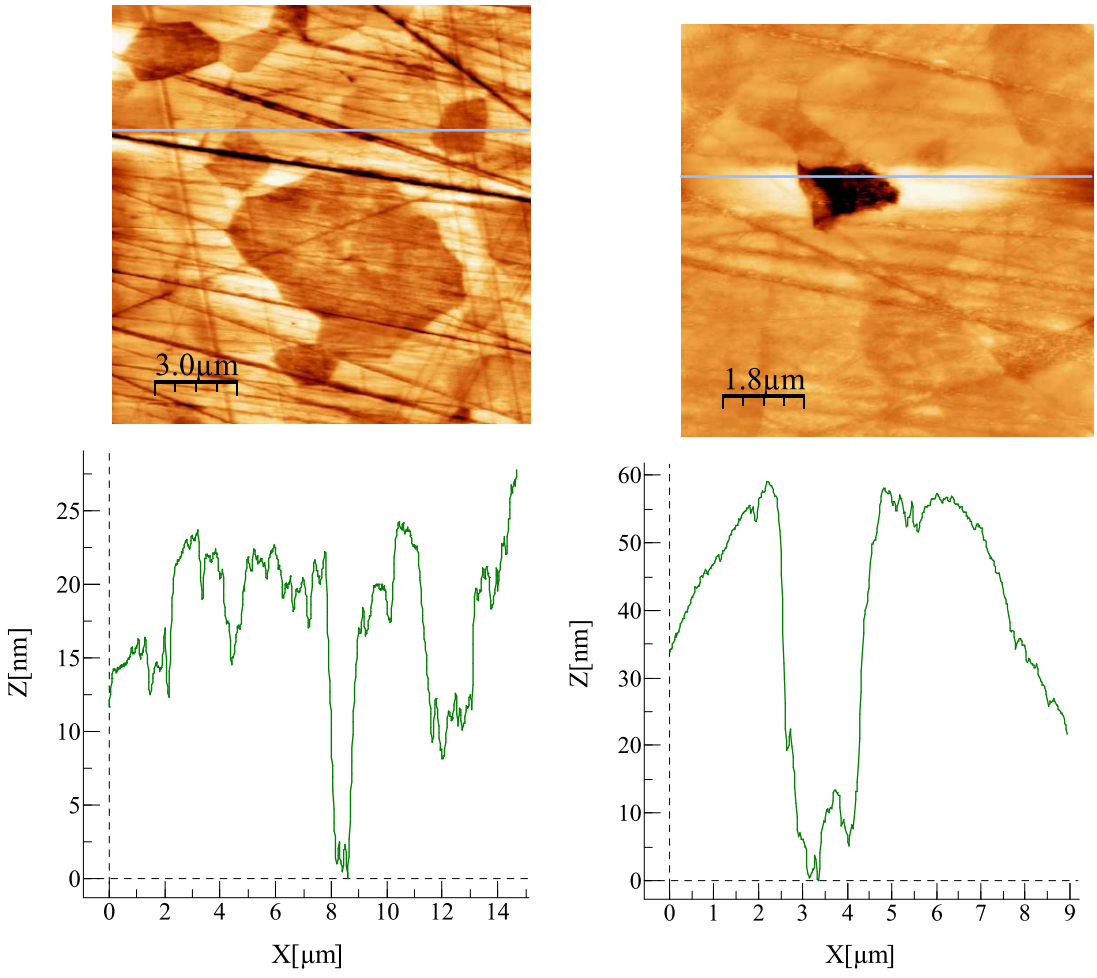

(a) Pole *(b) Pole*

Figure 6.15: *AFM images and line profiles showing shallow grain removal on the alumina ceramic heads after 5 million cycles of wear under standard conditions.*

Chapter 7

Results - Standard 38 mm Zirconia Toughened Alumina

A set of six, 38 mm diameter zirconia toughened alumina (ZTA) femoral heads were paired with as cast CoCrMo acetabular cups, as shown in Figure 7.1.

Joints were paired to give radial clearances close to 100 μm, as shown in Table 7.1

7.1 Standard Wear Testing

Testing was found to give low wear rates for both the ZTA heads and CoCrMo cups as shown in Figures 7.2 and 7.3. As can be seen from Figure 7.2, the ZTA head wear fluctuated close to zero throughout the test, in a similar way to that seen with the standard 38 mm alumina heads. The loaded soak control followed the same

Figure 7.1: *38mm ZTA head and as-cast CoCrMo alloy cup*

Station	Head	Dimension (mm)	Cup	Dimension (mm)	Radial Clearance (μm)
1	6	18.974	# 10	19.063	89
2	11	18.968	# 9	19.063	95
3	1	18.977	# 11	19.087	101
4	10	18.970	# 5	19.062	92
5	5	18.971	# 4	19.062	91
Control	4	18.973	# 8	19.063	89

Table 7.1: *38 mm ZTA against CoCrMo pairings and radial clearances for the standard wear test.*

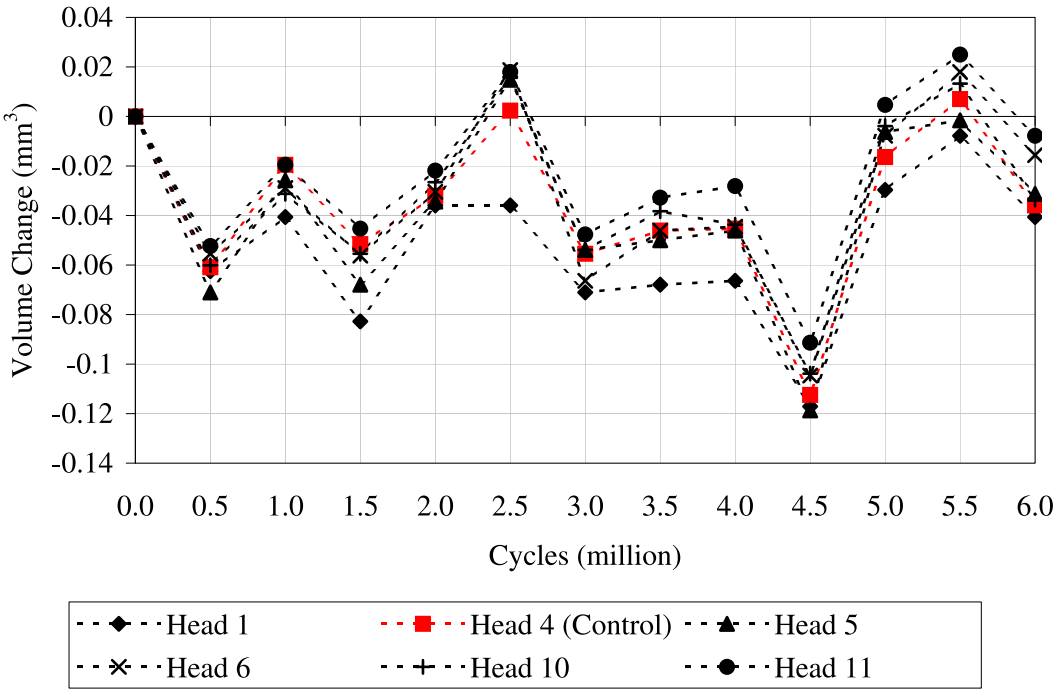

Figure 7.2: *Volume change of 38 mm ZTA femoral heads under standard wear testing.*

pattern and magnitude of volume fluctuations as the active stations, therefore it was concluded that the volume change was due to changes in the environment during the weighing process rather than wear of the bearings during simulation. Figure 7.3 shows the change in volume recorded for the CoCrMo cups during wear testing. As was expected the control cup wore less than the active stations which initially

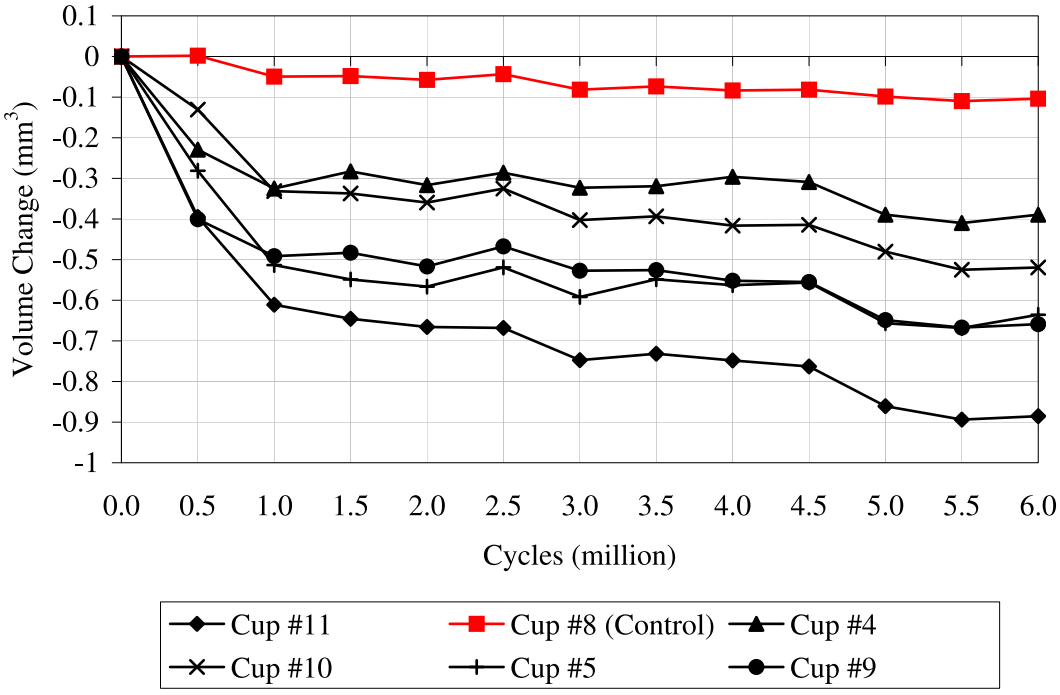

Figure 7.3: *Volume change of 38 mm as-cast CoCrMo cups (from ZTA test) under standard wear testing.*

showed an increased wear rate due to running-in of the bearing surface. Variations were seen between cups with some completing running in wear by 0.5 million cycles, whilst some took 1.0 million cycles for running in to be complete. Slight increases in wear was seen between 2.5-3.0 million cycles and 4.5-5.0 millions which cannot be explained and are not thought to be a significant change in wear, however it is important to note that after both episodes the wear returned to the lower wear rate seen previously.

The adjusted wear of the ZTA heads and CoCrMo cups is shown in Figure 7.4. The heads fluctuated around zero for the entire wear test. By 6 million cycles, 2 of the heads were found to gain volume (≈0.02 - 0.03 mm^3) and 1 head was found to decrease in volume (≈0.005 mm^3). Two heads returned to the same volume as the unworn samples. In contrast to the heads, all cups were found to decrease in volume. As mentioned previously, the time taken for running in to be complete varied between cups. Therefore the running in wear rate for two cups (# 4 and # 9) was taken between 0-0.5 million cycles, and for the remaining 3 (# 5, # 10 and # 11) the running in was considered to be complete by 1.0 million cycles. Wear

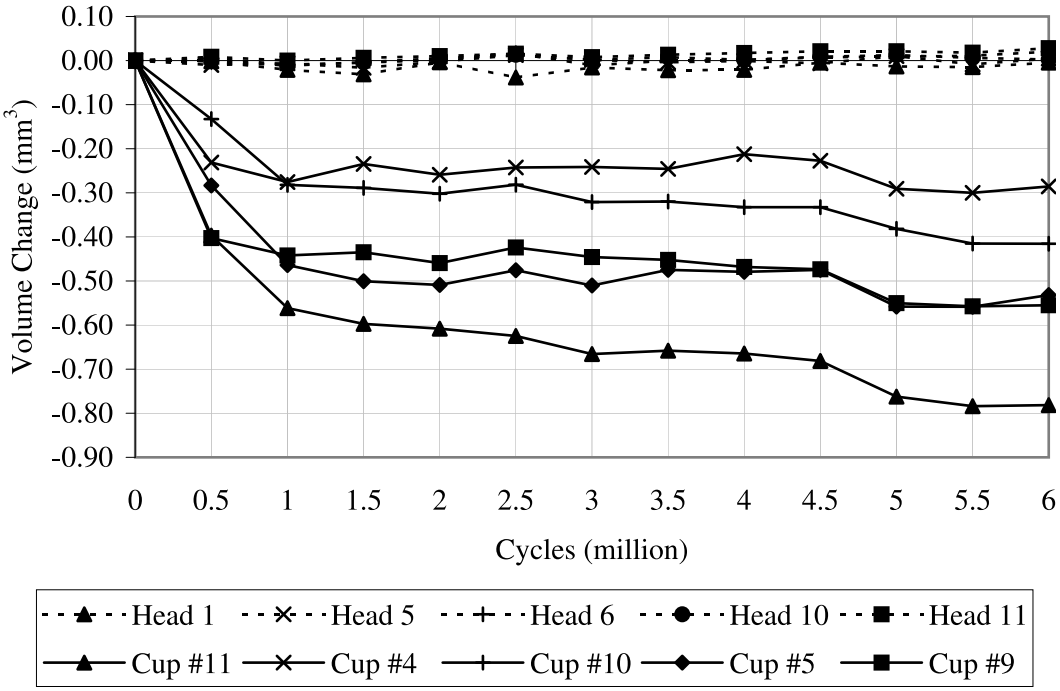

Figure 7.4: *Volume change for 38 mm ZTA:CoCrMo under standard wear (taking account of loaded soak control).*

rates were calculated for each individual cup and a mean value (mean ± C.I.) for all 5 active stations.

As can be seen from Table 7.2 a large variation in both steady state and running in wear rates were found between bearings. Cups #9 and #11 showed nearly twice the running in wear rates of cups #4 and #10 and a 4 fold increase compared with cup #5. The steady state wear rates also varied significantly with cup #11 (0.044 mm^3/million cycles) having a wear rate nearly 7 fold greater than that of cup #4. It is important to note that cup #11 was paired with head 1, which as will be noted later, had a considerably different initial surface topography compared with the other heads, and may be an explanation for the increased wear rate of that cup.

Mean running in and steady state wear rates were calculated for the 5 active stations. The average wear rates for the two cups which had completed running in by 0.5 million cycles was 0.634 ±0.737 mm^3/million cycles (mean ± 95% C.I.) and 0.016 ±0.003 mm^3/million cycles for running in and steady state wear rates respectively. The average wear rates for the three cups which had completed running in by 1.0 million cycles was 0.373 ±0.108 and 0.028 ±0.007 mm^3/million cy-

Cup	RI Cycles (millions)	RI Wear Rate (mm^3/mc)	SS Cycles (millions)	SS Wear Rate (mm^3/mc)
# 4	0-0.5	0.463	0.5-6.0	0.007
# 5	0-1.0	0.266	1.0-6.0	0.013
# 9	0-0.5	0.805	0.5-6.0	0.026
# 10	0-1.0	0.463	1.0-6.0	0.028
# 11	0-1.0	0.794	1.0-6.0	0.044

Table 7.2: *Individual 38 mm CoCrMo cup wear rates under standard wear conditions (ZTA test). (RI = Running in, SS = Steady state)*

cles respectively. If all 5 active stations were considered to have completed running in by 1.0 million cycles the steady state average wear rate for all 5 cups was 0.023 $\pm$0.005 mm^3/million cycles .

7.2 Friction Testing

Friction tests were carried out on 2 pairs of components, initially and after 5 million cycles of wear and are shown in Figure 7.5. Stribeck curves were plotted to indicate the lubrication regime under which the joints were operating, which allowed a comparison of the worn and unworn bearings.

The friction factors of the unworn samples did not differ from those samples worn to 5 million cycles. The curves indicated that the joints were working in a lubrication regime close to full fluid film lubrication which was indicated by the slight increase in friction factor found with the highest Sommerfeld numbers. The minimum friction factor was found between $1E^{-9}$ and $1E^{-8}$ with increases in friction factor found either side of this value. All viscosities of water based CMC lubricants showed lower friction factors compared with when bovine serum based CMC lubricants were used. All friction factors were < 0.1 with the water based CMC lubricants, except for water after 5 million cycles of wear.

Theoretical calculations were carried out to determine the minimum film thickness and associated lambda values to investigate the theoretical lubrication regime

Cycles (millions)	Head Rms (μm)	Cup Rms (μm)	H min (μm)	λ	Friction factors CMC*/BS**
0	0.010	0.007	0.07	>3	0.001/0.049[1]
					0.006/0.057[2]
0.5	0.012	0.012	0.07	>3	-
2	0.014	0.012	0.07	>3	-
5	0.011	0.009	0.07	>3	0.008/0.045[1]
					0.022/0.091[2]
6	0.011	0.008	0.07	>3	-

* CMC η=0.001 Pa s^{-1}, **BS η=0.0013 Pa s^{-1}

[1] = head 1 cup 11, [2] = head 6, cup 10

Table 7.3: *Theoretical minimum film thickness and lambda values for 38mm ZTA heads against CoCrMo cups*

under which the joints should operate.

The results, shown in Table 7.3, revealed theoretically the bearings were acting within full fluid film lubrication with λ >3 for all rms roughness values. This fitted with the low experimental friction factors and shape of the Stribeck curves.

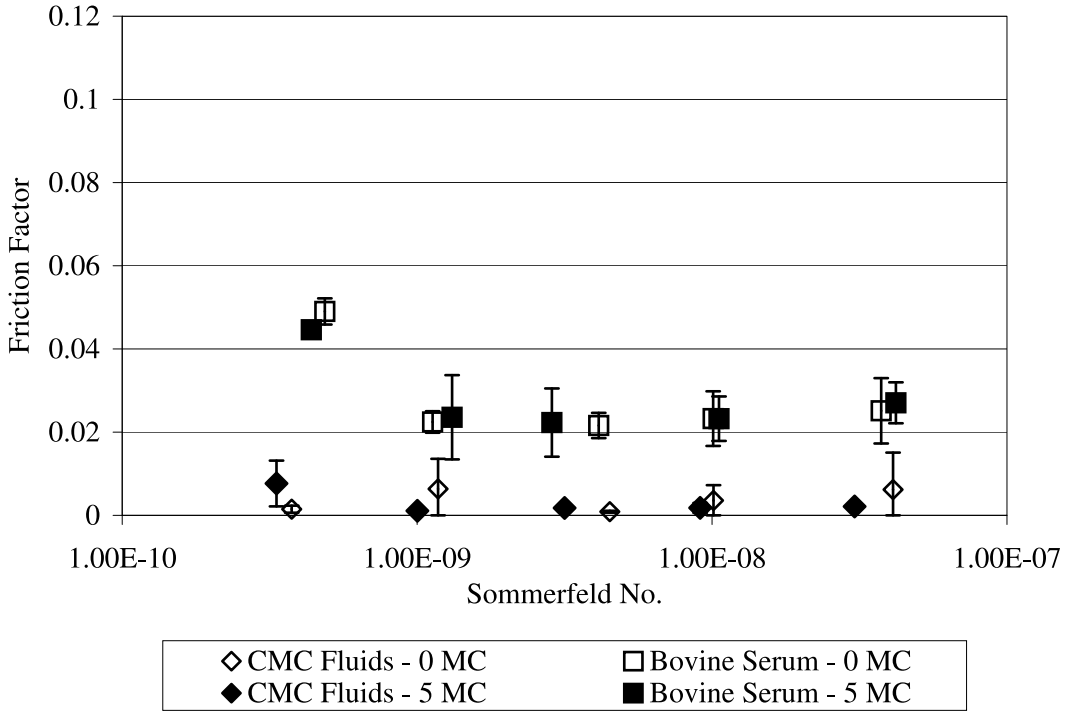

(a) Head 1 Cup 11

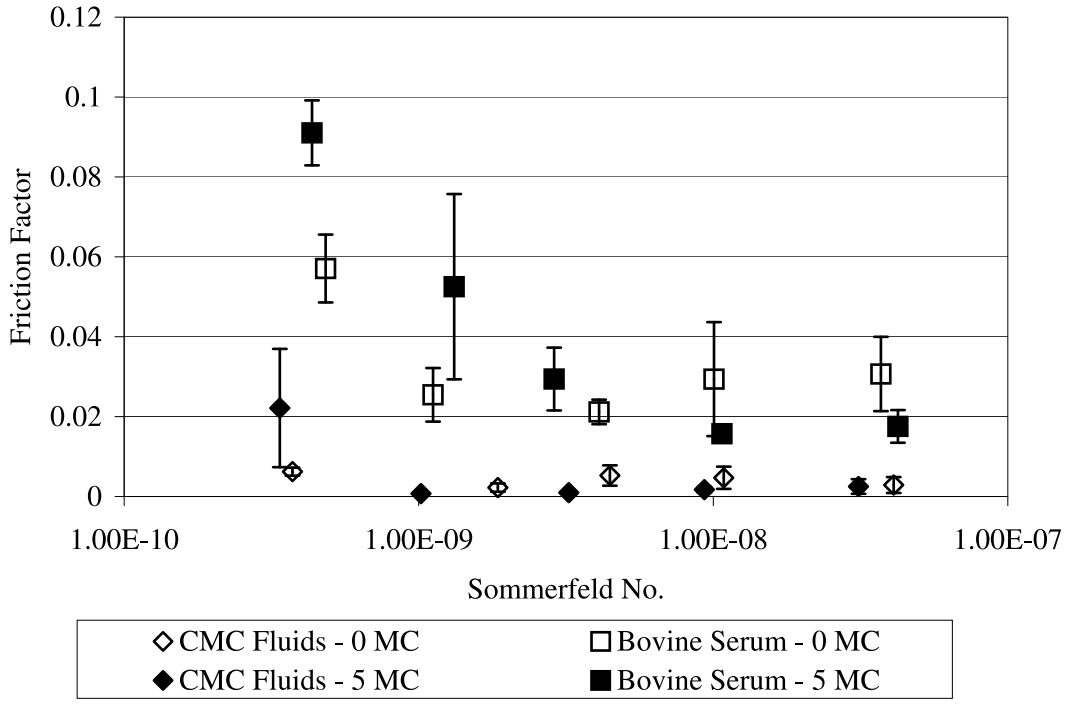

(b) Head 6 Cup 10

Figure 7.5: *Stribeck plot of 38 mm ZTA heads against CoCrMo cups, comparing unworn to 5 million cycles using lubricants of both water based CMC and bovine serum based CMC lubricants*

7.3 Surface Analysis

7.3.1 Non contacting Interferometry

Figure 7.6 shows the surface topography taken throughout testing.

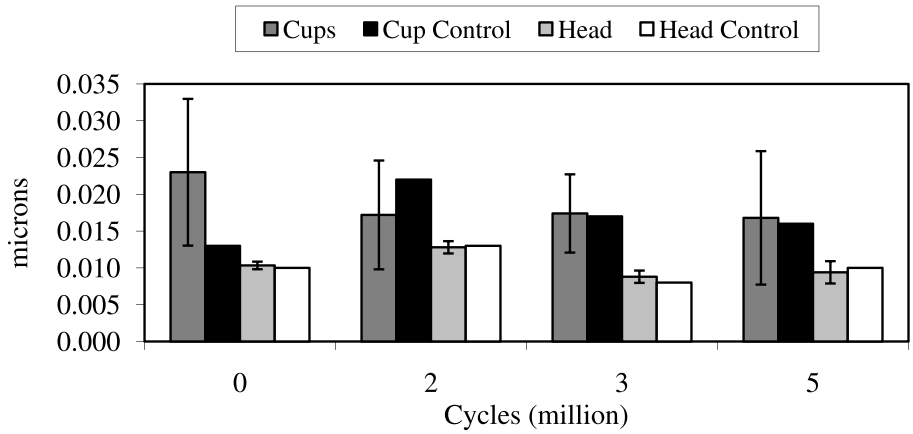

(a) Root mean squared roughness

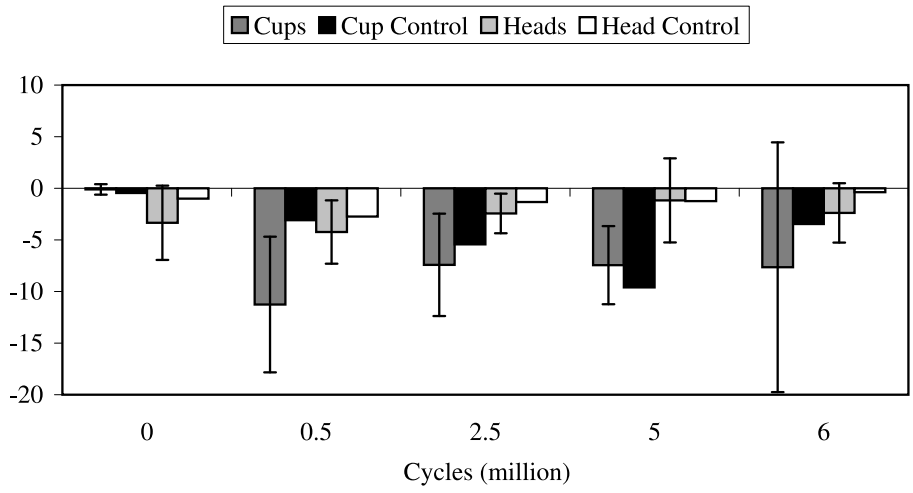

(b) Skewness

Figure 7.6: *Surface topography of 38 mm ZTA:CoCrMo components under standard wear simulator conditions.*

The rms roughness of the metallic cups increased in the first 0.5 million cycles from and initial value of 0.007 μm to 0.012 μm, after with a decrease in roughness seen for 2.5, 5 and 6 million cycles. By 6 million cycles of wear the rms roughness had returned close to the initial value of 0.008 μm. The control cup in contrast to the active stations, remained constant (0.006/0.007 μm) throughout testing. The

ceramic heads had a slightly higher roughness (compared with the cups) throughout wear testing (initially 0.010 μm). A similar pattern to that seen for the cups was found for the heads with an increase from the initial roughness to a peak at 2.5 million cycles (0.010 to 0.014 μm) followed by a decrease in roughness to 6 million cycles. The control head rms roughness followed a similar pattern to the active stations with relatively little change throughout testing. It must be strongly noted that the changes in rms roughness were extremely small, and one may say insignificant.

The skewness measurements were found to follow an expected trend throughout wear testing. The initial cups showed a slightly positive value, indicating sharper peaks compared with valleys, which was explained by the carbides which projected from the surface of the as-cast metallic cups. However by 0.5 million cycles the skewness was considerably more negative due to carbide removal, abrasive scratching and pitting of the matrix. By 2.5 million cycles the skewness was less negative as the softer matrix material was worn away, because of the decreased protection from the harder carbide components. This therefore decreased the sharpness of the valleys compared with the peaks. Following this the skewness was found to remain at a similar value up until 6 million cycles possibly as an equilibrium of carbide and matrix material removal was reached. The control cup was also found to increase in skewness thought to be caused by micro motion between the bearing surfaces leading to pitting or carbide removal. The control cup surface topography was not abrasively scratched as was found for the active stations. The values of skewness of the control cup at 2.5, 5 and 6 million cycles fell within the standard deviations of the active stations therefore the change in skewness of the cups may not be significant enough to be considered different to the control station. The ceramic heads were consistently found to have a less negative skewness compared with the cups. Occasional light scratching and grain removal may be the explanation for the negative skewness however the values are close to zero suggesting that the tendency for the surface to have sharper valleys compared with peaks was extremely small, and in fact the surfaces are evenly distributed around the mean line.

Figure 7.7 shows typical micrograph of the metallic cups throughout standard wear testing. The modest change in rms roughness can clearly be seen as the images

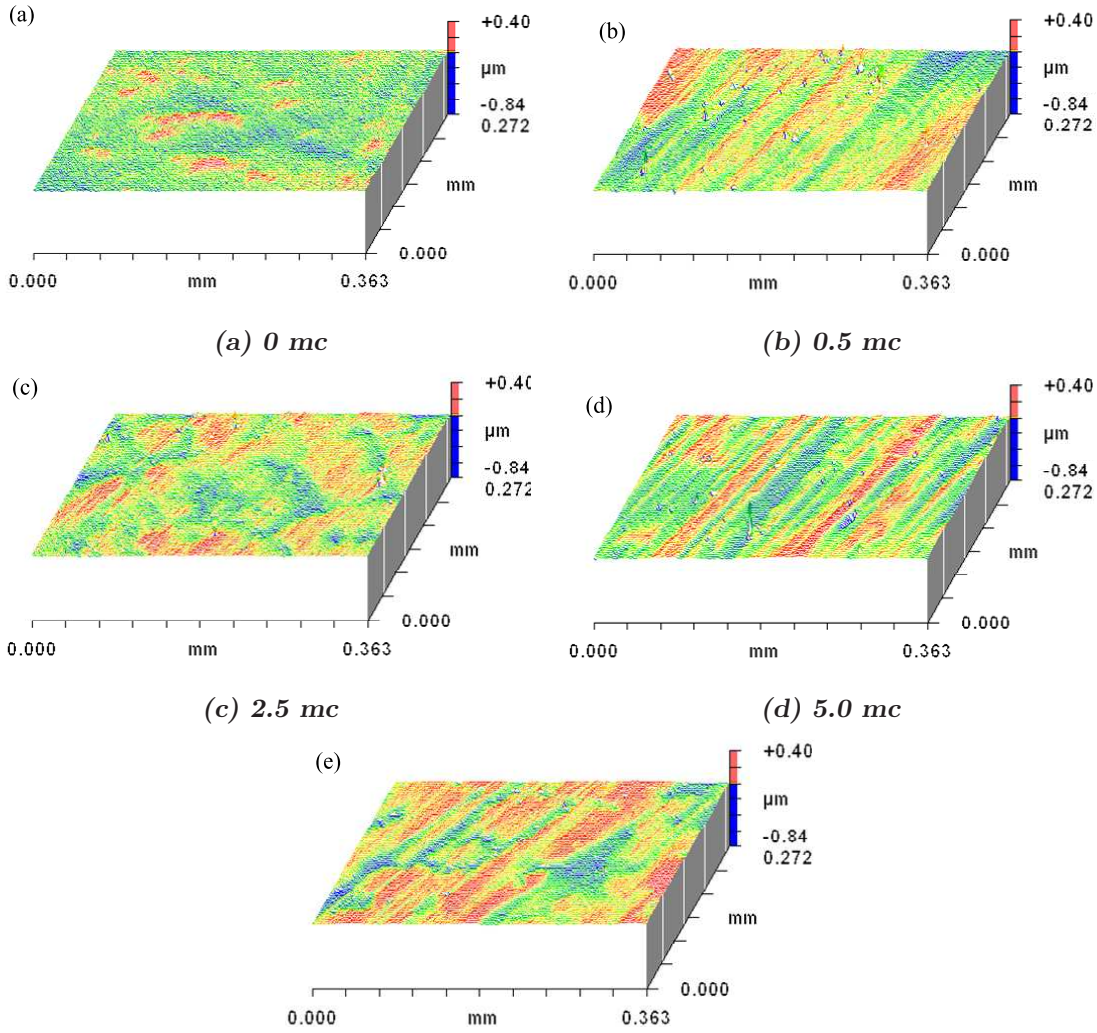

(a) 0 mc ***(b) 0.5 mc***

(c) 2.5 mc ***(d) 5.0 mc***

(e) 6.0 mc

Figure 7.7: *Zygo 3D profiles of 38 mm CoCrMo cups (ZTA test)*

show little variation in topography. The carbides were not as visible in the micrographs of the unworn surface as was seen for the alumina test, but the surfaces were free from abrasive scratches and pitting indicating the surfaces were unworn. By 0.5 million cycles of wear, pitting of the matrix was noticed and more negatively skewed topography was found (see Figure 7.8). Directional scratches and wear was also seen. By 2.5 million cycles, the pitting was not as obvious as the matrix appeared worn and the surface relatively smooth. The micrographs at 5 and 6 million cycles were similar to that found at 2.5 million cycles.

The micrographs shown in Figure 7.9 indicated that little change in surface topography occurred to the ZTA head. The images indicated a smooth surface with

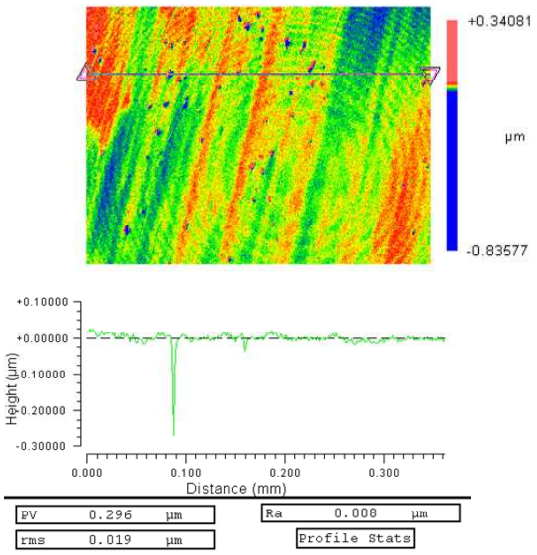

Figure 7.8: *Line profile showing pitting of the metallic cups seen after 0.5 million cycles of standard wear*

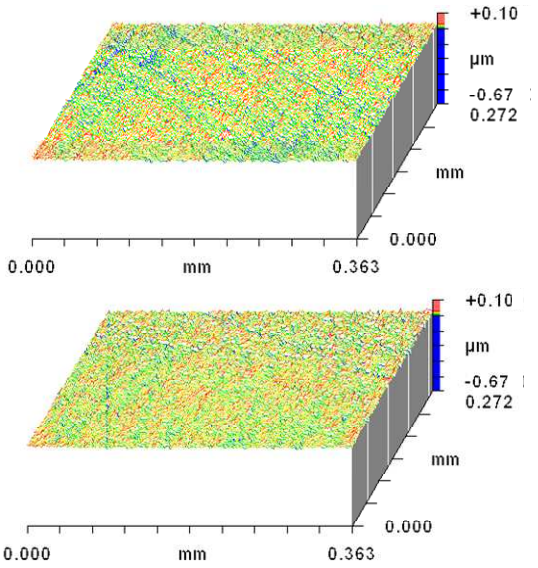

Figure 7.9: *Zygo 3D micrographs of ZTA heads*

a slight predominance for negative skewness shown by the z-scale bar on the left hand side of the image.

The micrographs (Figure 7.7 and Figure 7.9) show typical topography for the majority of the cups in the current test. However initial simulator set-up and friction testing, carried out on 2 of the cups, resulted in damage to the unworn topography. A relatively large scratch was seen on cup #9 during simulator set-up and protein was found deposited in the wear patch after friction testing, images of which can be

seen in Figures 7.10 and 7.11.

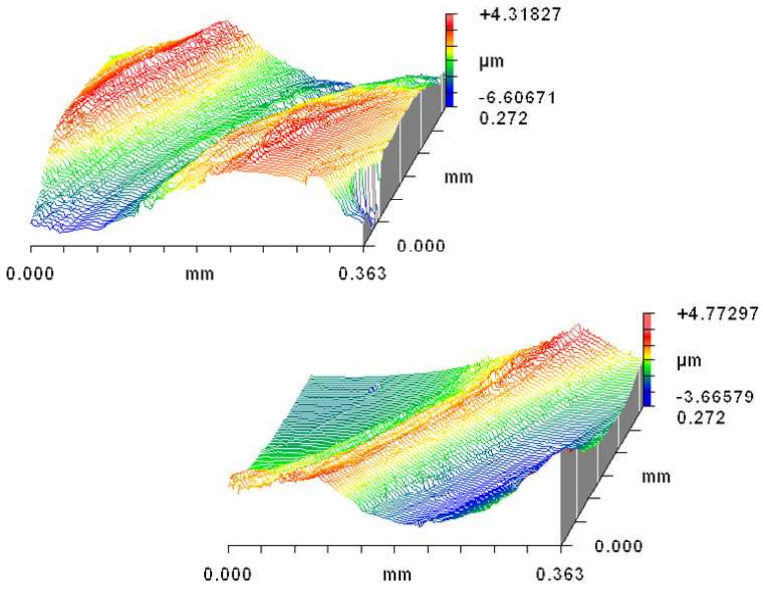

Figure 7.10: *Damage caused by simulator setup(cup #9)*

The damage on cup #9 and #10 due to friction and simulator set-up did not appear to have an effect on the wear of these components as they followed similar wear patterns to the other active stations. Cup #11, which showed scratching, protein deposition and smudging of the matrix around the carbides after friction testing, showed the most wear out of the 5 active stations. However, it must be noted that cup #11 was paired with head 1, which as will be seen in the following AFM images, had significant holes and damage to the ceramic surface before testing, and therefore may be partly responsible for the greater wear rate of that bearing couple. It is likely that the protein seen on cup #11 after friction testing was worn off during the initial stages of wear and therefore did not have a significant effect. However, the presence of protein deposition in the wear patch seen after friction indicates that even during 41 cycles during friction testing, protein in the lubricant precipitates and deposits on to the surface.

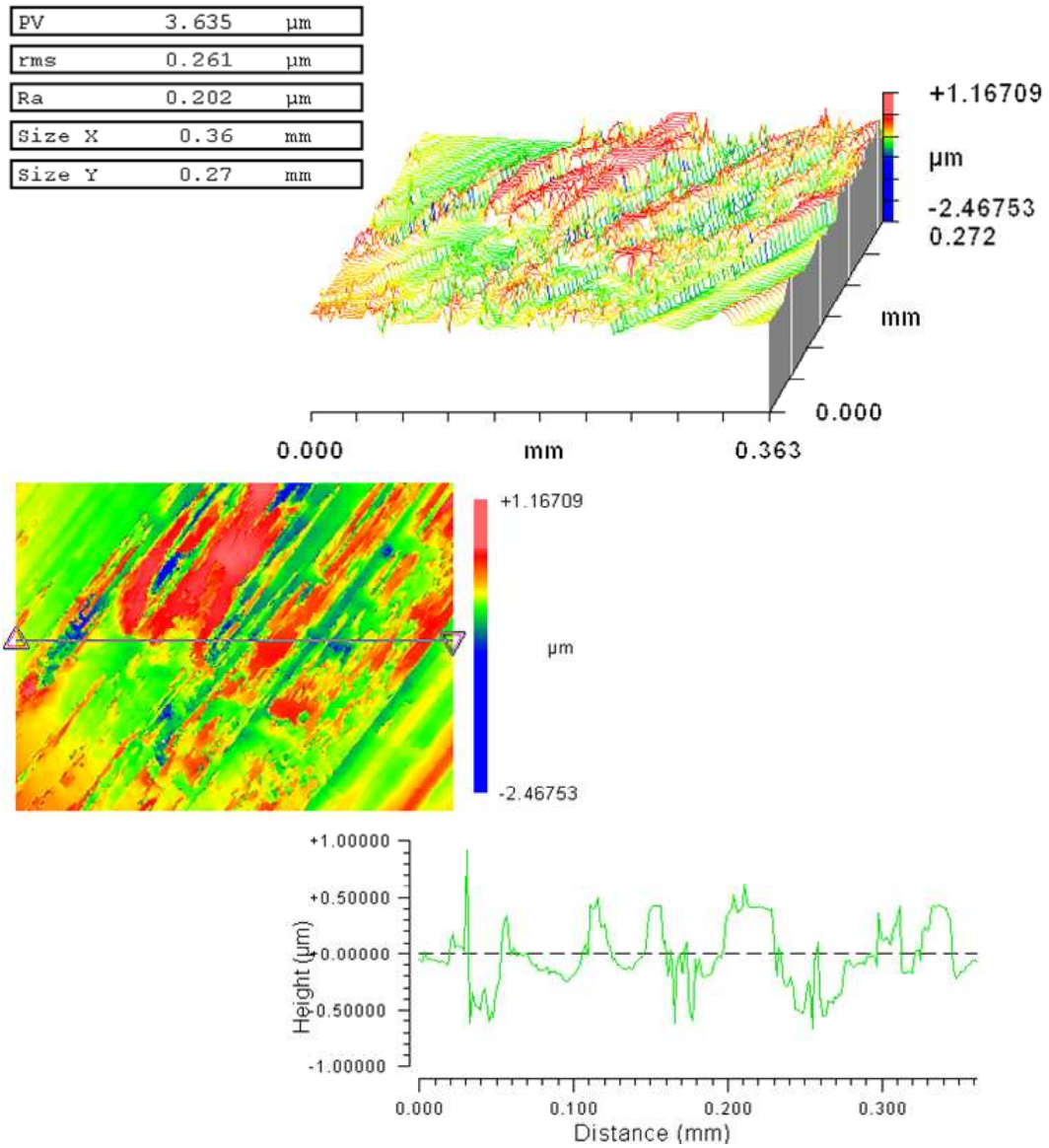

Figure 7.11: *Deposit left on cup after friction(cup #11)*

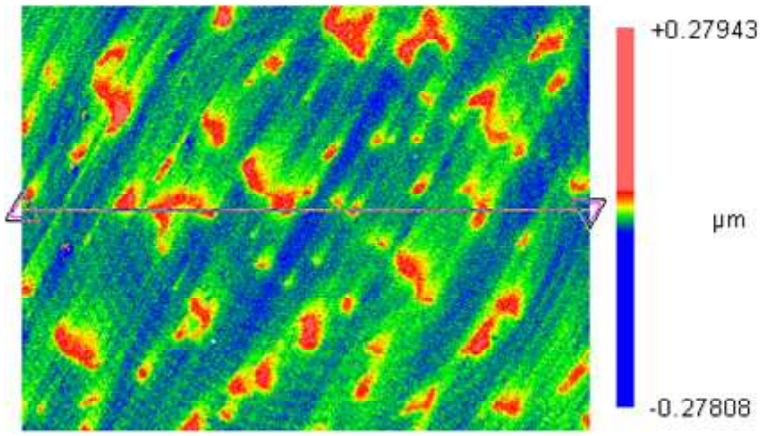

Figure 7.12: *Smudged carbides after friction(cup #11)*

7.3.2 Optical Microscopy

Micrographs were taken of the unworn surface and after 2.5, 5 and 6 million cycles of wear.

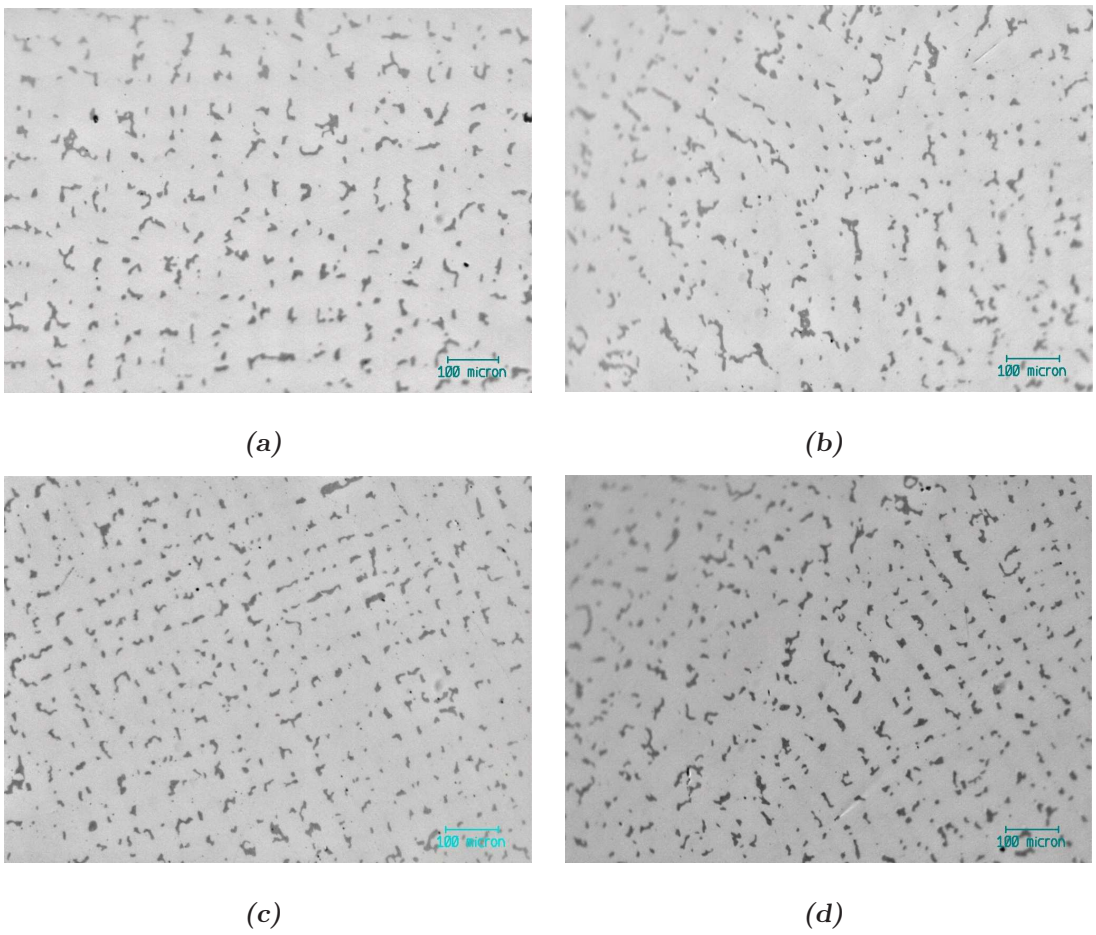

Figure 7.13: *Optical micrographs of the unworn surface of the 38mm CoCrMo cups (ZTA test) metallic cup clearly showing the irregularly shaped darker carbides projecting from the surface.*

As Figure 7.13 demonstrates, the unworn surfaces clearly showed contrasting carbides which were irregular blocky structure which projected from the matrix. The topography in some of the micrographs appeared to show a regular pattern to the carbides (Figure 7.13(c)), often forming a grid pattern whilst some of the other cups appeared to be more random in distribution (Figure 7.13(b)).

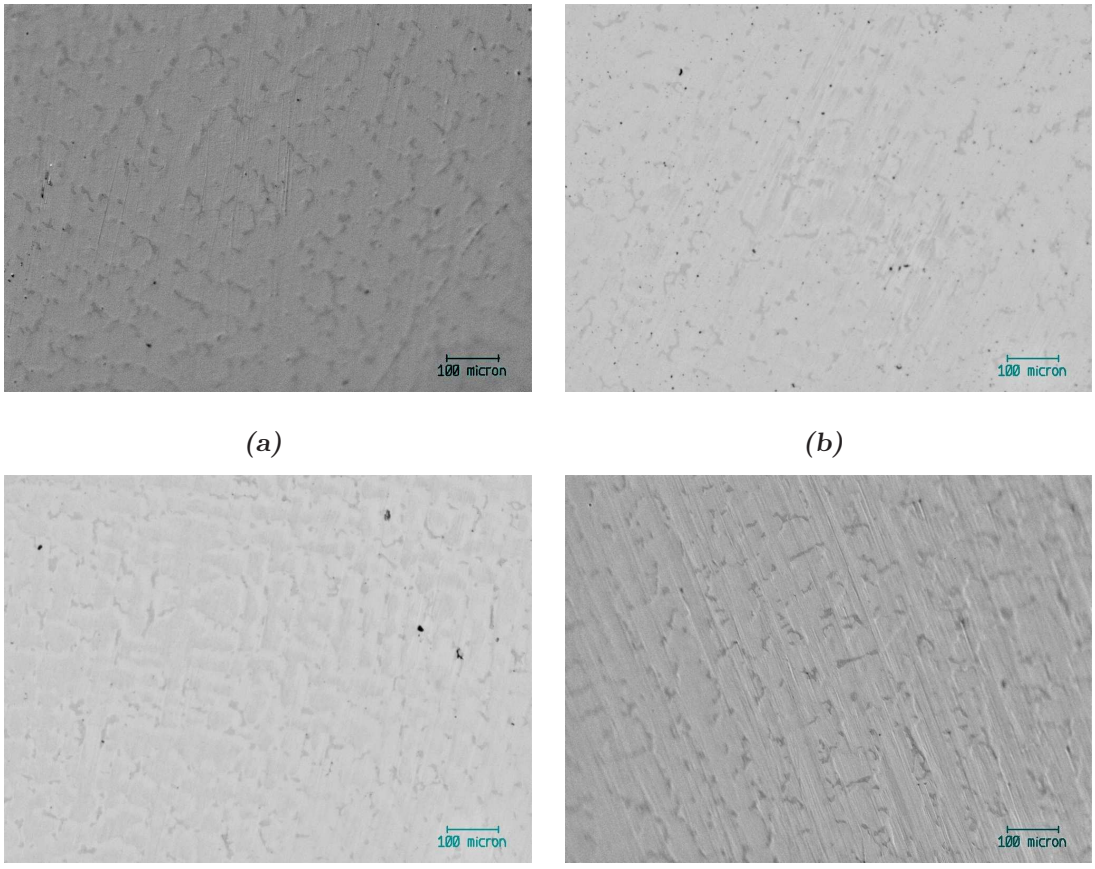

(a) *(b)*

(c) *(d)*

Figure 7.14: *Optical micrographs showing the metallic cups after 2.5 million cycles of wear in a standard wear simulator. All micrographs showed little abrasive or adhesive wear, however the contrast between the carbides and matrix decreased suggesting smoothing or removal of the carbides.*

After 2.5 million cycles of wear, the majority of the topography remained relatively unchanged, as shown in Figure 7.14. The carbides appeared smoothed and even though the direction of motion was apparent on the surfaces through deformation of the matrix, only light abrasive scratching evident on the surface. Small areas of scratching and pitting were observed within the wear patch which are shown in Figure 7.15.

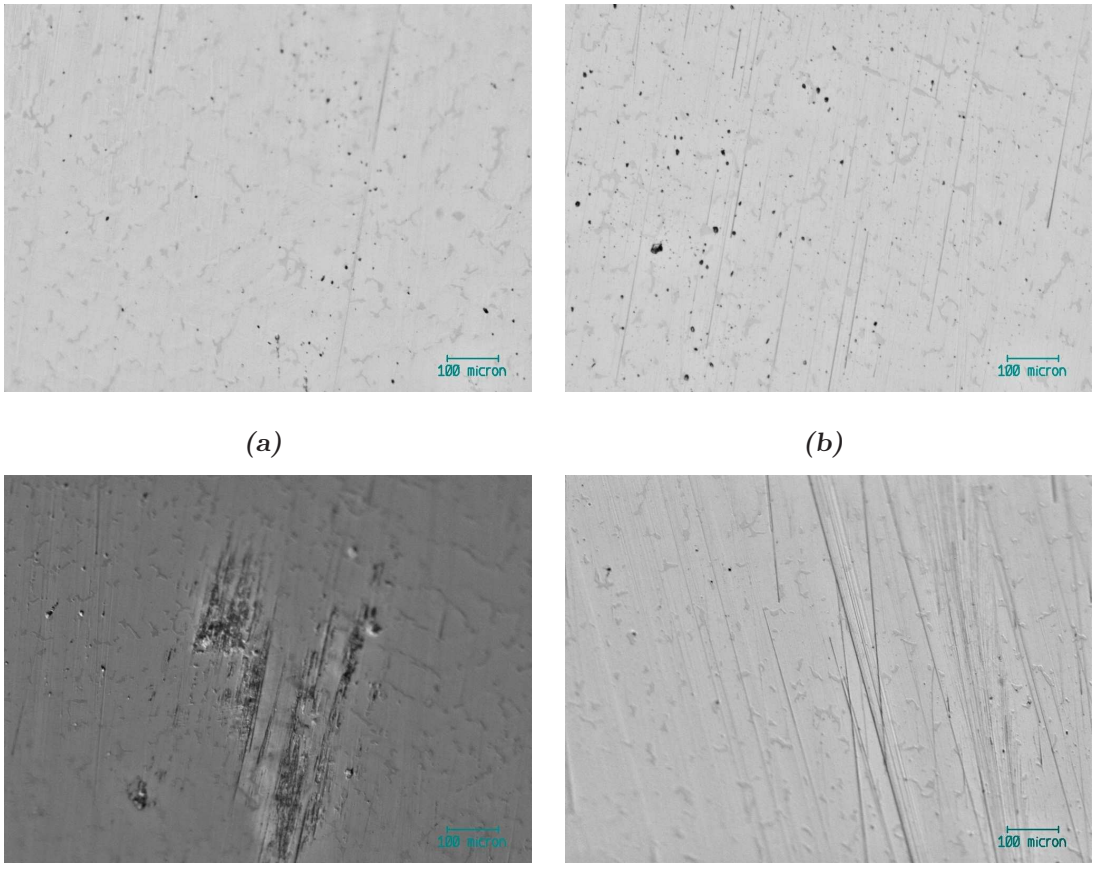

(a) *(b)*

(c) *(d)*

Figure 7.15: *Optical micrographs showing abrasive scratches and pitting of the metallic cups after 2.5 million cycles in a standard wear simulator. Isolated areas of significant damage were also found (sub figure 7.15(c)*

After 5 million cycles of wear, the surfaces remained relatively undamaged with only occasional areas of scratching and pitting, as shown in Figure 7.16. The unworn surfaces were identical to those shown in Figure 7.13.

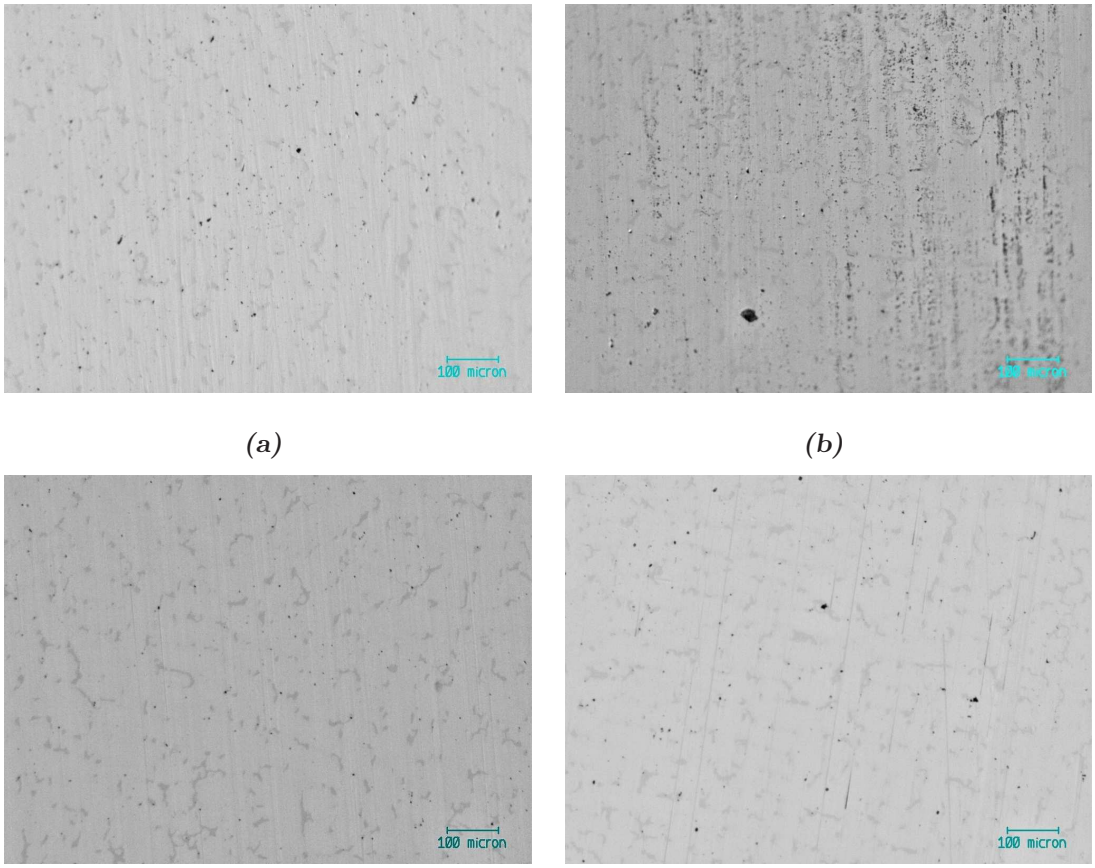

(a) *(b)*

(c) *(d)*

Figure 7.16: *Optical micrographs showing the metallic cups after 5.0 million cycles of wear in a standard wear simulator. All micrographs showed little abrasive or adhesive wear, however the contrast between the carbides and matrix decreased suggesting smoothing or removal of the carbides.*

Figure 7.17 clearly shows the edge of the wear track which allowed direct comparison between the surface topography of the worn and unworn surface which highlights the different contrasting colours of the worn and unworn carbides. The unworn surfaces remained un-changed with carbides projecting from the surface. Within the worn section, the motion direction is obvious and the carbides are less apparent.

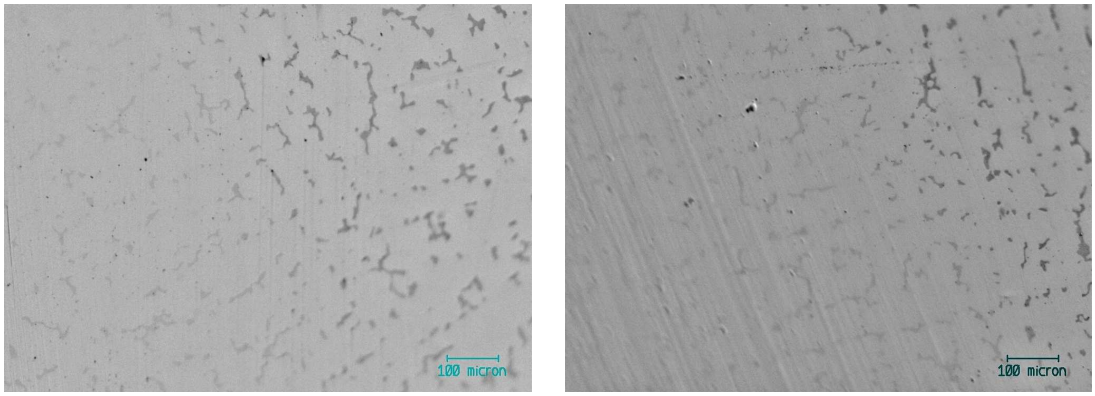

(a) *(b))*

Figure 7.17: *Optical micrographs showing the edge of the wear track. Both sub figures shown the worn surface on the left and the unworn surface on the right side of the images*

Figure 7.18 shows the limited changes in surface topography of the metallic cups was seen between 5 and 6 million cycles of wear. As found between during the early wear, the majority of the cups remained undamaged with only smoothed carbides and light wear of the surfaces allowing the direction of motion to be determined. Small random areas within the cups revealed occasional pitting and abrasive or third body scratches. The limited damage may be attributed to the un-damaged and un-featured surface of the ceramic cups, as will be shown by the AFM analysis.

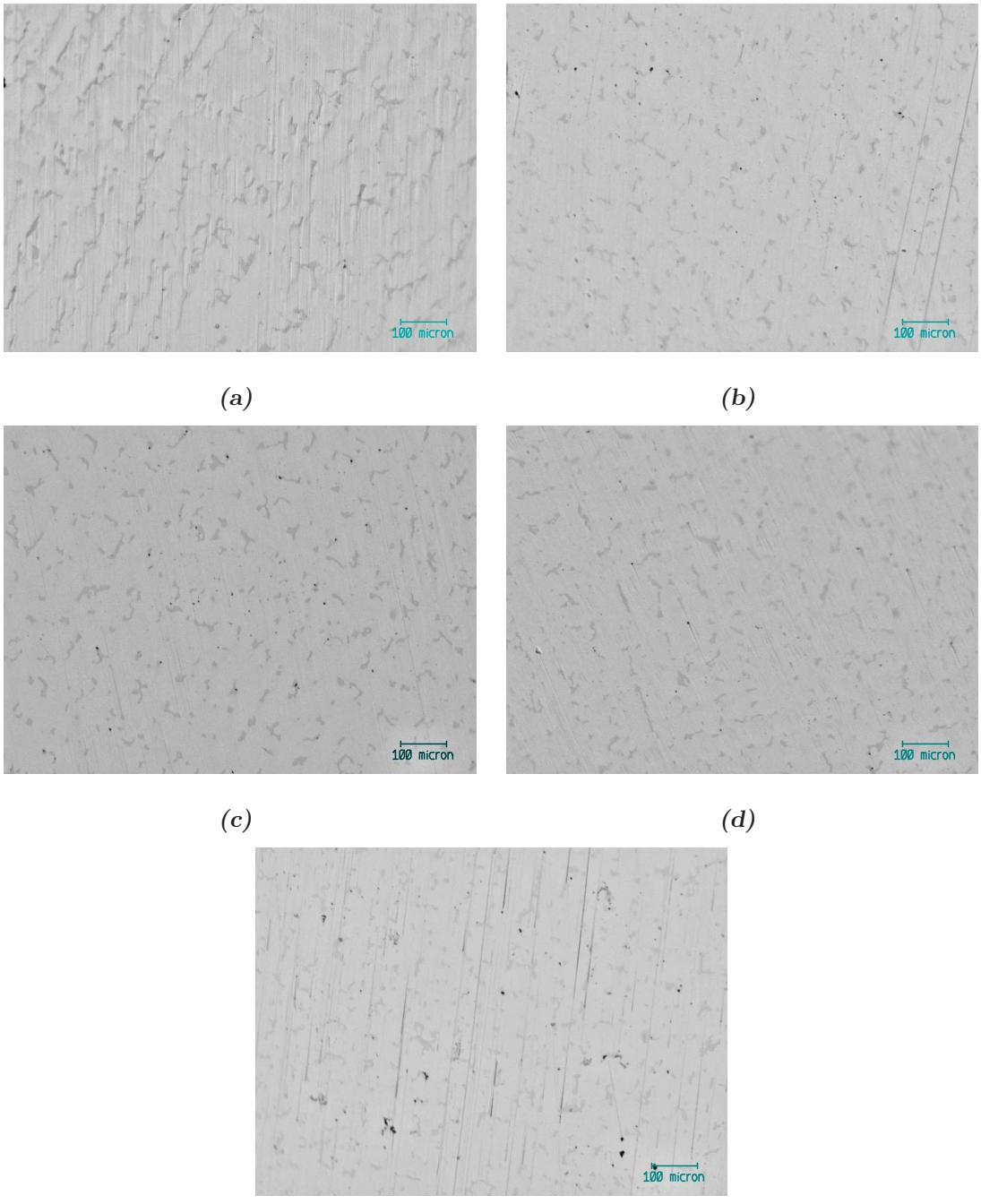

(a) *(b)*

(c) *(d)*

(e)

Figure 7.18: *Optical micrographs showing limited abrasive scratches and pitting of the metallic cups after 6 million cycles in a standard wear simulator.*

7.3.3 Atomic Force Microscopy

Micrographs of each unworn ceramic head were taken to record the surface topography before testing commenced.

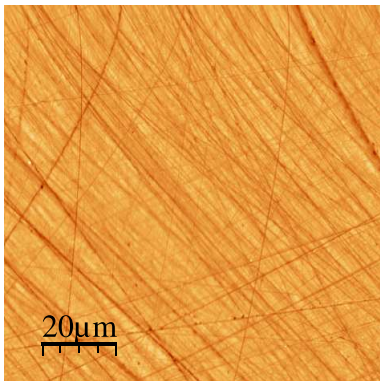

(a) Head 4

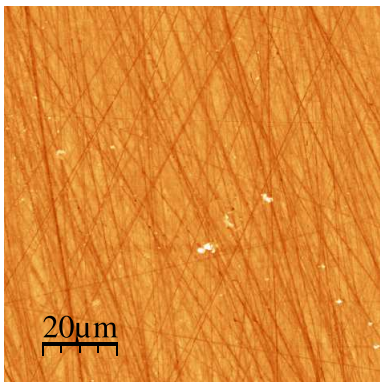

(b) Head 5

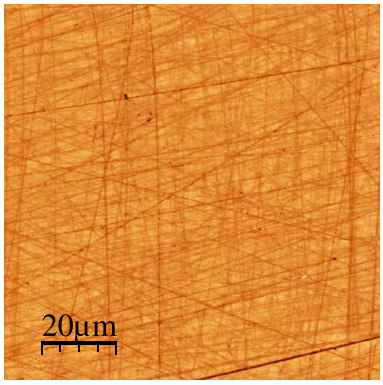

(c) Head 6

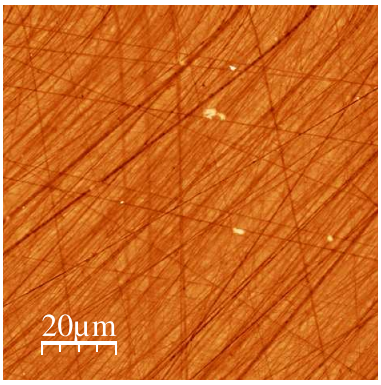

(d) Head 10

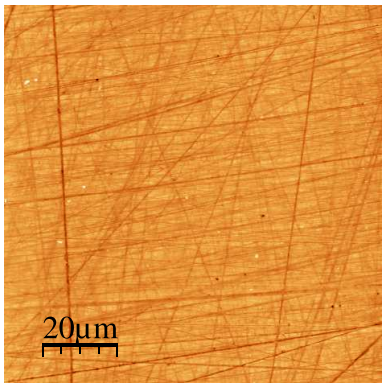

(e) Head 11

Figure 7.19: *AFM micrographs of unworn 38mm ZTA heads on the pole showing random polishing scratches.*

Figure 7.19 shows micrographs of the unworn surfaces of the pole of the head. The majority of the heads (heads 4, 5, 6, 10 and 11) showed polishing scratches which were randomly orientated, and no grains were visible. The images of head 4 and head 10 show the effects of thermal drifting at the top which is not a feature of the ceramic material but of the AFM equipment. In contrast head 1 showed significant damage and grain removal on the pole. The polishing scratches were less apparent however this may be due to the deep holes which resulted in the scratches becoming an insignificant feature. The holes varied in depth some as deep as 0.25 μm as shown in Figure 7.20. Images taken at 45 degrees to the horizontal (Figure 7.21), the damage was less obvious and the irregular polishing scratches are evident.

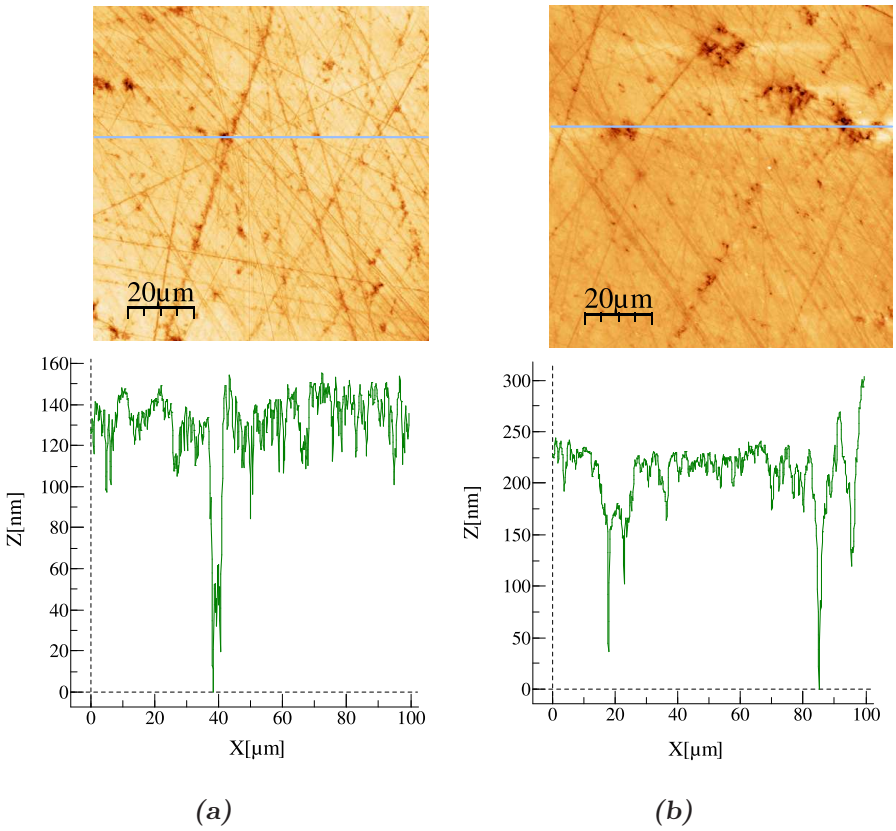

Figure 7.20: *AFM micrographs of 38 mm unworn ZTA head 1 showing initial damage on the pole.*

After 5 million cycles of standard wear the surface topography did not change considerably compared with the unworn surfaces. The polishing scratches, as seen on the unworn surfaces, remained noticeable. Randomly distributed very occasional

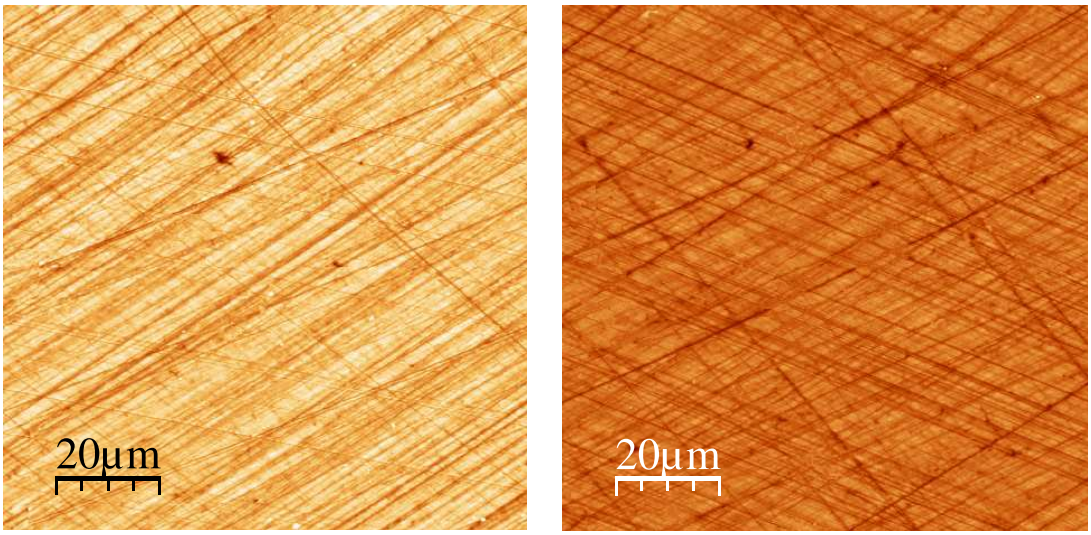

(a) *(b)*

Figure 7.21: *AFM micrographs of 38 mm unworn ZTA head 1 at 45 ^{0} to the pole showing polishing scratches.*

shallow grains were detectable on the pole of some of the heads, however this was not the dominant feature of the surface and was only noticeable after changing the contrast of the images to highlight the grains. Typical heads are shown in Figure 7.22. After 5 million cycles of wear, head 1 showed a similar topography compared with the unworn surface with grains removed on the pole. Although it was difficult to quantify the amount of grain removal, it did not appear that the quantity of grains removed had increased from the initial unworn surface, with wear. The image and line profile are shown in Figure 7.23.

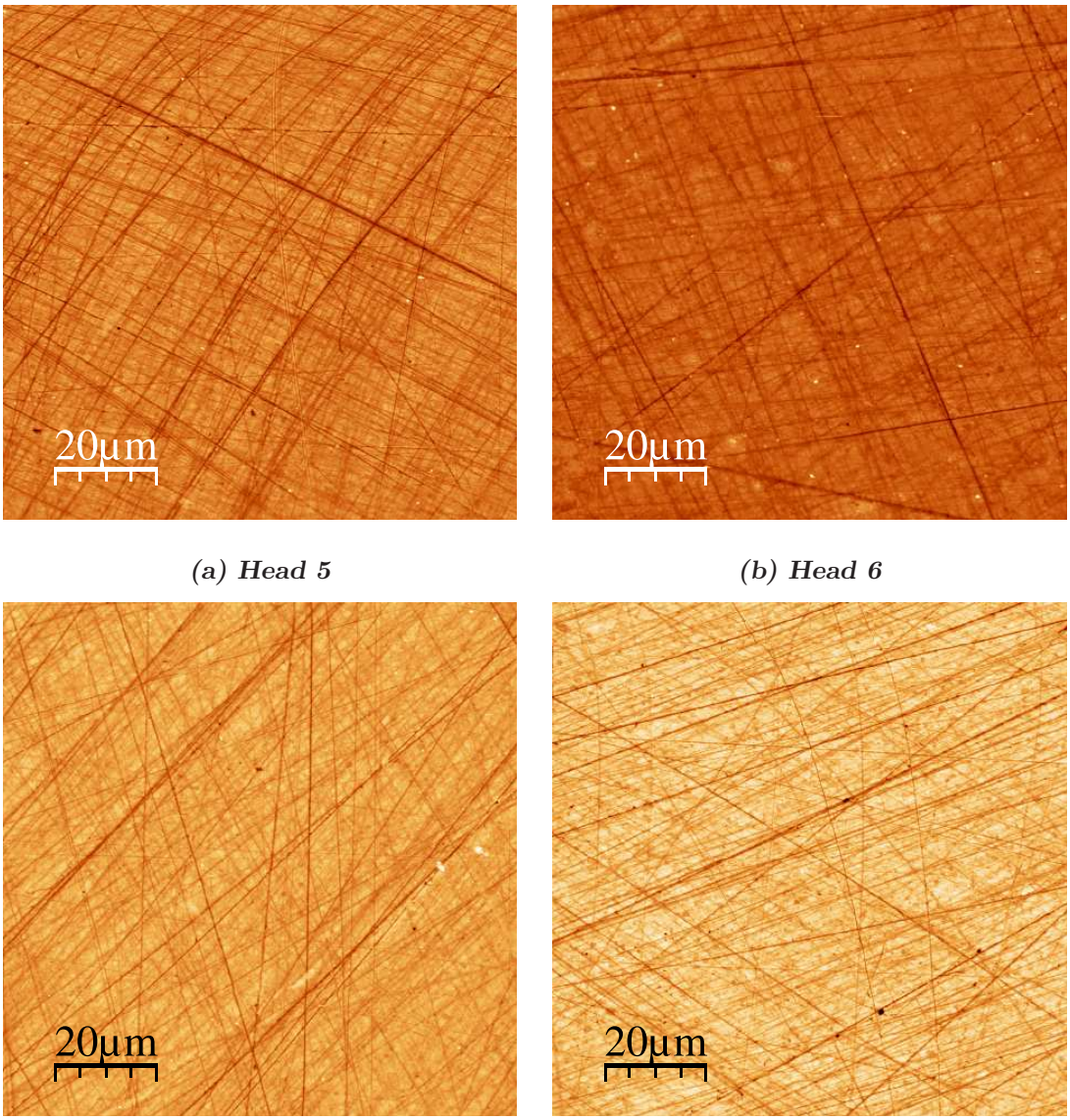

(a) Head 5 *(b) Head 6*

(c) Head 10 *(d) Head 11*

Figure 7.22: *AFM micrographs of pole of the head after 5 million cycles of wear in a standard wear simulator, showing polishing scratches similar to that found on the unworn surfaces.*

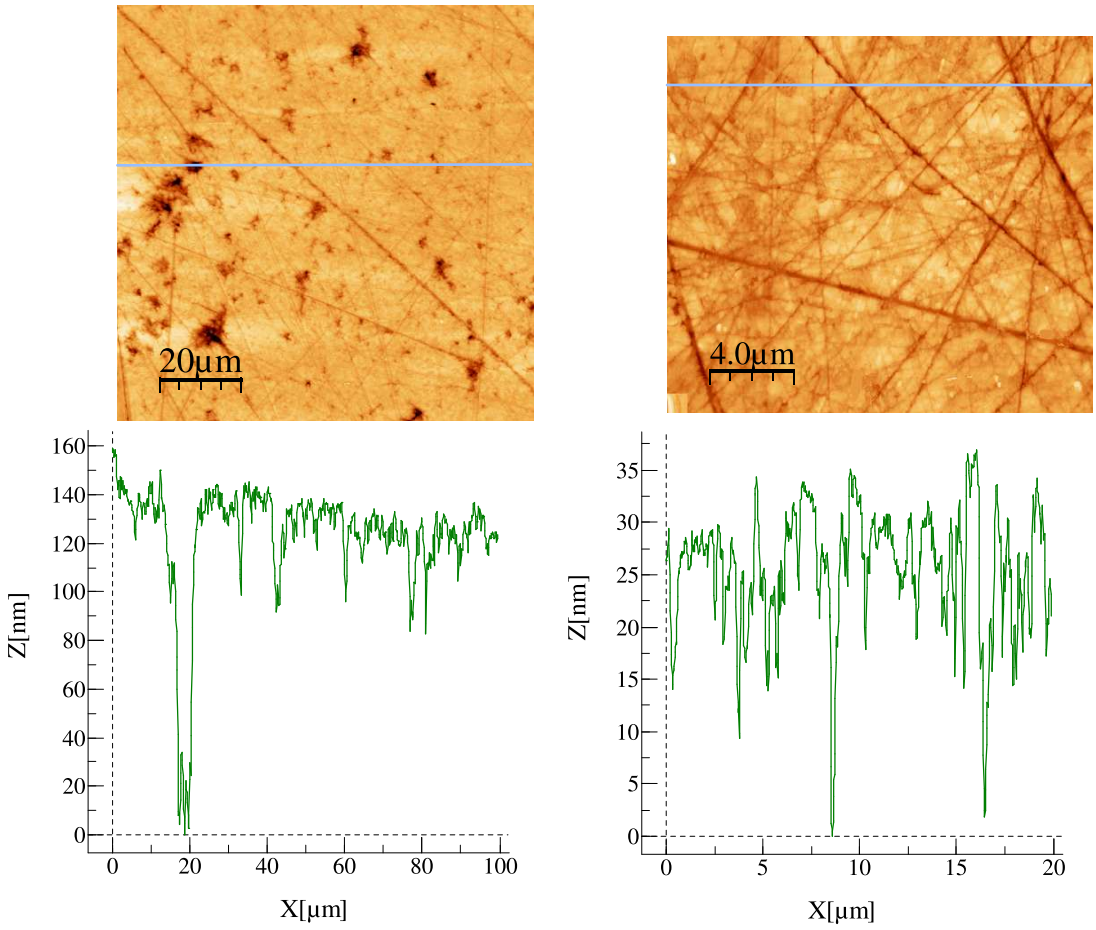

(a) Head 1 *(b) Head 11*

Figure 7.23: *AFM micrographs and line profiles of head 1 and 11 on the pole after 5 million cycles of standard wear showing similar topography to the unworn surfaces.*

7.3.4 Deposition

The white substance deposited during wear testing was stained blue using non permanent ink. This allowed the wear patch on the pole of the heads to be visualised. The blue coloured deposit surrounding the circular wear patch indicated the position between the head and cup where close contact occurred. Figure 7.24 shows the 6 heads after a 0.5 million cycles period of wear (between 4.5 and 5 million cycles of wear). This was typical of each 0.5 million cycles wear period.

No deposition was found on the loaded control joint. A clear circular wear patch was visible on the pole of the active stations with scratches running into the deposit as a result of two body of three body abrasive wear. It can be seen from these images that the majority of the metal transfer occurred outside the wear patch. Head 5 has an area of metal transfer on the pole, which is thought to have occurred during simulator setup/take down during the previous 0.5 million cycles.

(a) Head 1

(b) Head 4

(c) Head 5

(d) Head 6

(e) Head 10

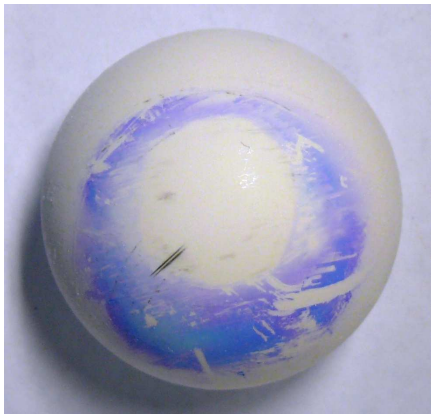

(f) Head 11

Figure 7.24: *Stained deposition after 0.5 million cycles of standard wear (total of 5 million cycles) on ZTA 38mm heads.*

Chapter 8

Results -'Microseparation' of 38 mm alumina heads against CoCrMo cups

A set of six, 38 mm diameter alumina heads and as-cast CoCrMo alloy cups were tested under 'microseparation' conditions. The components were similar to those described in Chapter 6 and were paired to give radial clearances as close to 100 μm.

Station	Head	Dimension (mm)	Cup	Dimension (mm)	Radial Clearance (μm)
1	06248-33	18.970	#6	19.065	95
2	06248-31	18.971	#2	19.073	102
3	06248-36	18.971	7	19.073	102
4	06276-05	18.969	8	19.065	96
5	06248-38	18.971	#1	19.071	100
Control	6276-07	18.969	#7	19.071	102

Table 8.1: *38 mm alumina against CoCrMo joint pairings and radial clearances for the microseparation loading pattern wear test.*

8.1 Wear Results

Wear testing was carried out under microseparation conditions which incorporated medial/lateral displacement into the swing phase of the walking cycle. Figure 8.1 shows the volume change of the alumina heads over 5 million cycles of wear, which shows the active and control stations remained close to zero throughout the test. At 5 million cycles some heads had very slightly increased in volume and some had slightly lost volume with some remaining the same volume. It was therefore concluded that the volume changes detected was as a result of environmental influences during the weighing process and not during *in vitro* simulation. The trend and magnitude of volume fluctuations were similar to that seen for the alumina heads under standard wear conditions.

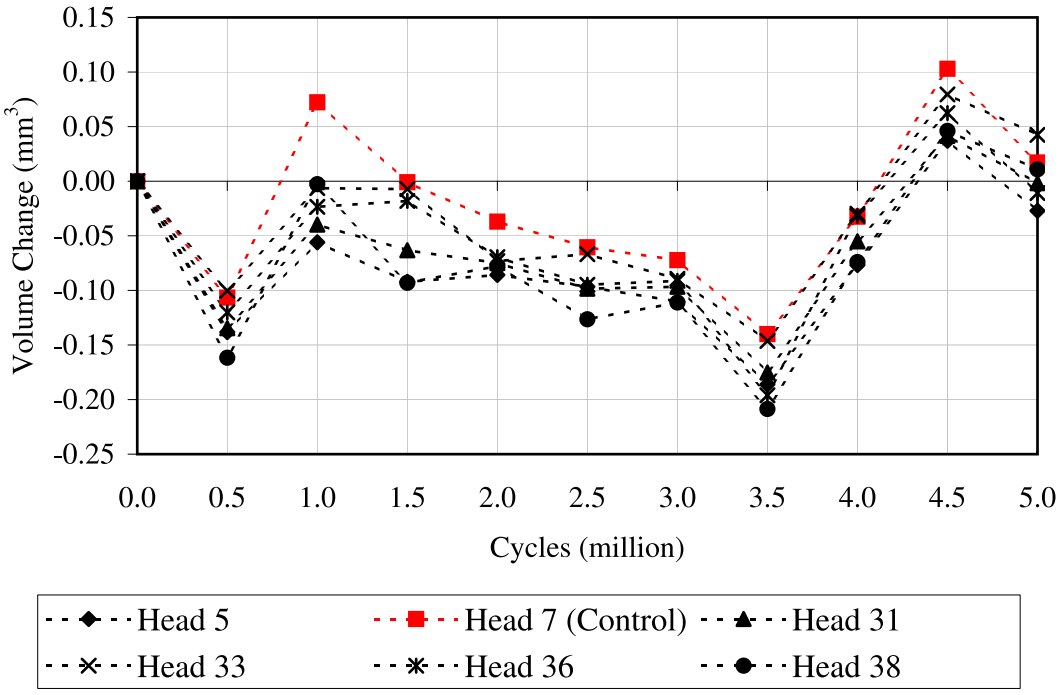

Figure 8.1: *Volume change of 38 mm alumina femoral heads under microseparation wear conditions.*

In contrast to the ceramic heads, the metallic cups (Figure 8.2) showed a considerable change in volume with number of cycles. The wear phases (i.e. running in and steady state) were not as distinct as the standard tests. The wear rates of individual cups varied between 0.5 million cycles weighing points, therefore it was

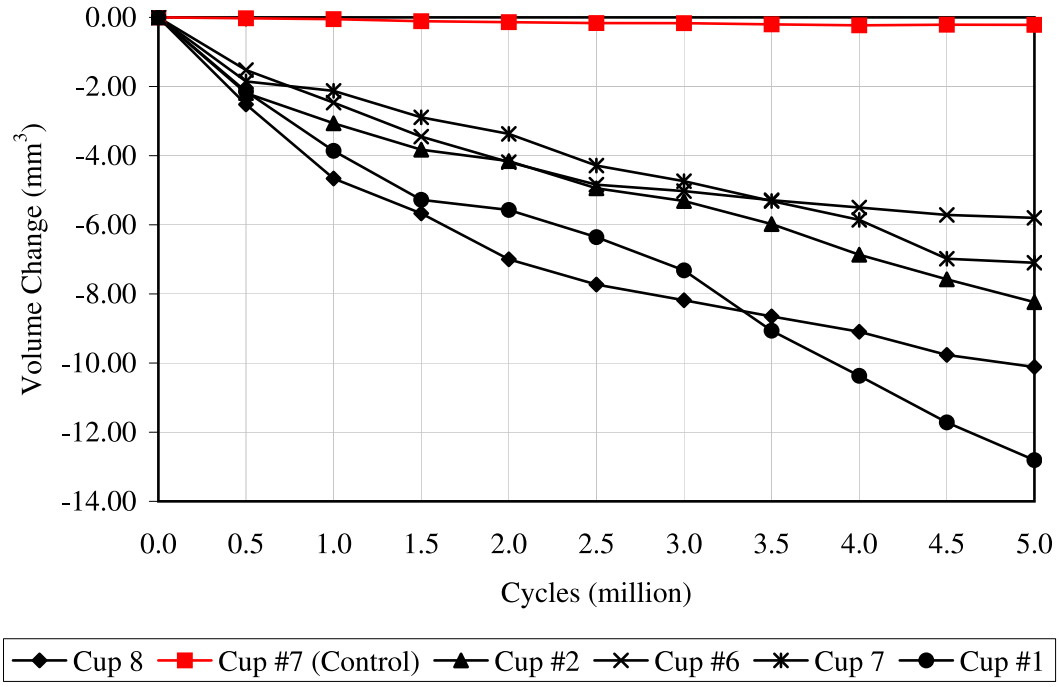

Figure 8.2: *Volume change of 38 mm as-cast CoCrMo acetabular (from alumina test) cups under microseparation wear conditions.*

difficult to determine a fair wear rate for this data. Figure 8.3 shows the corrected head and cup volume change taking account of the loaded control which highlights the difference in volume change between the ceramic and metal components. The wear of the ceramic components was negligible when compared with the metal cups as shown in Figure 8.3.

Although distinct running in and steady state wear phases were not present with these data, it was decided that a relatively stable wear rate was established after 1 million cycles. Therefore to maintain similar analysis compared with the standard alumina test, a running in wear rate between 0-1 million cycles and a steady state wear rate between 1-5 million cycles was calculated. Individual wear rates were calculated for each metallic cup, as shown in Table 8.2 and an overall average wear rate for all 5 active stations was determined. R^2 values are presented to show the amount of variability accounted for by the regression line.

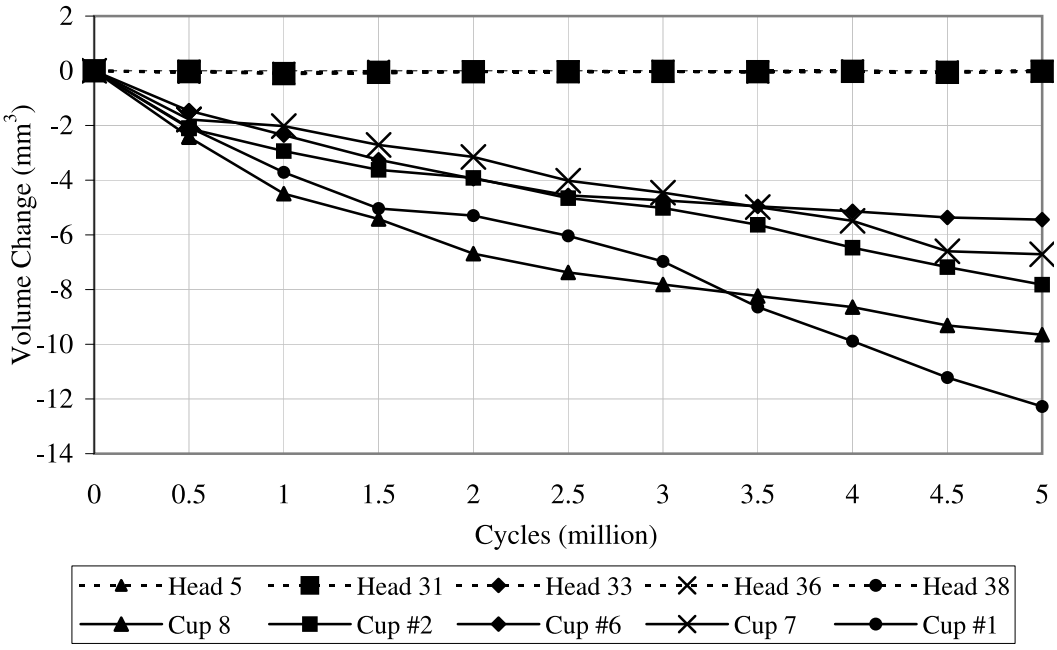

Figure 8.3: *Volume change of 38 mm alumina:CoCrMo under microseparation wear conditions (taking account of loaded soak control).*

Cup	RI Wear Rate (mm^3/mc)	r^2	SS Wear Rate (mm^3/mc) 1-3MC|1-5MC	r^2
# 1	-3.7141	0.99	-1.5033 |2.1522	0.96/0.98
# 2	-2.9361	0.94	-1.0390|-1.2096	0.98/0.99
# 6	-2.3537	0.98	-1.2140|-0.7158	0.95/0.88
7	-2.0216	0.84	-1.2358|-1.2019	0.99/0.99
8	-4.4945	0.99	-1.7000|-1.2356	0.97/0.96

Table 8.2: *Individual 38 mm CoCrMo cup wear rates under microseparation wear conditions(alumina test).*

Considerable wear rates were found for both the running in and steady state wear. It is important to note that in this case the wear rates were greatly dependent on the number of cycles tested. If testing were complete by 3 million cycles rather than 5 million cycles, the steady state wear rate would have differed for a number of stations as shown in Table 8.2. For example cup #6 has nearly half the wear rate when taken between 1-3 million cycles compared with 1-5 million cycles.

Average wear rates for the 5 active stations, taking running in between 0-1 million cycles and steady state between 1-5 million cycles, produced wear rates of 3.04 $\pm$0.673 mm^3/million cycles (mean 95% C.I.) and 1.35 $\pm$0.154 mm^3/million cycles respectively. As with the previous tests, the ceramic heads were considered to have zero wear.

8.2 Friction Testing

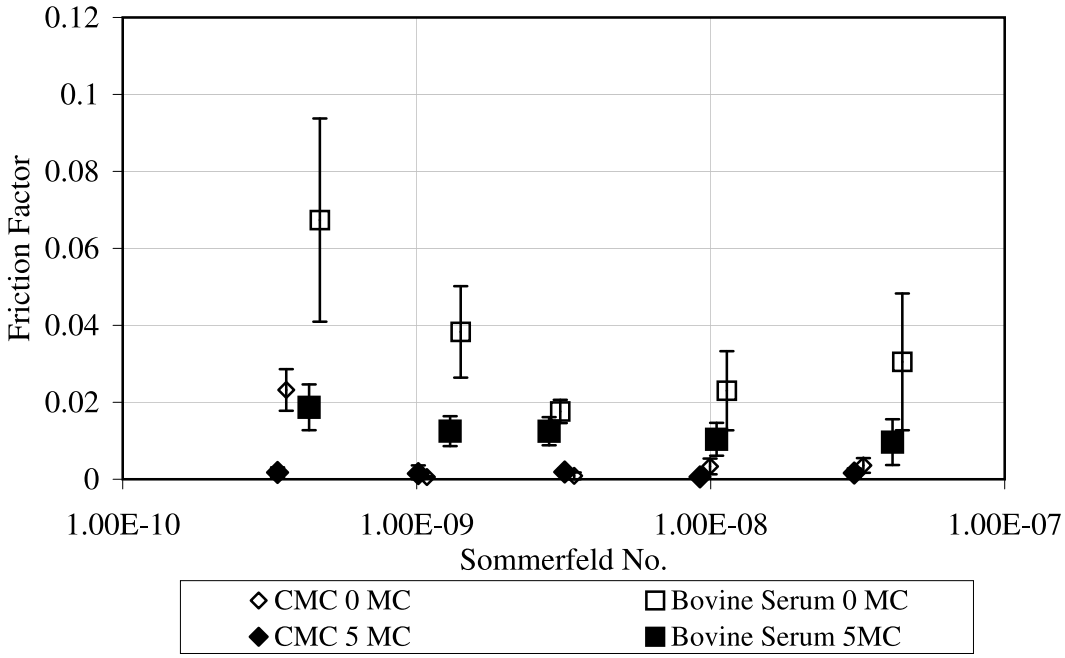

Figure 8.4: *Stribeck plot of unworn 38mm alumina: CoCrMo and after 5 million cycles of wear (MXS conditions) tested under water based and bovine serum based CMC fluids as lubricants.*

Two bearing couples were friction tested (Head 5/Cup 8 (Figure 8.4) and Head 31/Cup 2 (Figure 8.5)) initially and after 5 million cycles under microseparation

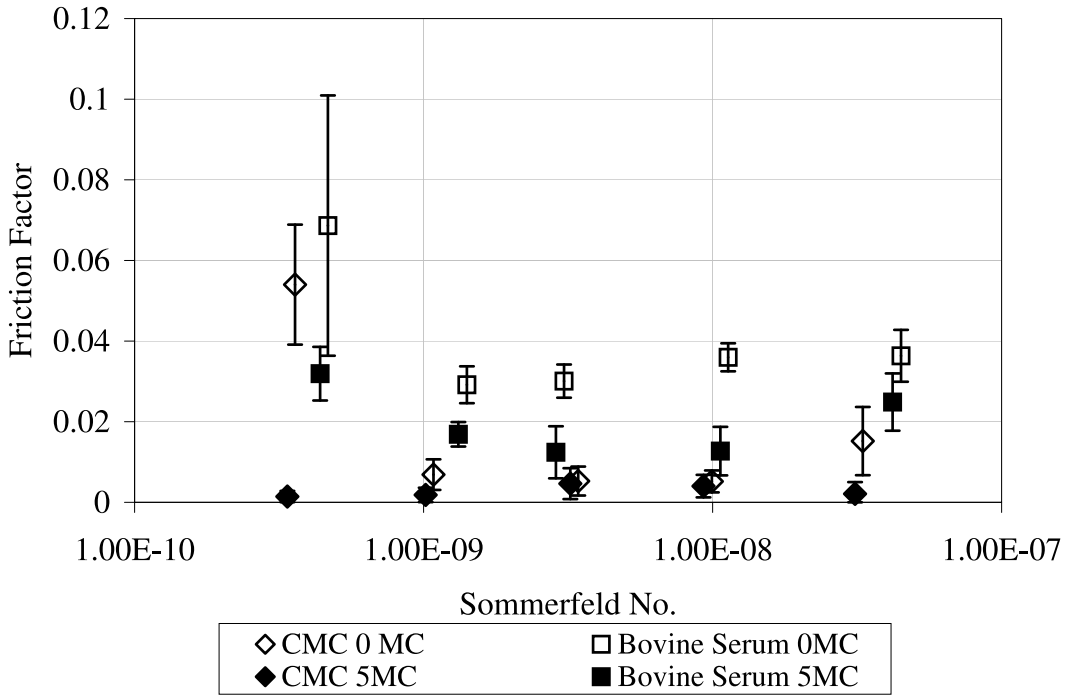

Figure 8.5: *Stribeck plot of unworn 38mm alumina: CoCrMo and after 5 million cycles of wear (MXS conditions) tested under water based and bovine serum based CMC fluids as lubricants.*

wear testing. Both bearings showed similar results. The initial friction factors indicated the joints were working close to full fluid film lubrication, showing peaks in friction factor at the extreme viscosities (0.001 Pa s and 0.1 Pa s) with a minimum friction factor at approximately 0.01 Pa s. In both cases when water based CMC lubricants were used, the friction factors were lower than when bovine serum based CMC fluids were used. After 5 million cycles of a drop in friction factor was seen from all bovine serum based lubricants. The CMC based lubricants showed similar very low friction factors at 0 and 5 million cycles.

As with the previous testing, theoretical calculations were carried out to determine the minimum film thickness and corresponding lambda value as shown in Table 8.3.

Initially the results showed a lambda value greater than 3, suggesting the joints would operate in full fluid film lubrication which was supported by the shape of the curve and low friction factors found from experimental results. However, theoretically the results showed the lambda value to become less than 3 ($\lambda = 2.7$) which

Cycles (millions)	Head Rms (μm)	Cup Rms (μm)	H min (μm)	λ	Friction factors CMC*/BS**
0	0.008	0.007	0.07	>3	0.054/0.067[1]
					0.023/0.067[2]
0.5	0.008	0.023	0.07	= 2.8	-
2.5	0.008	0.020	0.07	>3	-
5	0.008	0.024	0.07	= 2.7	0.0014/0.032[1]
					0.0018/0.019[2]

* CMC η=0.001 Pa s^{-1}, **BS η=0.0013 Pa s^{-1}

[1] = head 31, cup 2, [2] = head 5 cup 8

Table 8.3: *Theoretical minimum film thickness and lambda values for 38 mm alumina against CoCrMo under microseparation conditions.*

would suggest mixed lubrication. The experimental results showed a decrease in friction factor for the bovine serum after 5 million cycles of wear, and similar results for the CMC lubricants suggesting the lubrication had remained similar to the initial results or had slightly improved as lower friction factors were recorded. A discussion relating theoretical lambda values to experimental results, and the limitations can be found in Chapter 13.

8.3 Edge Contact

Edge contact occurred between the head and the rim of the cup as a result of separation and relocation during simulation. Each active station showed one flattened lip often with a second superimposed on the top of the original lip. This is illustrated in Figure 8.6(b). The head showed three areas of interest, namely, the wear on the pole, a region of metal transfer and an area of stripe wear. The metal region was as a result of dislocation of the head, whilst the stripe region was due to impact during relocation. These are highlighted in Figure 8.6(a). The area of stripe wear on the head was only discovered after 5 million cycles of wear therefore data is only

available for this period.

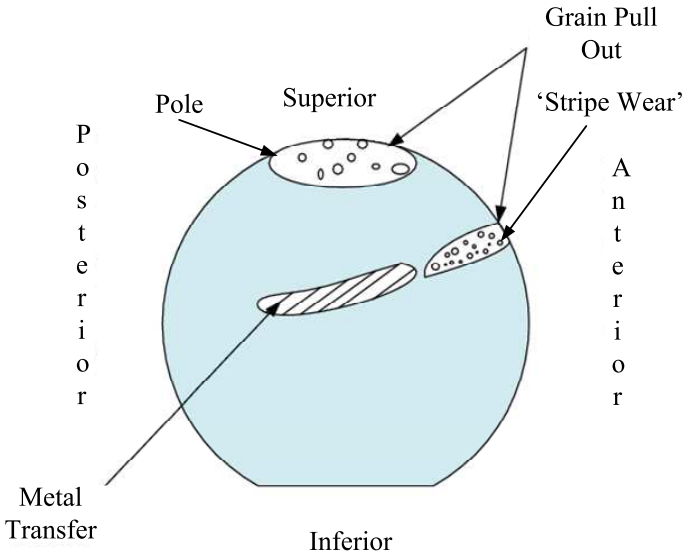

(a) Regions of wear on the alumina head

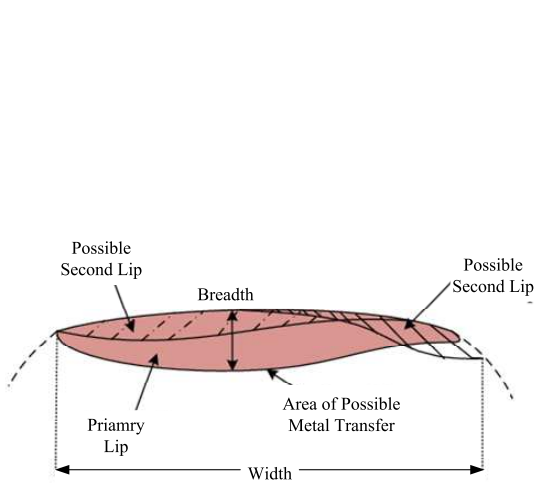

(b) Cup flattened lip

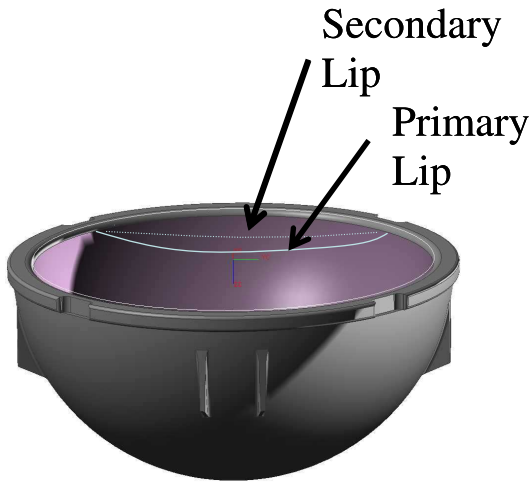

(c) Cup flattened lip

Figure 8.6: *Schematic diagram showing the different regions of wear and metal transfer on the ceramic head and the flattened lip region on the rim of the metal cup, after wear under microseparation conditions.*

The flattened lip area was measured periodically throughout testing. A micrometer was used to measure the width and breadth (see Figure 8.6(b)). The size of the lip did not considerably increase with number of cycles. All cups showed similar width and breadth measurements. Accurate measurement of the lip was difficult, especially on the posterior side of the cup (as viewed while positioned in the simula-

tor) as the edge was not clearly defined in some cases. Figure 8.7 shows the results of these measurements.

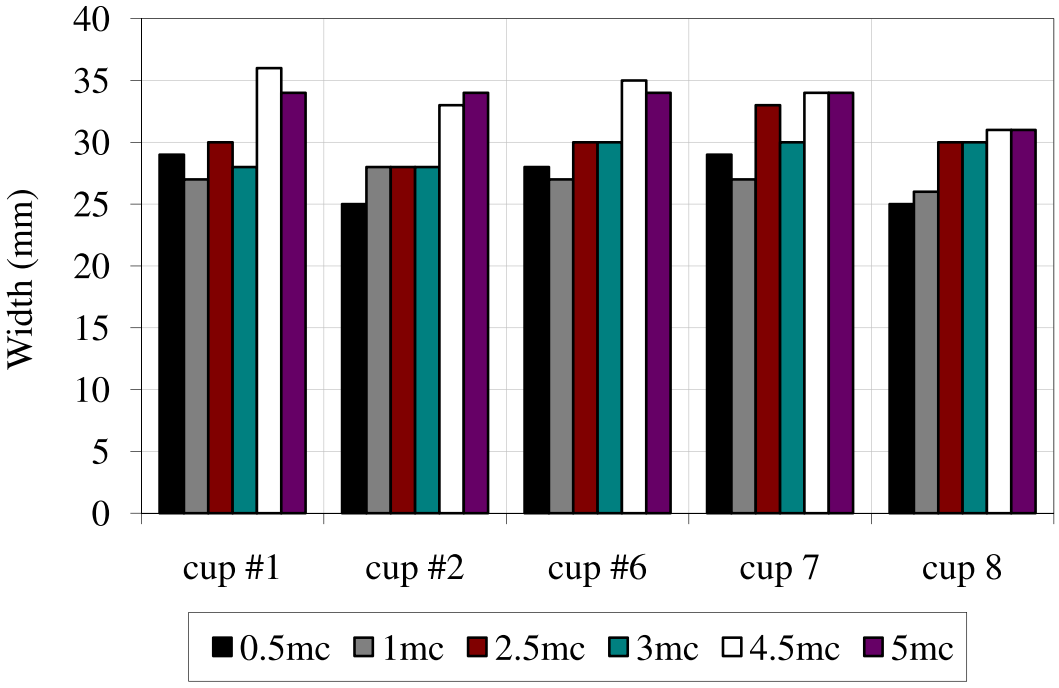

(a) Width

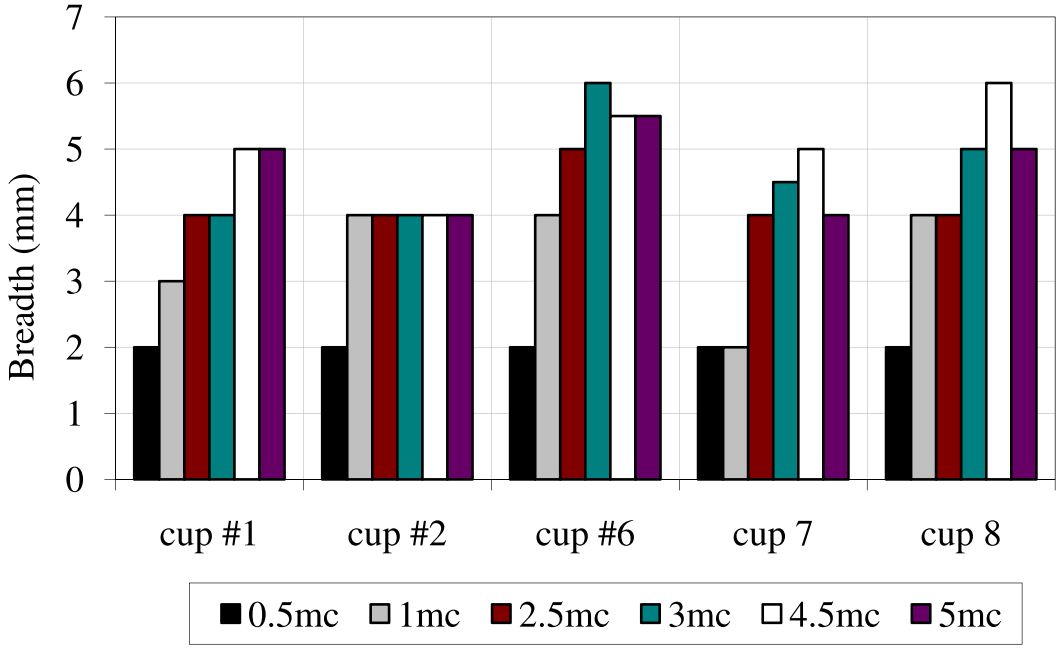

(b) Breadth

Figure 8.7: *Dimensions of the flattened lip which formed on the metallic cup due to edge contact during the 38 mm alumina microseparation test*

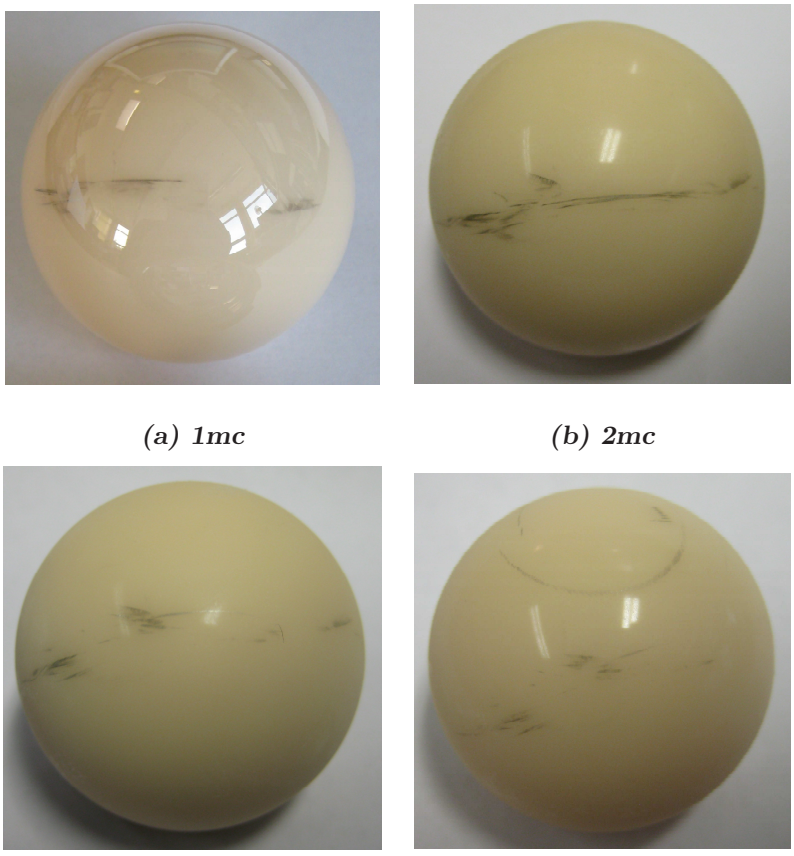

(a) 1mc *(b) 2mc*

(c) 3mc *(d) 5mc*

Figure 8.8: *Digital images showing the progression of metal transfer with number of cycles of a typical alumina head. Metal transfer is thought to be as a result of dislocation of the head from the cup when the hip is extended.*

Digital images were taken to show the metal transfer on the head (Figure 8.8) and the flattened lip on the cup (Figures 8.9 and 8.10). The metal transfer on the head changed as the wear progressed, and the metal was transferred and removed. The lip was visible by eye (see Figure 8.11) however the edges became less distinguishable from the main surface of the cup as the test progressed. Although the width and breadth only increased slightly with number of cycles, it is likely that an increase in the depth (not measured) was the cause of the observed increase in wear rate compared with the standard wear test. A dull patch, possibly a mixture of deposit and metal particles, was often observed on the edge of the flattened lip. This is shown in Figure 8.10.

(a) 1mc *(b) 2mc*

(c) 3mc *(d) 5mc*

Figure 8.9: *Digital images showing the progression of flattened lip formation on the metallic cup over the progression of the wear test. The flattened lip has been highlighted with a non permanent pen.*

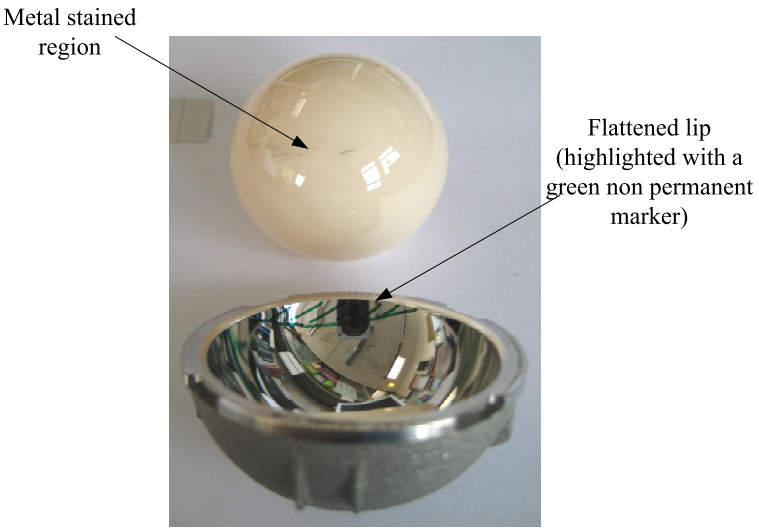

Figure 8.10: *Annotated image showing the flattened lip on the metallic cup and metal transfer on the ceramic. The lip has been highlighted with a non permanent pen.*

(a) 1mc ***(b) 2mc***

Figure 8.11: *Digital images showing the flattened lip (without markings using a non permanent pen) and a dull patch found on the edge of the lip (see arrow).*

8.4 Surface Analysis

8.4.1 Non Contacting Interferometry

Non contacting interferometry was used to investigate the change in rms roughness and skewness of the surfaces, the results of which are shown in Figures 8.12 and 8.13. Microseparation of the head and cup during the swing phase of the walking cycle resulted in edge contact and a flattened lip formation on the rim of the cup. Limited access to the lip contact area resulted in the measurements being taken within the wear patch as with the standard walking cycle test components. The rms roughness of the wear patch of the cups significantly increased between the first 0.5 million cycle wear phase after which the roughness was not found to change considerably up to 5 million cycles of wear. The control cup was also found to increase in roughness after 0.5 million cycles which was thought to be due to impact between the head and cup when the load was decreased during the swing phase of the test resulting in separation of the control components. When the load increased during the stance phase, the metallic surface became damaged with carbide fracture and removal, even though motion was not occurring. In contrast the roughness of the pole of the ceramic head did not change throughout the test.

The skewness of the cups became considerably more negative as the test progressed. Initially the unworn surfaces were positively skewed due to the as-cast structure, however by 0.5 million cycles, the skewness of the cups was negative, and became more negatively skewed as the test progressed. The skewness of the ceramic heads followed a similar trend to the cups increasing between 0-2.5 million cycles, however little change occurred between 2.5 and 5 million cycle of wear. Larger error bars were found showing the heterogeneous nature of the structure.

Three regions of interest on the heads were measured after 5 million cycles of wear, namely the pole, the metal stained region and an area of wear at approximately 33 degrees to the horizontal on the anterior side of the head. The results of these measurements are shown in Figure 8.14. The stripe region (and the pole) had holes resulting from removed grains, as will be seen from the AFM micrographs shown in section 8.4.4. The rms roughness was marginally greater in the metal stained and

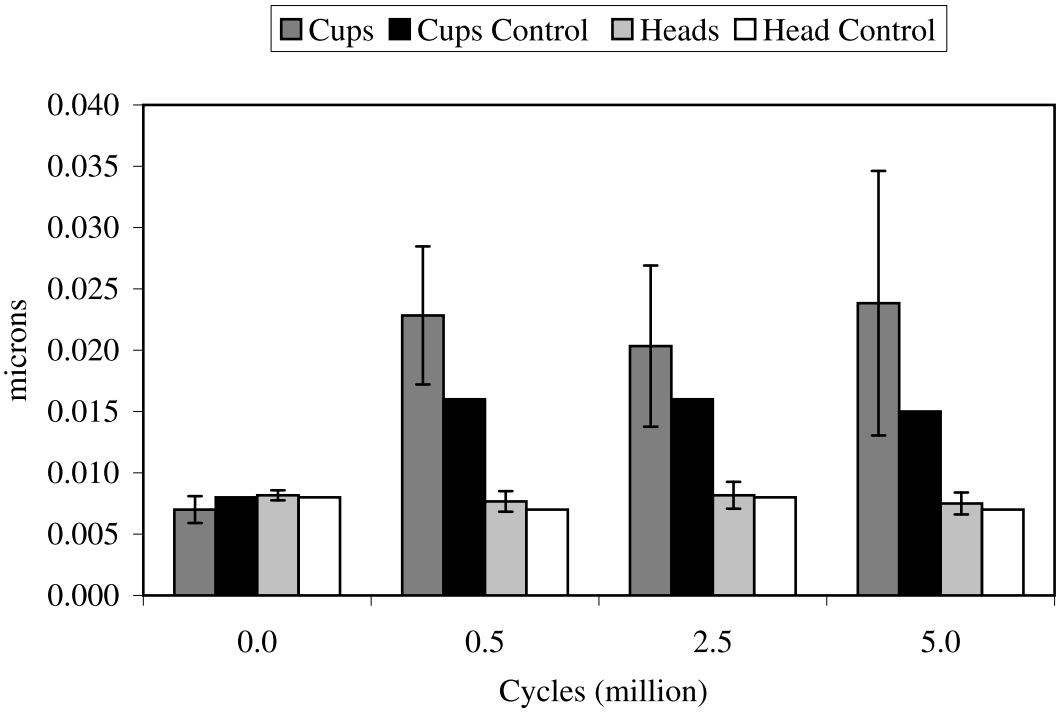

Figure 8.12: *RMS roughness values for the 38mm alumina test carried out under microseparation conditions.*

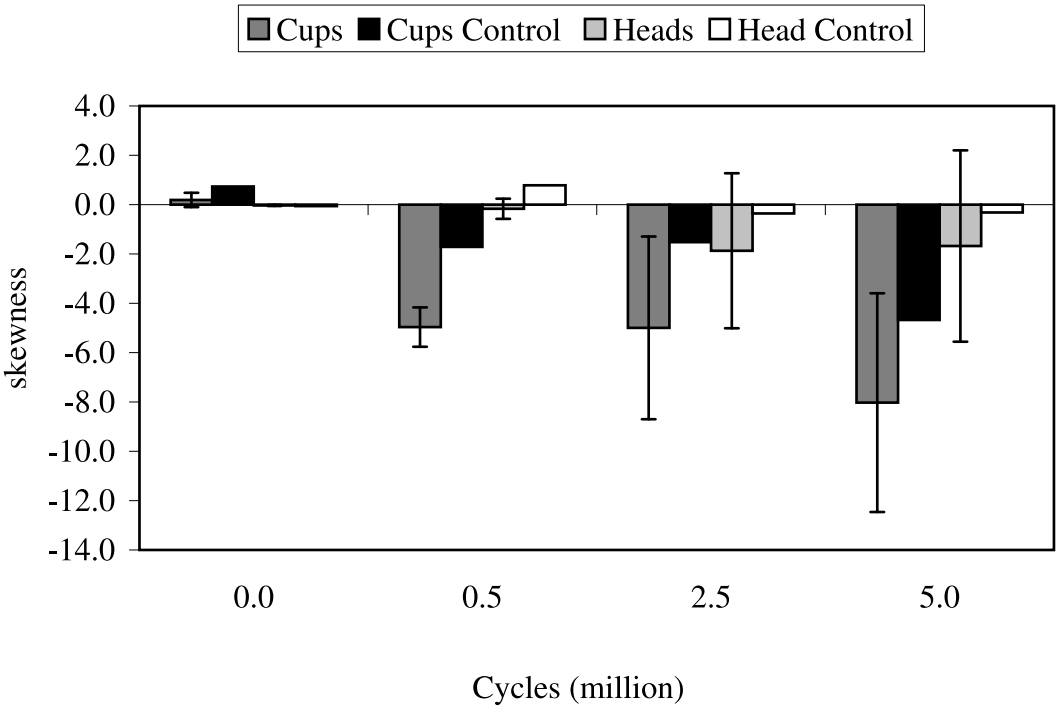

Figure 8.13: *Skewness values for 38mm alumina test carried out under microseparation conditions.*

stripe wear region compared with the pole although the standard deviation bars overlapped. A noticeable increase in standard deviation for the roughness values was observed in the measured regions away from the pole due to the heterogeneous nature of the impact regions. The skewness in the three regions of interest varied as expected with a positive skewness found in the metal region and a negative skewness on the pole and stripe wear region, resulting from grain removal in these areas.

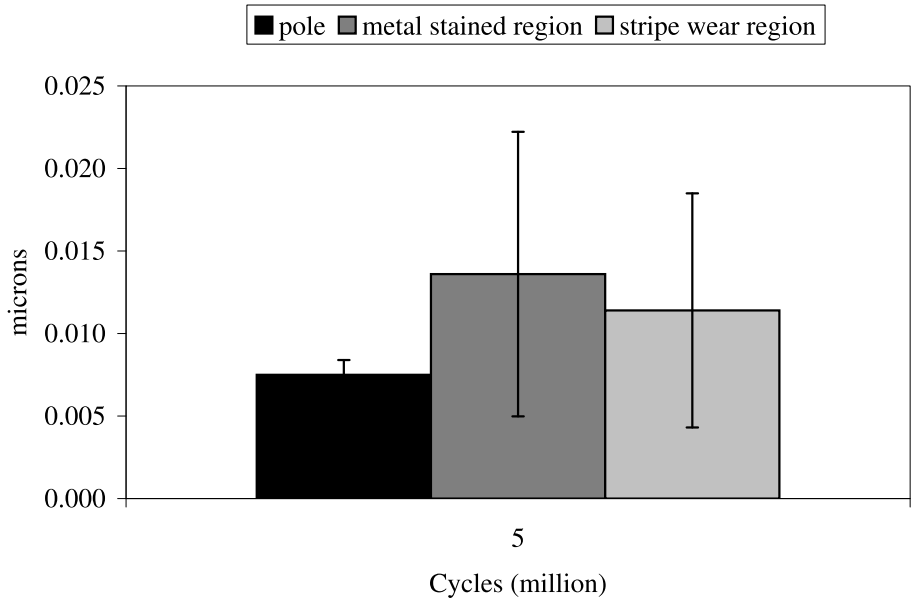

(a) RMS roughness

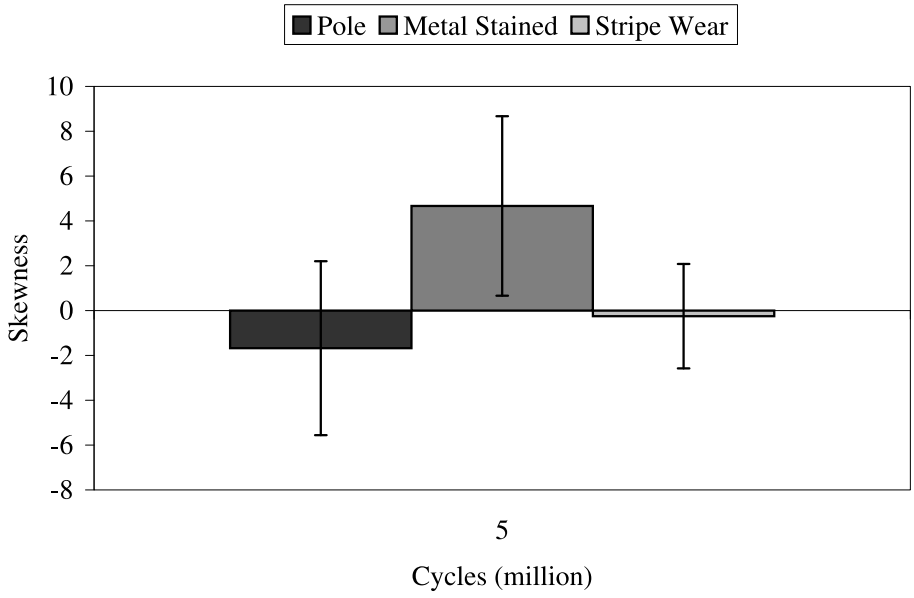

(b) Skewness

Figure 8.14: *Comparison of rms roughness and skewness values on the pole of the head, in the metal stained region and the stripe wear region, after 5 million cycles of wear under microseparation conditions.*

8.4.2 Optical Microscopy

Optical micrographs of both the wear track and the lip which formed due to edge contact between the head and cup, were taken periodically throughout testing. The images of the unworn cups were the same as those found for the standard Alumina and ZTA tests. Micrographs were taken at 0.5, 1.0, 1.5, 2.5 and 5 million cycles.

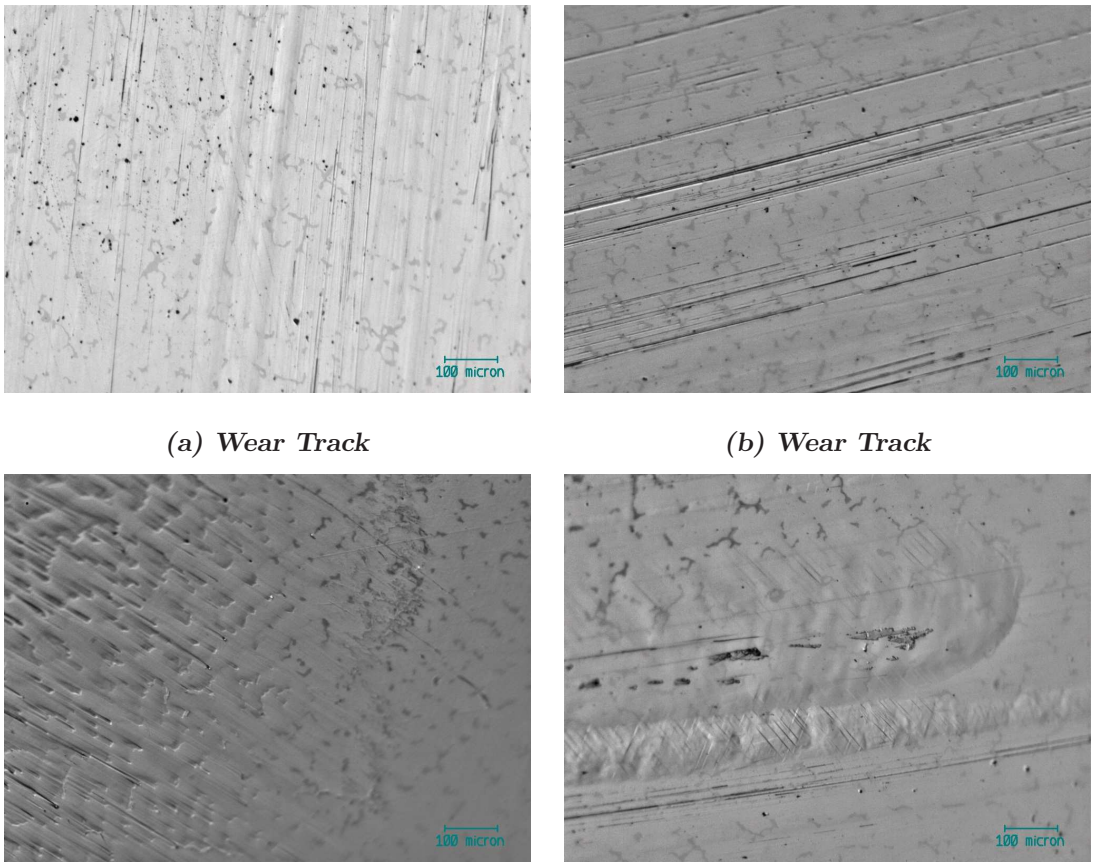

(a) Wear Track ***(b) Wear Track***

(c) Edge Wear Track ***(d) Edge Wear Track***

Figure 8.15: *Optical images taken of the as-cast CoCrMo cups (alumina microseparation test)after 0.5 million cycles. The dominant features of each sub figure are; (a) pitting, adhesive and abrasive wear, (b) abrasive wear, (c) deformation of the matrix through adhesive wear or carbide removal, (d) regular sharp edged deformation on the edge of the wear track.*

The micrographs in the wear track of the cups after 0.5 million cycles of wear (see Figure 8.15) showed significant damage to the surface topography. Smoothing

of the carbides and abrasive wear was evident in the flexion/extension direction. On the edge of the wear track (see Figure 8.15) regular impact marks were evident as a result of head displacement and relocation. Regions of 'pulled' or deformed matrix material could also be seen at the edge of the wear track showing plastic deformation of the matrix material occurred during simulation.

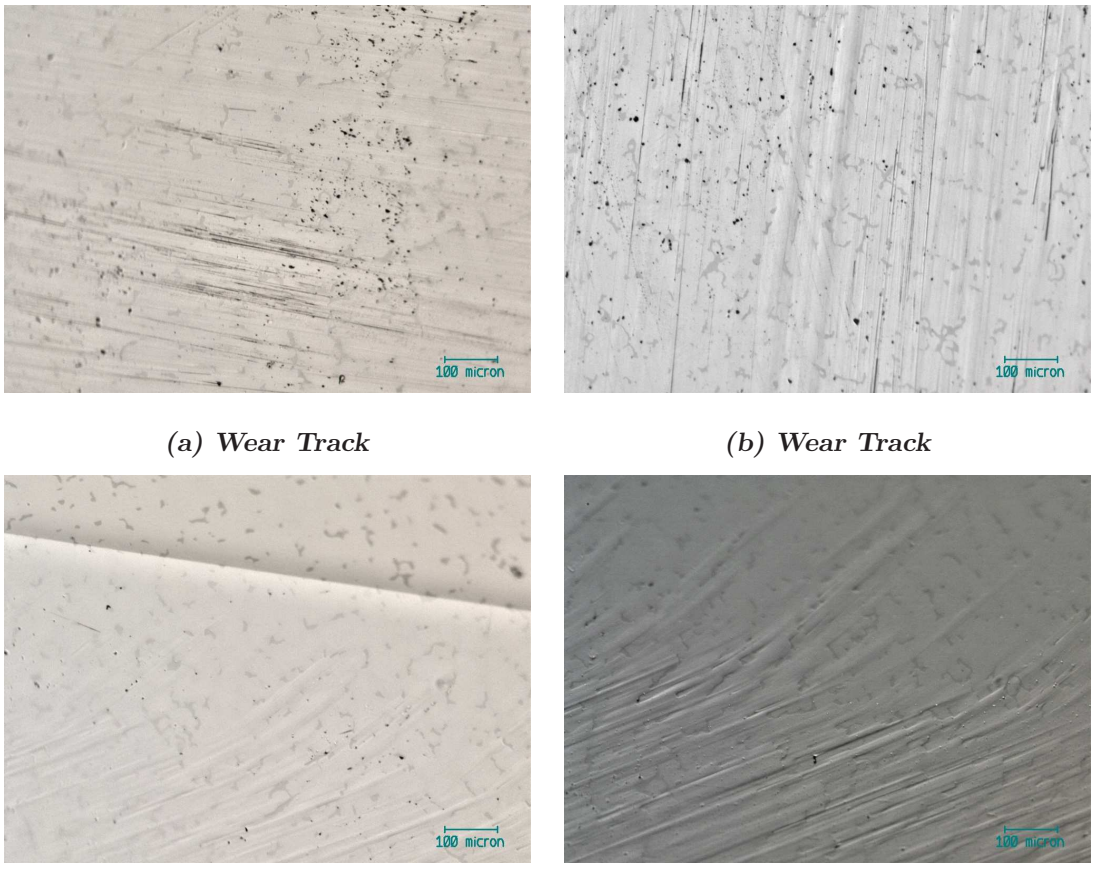

(a) Wear Track ***(b) Wear Track***

(c) Edge Contact Region ***(d) Edge Contact Region***

Figure 8.16: *Optical images taken of the as-cast CoCrMo cups (alumina microseparation test) after 1.0 million cycles. The dominant features of each sub figure are; (a) pitting and 'comet tail' adhesive wear, (b) pitting, abrasive and adhesive wear, (c)deformation of the surface with little pitting of abrasive wear, (d)deformation of the matrix and adhesive wear leading to abrasive wear.*

After 1 million cycles of wear (Figure 8.16), the wear track showed similar features of abrasive scratching, smoothed carbides and pitting. The surface was found to be undulating in nature, with raised bands possibly as a result of plastic de-

formation during relocation of the head. The edge contact region showed a clear boundary between the flattened lip and the main body of the cup (Figure 8.16(c)). Both the wear track (especially the superior side) and the lip showed the 'pulled' matrix possibly as a result of poor lubrication resulting in adhesive contact between the head and cup which pulled the matrix in the direction relocating the matrix as it moved. Significant contrast was seen between the carbides in the lip region and the unworn material, highlighting the carbides had been worn smooth or fractured and removed.

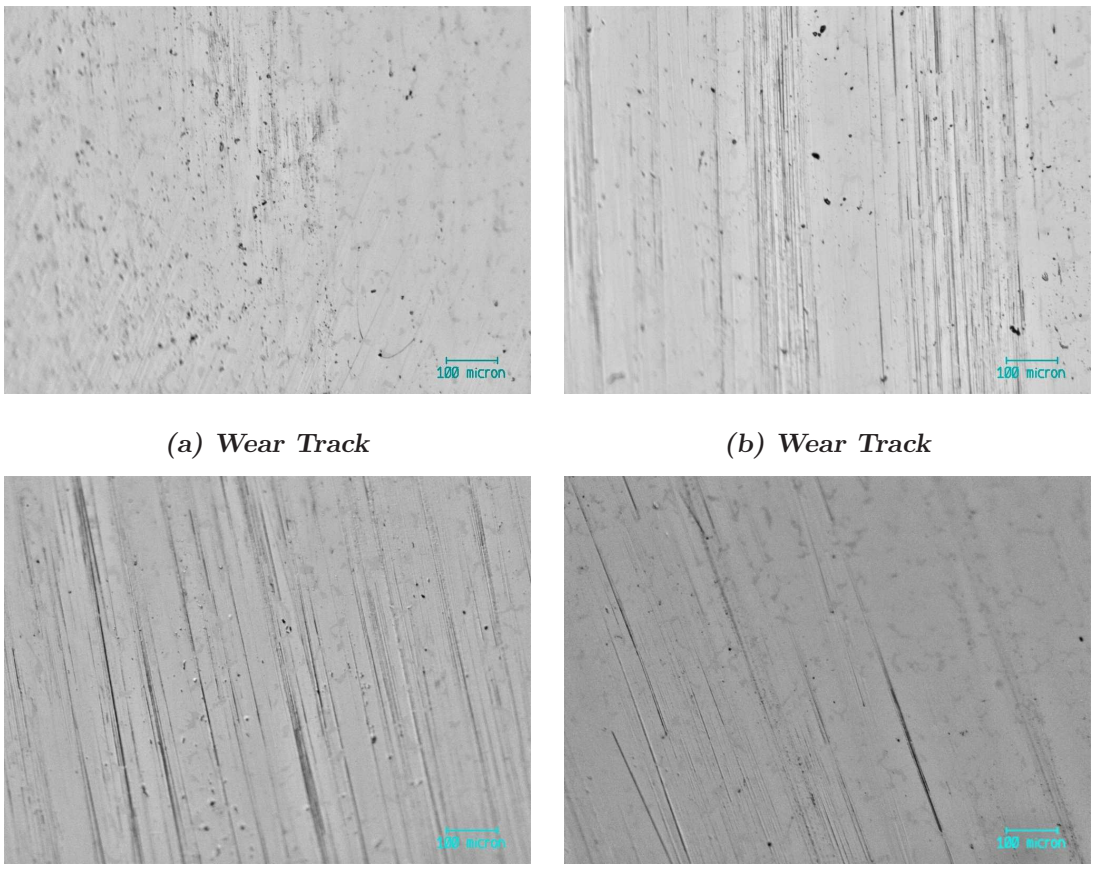

(a) Wear Track ***(b) Wear Track***

(c) Wear Track ***(d) Wear Track***

Figure 8.17: *Optical images taken of the as-cast CoCrMo cups (alumina microseparation test) after 1.5 million cycles in the wear track. The dominant features of each sub figure are; (a) pitting, (b) pitting, abrasive and adhesive wear, (c) pitting and abrasive wear, (d) abrasive and adhesive wear.*

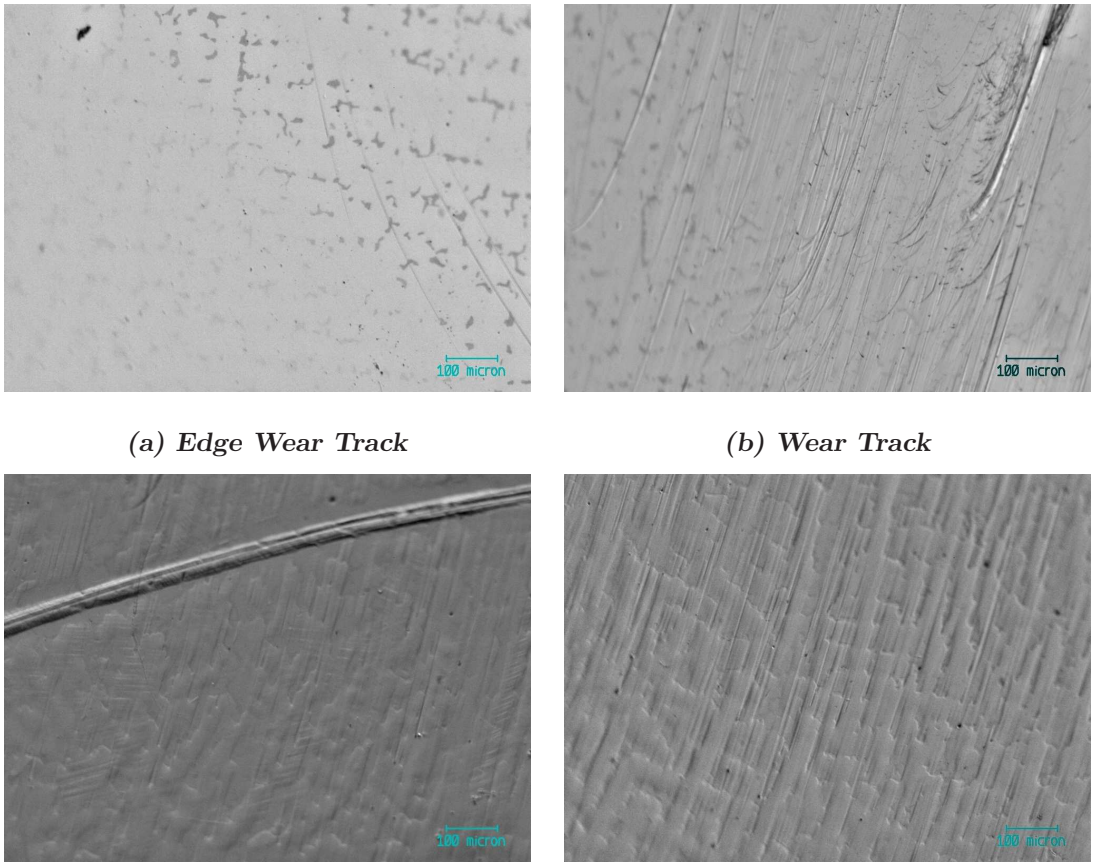

(a) Edge Wear Track ***(b) Wear Track***

(c) Wear Track ***(d) Wear Track***

Figure 8.18: *Optical images taken of the as-cast CoCrMo cups (alumina microseparation test) after 1.5 million cycles showing isolated features. The dominant features of each sub figure are; (a) contrast between worn and unworn carbides at the edge of the wear track, (b)'wispy' abrasive wear, (c) raised feature and deformation of the surface, (d) adhesive wear of the carbides and matrix resulting in deformation of the surface.*

As with previous cycles after 1.5 million cycles of wear under microseparation conditions, a heterogeneous surface topography was found. Generally the damage in regions within the central wear patch, caused by the pole of the head, showed abrasive wear and pitting as shown in Figures 8.18 and 8.17. However isolated features were also visible within the wear track such as the 'pulled' matrix material as seen in previous images. Again regular impact marks could be seen (Figure 8.18(c)) be seen in the superior region of the cup as a result of head re-location. 'Wispy' abrasive scratches were noticeable on the superior region as a result of possibly ceramic or carbide third body particles in the lubricant.

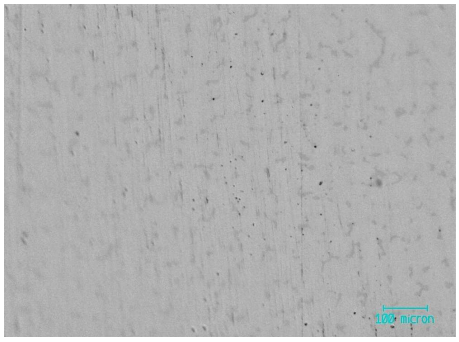

(a) Edge contact lip

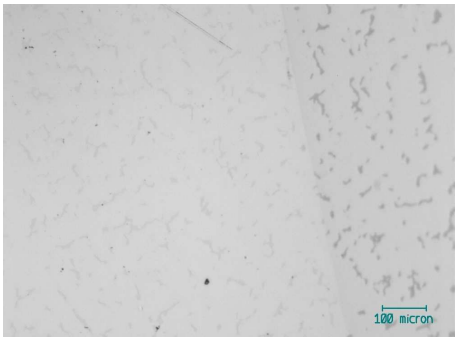

(b) Boundary between lip and unworn area

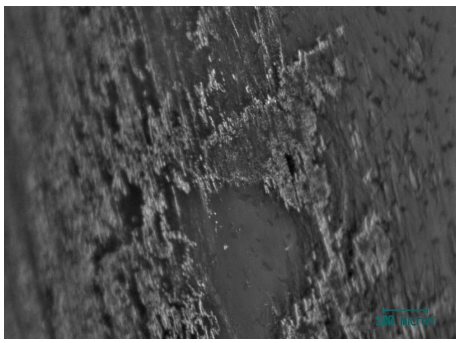

(c) Transfer on the edge of the lip

(d) Transfer within the lip

Figure 8.19: *Optical images taken of the as-cast CoCrMo cups (alumina microseparation test) after 1.5 million cycles showing the region of edge contact. The dominant features of each sub figure are; (a) smooth unfeatured surface, (b) distinct contrast between the worn and unworn carbides at the edge of the flattened lip, (c) dull transfer on the edge of the flattened lip, (d) dull transfer within the flattened lip.*

Metal transfer was also evident in certain areas along the boundary between the lip and unworn material (Figure 8.19(c)) which may be a result of repeated transfer of metal between the head and cup during repeated impacts. On one of the active heads, metal transfer was also seen within the flattened lip area (Figure 8.19(d)).

Micrographs taken after 2.5 and 5 million cycles of wear showed similar features to those reported previously. The central wear patch showed a heterogeneous topography with abrasively worn areas and smooth, relatively un-damaged, areas within the same cup. Pitting of the metal was also evident in places. The 'pulled' matrix was found in the superior region of the cup along with the 'wispy' third body wear features. As previously found, metal transfer was seen on the edge of the flattened lip. More damage was seen on some areas within the flattened lip compared with images from previous cycles however it must be noted that the surfaces were extremely heterogeneous in nature and therefore it is difficult to generalise over the 5 active cups. A second lip was found to form on top of the primary lip on some cups. This feature is shown in Figure 8.20

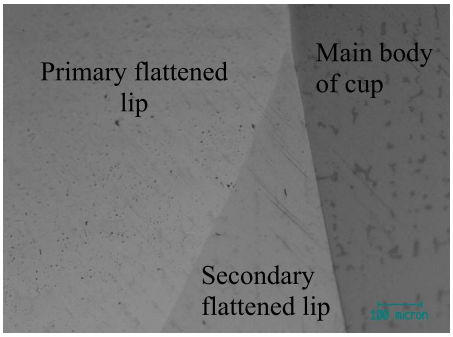

Figure 8.20: *Optical image taken at 5 million cycles showing second lip formation on top of the first lip as a result of edge contact.*

8.4.3 Scanning Electron Microscope

SEM images were taken of the metallic cup to investigate the change in structure of the carbides within the matrix. Micrographs of the unworn surface show porous carbides within the continuous matrix as shown in Figure 8.21. The carbides appeared to be flat within the matrix.

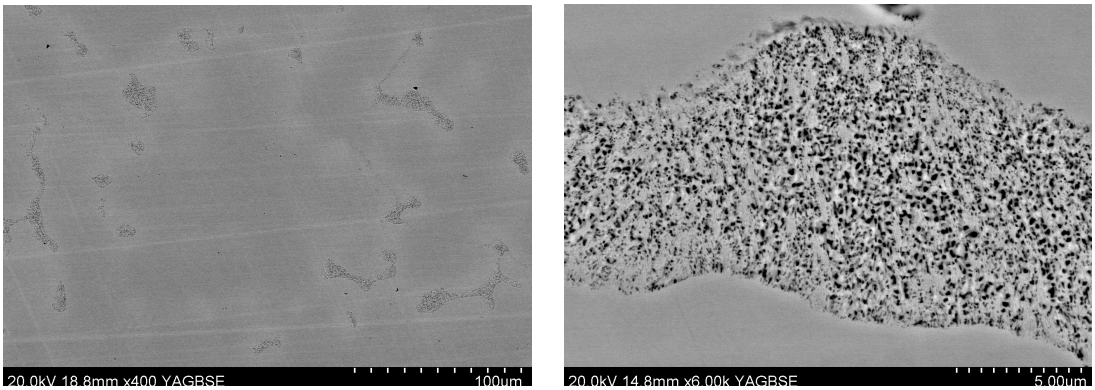

(a) *(b)*

Figure 8.21: *SEM micrographs of unworn metallic surfaces showing flat porous carbides within matrix. An open porous structure was found.*

The flattened lip caused by edge contact showed similar flat carbides, however the porous structure appeared smudged as a result of the head sliding into the cup. An example of this can be seen in Figure 8.22.

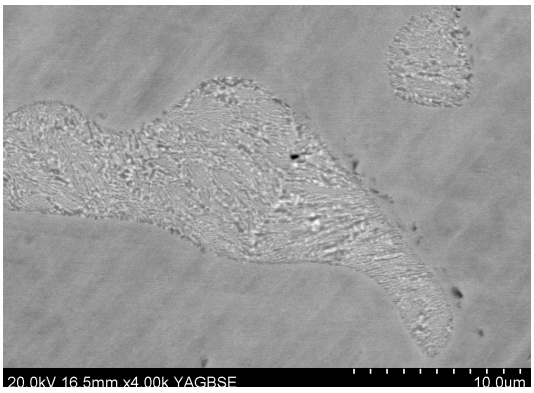

Figure 8.22: *SEM micrograph of a magnified carbide within the flattened lip on the metallic cup showing 'smudging' of the porous structure due to edge contact with the head.*

Partial fracture of the carbides was seen within the wear patch. This can clearly be seen in Figure 8.23. The porous structure can be seen deep within the matrix material. The majority of carbides were a similar level to the matrix material. Scratches were seen running through the carbides therefore the abrasive material must have been of similar or greater hardness suggesting they were bits of alumina or carbide . The majority of the fractured carbides did not appear to have a corresponding abrasive comet tail suggesting the particle was removed and taken away from the origin through the lubricant, rather than becoming attached to the opposing surface and coming indented into the surface which would have resulted in an abrasive wear scratch.

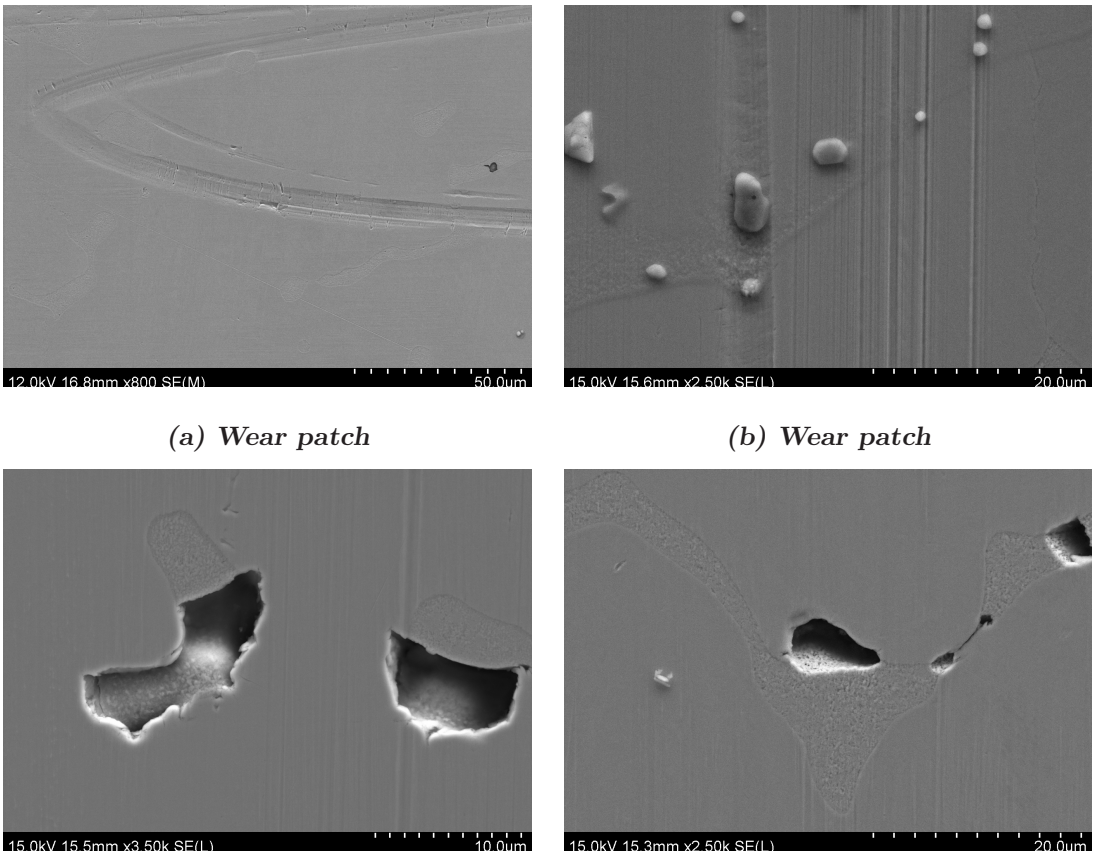

(a) Wear patch ***(b) Wear patch***

(c) Wear patch ***(d) Wear patch***

Figure 8.23: *SEM micrographs of wear patch, (a) abrasive wear which continues through the carbides and the matrix, (b) abrasive scratches and wear debris, (c) partial carbide removal, (d) partial carbide removal.*

8.4.4 AFM

Initial micrographs revealed polishing/machining marks as seen for the standard alumina heads. The scratching was in region of tens of nanometres deep. Micrographs (see Figure 8.24) taken on the pole showed more random polishing scratches compared with images taken at approximately 45^o which were more regular in orientation.

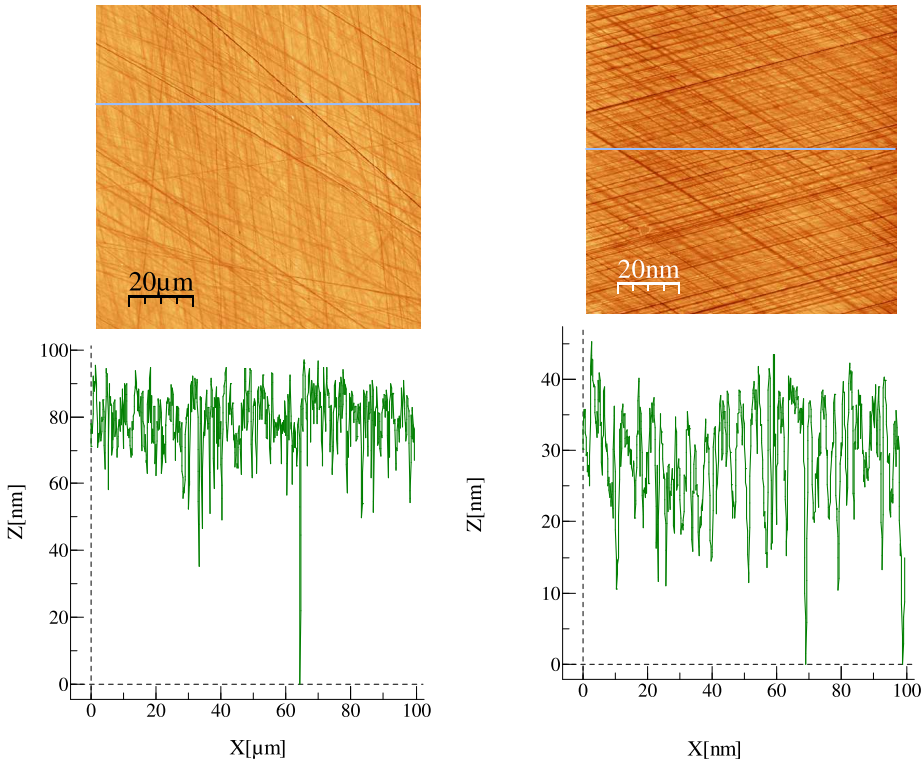

(a) Pole - 100 µm scan ***(b) Approx. 45°100 µm scan***

Figure 8.24: *AFM images of the unworn alumina heads used for microseparation wear testing.*

Micrographs taken on the pole of the ceramic heads after 2.5 million cycles of wear under microseparation conditions revealed shallow holes where grain pull out had occurred. The metal transfer within the dislocation region was nanometres thick (see Figure 8.25).

A number of images were taken in the metal transfer region after 3 million cycles, which revealed occasional grain removal in addition to the metal transferred. Although impact was obviously occurring between the head and cup, this was not

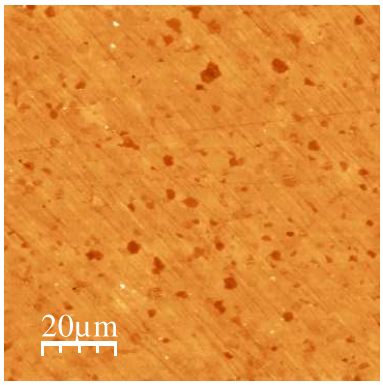

(a) Pole - 100 µm scan

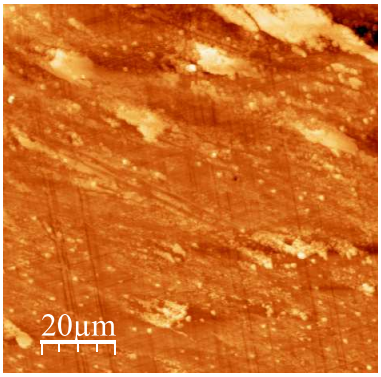

(b) Metal transfer - 100 µm scan

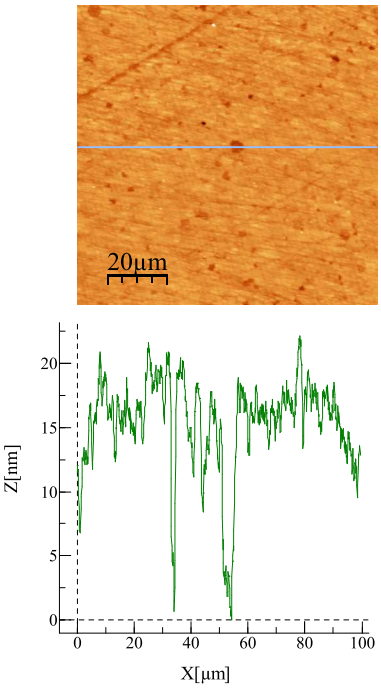

(c) Pole - 100 µm scan

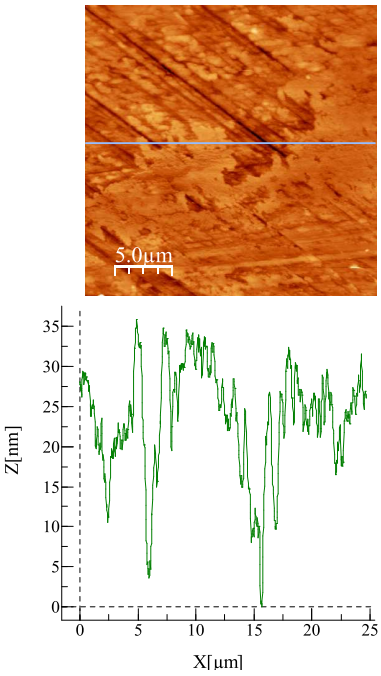

(d) Metal transfer - 125 µm scan

Figure 8.25: *AFM images of the alumina head (microseparation test) after 2.5 mc. (a) & (c) shallow grain pull out, (b) & (d) metal transfer*

significantly damaging the underlying ceramic surface which maintained a low number of 3rd body particles limiting the abrasive wear of the surrounding area.

The final surface topography investigation carried out after 5 million cycles of wear highlighted an interesting discovery. A band of wear was found on the superior anterior quadrant of the head, noticed on all 5 active stations. The 'stripe' wear revealed grain removal as was seen on the pole of the head. This region was not previously noticed or recorded using the AFM as it was not visible by eye and was only accidentally noticed using the white light profilometer. Figure 8.26 shows the contrast between the three different regions. A digital image of the ceramic heads highlights the regions on the ceramic head with the stained deposit present.

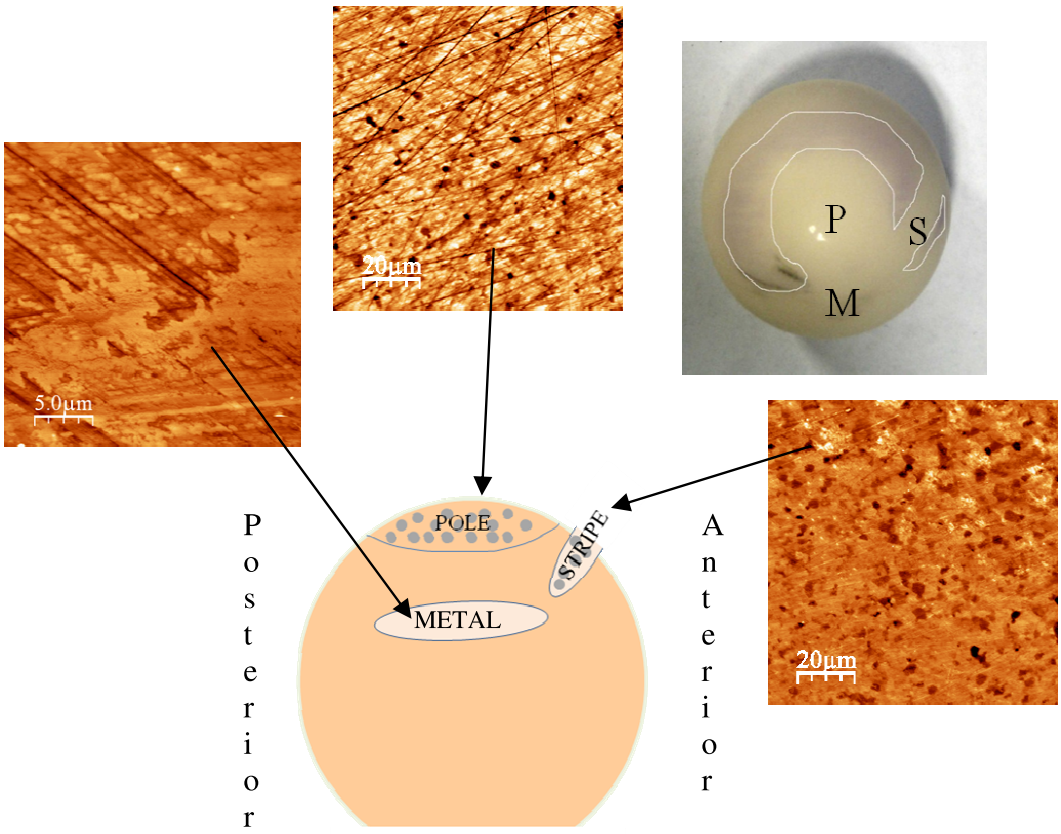

Figure 8.26: *AFM images showing the three different areas of interest on the alumina head from the microseparation test.*

8.5 Deposition

As with earlier tests, deposition was stained using non permanent ink. Images were taken at intervals throughout testing. Figure 8.27 shows the progression of head 5 throughout the test. A u-shaped pattern was found on the pole of the heads, clearly showing the contact area on the pole where the substance was not found deposited. Deposition was not found in the lateral segment where rim contact occurred. A straight edge in the deposition was visible in the region of stripe wear, as a result of the head impacting the cup upon relocation as was highlighted in Figure 8.26.

(a) 0.5 mc *(b) 1 mc* *(c) 1.5 mc*

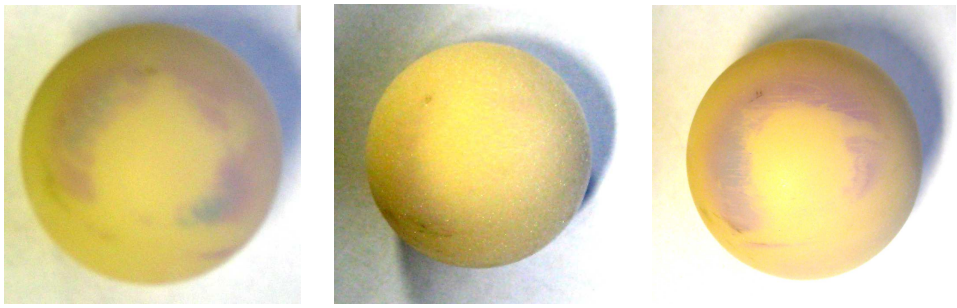

(d) 2.0 mc *(e) 3.5 mc* *(f) 4.0 mc*

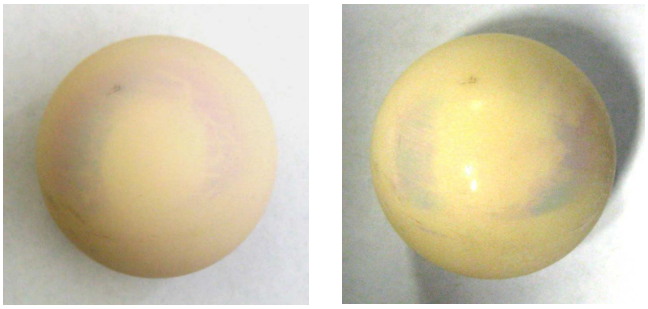

(g) 4.5 mc *(h) 5.0 mc*

Figure 8.27: *Digital images showing the stained deposit at various stages throughout testing under microseparation conditions.*

Chapter 9

Results -'Microseparation' of 38 mm ZTA heads against CoCrMo cups

A set of six, 38 mm diameter ZTA heads and as-cast CoCrMo cups were tested under 'microseparation' wear conditions. The components were similar to those described in Chapter 7 and were paired to give radial clearances close to 100 μm.

Station	Head	Dimension (mm)	Cup	Dimension (mm)	Radial Clearance (μm)
1	37	18.979	1	19.076	97
2	38	18.978	#2	19.068	90
3	1	18.985	3	19.083	98
4	15	18.978	#4	19.068	90
5	32	18.980	5	19.076	96
Load Control	26	18.981	4	19.081	100
Soak Control	14	18.980	2	19.071	91

Table 9.1: *38 mm ZTA against CoCrMo joint pairings and radial clearances for tests under microseparation wear conditions.*

9.1 Wear Results

Similar displacement conditions to those described in Chapter 8 were used in the current test. As with previous tests the ZTA head volume change fluctuated around zero for the entire test as shown in Figure 9.1. The load and soak control heads fluctuated with the same trend and magnitude as the active stations suggesting that the volume change measured was due to external factors during the weighing process rather than attributed to wear. In contrast the metal cups showed a large volume change, with a mean volume loss of 9.43 mm^3 after 5 million cycles of wear (see Figure 9.2). As with the microseparation test involving alumina heads against CoCrMo cups, the running in and steady state wear phases were not as distinct as found for standard testing. Steady state wear was established in all cups by 2 million cycles, however cup #2 and cup 3 appeared to have established steady state wear earlier by 1.5 million cycles. However for consistency between all cups, running in wear was taken between 0-2 million cycles, and steady state between 2-5 million cycles.

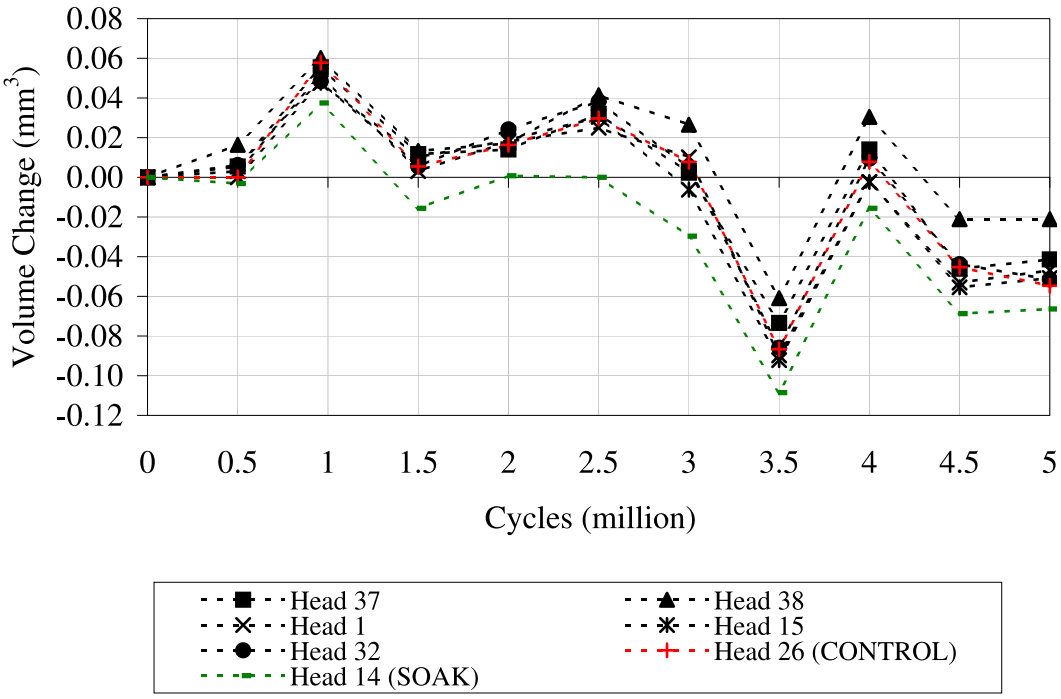

Figure 9.1: *Volume change of 38 mm ZTA femoral heads under microseparation wear conditions.*

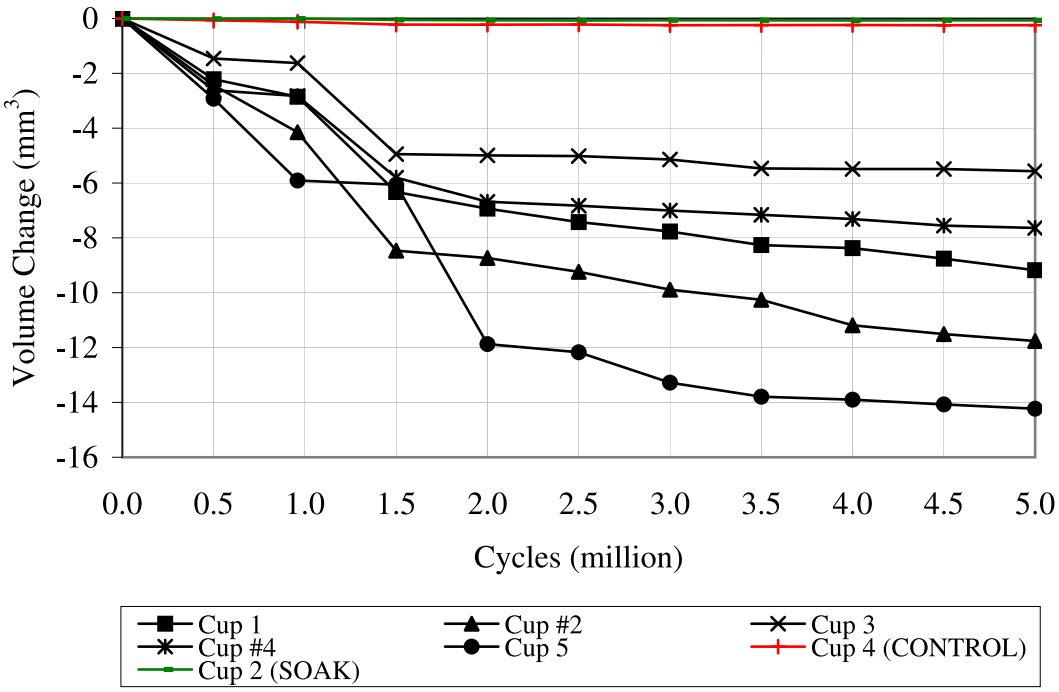

Figure 9.2: *Volume change of 38 mm as-cast CoCrMo acetabular cups (from ZTA test) under microseparation conditions.*

The data for the heads and cups was adjusted using the same method as previous tests to incorporate the loaded control components. This allowed the true wear to be determined and is shown in a combined graph of both the heads and cups, in Figure 9.3. The individual head volume changes became indistinguishable shown against the larger volume change of the cups.

The running in wear rates were considerably higher than the steady state wear for all cups. With the exception of cup #2 a trend was found which showed a higher running in wear rate resulted in a high steady state wear rate. Average running in and steady state wear stages were 3.82 $\pm$0.614 (r^2= 0.88) and 0.623 $\pm$0.252 (r^2= 0.43) respectively.

Cup	RI Wear Rate (mm^3/mc)	r^2	SS Wear Rate (mm^3/mc)	r^2
1	3.4849	0.96	0.7078	0.99
# 2	4.5855	0.97	1.0585	0.98
3	2.5871	0.90	0.2086	0.87
#4	3.1990	0.95	0.3239	0.99
5	5.2426	0.91	0.8138	0.88

Table 9.2: *Individual 38 mm CoCrMo cup wear rates under microseparation wear conditions(ZTA test).*

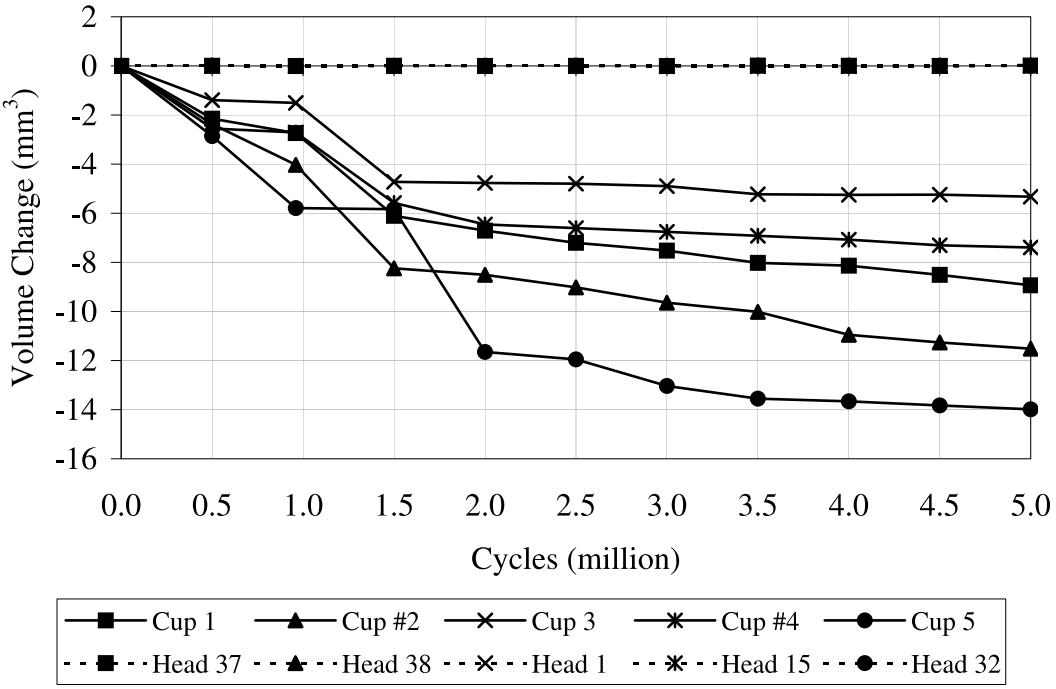

Figure 9.3: *Adjusted volume change of 38 mm ZTA:CoCrMo under microseparation wear conditions (taking account of loaded soak control).*

9.2 Friction

Friction testing was carried out on two pairs of components, initially and after 5 million cycles of wear under microseparation conditions. The results are shown in Figure 9.4. The results at 5 million cycles were undertaken by a 4th year project student, Emma Tonks, under the cosupervision of the author for the practical work.

Similar friction factors were found before and after wear testing with the exception of the two highest viscosities of bovine serum based lubricant. Generally the water based lubricants showed lower friction factors than the bovine serum lubricants, as was found for previous ceramic on metal combinations. The water based lubricants showed similar friction factors and shape of the curve before and after wear testing, indicative of full fluid film lubrication with low friction factors. Interestingly the bovine serum lubricants showed opposing trends, before and after wear testing, although the range of friction factors were similar in both cases. Initial results showed a decrease in friction factor with increasing Sommerfeld number, to a minimum, after which the friction factors increase. After wear the results showed a distinct decrease in friction factor with increasing Sommerfeld number. The low friction factors suggested the joints were operating within the mixed lubrication regime where asperity contact was occurring, after 5 million cycles of wear.

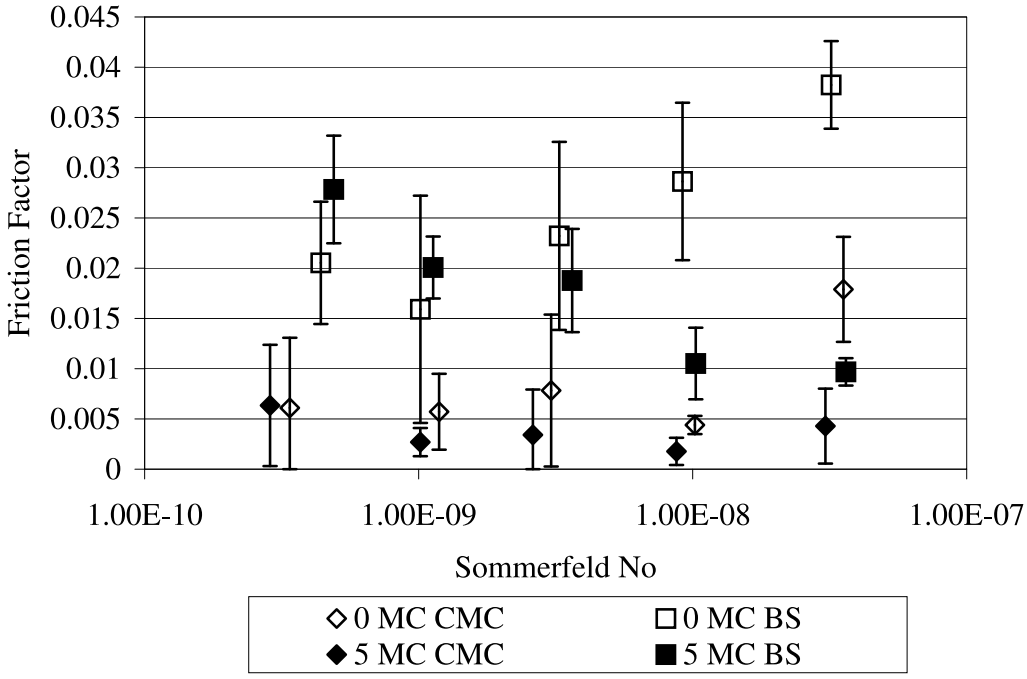

(a) Head 37:Cup 1

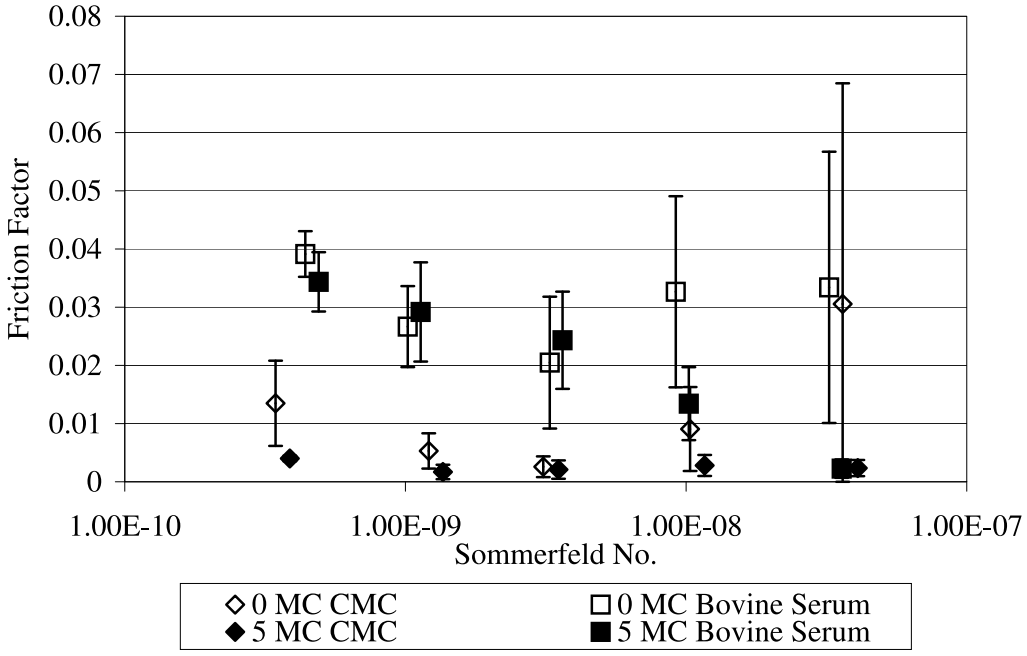

(b) Head 38:Cup 2

Figure 9.4: *Stribeck plots of 38mm ZTA:CoCrMo components before and after 5 million cycles of wear under microseparation conditions. The unworn and worn results were undertaken on different wear simulators.*

9.3 Surface Analysis

9.3.1 Digital Images

Digital images were taken of the cups throughout wear testing which allowed the progression, size and location of the flattened lip, as a result of edge impact, to be monitored. Figure 9.5 shows the flattened lip progression on cup #2 after 0.5, 2.5 and 4.5 million cycles, by which time a second lip had formed.

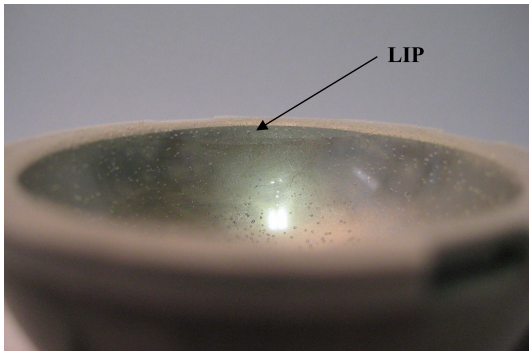

(a) Cup #2 - 0.5mc

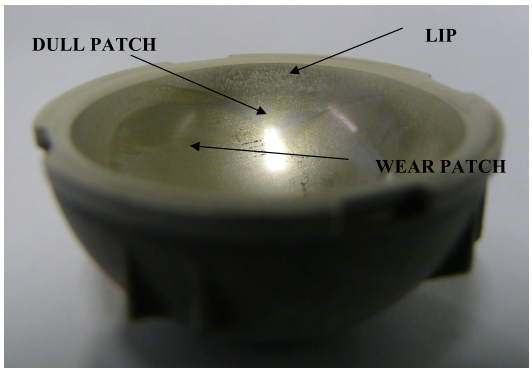

(b) Cup #2 - 2.5mc

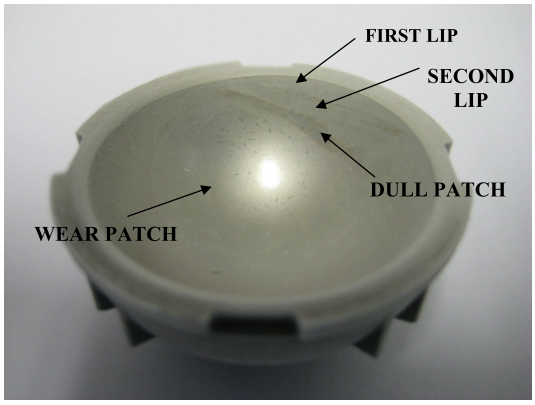

(c) Cup #2 - 4.5mc

Figure 9.5: *Digital images of the metal cup (ZTA test) showing the flattened lip, dull area and wear patch of cup #2 at 0.5, 2.5 and 4.5 million cycles.*

The size of the lip (both width and breadth) increased with number of cycles as shown in Figure 9.6. Some cups developed a second lip which were superimposed on top of the first lip, and a dull patch, thought to be a protein/metal agglomerate, appeared on the edge of the lip (see Figure 9.5). The definition of the lip became less obvious with number of cycles, and the bottom edge became difficult to differentiate

from the wear patch. All cups showed similar dimensions of width and breadth of the lip throughout the test. Until 3 million cycles the width of the lip in cup 3 was smaller than the other cups, however it increased to the size of the other cups by 5 million cycles. Cup 3 also showed the smallest breadth measurement throughout testing. Interestingly this cups showed the lowest running in and steady state wear rates.

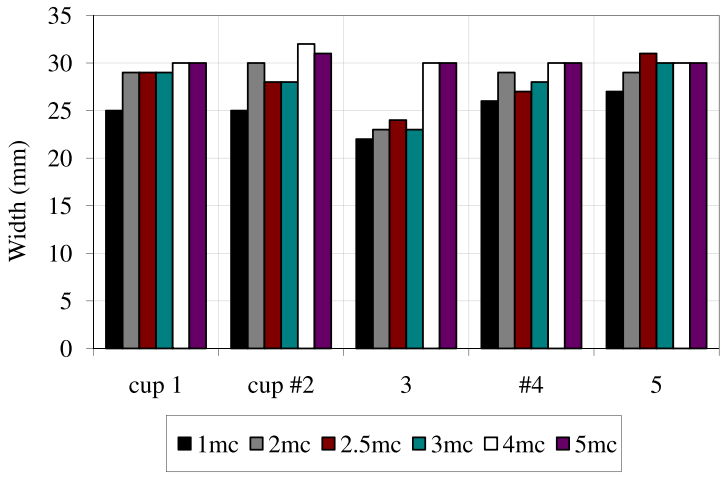

(a) Width

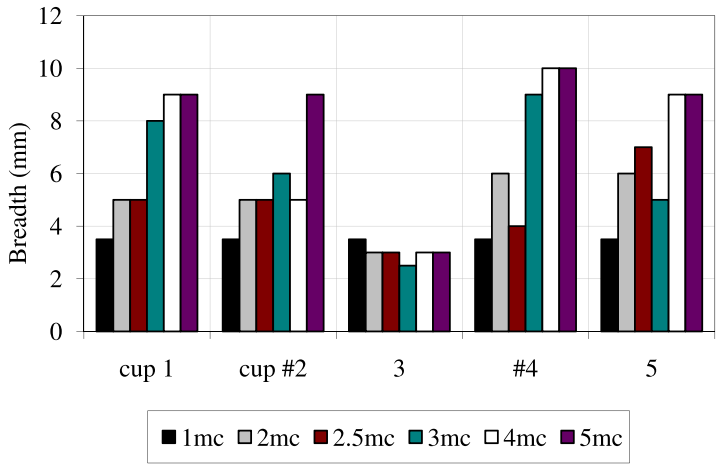

(b) Breadth

Figure 9.6: *Dimensions of the flattened lip on the metallic cup (ZTA test) which formed as a result of edge impact between the head and the rim of the cup*

9.3.2 Non contacting Interferometry

Three areas on of the ZTA heads were investigated. These were the pole, the metal transfer region which was located at approximately 33^o to the horizontal on the lateral side of the head, and a 'stripe' wear region located in the superior lateral region of the cup.

Figure 9.7 shows two examples of the ZTA heads indicating the three regions of interest. The red areas indicate deposition found after a 0.5 million cycle period of wear testing.

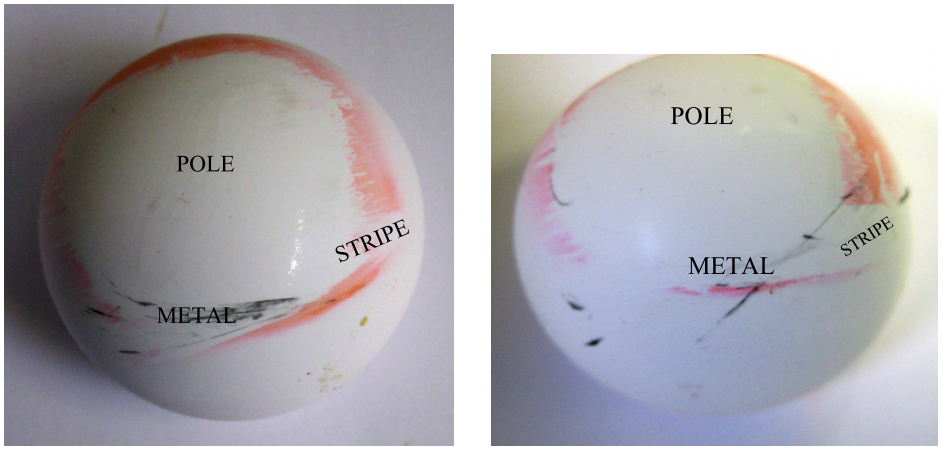

(a) Head 1 ***(b) Head 15***

Figure 9.7: *Regions of interest on ZTA heads*

Surface measurements using the non contacting interferometer were taken on the pole up to 1 million cycles, after which the instrument was unavailable for measurements. The root mean squared roughness and skewness measurements are shown for 0, 0.5 and 1.0 million cycles in Figures 9.8

The rms roughness of the metallic cups increased from 0.011 μm to 0.029 μm by 0.5 million cycles after which the roughness decreased to 0.020 μm. The control cup increased in roughness steadily over the three measurements from 0.011 μm at 0 million cycles to 0.020 μm after 1.0 million cycles therefore showed similar results to the active stations. The head rms roughness did not change considerably over 1 million cycles of wear. The standard deviation of the heads was smaller than those for the cups, highlighting the heterogeneous nature of the cup surfaces.

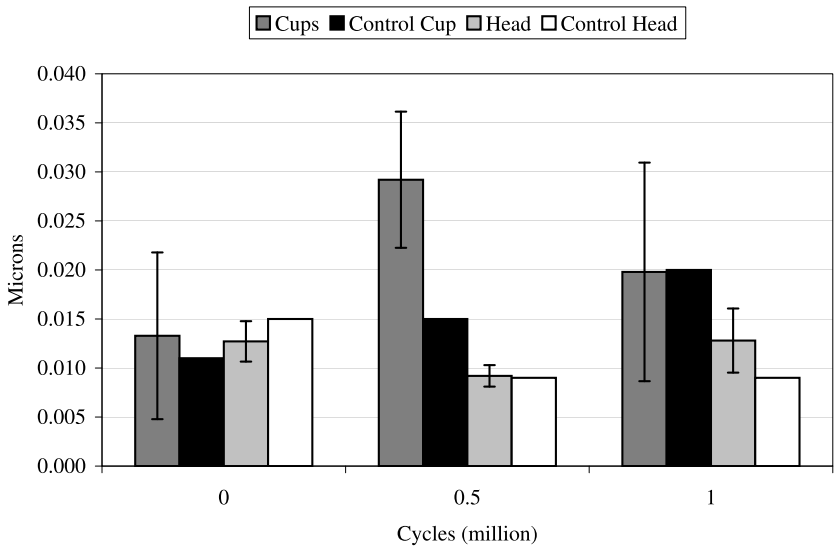

(a) RMS roughness

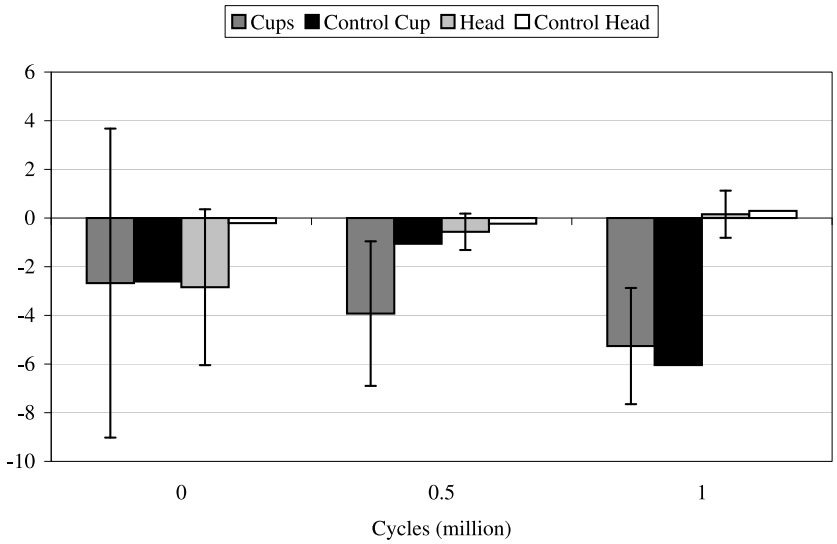

(b) Skewness

Figure 9.8: *Surface topography data from the 38 mm ZTA test under microseparation conditions up until 1 million cycles.*

After 1 million cycles the rms roughness and skewness of the heads was quantified using two different AFM analytical software packages. The topography of the metal cups could not be measured after 1 million cycles.

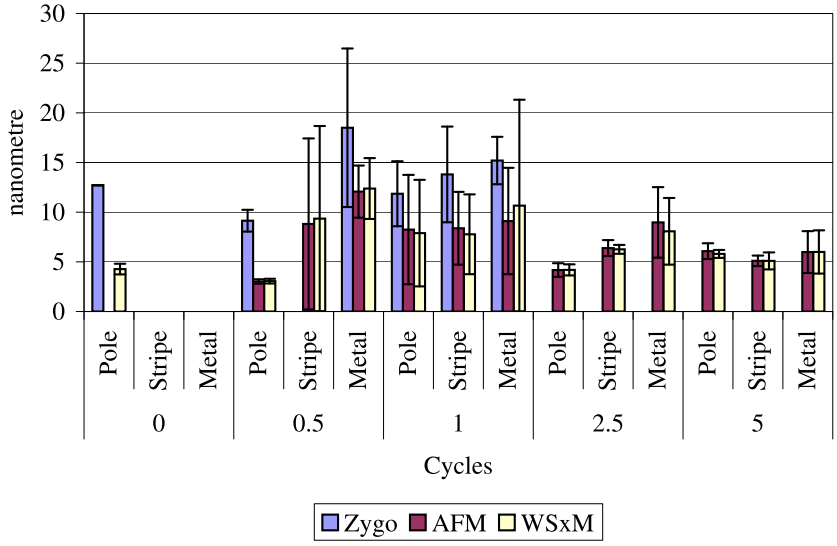

(a) RMS roughness

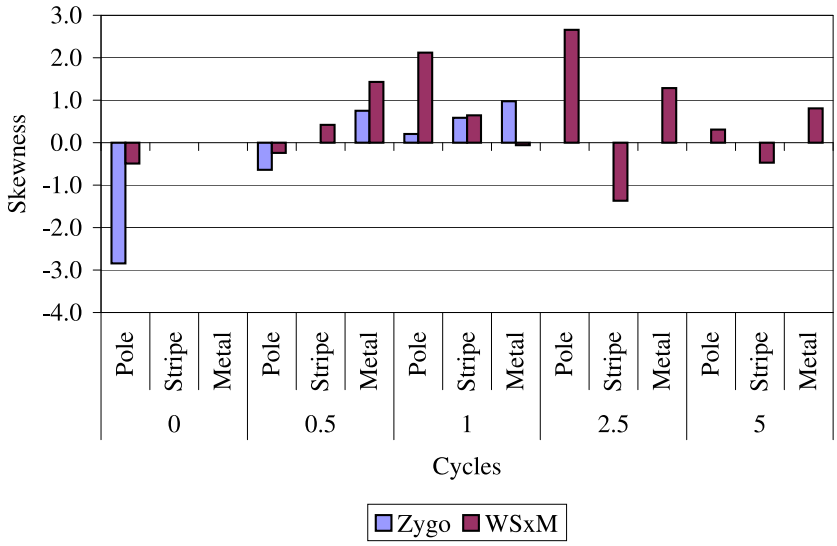

(b) Skewness

Figure 9.9: *A comparison of rms roughness and skewness values of the ZTA heads from the 38 mm ZTA test under microseparation conditions, analysed using the Zygo, AFM and WSxM software.*

Figure 9.9 combines the results of rms roughness's from the non contacting interferometer (Zygo), AFM software and WSxM surface topography packages. The

absolute rms roughness values vary considerably between techniques however the general trends of roughness follow the similar patterns for all methods of analysis. After 2.5 million cycles, the metal region showed a slightly higher roughness than the stripe or pole regions, however after 5 million cycles the results for all three regions were similar. It must be noted that the skewness values were close to zero for all measurements, showing little variation in the tendency for sharp peaks and valleys, over the surface. Detailed analysis showed that initially the unworn surfaces showed a negative skewness value, likely to be due to the polishing scratches resulting in deep valleys. After 1 million cycles, all three areas of interest showed a positive skewness. The results after 2.5 and 5 million cycles showed the stripe wear region to be negative, probably as a result of grain removal, whereas the pole and metal regions were slightly positive.

9.3.3 Surface Imaging

Analysis of the unworn surfaces using non contacting profilometery revealed differences in the z-scale position of the carbides on the unworn surfaces between metal cups. Cups 1, 2 and #4 showed relatively smooth carbides whilst cups #2, 3, 4, and 5 showed carbides which protruded from the surface to a greater extent. An example of this can be seen in Figure 9.10 which compares two cups shown at the same scale, to highlight the differences in carbide position.

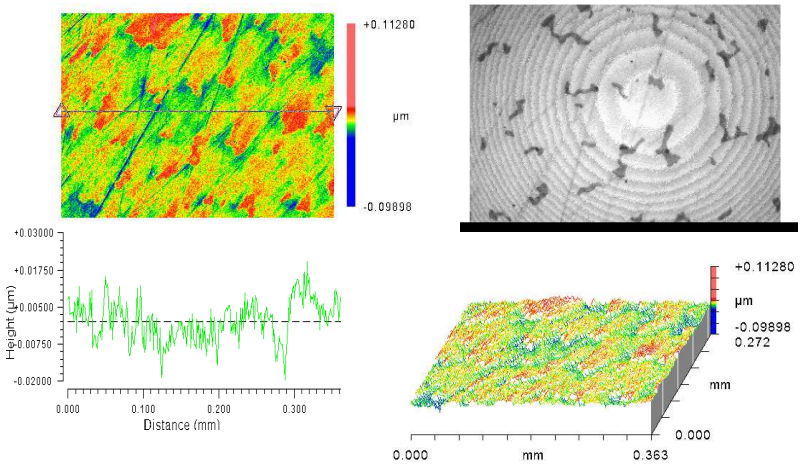

(a) Cup 1 - unworn

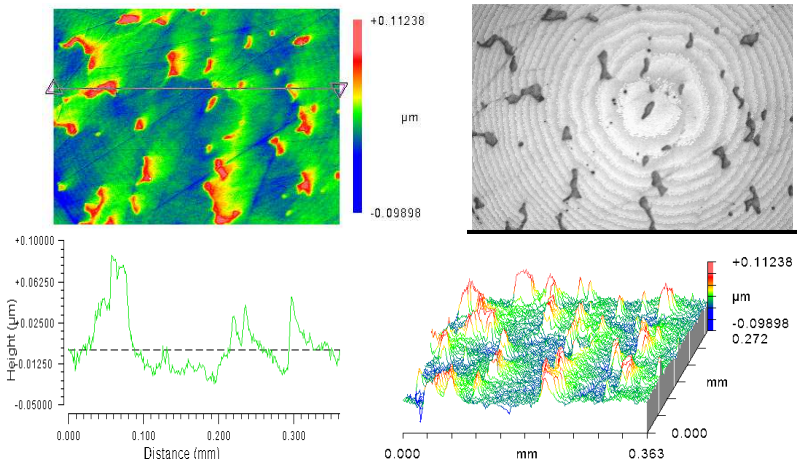

(b) Cup 2 - unworn

Figure 9.10: *Non contacting profilometer micrographs showing the difference in carbide height within different unworn cups (ZTA mxs test) (a) smooth carbides compared with the matrix material, (b) protruding carbides, showing a greater contrast to the matrix material.*

However, this difference between the unworn cups did not appear have an effect on the wear rates which showed similar wear rates (see Table 9.2).

The difference in carbide position was not as significant by 0.5 and 1.0 million cycles of wear all surfaces showing a relatively smooth topography. Images of cup 1 (initially smooth carbides) and cup 3 (initially protruding carbides) at 0.5 and 1.0 million cycles are shown in Figure 9.11. Images are shown at the same scale for comparison. The flexion/extension direction could be identified using abrasive scratches and deformation of the matrix material.

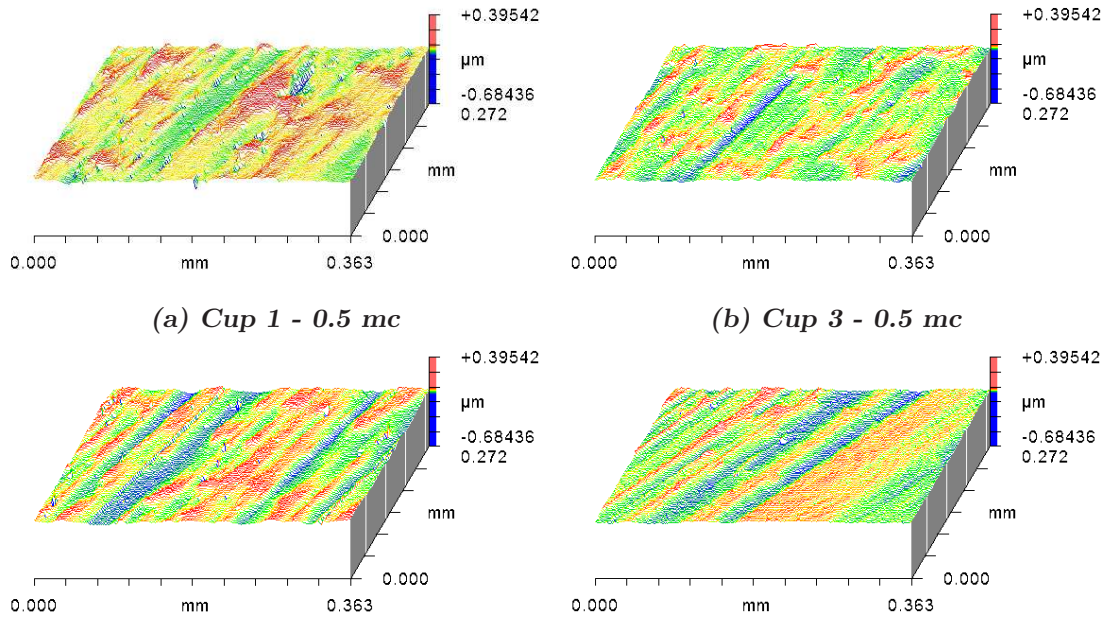

(a) Cup 1 - 0.5 mc

(b) Cup 3 - 0.5 mc

(c) Cup 1 - 1 mc

(d) Cup 3 - 1 mc

Figure 9.11: *Non contacting profilometer micrographs which compare the surface topography of the metal cup (ZTA test) after 0.5 and 1 million cycles of wear under microseparation conditions.*

The surface topography maps showed small holes in the surface likely to be pitting as a result of adhesive or corrosive wear. The carbides appeared flattened or smoothed and were not the dominant feature of the surface.

Areas of deposit (possibly protein) on the pole and 'stripe wear' areas were found using atomic force microscopy, which was not evident by eye. However these areas did not appear to increase the roughness of the surfaces. Figure 9.12 shows an example of images taken within the three different areas on head 32. The small

peaks randomly distributed across the surface are thought to be as a result of a deposit left on the surface during wear testing.

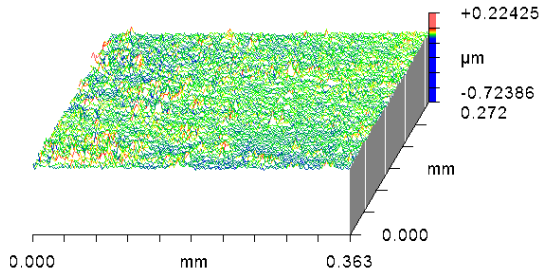

(a) Pole

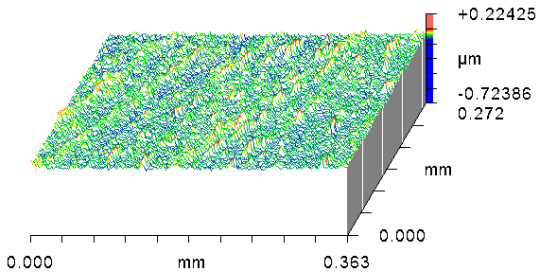

(b) Metal transfer region

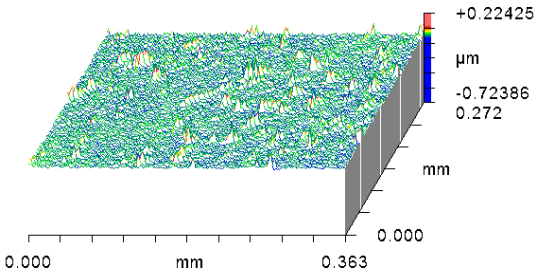

(c) Stripe

Figure 9.12: *Non contacting profilometer micrographs showing the surface topography a typical ZTA head after 1 million cycles of wear under microseparation conditions. The three areas of interest were the pole, the metal transfer region and the area where stripe wear was thought to occur.*

Although Figure 9.12 shows an area of the pole where deposit was found, there were also areas where the surface was unchanged from the initial samples.

9.3.4 Optical Microscopy

Optical micrographs of the unworn surfaces showed similar features to previous tests. Carbides could clearly be seen within the matrix although some cups had carbides which protruded out of the surface more than others which can be seen from the difference in contrast between carbide and matrix material shown in Figure 9.13.

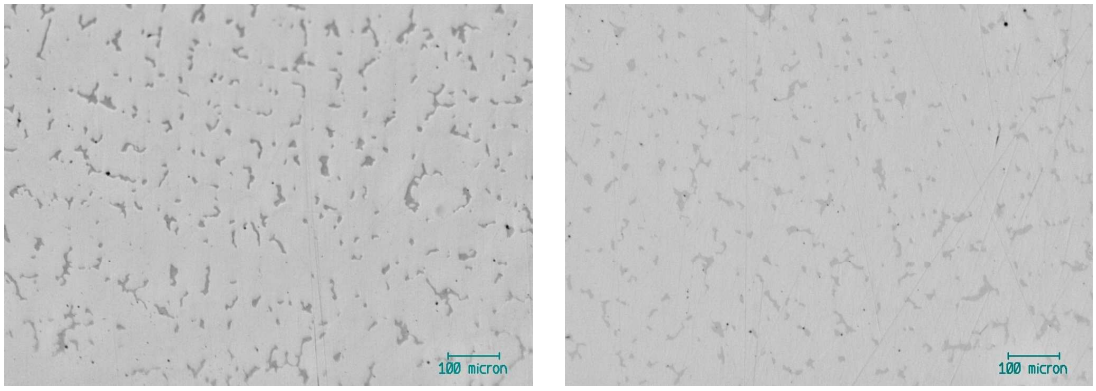

(a) Cup #2 - Unworn ***(b) Cup 16 - Unworn***

Figure 9.13: *Optical images of the unworn as-cast CoCrMo cups (ZTA microseparation test) (a) protruding carbides shown by the greater contrast between carbide and matrix, (b) flatter carbides shown by less contrast between carbides and matrix material.*

After 0.5 million cycles of wear, significant amounts of pitting and surface damage was observed. Tiny holes were present in the wear patch in both the matrix material, which may be as a result of adhesive or corrosion wear, and within some of the carbides. The individual carbides were less obvious and they contrasted less with the surrounding matrix material. Deposit left during wear testing was found to highlight the raised matrix structure, often surrounding the carbides. This can be seen in Figures 9.14(c) and 9.14(d).

Imaging of the edge contact region of the cup after 0.5 million cycles revealed a distinct flattened lip on the superior lateral edge of the cup. The contrast between the carbides and matrix material within this area was less than that of the unworn area showing that the carbides had been worn smooth or been removed. Very little abrasive scratching was found, however 'comet tails' corresponding to small holes

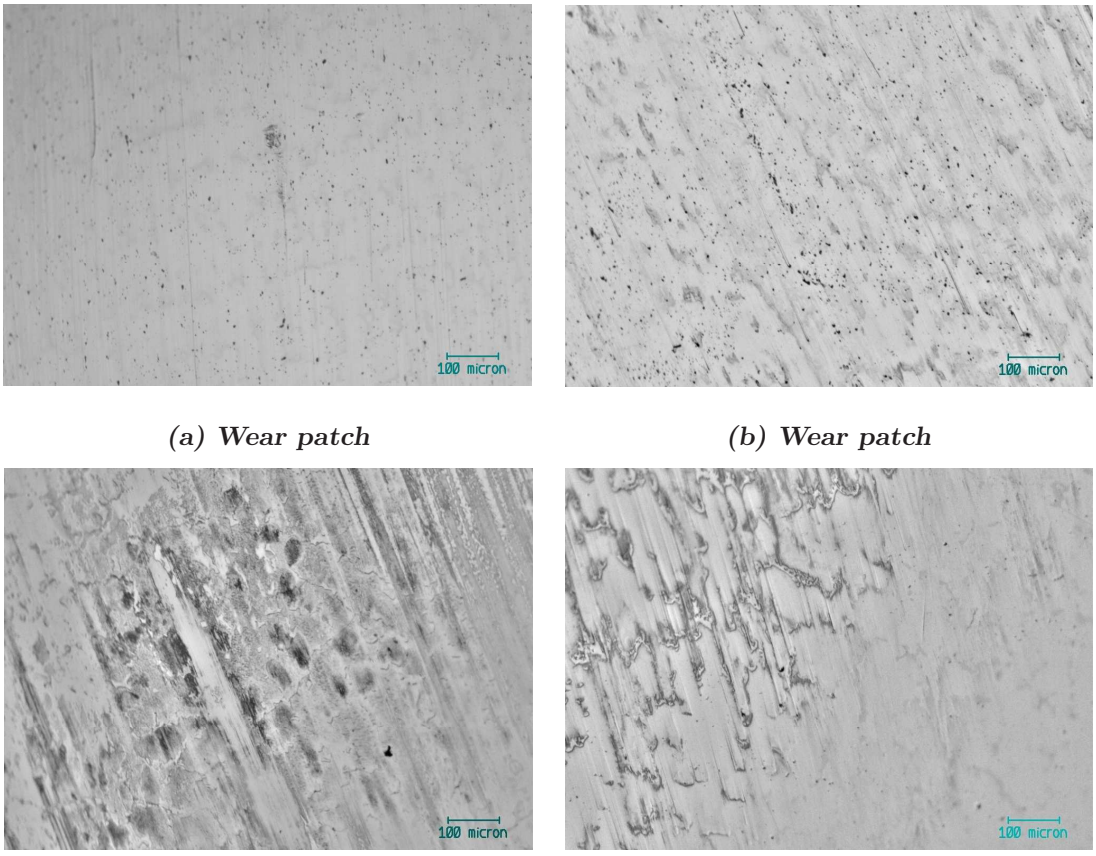

(a) Wear patch ***(b) Wear patch***

(c) Edge of wear patch ***(d) Wear patch***

Figure 9.14: *Optical images taken of the as-cast CoCrMo cups (ZTA microseparation test) in the wear patch after 0.5 million cycles. The dominant features in each sub figure are; (a) pitting, (b) pitting and adhesive wear, (c) & (d) transfer at the edge of the wear patch.*

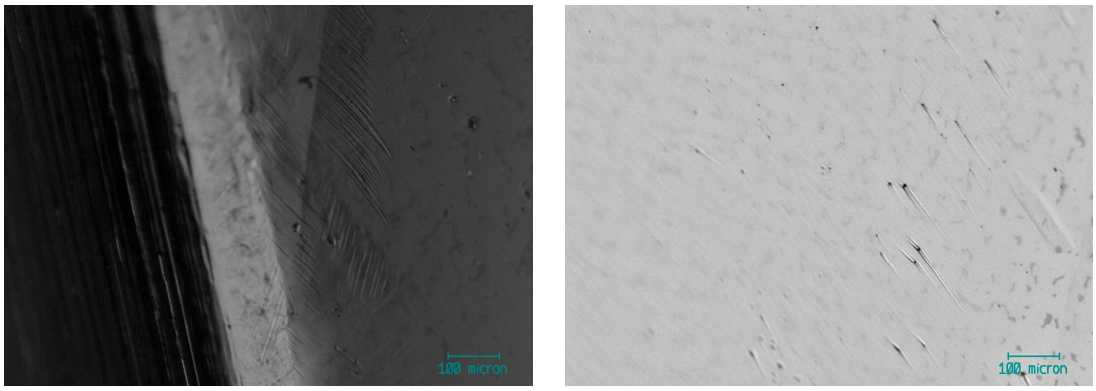

(a) Flattened lip *(b) Flattened lip*

Figure 9.15: *Optical images taken of the as-cast CoCrMo cups (ZTA microseparation test) after 0.5 million cycles. (a) regular impact marks on the edge of the flattened lip (b) adhesive wear showing 'comet tails' either side of the hole*

were present within some areas of the lip. Figure 9.15 highlights the edge of the lip and the smooth surface with limited adhesive wear. Interestingly abrasive scratches were present from both sides of the holes.

Similar micrographs were taken after 1 million cycles. The wear patch of all cups revealed a heterogeneous topography with areas of relatively little wear, and areas with a significant change in topography. Pitting was found to be a major feature on all active cups and areas of material transfer or material deposition. Abrasive scratches were evident, but not as the dominant feature.

Figure 9.16 presents micrographs which show the range of topography found within the wear patch after 5 million cycles of wear under microseparation conditions. Areas were found where little abrasive damage had occurred with only a change in the contrast of the carbides within the matrix (see Figure 9.16(a)). Areas were also imaged where significant abrasive damage was evident as a result of both carbides and matrix removal possibly due to adhesive wear. These wear particles may then have acted in third body abrasive wear (see Figure 9.16(b) to 9.16(d)). Wispy abrasive wear was found within the wear patch as a result of third body particles (Figure 9.16(b)).

After 5 million cycles, the flattened lip (resulting from edge contact) was imaged

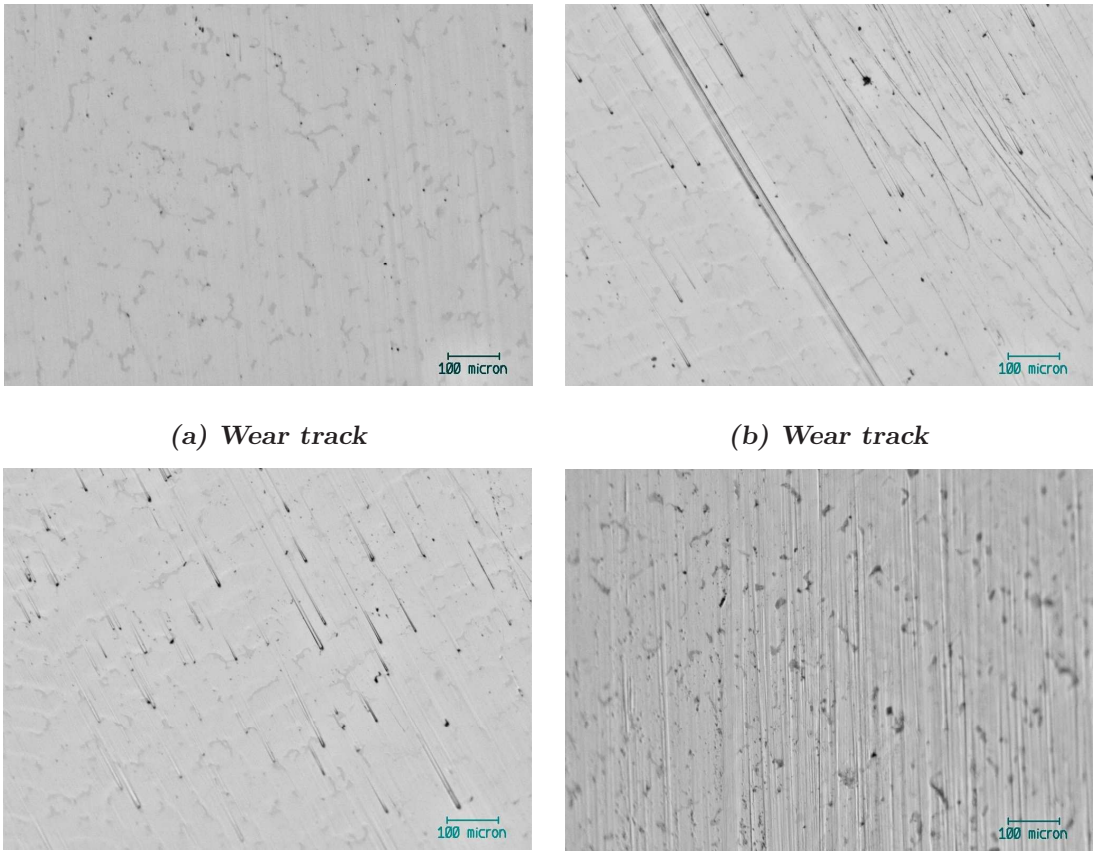

(a) Wear track ***(b) Wear track***

(c) Wear track ***(d) Wear track***

Figure 9.16: *Optical images taken of the as-cast CoCrMo cups (ZTA microseparation test) after 5 million cycles. The dominant features of each sub figure are; (a) smooth un-featured surface, (b) abrasive and adhesive wear, c) pitting and adhesive wear with corresponding 'comet' tails, (d) abrasive wear and possible carbide removal.*

which revealed several surface features as shown in Figure 9.17. Generally the area showed a relatively undamaged topography with only a decrease in contrast between the carbides and matrix (see Figure 9.17(a)). Along the edge of the lip, a dull transfer of material was evident which varied in severity (see Figure 9.17(f)). Abrasive scratches were seen within the transfer. Occasional areas of more significant abrasive damage were also found (see Figure 9.17(b)). On some cups, more than one lip developed on top of the original lip which is shown in Figure 9.17(e).

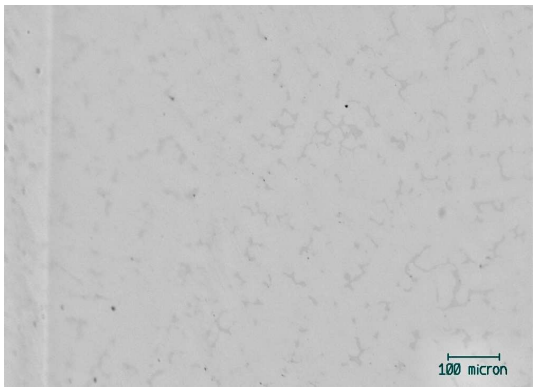

(a) Flattened lip

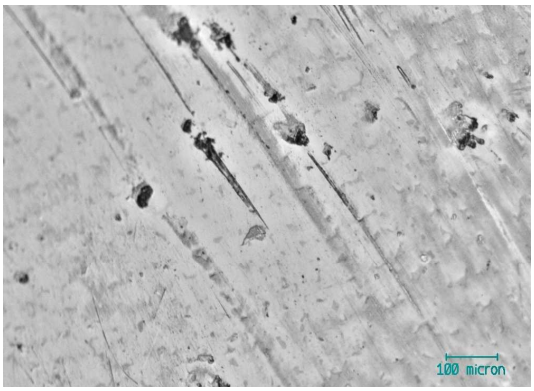

(b) Flattened lip

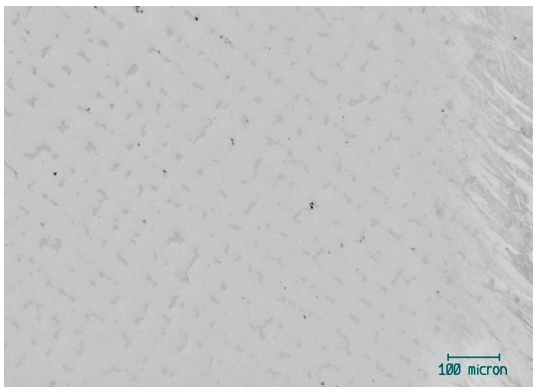

(c) Flattened lip

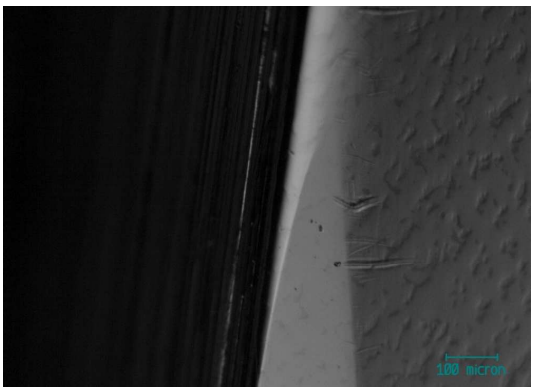

(d) End flattened lip

(e) Outside edge of flattened lip

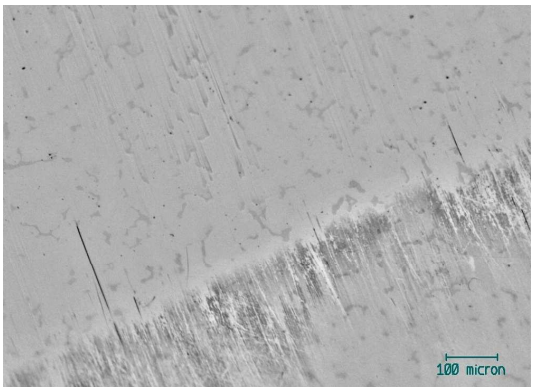

(f) Inside edge Flattened lip

Figure 9.17: *Optical images taken of the lip on the as-cast CoCrMo cups (ZTA mxs test) after 5.0 million cycles. The dominant features of each sub figure are; (a)&(c) smooth un-featured surface, (b) significant adhesive wear leading to abrasive scratches, d) smooth end of flattened lip, (e) start of the formation of a second lip on top of the primary lip, (f) dull transfer on the inside edge of the flattened lip.*

9.3.5 AFM

The main objective of AFM analysis was to examine the surfaces of the ceramic heads to discover whether grain pull out was evident. The three areas of interest were the pole, metal transfer which occurred at approximately 33 degrees to the horizontal and a region of 'stripe wear' which was expected due to edge contact. This region was not visible by eye and therefore AFM analysis was required to investigate whether a change in surface topography was evident.

All unworn surfaces were similar to those found previously for the standard ZTA test (see Figure 9.18). Random polishing scratches were evident on the pole, and the grain structure could not be identified. Occasional deeper scratches were found which were approximately 20 nm deep.

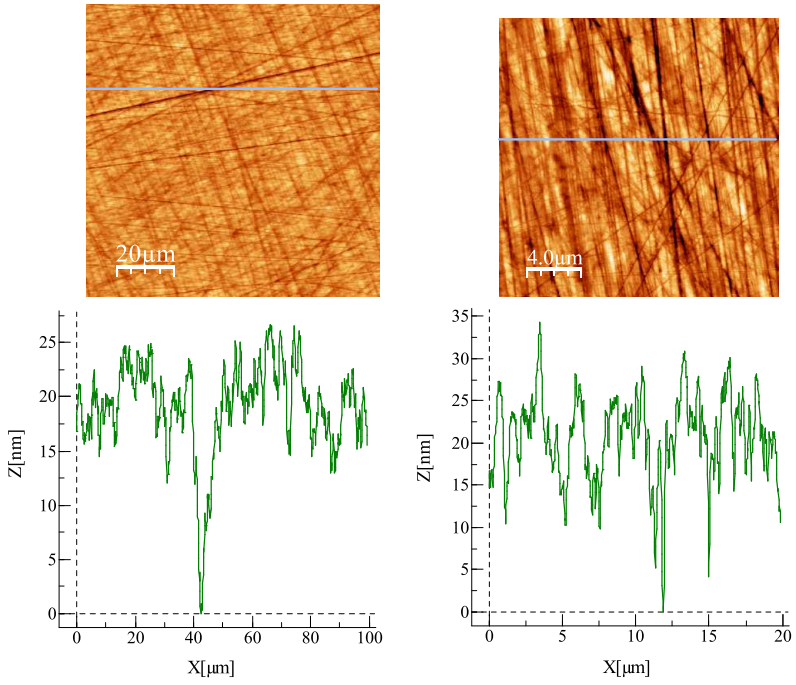

(a) Unworn ***(b) Unworn***

Figure 9.18: *AFM micrographs and line profiles of the unworn 38 mm ZTA heads (microseparation wear test) showing irregular polishing scratches.*

After 0.5 million cycles, occasional grains were noticeable on the pole of the head. The grains were extremely shallow, in the region of tens of nanometres. The polishing scratches were marginally less obvious. Thin layers of transfer could

be seen within the metal transfer region, however a stripe region was not identified. Figure 9.19 compares an image which was taken on the pole of the head which shows occasional grain removal, Figure 9.19(a), with an image from the metal transfer region, Figure 9.19(b). Grain removal and polishing scratches were not obvious within the metal transfer region.

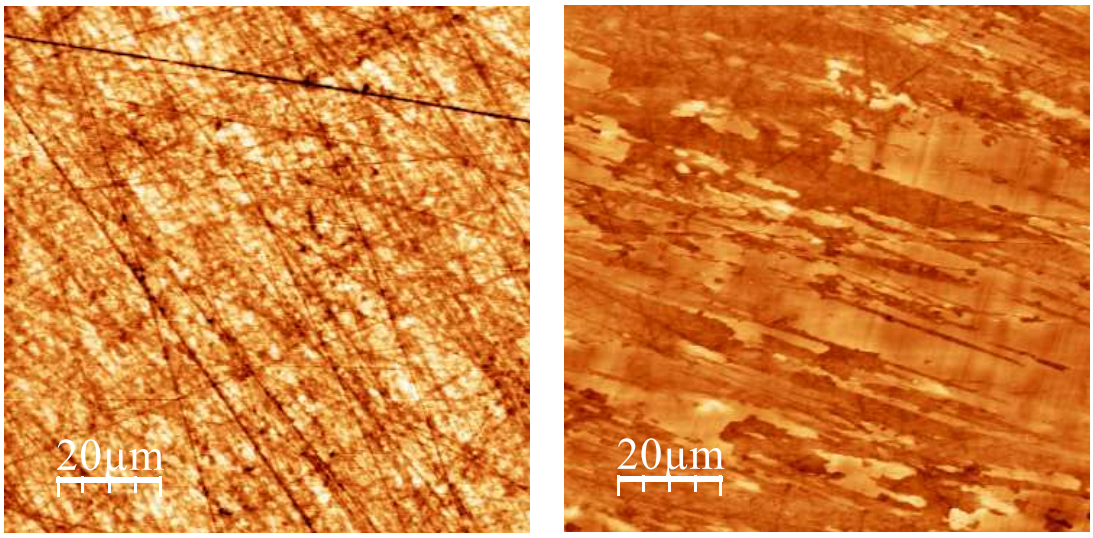

(a) Pole ***(b) Metal region***

Figure 9.19: *AFM micrographs of the 38 mm ZTA heads after 0.5 million cycles of microseparation wear testing comparing (a) grain pull out on the pole, (b) metal transfer as a result of head dislocation during extension.*

After 2.5 million cycles shallow grains were noticeable on all heads. Polishing scratches were less evident as the grains became more obvious, as shown in Figure 9.20. Line profiles confirmed the depth of the removed grains to be tens of nanometres deep. The metal transfer region was found on all active station heads, a typical image of which is shown in Figure 9.21. Areas around the pole were imaged to investigate whether a stripe wear region had formed, however, a similar topography to the unworn surfaces was observed.

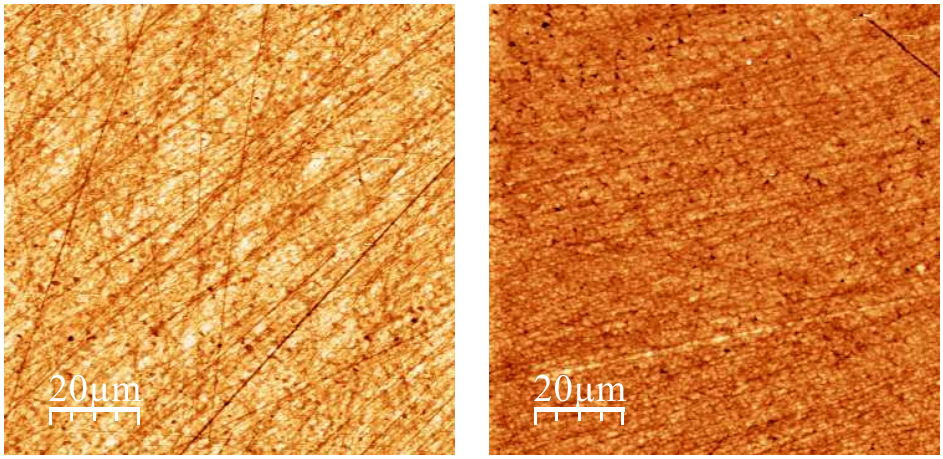

(a) Head 1 - Pole *(b) Head 15 - Pole*

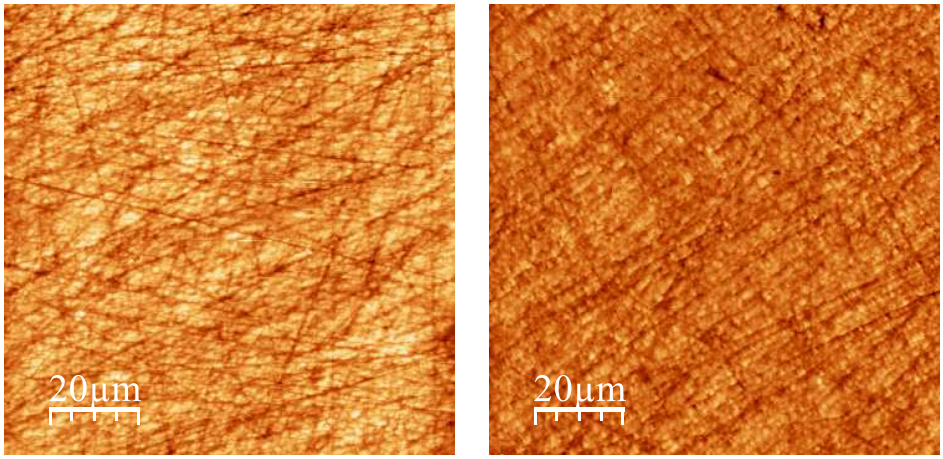

(c) Head 26 - Pole *(d) Head 32 - Pole*

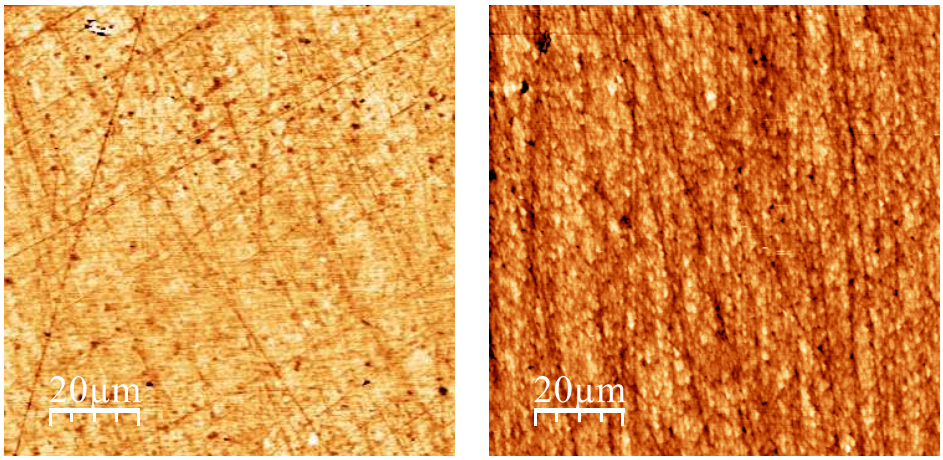

(e) Head 37 - Pole *(f) Head 38 - Pole*

Figure 9.20: *AFM micrographs of the pole of the 38 mm ZTA heads after 2.5 million cycles (mxs test) testing showing polishing scratches and occasional grain pull out.*

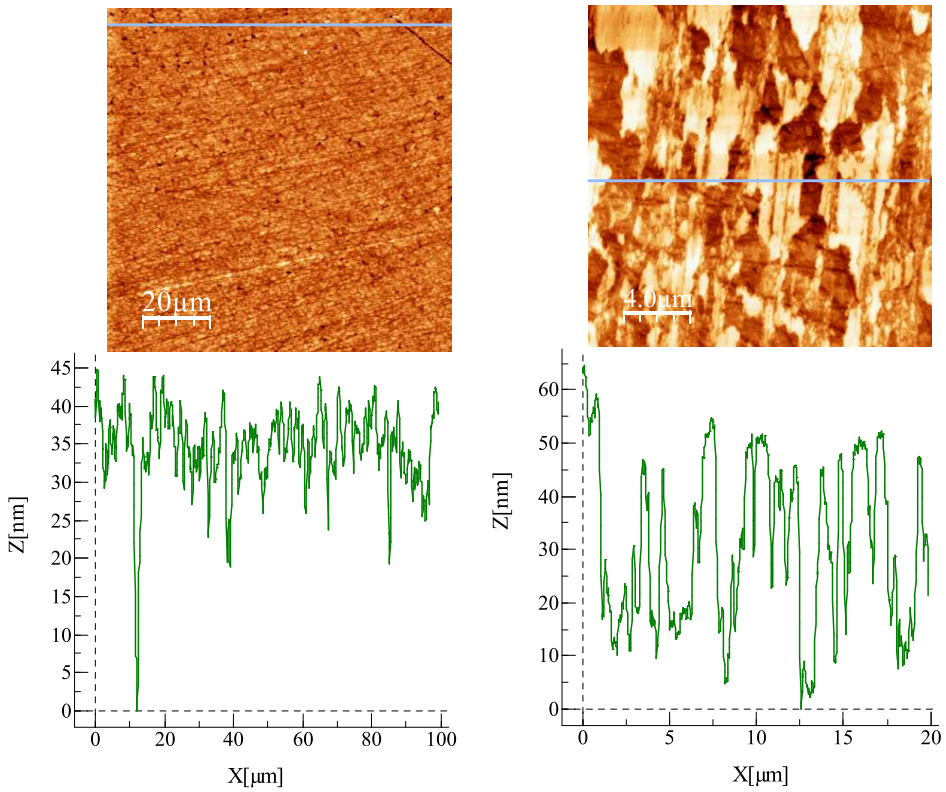

(a) Head 15 - Pole *(b) Head 15 - Metal transfer region*

Figure 9.21: *AFM micrographs showing line profiles of the pole and metal region of the 38 mm ZTA heads after 2.5 million cycles.*

After 5 million cycles of wear under microseparation conditions shallow grain removal was evident on the pole of all heads. The metal transfer region showed thin layers of metal, however only very occasional grains were removed. A small area of 'stripe wear' was found on the superior anterior segment of the head where removed grains were evident. The area of grain removal on both the pole and stripe wear regions was found to correspond to the area on the head where no deposition was located after wear testing. An example of these three areas are shown in Figure 9.22. The quantity of grains removed was similar on the pole and within the stripe wear region. The pole, metal and stripe wear regions can be seen on the digital image of the head when the deposit was still present.

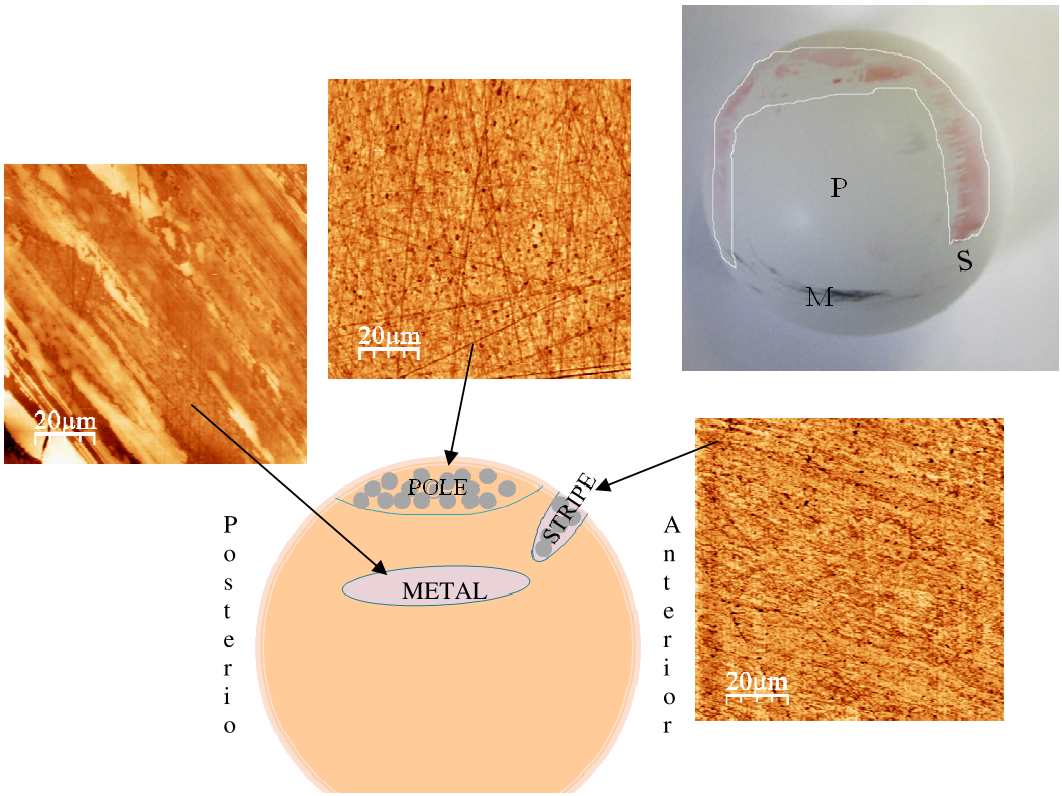

Figure 9.22: *AFM images showing the three different areas of interest on the ZTA head from the microseparation test.*

9.4 Protein Staining

The deposit found on the heads and cups was stained as with previous tests to monitor the location and any changes to the deposit throughout testing.

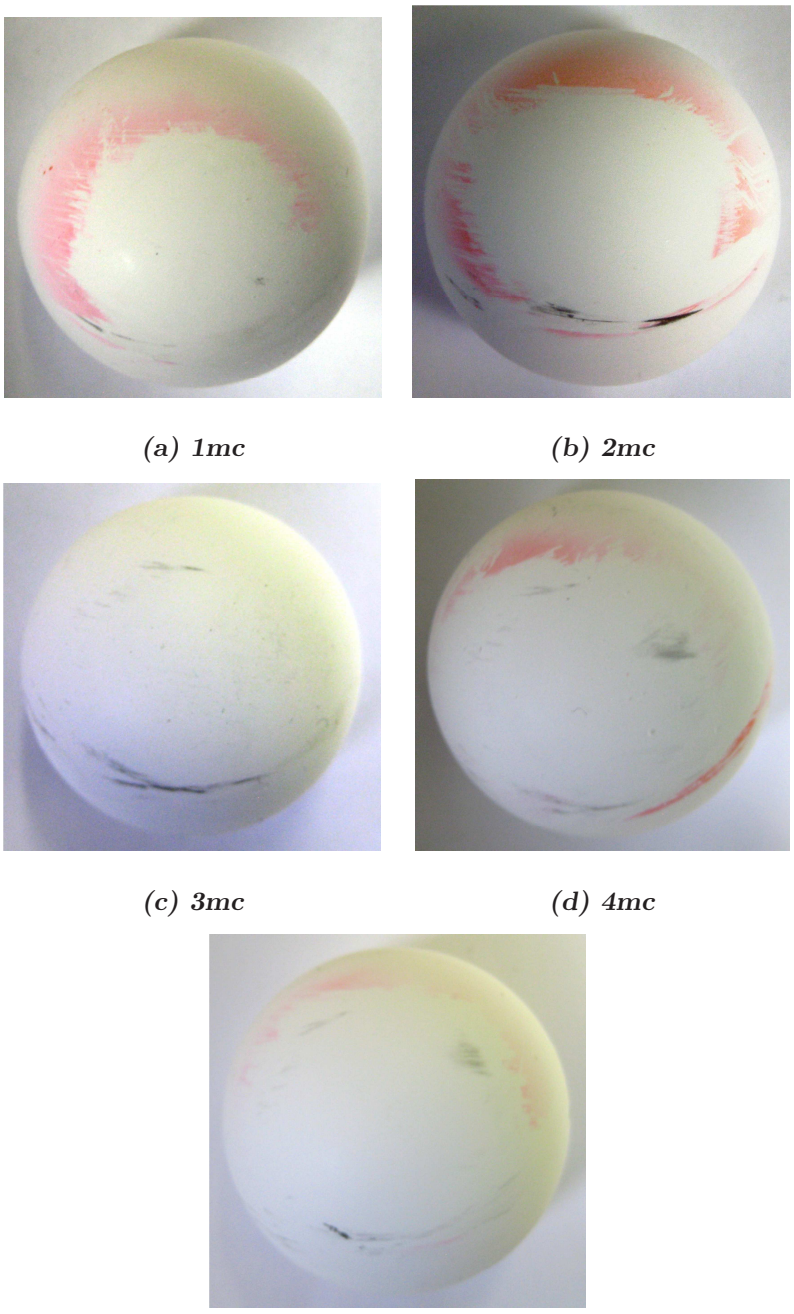

(a) 1mc *(b) 2mc*

(c) 3mc *(d) 4mc*

(e) 5mc

Figure 9.23: *Digital images of dyed deposit on the ZTA heads over a 5 million cycle microseparation wear test.*

The deposit was recorded after each 0.5 million cycle wear period, over 5 million cycles, an example of which is shown in Figure 9.23. The amount of deposit appeared to vary between 0.5 million cycles time periods. The most deposit found during the first 2 million cycles compared with the last 2 million cycles. Digital images of the metallic cups revealed deposit surrounding the wear patch in the superior lateral region of the cup. Scratching could be seen within the deposit however this did not appear to damage the underlying surfaces. The wear patch was slightly off centre as a result of relocation of the head into the cup. Figure 9.24 shows the metallic cups with the corresponding head after 2.5 million cycles of wear. From the images it appears that the contact areas of the head and cup were not exactly the same shape and size with a larger 'clear' area visible on the heads compared with the cups.

Figure 9.24 shows examples of different heads at the 2.5 million cycle wear interval.

(a) Station 1

(b) Station 1

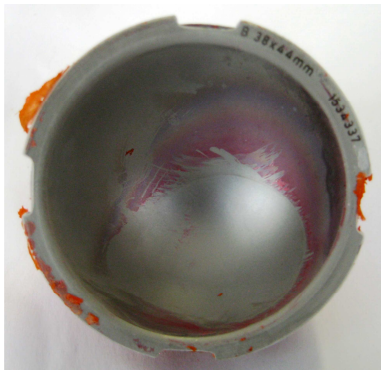

(c) Station 3

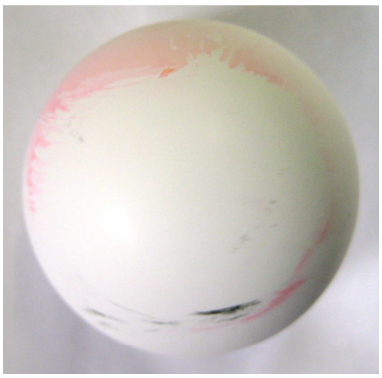

(d) Station 3

(e) Load Control

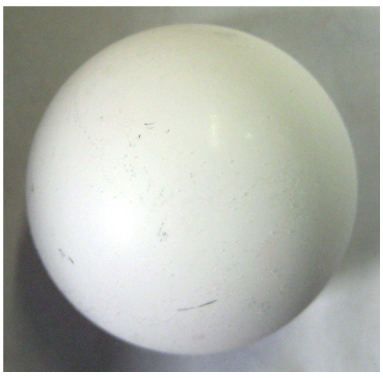

(f) Load Control

Figure 9.24: *Digital images of dyed deposit on the head and corresponding cups after 2.5 million cycles of microseparation test. Figures (e) and (f) show the loaded control with no deposit.*

Chapter 10

Results - Third Body Alumina Particle Testing of 38 mm Alumina and ZTA Joints

Pre-worn 38 mm alumina and ZTA heads and as-cast CoCrMo alloy cups were tested under standard walking conditions, with the addition of 0.5g of alumina particles in the lubricant. Chapters 6 and 7 show the results of the components previously tested under standard conditions before the third body particle testing. Throughout this chapter, the alumina heads against CoCrMo cups will be called the alumina test, and the ZTA heads against CoCrMo cups will be called the ZTA test.

10.1 Wear Results

A standard walking cycle loading pattern was implemented for 2 million cycles with the addition of alumina powder to the lubricant (stage 1). Following this a further 1 million cycles was undertaken with 'clean' lubricant (stage 2), to observe if the wear rates returned to the original steady state wear rates reported in Chapters 6 and 7. The ZTA test was continued for a further 0.5 million cycles (total 1.5 million cycles) with clean lubricant to confirm the wear rate after the particle testing. The results of these wear tests are shown in Figures 10.1, 10.2, 10.3 and 10.4. The stations with particles included in the lubricant are highlighted in orange.

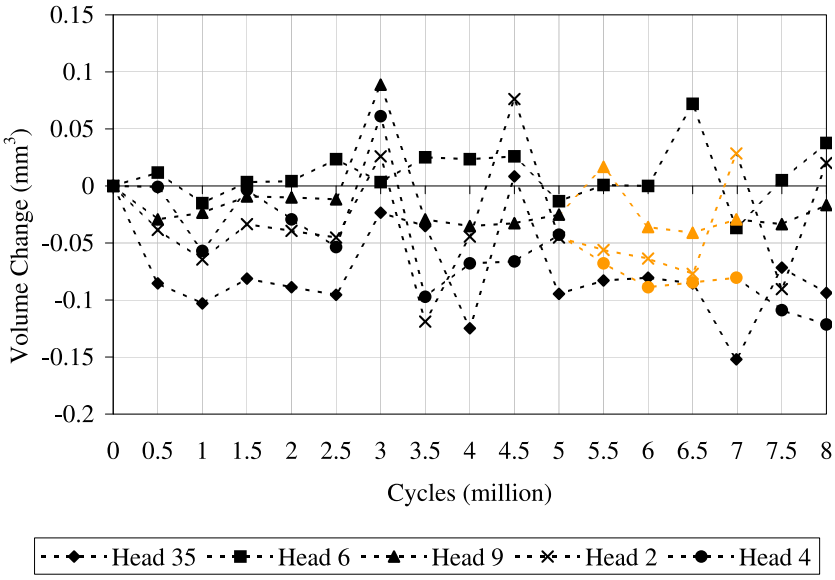

Figure 10.1: *Volume change of 38 mm alumina femoral heads under standard walking cycle conditions with and without the addition of alumina particles to the lubricant. (0-5 mc standard wear testing, 5-7 mc = Stage 1, 7-8 mc = Stage 2).*

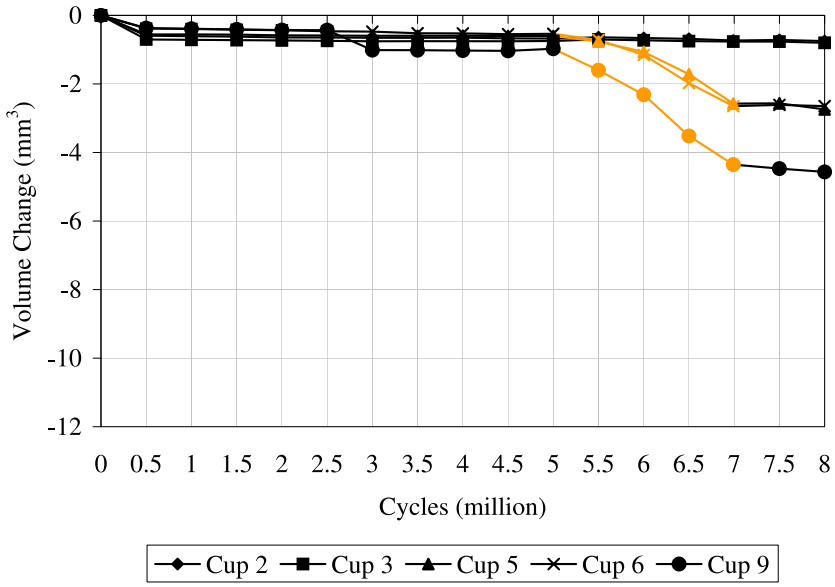

Figure 10.2: *Volume change of 38 mm CoCrMo acetabular cups (corresponding to the alumina heads) under standard walking cycle conditions with and without the addition of alumina particles to the lubricant. (0-5 mc standard wear testing, 5-7 mc = Stage 1, 7-8 mc = Stage 2).*

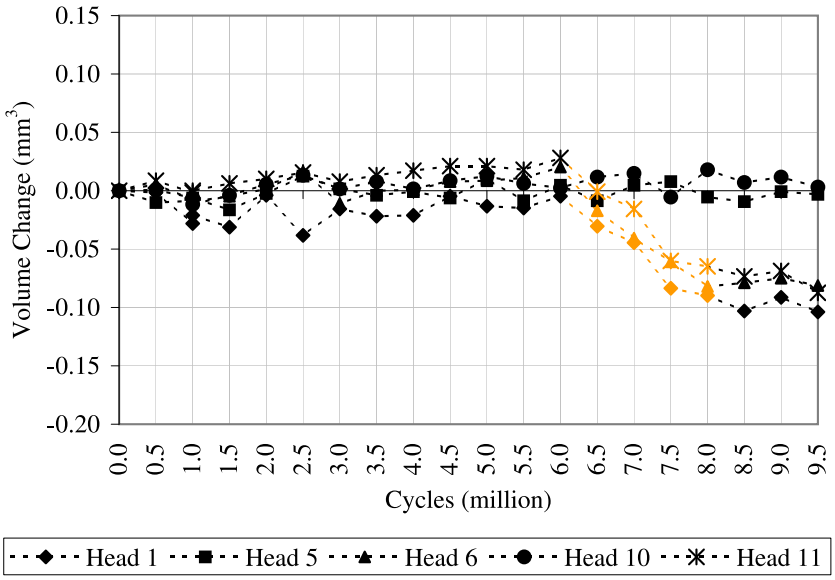

Figure 10.3: *Volume change of 38 mm ZTA femoral heads under standard walking cycle conditions with and without the addition of alumina particles to the lubricant. (0-6 mc standard wear testing, 6-8 mc = Stage 1, 8-9.5 mc = Stage 2).*

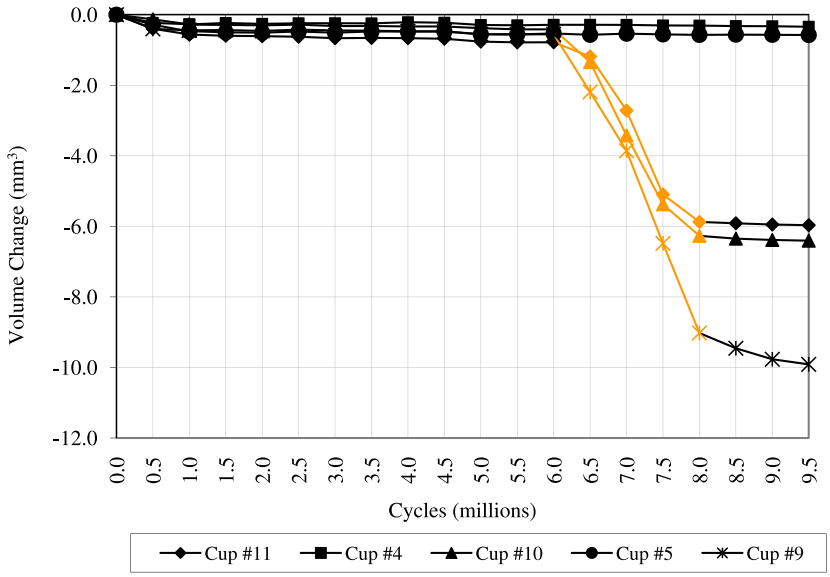

Figure 10.4: *Volume change of 38 mm CoCrMo acetabular cups (corresponding to the ZTA heads) under standard walking cycle conditions with and without the addition of alumina particles to the lubricant. (0-6 mc standard wear testing, 6-8 mc = Stage 1, 8-9.5 mc = Stage 2).*

	Station	Cup	Stage 1 (mm^3/mc)	Stage 2 (mm^3/mc)	Stage 1+2 (mm^3/mc)
ALUMINA TEST					
	1	9	1.721	0.212	
	2	6	1.119	0.001	
	3	5	0.976	0.170	
	4	2	0.041	0.016	0.037
	5	3	0.041	0.037	0.036
ZTA TEST					
	1	#10	3.145	0.089	
	2	#9	4.245	0.595	
	3	#11	2.816	0.063	
	4	#5	0.006	0.003	0.007
	5	#4	0.010	0.021	0.016

Table 10.1: *Individual CoCrMo cup wear rates from the 38 mm standard walking cycle conditions during third body particle testing.*

Wear rates were calculated for different stages of wear (stage 1 and stage 2). The results are shown in Table 10.1. Particles were added to the lubricant of stations 1, 2 and 3. For the two stations where only 'clean' lubricant was used for the entire test, one wear rate was calculated for the entire test. This is labeled Stages 1+2.

Average wear rates were calculated for the two groups of data (i.e. particle stations and non particle stations) and are shown in Table 10.2. The data represents the mean and the 95% confidence interval for the combined normalised data.

The addition of alumina particles to the lubricant had a greater effect on the wear of the cups corresponding to the ZTA heads compared with the cups corresponding to the alumina heads with wear rates of 1.272 $\pm$0.245 and 3.402 $\pm$0.485 for the alumina and ZTA tests respectively. The wear rate of the cups from the ZTA test was over two fold greater than the cups from the alumina test. During stage 2 of the wear test, the ZTA test cup wear rate was twice that of the alumina test. For

	ALUMINA TEST mm^3/mc	ZTA TEST mm^3/mc
Particle stations Stage 1 (2mc)	1.272 ± 0.245	3.402 ± 0.485
Particle stations Stage 2 (1/1.5mc)	0.127 ± 0.102	0.249 ± 0.181
No particle stations Stage 1 (2mc)	0.041 ± 0.014	0.008 ± 0.011
No particle stations Stage 2 (1/1.5mc)	0.027 ± 0.042	0.012 ±0.017
No particle stations Stage 1 + Stage 2 (3/3.5mc)	0.036 ± 0.018	0.010 ± 0.006

Table 10.2: *Average CoCrMo cup wear rates of the 38 mm standard waking cycle conditions during third body particle testing (mean±95% C.I.).*

both tests the wear was considerably higher after particle testing compared with the stations lubricated with 'clean' lubricant throughout the entire test.

Interestingly, the ZTA head wear rate was also found to increase due to the presence of third body alumina particles within the lubricant, whereas the alumina heads did not change. The individual and average wear rates of the heads are shown in Tables 10.3 and 10.4. A positive wear rate represented a volume loss, and a negative wear rate represented a volume gain.

No change in wear rate of the alumina heads was observed between stages 1 and 2, as the heads showed random fluctuations not thought to be due to the 3rd body alumina particles. However a considerable increase in wear was found for the ZTA heads during stage 1 compared with stage 2 (0.006 mm^3/mc in stage 2 compared with 0.046 mm^3/mc in stage 1). The wear rates of the stations with 'clean' lubricant remained low for the duration of the test (compared with particle stations), however the wear rates of the alumina heads were considerably higher than the ZTA heads. A small gain in volume was found for the alumina head during stage 2 of the test however this is not a trend typical over the whole test.

The lubricant was collected from certain stations after each 0.5 million cycle stage. A significant difference in colour was observed between the alumina test and ZTA test. The lubricant from the ZTA test was considerably darker, suggesting a greater number of metal particles were present. The alumina test lubricant remained

	Station	Head (mm^3/mc)	Stage 1 (mm^3/mc)	Stage 2 (mm^3/mc)	Stage 1+2
ALUMINA TEST					
	1	4	0.027	0.041	
	2	2	-0.008	0.008	
	3	9	0.036	0.013	
	4	35	0.048	-0.058	0.016
	5	6	0.005	-0.075	-0.004
ZTA TEST					
	1	6	0.048	-0.001	
	2	11	0.047	0.013	
	3	1	0.043	0.006	
	4	10	0.004	0.008	0.003
	5	5	-0.005	-0.003	-0.001

Table 10.3: *Individual wear rates of the 38 mm heads tested under standard walking cycle conditions during third body particle tests.*

	ALUMINA Head mm^3/mc	ZTA Head mm^3/mc
Particle stations Stage 1 (2mc)	0.019 ± 0.027	0.046 ± 0.005
Particle stations Stage 2 (1/1.5mc)	0.012 ± 0.007	0.006 ± 0.007
No particle stations Stage 1 (2mc)	0.026 ± 0.036	-0.001 ± 0.009
No particle stations Stage 2 (1/1.5mc)	-0.066 ± 0.059	0.002 ±0.027
No particle stations Stage 1 + Stage 2 (3/3.5mc)	0.006 ± 0.020	0.001 ± 0.003

Table 10.4: *Average wear rates of the 38 mm heads tested under standard walking cycle conditions during third body particle tests (mean±95% C.I.).*

a similar colour as the original diluted serum however was more opaque. Figure 10.5 shows the frozen lubricant from the particle test. The darker serum supported the higher wear rates seen for the ZTA test cups, compared with the alumina test.

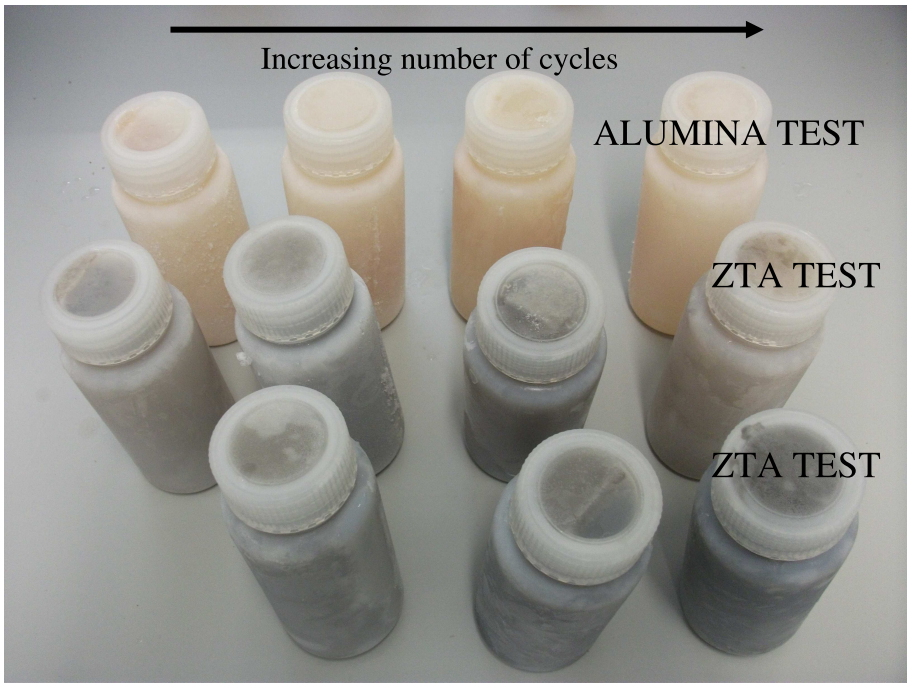

Figure 10.5: *Frozen serum from the third body particle test. The top row shows serum saved from an alumina test station, and the bottom two rows show the darker serum found from two stations from the ZTA test stations.*

10.2 Friction testing

Low friction factors were found for the components after standard wear testing for both the alumina and ZTA components and the Stribeck curve indicated a lubrication regime close to full fluid film. Figures 10.6 and 10.7 show the results of friction tests carried out at the end of standard wear testing, which are compared with the friction results after 2 million cycles of particle testing (final tests on the alumin heads carried out by a 4th year student under the cosupervision of the author for the practical work).

Interestingly a small increase in friction factors were found for the ZTA:CoCrMo

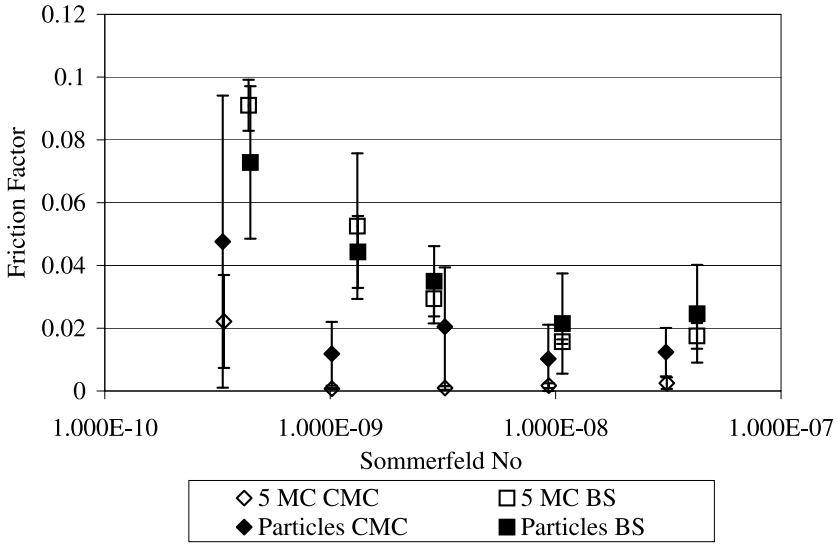

Figure 10.6: *Stribeck Plot of a 38 mm ZTA:CoCrMo component tested after 5 million cycles of standard wear testing, 2 million cycles with alumina particles incorporated into the lubricant and 1.5 million cycles of standard wear testing.*

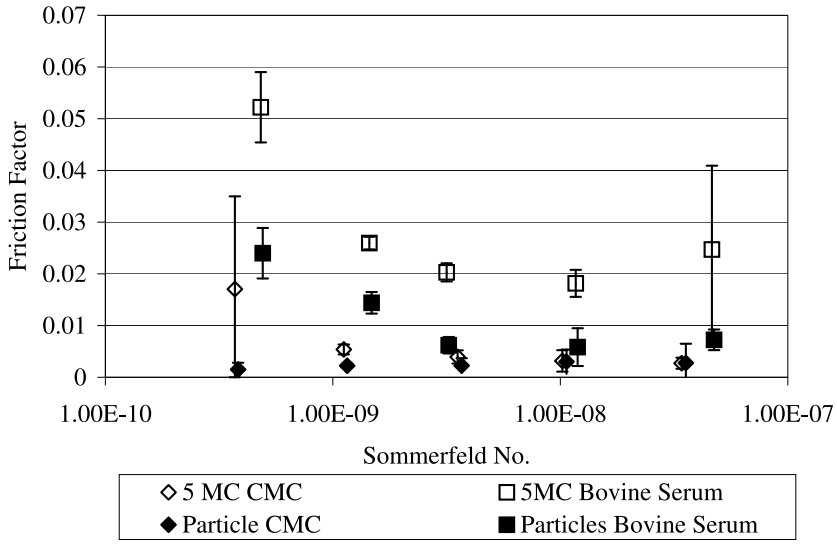

Figure 10.7: *Stribeck Plot of a 38 mm Alumina:CoCrMo component tested after 5 million cycles of standard wear testing, 2 million cycles with alumina particles incorporated into the lubricant and 1.0 million cycles of standard wear testing.*

couple after particle testing had occurred, for all lubricants except the two lowest viscosities of bovine serum based lubricants. All friction factors were less than 0.1. When bovine serum based lubricants were used, a decrease in friction factor was found with increasing Sommerfeld number with a slight increase in friction factor found for the highest viscosity, which was indicative of full fluid film lubrication. The majority of tests using water based lubricants resulted in friction factors of less than 0.04 with a slight trend of a decreasing friction factor with increasing Sommerfeld number, however not as distinct as when bovine serum based lubricants were used.

In contrast a decrease in friction factor was seen for the Alumina:CoCrMo couple when tested with bovine serum lubricants, after particle testing. With the exception of the lowest viscosity of water based lubricants (deionised water), the friction factors were similar after standard wear testing and after particle testing. All friction factors were less than 0.06 which is lower than that found for the ZTA test. The shape of the curve and the low friction factors indicated that the joints were working close to full fluid film lubrication.

Theoretical lubrication calculations provided minimum film thickness and lambda values as shown in Table 10.5.

	Cycles (millions)	Head Rms (μm)	Cup Rms (μm)	H min (μm)	λ	Friction factors CMC*/BS**
Alumina	0	0.009	0.013	0.07	>3	0.017/0.052[1]
	1	0.011	0.011	0.07	>3	-
	2	0.011	0.007	0.07	>3	-
	3	0.017	0.012	0.07	>3	0.002/0.024[1]
						0.011/0.029[2]
ZTA	0	0.013	0.010	0.07	>3	0.022/0.091[3]
	1	0.011	0.011	0.07	>3	-
	2	0.013	0.007	0.07	>3	-
	3	0.016	0.009	0.07	>3	0.47/0.073[3]

* CMC η=0.001 Pa s^{-1}, **BS η=0.0013 Pa s^{-1}

[1] = head 4, cup 9, [2] = head 2 cup 6, [3] = head 6 cup #10

Table 10.5: *Theoretical minimum film thickness and lambda values for 38 mm 3rd body wear tests.*

10.3 Surface Analysis

10.3.1 Non contacting Interferometry

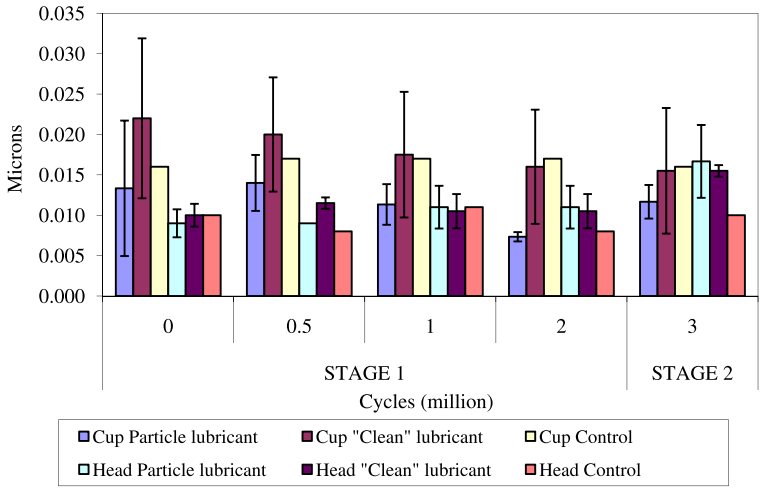

(a) Alumina RMS Roughness

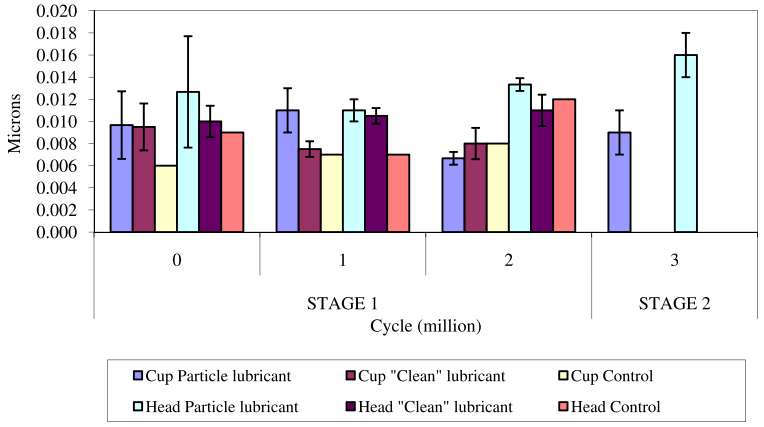

(b) ZTA RMS Roughness

Figure 10.8: *Rms roughness values of the alumina:CoCrMo and ZTA:CoCrMo components during the alumina particle testing.*

Surface analysis was carried out at 0, 0.5, 1, 2 and 3/3.5 million cycles of wear. This included 4 measurements during stage 1 when particles were included in the lubricant, and a measurement was taken at 3/3.5 million cycles at the end of stage 2 (clean lubricant). The results are presented in Figures 10.8 and Figures 10.9.The results of the ZTA test at 0.5 million cycles have been omitted as they were considered to be incorrect. No considerable difference was seen in roughness for any of the

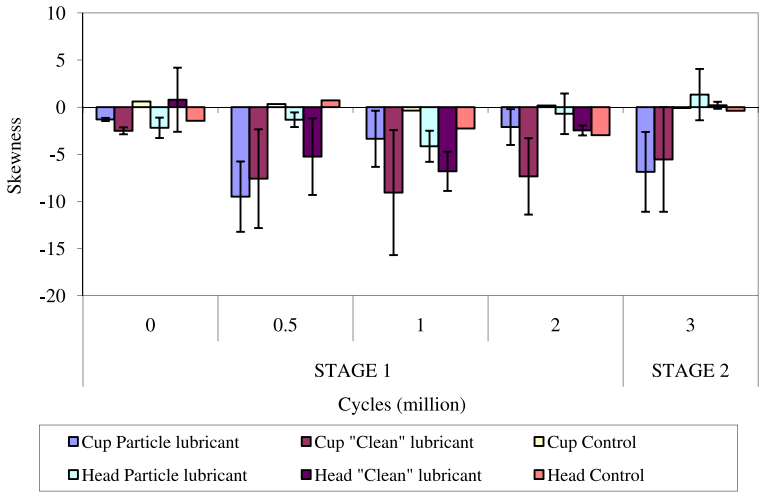

(a) Alumina Skewness

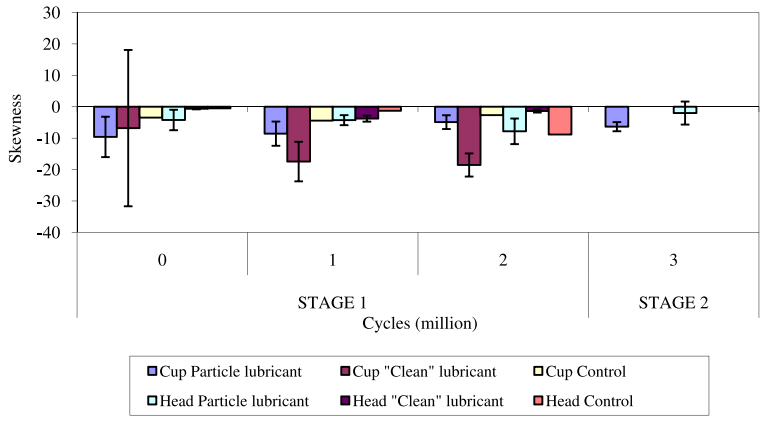

(b) ZTA Skewness

Figure 10.9: *Skewness values of the alumina:CoCrMo and ZTA:CoCrMo components during the alumina particle testing*

components. A slight decrease in both the particle and non particle stations was seen during stage 1. During stage 2, the roughness of the particle stations increased slightly. The control cup rms roughness remained the same throughout testing. No change in rms roughness of the alumina heads was noted during stage 1. A slight increase was seen for stage 2, as seen with the cups. The rms roughness of the cups from the ZTA test did not considerably change throughout testing with little change to the roughness of the heads.

The skewness values for the metallic cups of the alumina test, increased during the first 0.5 million cycles of testing as a result of the considerable increase in abrasive

third body scratches. However, as stage 1 progressed, the skewness of the cups in the particle stations decreased as the matrix material was worn and polished. The skewness of the non particle stations remained more negatively skewed throughout testing as a result of larger abrasive scratches and holes left from removed carbides. The head skewness value appeared relatively unaffected by third body particles. The skewness values for the ZTA test showed similar trends as the alumina test.

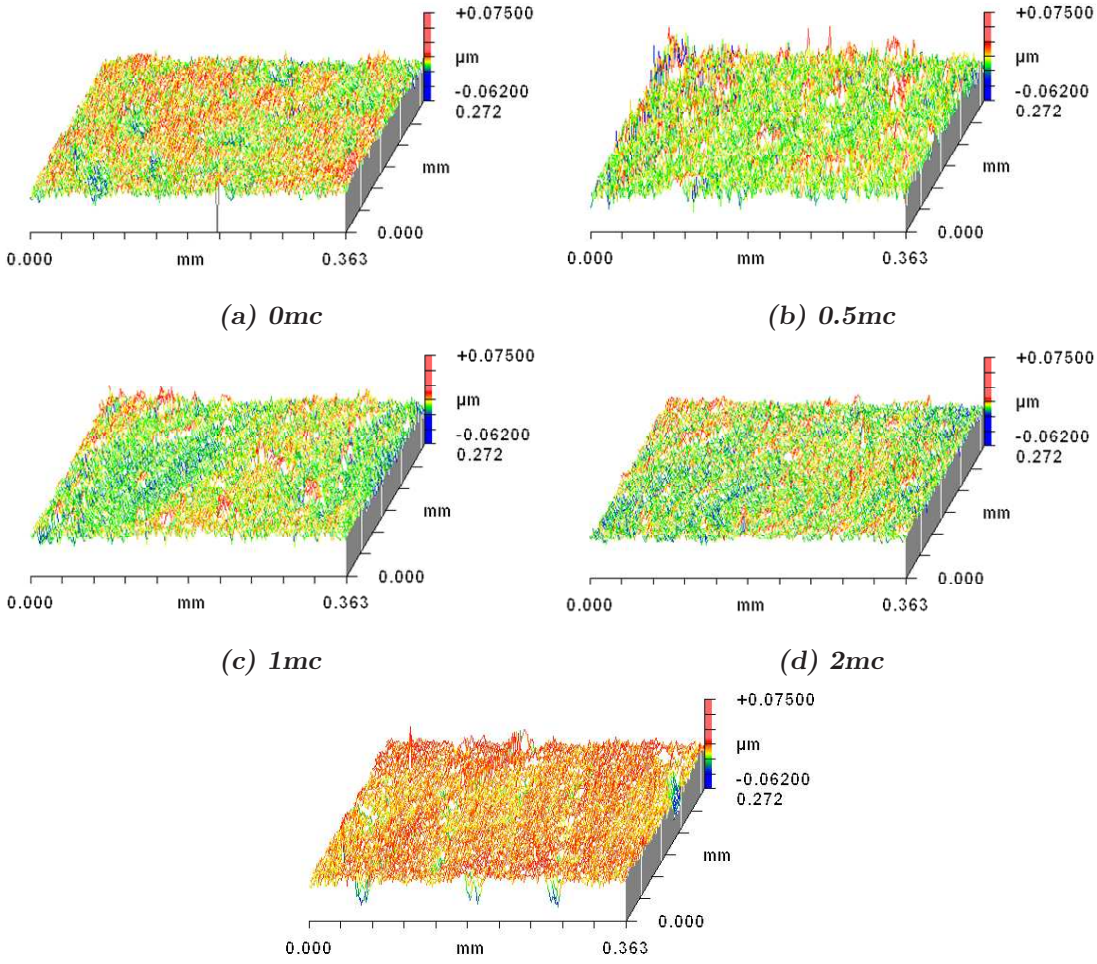

(a) 0mc *(b) 0.5mc*

(c) 1mc *(d) 2mc*

(e) 3mc

Figure 10.10: *3D Zygo plots of a wear patch of a metallic cup (from the alumina test) during the third body wear test. All images are shown at the same scale for comparison.*

The progression of surface topography of a metallic cup was monitored through 3D images. A typical cup progression (from the alumina test) is shown in Figures 10.10. The images within the Figure are shown at the same scale for comparison.

The topography did not appear to change significantly however closer inspection of the images revealed an interesting trend.

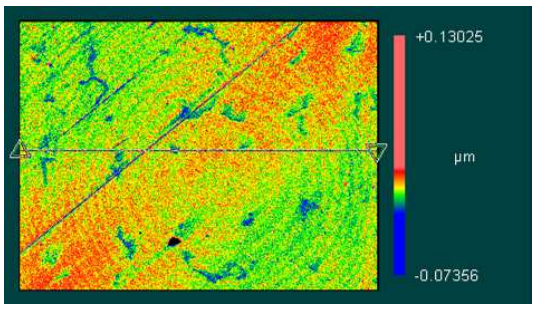

(a) Alumina test - Before particle test

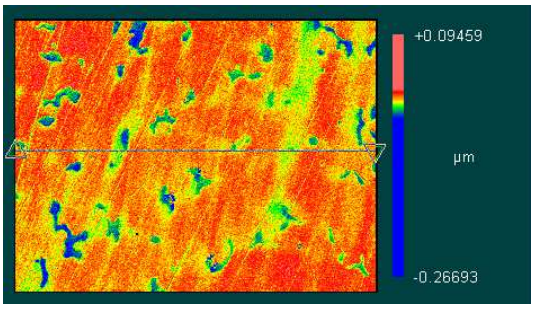

(b) ZTA test - Before particle test

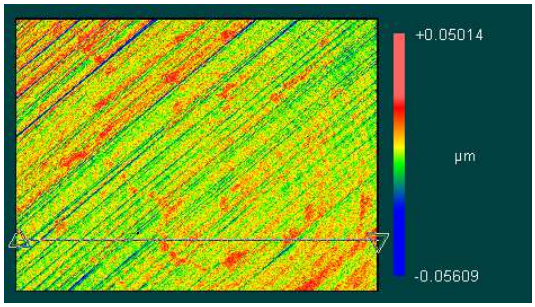

(c) Alumina test - After 2mc with particles included the in lubricant

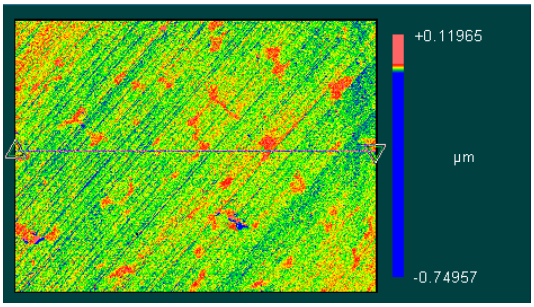

(d) ZTA test - After 2mc with particles included the in lubricant

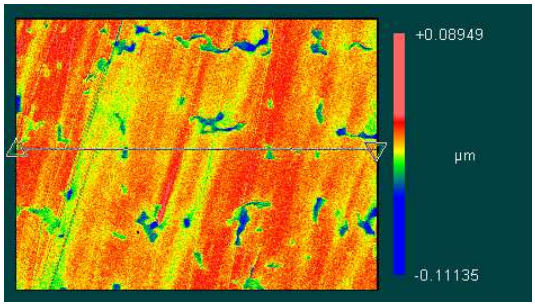

(e) Alumina test - After 1mc of clean lubricant

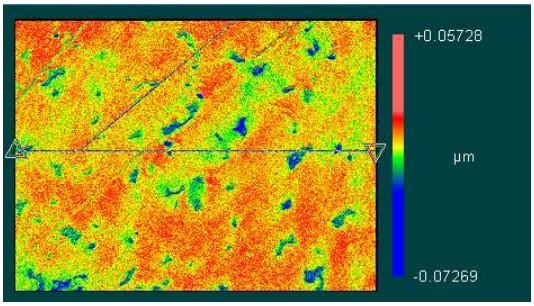

(f) ZTA test - After 1mc of clean lubricant

Figure 10.11: *Zygo micrographs showing holes and protruding carbides within the metallic cups.*

Rescaling the images allowed individual surface features to be seen. Before third body testing, the images of the metallic cups revealed holes left from removed or worn carbide (see Figure 10.11(a) and 10.11(b)). However, after 2 million cycles of wear with third body particles present, the carbides appear to stick out of the matrix material as the softer matrix material had been worn away (see Figures 10.11(c)

and 10.11(d)). After a further 1/1.5 million cycles of clean lubricant, the holes became apparent where carbides were once present (see Figures 10.11(e) and 10.11(f)). This trend was found for both the cups corresponding to the alumina and ZTA heads.

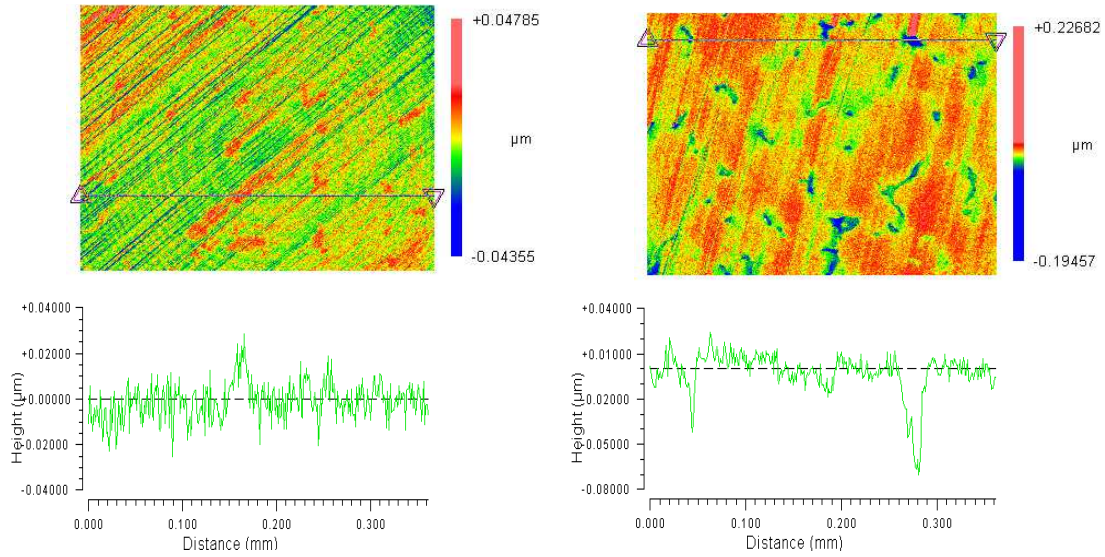

(a) After stage 1 ***(b) After stage 2***

Figure 10.12: *Line profiles from the cups from third body particles tests (cups corresponding to alumina test), showing the position of the carbides within the matrix.*

Figure 10.12 shows abrasive scratches (in the flexion/extension plane) on the metallic cups from the alumina test showing the carbides protruding from the surface and the holes left from removed carbides. Line profiles of the surfaces show the position of the carbides within the matrix material. A similar feature was found for the ZTA test.

10.3.2 Optical Microscopy

Optical images taken periodically revealed considerable damage to the metallic cups in the stations where additional alumina particles were added to the lubricant. A heterogeneous surface topography was found with abrasive and adhesive wear prevalent. In addition considerable areas appeared to have a layer of transfer (possibly metal and protein) on top of the original surface. Figures 10.13 and 10.14 shows a range of images taken during the 2 million cycles where particles were present in the lubricant.

The cup images from the alumina test showed regular parallel abrasive scratches in-line with the flexion/extension direction motion (see Figure 10.13). Wispy, less regular curved abrasive scratches were also evident and are shown in Figures 10.13(c) and 10.13(e). The transfer/deposition highlighted the topography and position of the carbides as shown in Figure 10.13(a) and Figure 10.13(c).

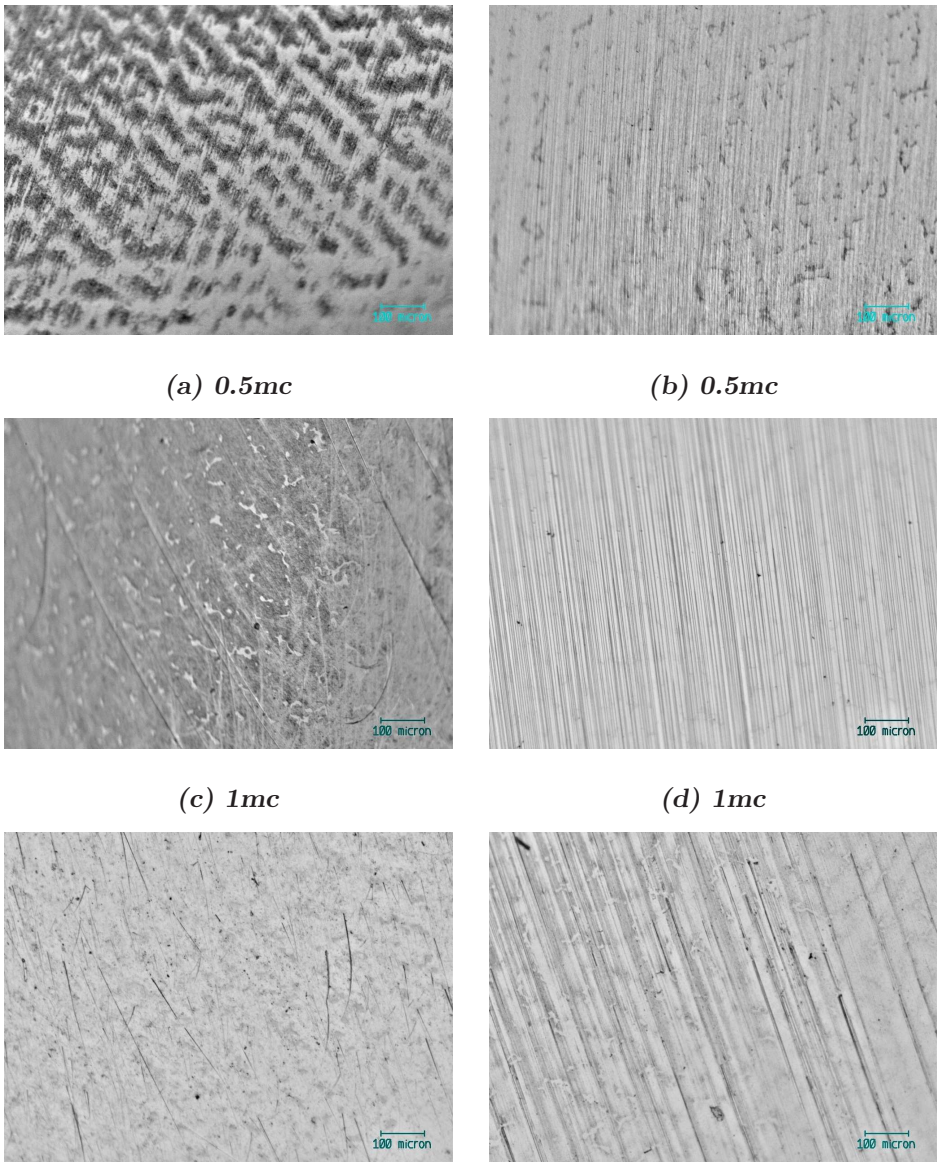

(a) 0.5mc *(b) 0.5mc*

(c) 1mc *(d) 1mc*

(e) 2mc *(f) 2mc*

Figure 10.13: *Optical images of the as-cast CoCrMo cups (alumina test) showing the progression of the surfaces when particles were included in the lubricant. (a) transfer or metal particles, (b), (d) % (f) fine abrasive scratches likely to be caused by third body particles, (c)transfer which highlights the wispy third body wear, (e) random abrasive scratches.*

The cup images from the ZTA test again showed parallel abrasive scratches in the flexion/extension direction (Figure 10.14). Areas were also found within the wear patch where no abrasive scratches were evident (Figure 10.14(d)) but the carbides were almost indistinguishable from the matrix material, suggesting they had been worn smooth.

Limited damage was seen on the metallic cups in 'clean' lubricant with occasional abrasive scratching and adhesive wear such as pitting. The alumina test typically showed shorter length abrasive scratches and a large proportion of area with very limited abrasive wear and pitting. The ZTA test cups with no particles within the lubricant revealed very little damage with only small amounts of pitting or abrasive wear.

The surfaces were also analysed after an additional period of wear where 'clean' lubricant was used for all stations. The surface topography of all cups appeared not to change, including the stations which previously incorporated alumina particles. Areas of parallel abrasive scratches and individual abrasive wear was seen within the wear patch of the cups. Areas with relatively little damage were also evident within the wear patch.

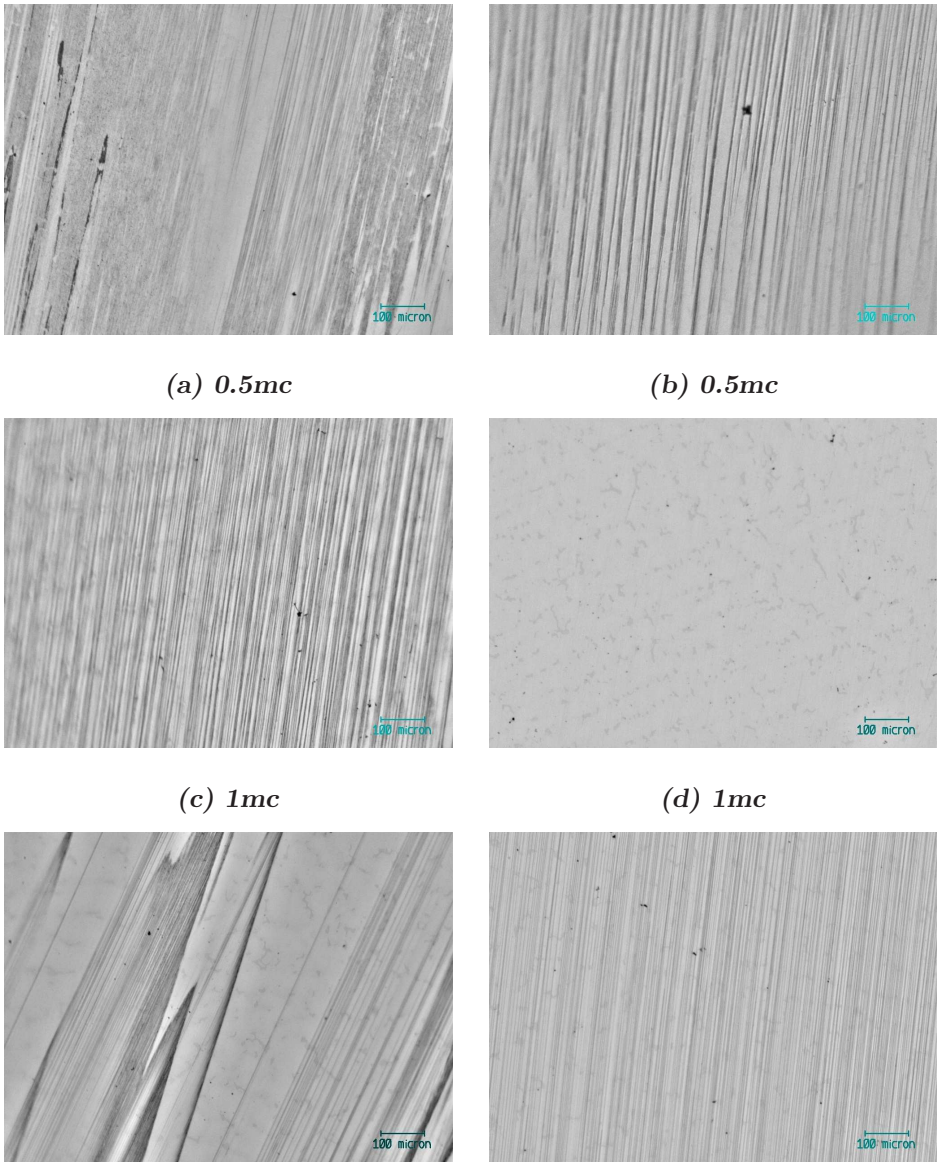

(a) 0.5mc *(b) 0.5mc*

(c) 1mc *(d) 1mc*

(e) 2mc *(f) 2mc*

Figure 10.14: *Optical images of the as-cast CoCrMo cups (ZTA test) showing the progression of the surfaces when particles were included in the lubricant. (a),(b),(c),(e),(f) abrasive scratches likely to be caused by third body wear particles, (d) smooth un-featured surface.*

10.3.3 Atomic Force Microscopy

Five million cycles of standard wear resulted in shallow grain pull out on the pole of the alumina heads. The holes were polygon shaped and tens of nanometres deep. After 0.5 million cycles of wear with additional particles within the lubricant the surface topography of the alumina heads changed. Grain pull out was more evident, with much deeper holes in addition to the shallow polygonal grains. The holes appeared to have developed in the direction of motion with a 'comet tail' forming as the grain was removed from the surface, holes were hundreds of nanometres deep. Images and line profiles of 100 μm and 20 μm scans are shown in Figure 10.15. In contrast micrographs of the alumina heads in the stations where 'clean' lubricant was used, revealed only shallow grain removal as was seen after 5 million cycles of standard wear (see Chapter 6). The loaded control head topography did not change from the unworn surface.

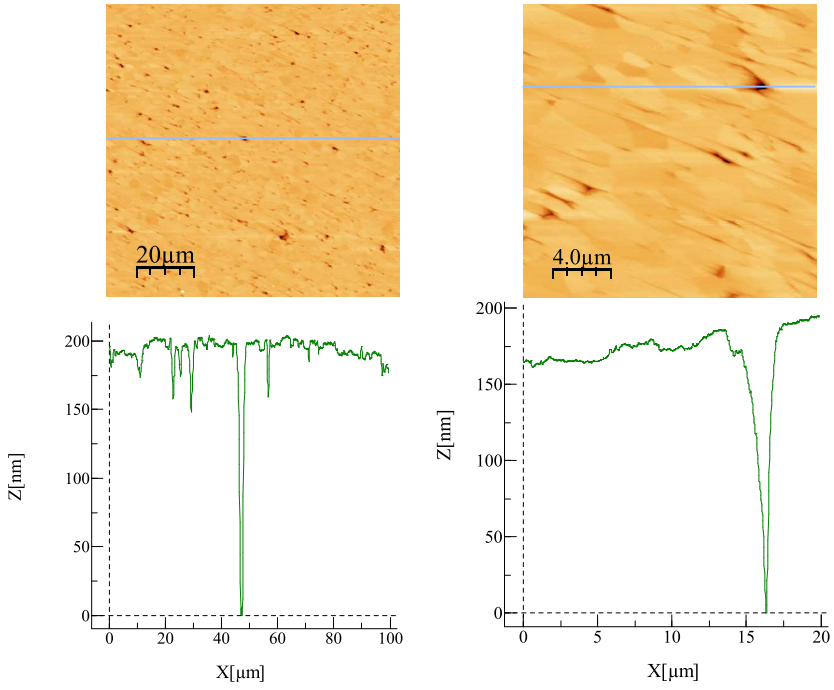

(a) Particles - 100 µm *(b) Particles - 20 µm*

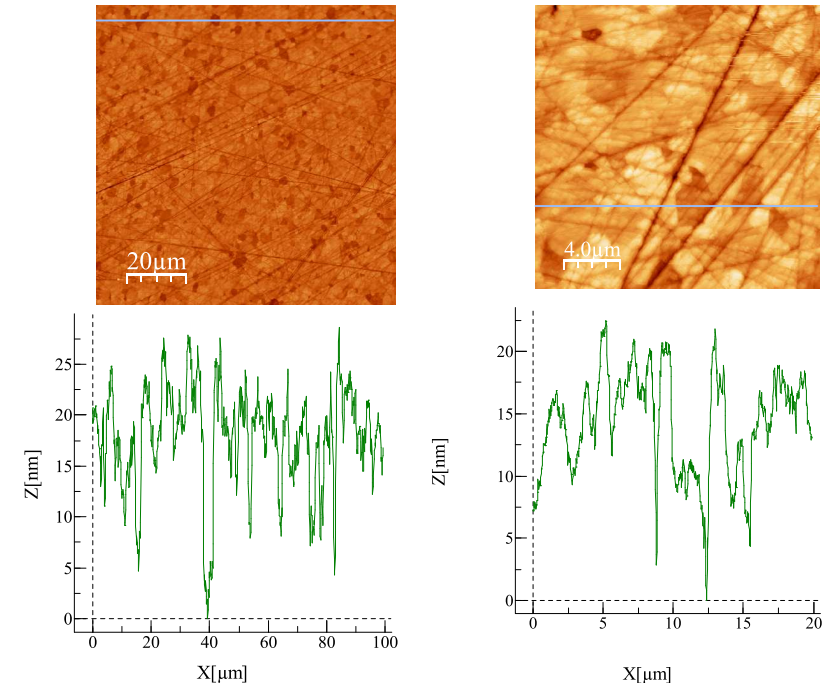

(c) Clean - 100 µm *(d) Clean - 20 µm*

Figure 10.15: *AFM images of alumina head after 0.5 million cycles of wear with (a) &(b) particles in the lubricant, (c) & (d) clean lubricant.*

Images taken after 1 and 2 million cycles revealed similar features to those seen after 0.5 million cycles as shown in Figure 10.16.

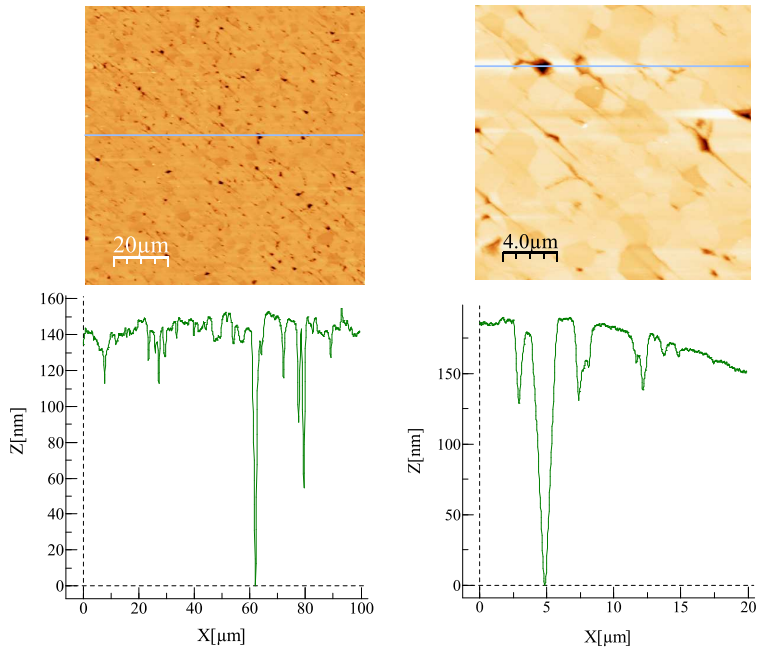

(a) Particles (Head 9) - 100 μm *(b) Particles (Head 9) - 20 μm*

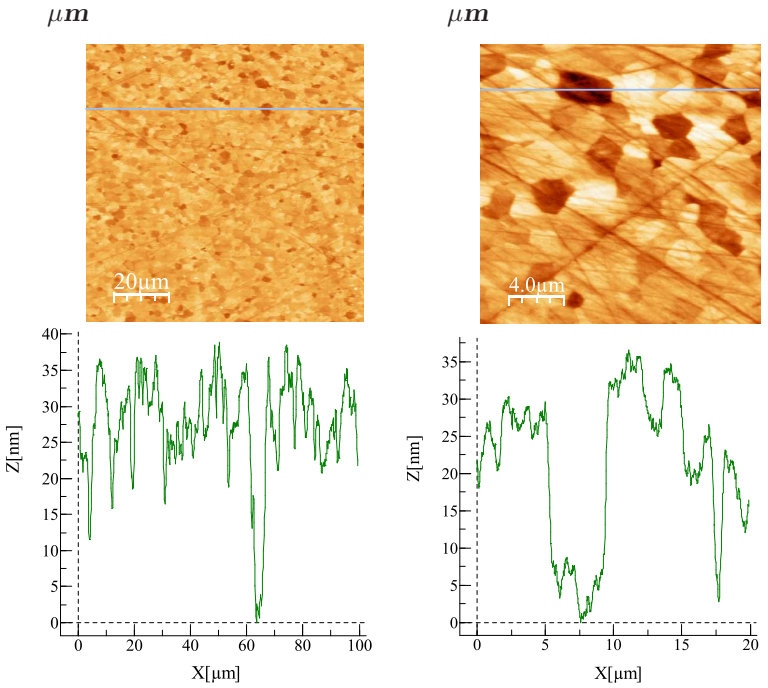

(c) Clean (Head 6) - 100 μm *(d) Clean (Head 6) - 20 μm*

Figure 10.16: *AFM images of alumina head after 2 million cycles with particle in the lubricant, (a) & (b), and with 'clean' lubricant, (c) & (d).*

A similar trend was found for the ZTA heads. The ZTA heads after 6 million cycles of standard wear testing showed very limited, occasional grain pull out on the pole. The addition of third body particles into the lubricant resulted in the removal of many grains. Figure 10.17 shows 100 μm and 20 μm scans of the pole of the heads after 0.5 million cycles. The holes were tens of nanometres deep, shallower than the alumina holes, and randomly distributed over the surface. Comet tail features as seen for alumina heads, were not present. The removed grains in the ZTA heads are thought to be predominantly ZrO_2 particles which are embedded within the alumina matrix. These were clearly seen the SEM image of the ZTA ceramic provided by Morgan Ceramics (see Figure 5.1). The components in the 'clean' lubricant stations had a topography similar to those of the unworn surfaces with randomly distributed polishing scratches. The grain structure was hardly visible.

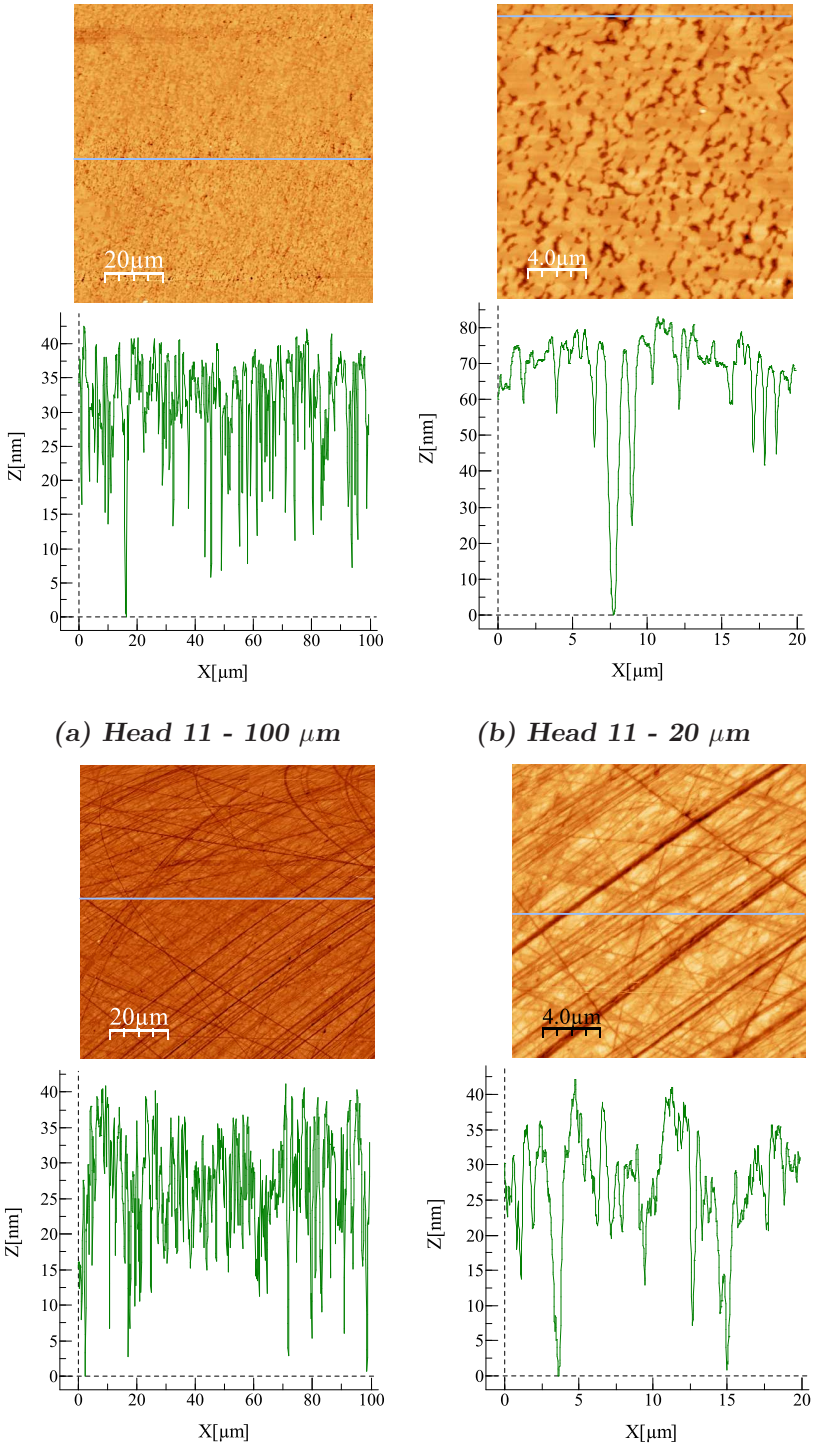

(a) Head 11 - 100 µm *(b) Head 11 - 20 µm*

(c) Clean (Head 10) - 100 µm *(d) Clean (Head 10) - 20 µm*

Figure 10.17: *AFM images of ZTA heads after 0.5 million cycles of wear with (a) & (b) particles in the lubricant, (c) & (d) clean lubricant.*

Head 1, which was found to be damaged before the standard testing, however a change in topography could still be seen (Figure 10.18).

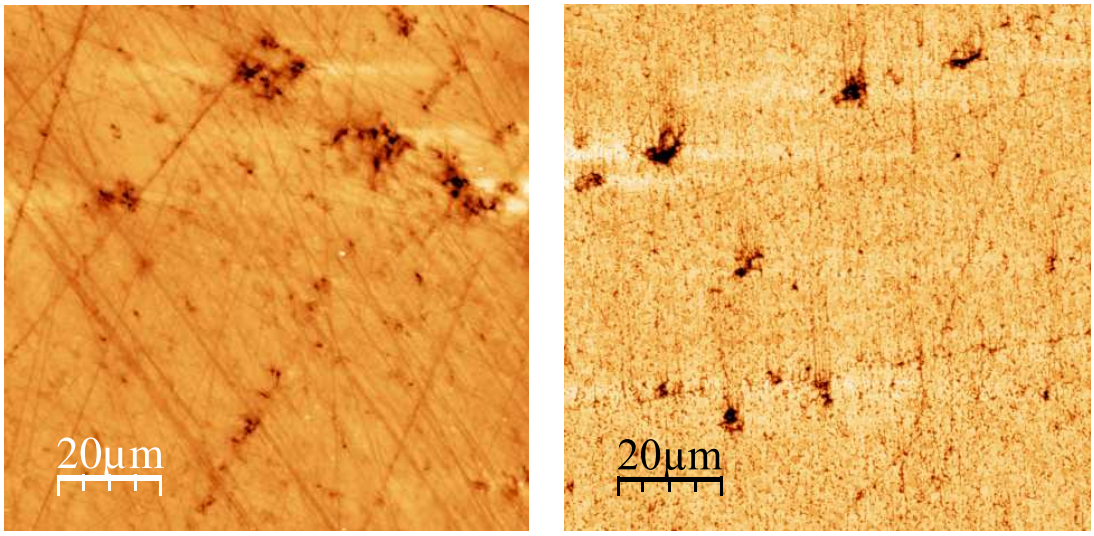

(a) 6 mc standard wear ***(b) 0.5 mc third body wear***

Figure 10.18: *AFM images of ZTA head 1 comparing the damage on head 1 after standard wear and 0.5 million cycles of third body wear.*

Images taken after 1 and 2 million cycles were similar to that after 0.5 million cycles. Figure 10.19 compares the topography of heads when particles were present with 'clean' lubricant stations at 2 million cycles. It also shows the difference between the two 'clean' lubricant stations as grains were more visible in head 10 compared with head 5.

During stage 2 (recovery period) little change was seen for either ceramic head material compared with the results at the end stage 1. Figures 10.20 shows the final surface topography micrographs.

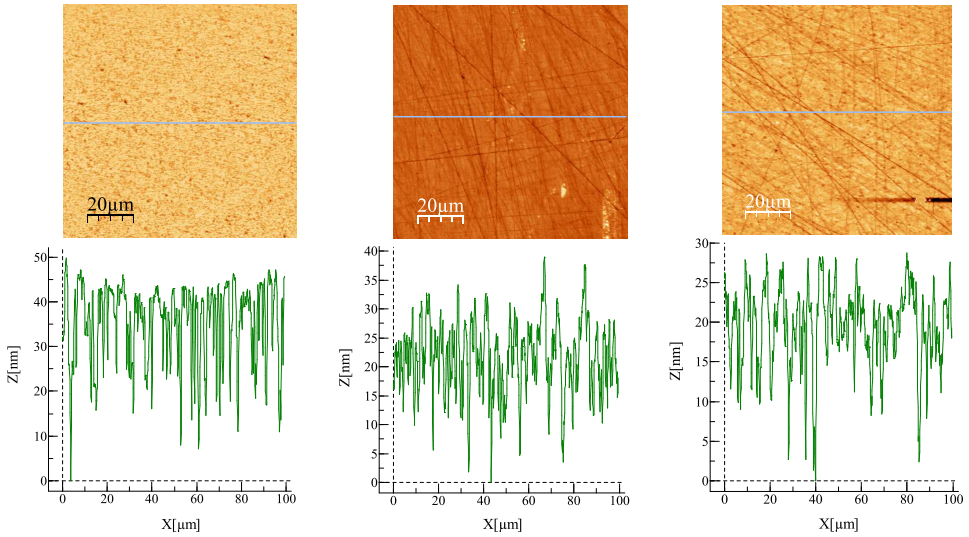

(a) Particles (Head 6) - 100 µm *(b) Clean (Head 5) - 100 µm* *(c) Clean (Head 10) - 100 µm*

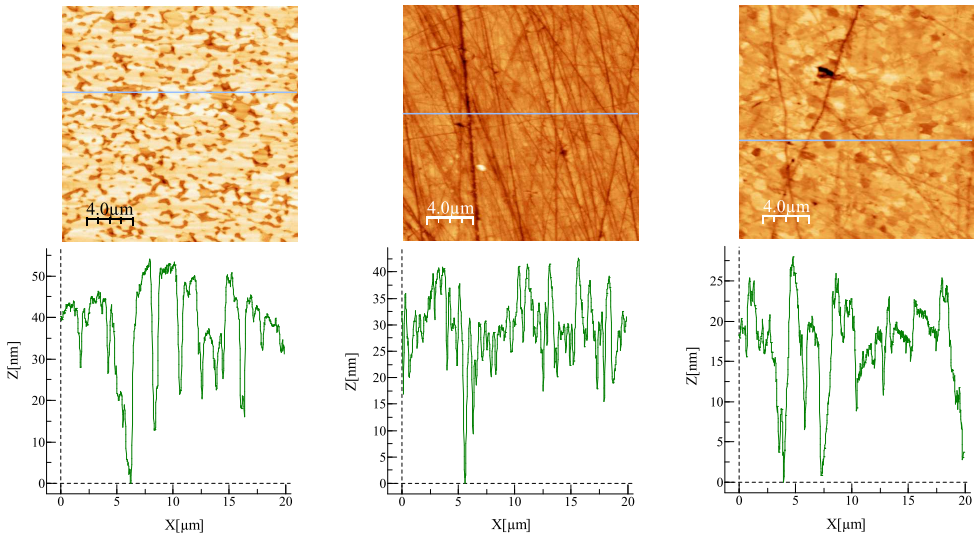

(d) Particles (Head 6) - 20 µm *(e) Clean (Head 5) - 20 µm* *(f) Clean (Head 10) - 20 µm*

Figure 10.19: *AFM images of ZTA heads after 2.0 million cycles of wear showing a component with particles in the lubricant (a & d) and a component worn with 'clean' lubricant (b, c, e & f).*

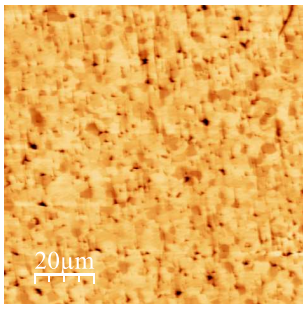

(a) Alumina, (particles)

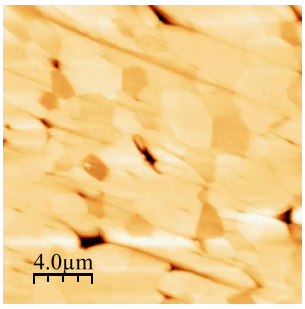

(b) Alumina, (particles)

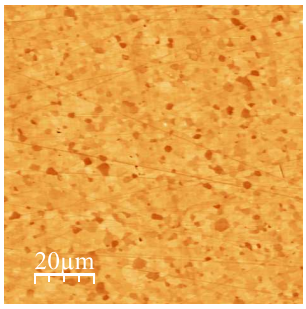

(c) Alumina, (clean)

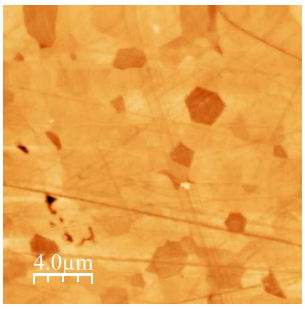

(d) Alumina, (clean)

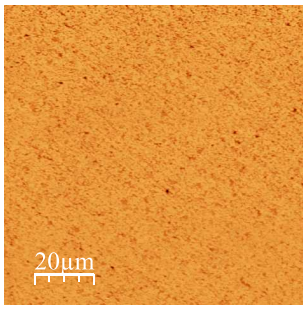

(e) ZTA (particles)

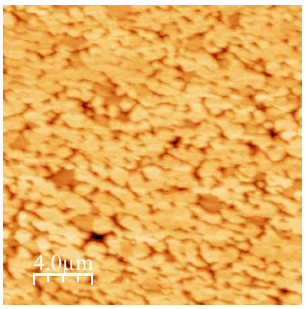

(f) ZTA (particles)

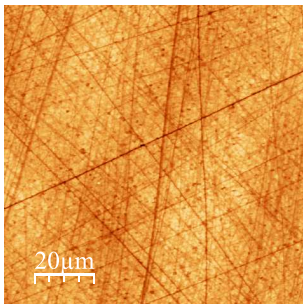

(g) ZTA, (clean)

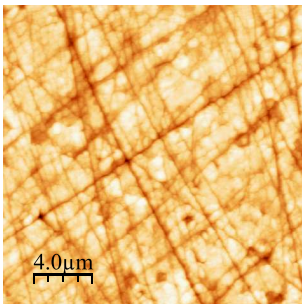

(h) ZTA, (clean)

Figure 10.20: *AFM images of alumina and ZTA heads after stage 2 of testing, (a) & (b) alumina head, particle lubricant, (c) & (d) alumina head, clean lubricant, (e) & (f)ZTA head, particles lubricant g) & h) ZTA head, clean lubricant.*

10.4 Deposition

During wear testing, a white substance was deposited onto the surface of the ceramic heads and metallic cups. The wear patch could clearly be identified on the pole of the head within the clear area which was enclosed within the deposit. Less deposit was seen on the components when particles were present in the lubricant compared with the 'clean' lubricant stations. Figure 10.21 and 10.22 show typical images taken during stage one of testing after 0.5 and 2 million cycles.

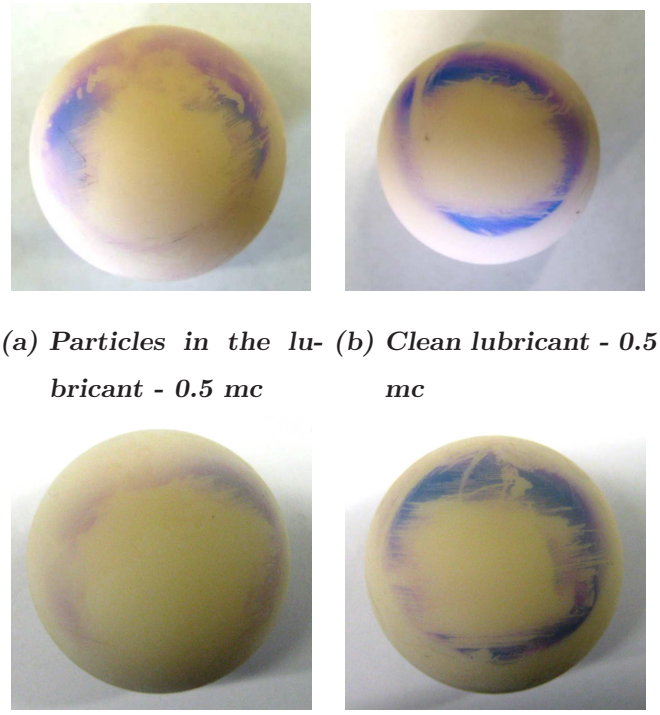

(a) Particles in the lubricant - 0.5 mc

(b) Clean lubricant - 0.5 mc

(c) Particles in the lubricant - 2 mc

(d) Clean lubricant - 2 mc

Figure 10.21: *Digital images of stained deposition on the alumina heads during third body particle testing taken at 0.5 million cycles (a & b) and 2 million cycles (c & d).*

(a) Particles in the lubricant - 0.5mc

(b) Clean lubricant - 0.5mc

(c) Particles in the lubricant - 2 mc

(d) Clean lubricant 2 mc

Figure 10.22: *Digital images of stained deposition on the ZTA heads during third body particle testing taken at 0.5 million cycles (a & b) and 2 million cycles (c & d).*

Figure 10.23 and 10.24 magnified images of the deposition and scratches which protrude into the deposition. By eye the underlying surface appeared undamaged.

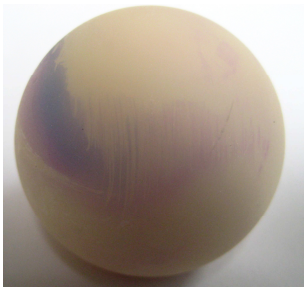

(a) Head 4

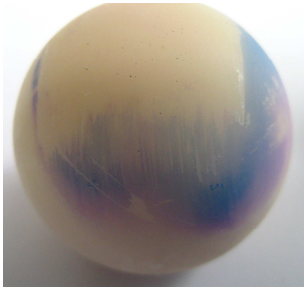

(b) Head 9

Figure 10.23: *Zoomed images of deposit on the alumina heads*

Figure 10.24 shows an image of an active station and the control station at the end of stage 2. The position and shape of the deposition was similar for all heads with the exception of the loaded control where no deposition was found. A rectangular shaped clear patch was found on the heads, however a circular clear patch was found on the cups. A greater amount of deposit was present on the ZTA heads compared with the alumina heads.

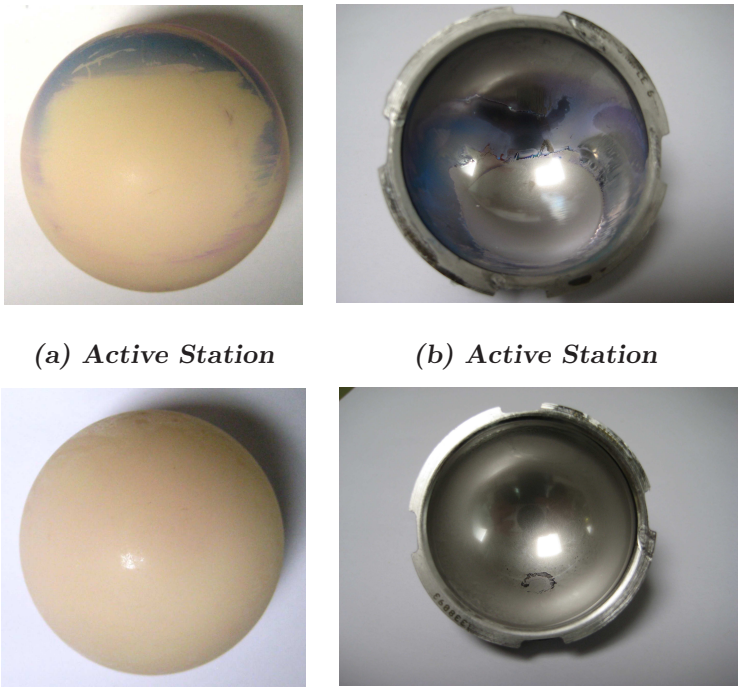

(a) Active Station ***(b) Active Station***

(c) Control Station ***(d) Control Station***

Figure 10.24: *Digital images of stained deposition on the alumina ceramic heads and corresponding metal cups after 0.5 million cycles of standard wear (end of stage 2), (a) & (b) stations which incorporate loading and motion, (c) & (d) loaded control station.*

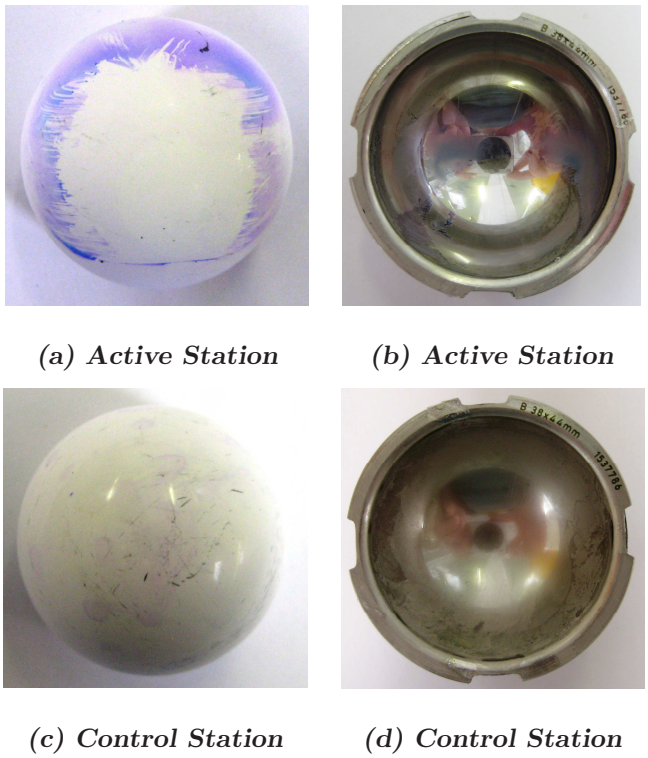

(a) Active Station *(b) Active Station*

(c) Control Station *(d) Control Station*

Figure 10.25: *Digital images of stained deposition on the ZTA ceramic head and corresponding metal cup after 0.5 million cycles of standard wear (end of stage 2). (a) & (b) stations which incorporate loading and motion, (c) & (d) loaded control station.*

Chapter 11

Results - Standard 60 mm Alumina heads against CoCrMo cups

A set of eight 60 mm ZTA heads and as-cast CoCrMo alloy cups were tested under standard walking conditions. Figure 11.1 shows a typical ZTA head and CoCrMo cup.

Figure 11.1: *60 mm ZTA femoral head and as-cast CoCrMo acetabular cup.*

Components were paired to give radial clearances close to 100 μm, as shown in Table 11.1.

Station	Head	Dimension (mm)	Cup	Dimension (mm)	Radial Clearance (μm)
1	9026-1	30.017	10	30.117	100
2	9032-3	30.017	7	30.117	100
3	9026-7	30.019	11	30.119	100
4	9026-3	30.014	16	30.114	100
5	9032-6	30.023	2	30.122	99
Control	9026-4	30.012	8	30.112	100
Soak	9032-5	30.018	13	30.117	99

Table 11.1: *60 mm ZTA against CoCrMo joint pairings and radial clearances for standard walking cycle wear test.*

The test included a loaded soak control which underwent loading and therefore was used to take account of mass fluctuations due to simulator set-up/take down and any fluid adsorption. In addition a soak control was placed in fresh lubricant every 0.5 million cycles and maintained at 37 ^{o}C for the duration of the test. Both controls were wash/dried/weighed as per the active stations. This component was used to monitor changes in mass due to the washing technique. Finally an environmental control was used to monitor mass changes due to the environment which was kept next to the balances. This helped with the understanding and eliminated errors due to changes in the balance rather than wear.

11.1 Wear Testing

The 60 mm ZTA heads fluctuated close to zero for the entire test, as shown in Figure 11.2. The three control heads (loaded soak, soak and environmental) followed a similar trend and volume change as the 5 active stations suggesting that the measured volume changes were due to environmental factors during the weighing process. For direct comparison with the 38 mm ZTA and other components, the loaded soak was used to adjust the results. In addition the soak control was also used to calculate the adjusted values and wear rates determined for both controls.

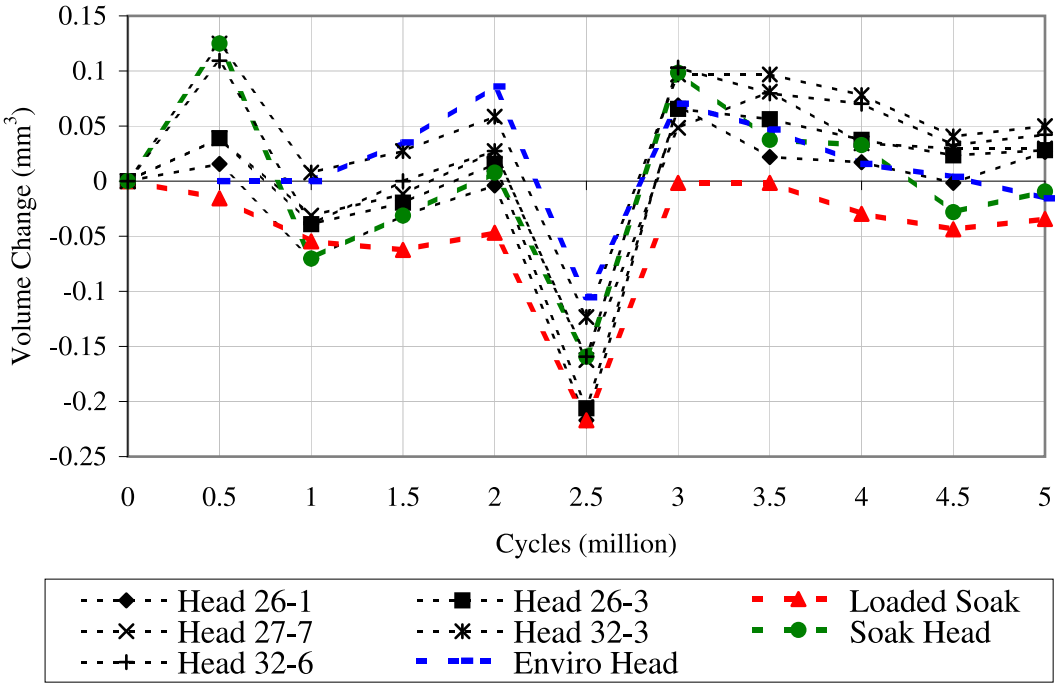

Figure 11.2: *Volume change of 60 mm ZTA femoral heads under standard wear testing.*

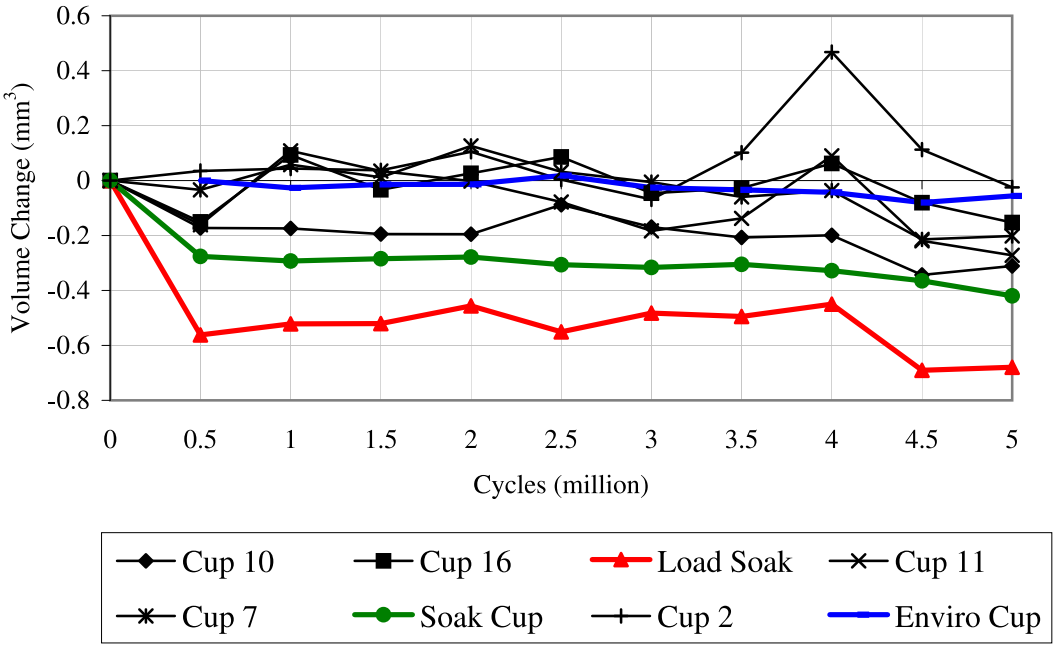

Figure 11.3: *Volume change of 60 mm as-cast CoCrMo cups (from ZTA test) under standard wear testing.*

Figure 11.3 shows that the 60 mm CoCrMo cups were also found to fluctuate close to zero for the entire wear test and a running in wear rate was not apparent.

Interestingly the loaded soak lost the greatest volume in the first 0.5 million cycles which was not expected. Adjusting using the control resulted in an apparent 'increase' in wear for the running in wear phase. Therefore, the control was used to adjust the results for the steady state wear only. Figure 11.4 shows the adjusted results (with the loaded soak), excluding the control in the first 0.5 million cycles. It is clear from this Figure that the difference in volume change between the heads and cups was not as different as found for previous tests (38 mm).

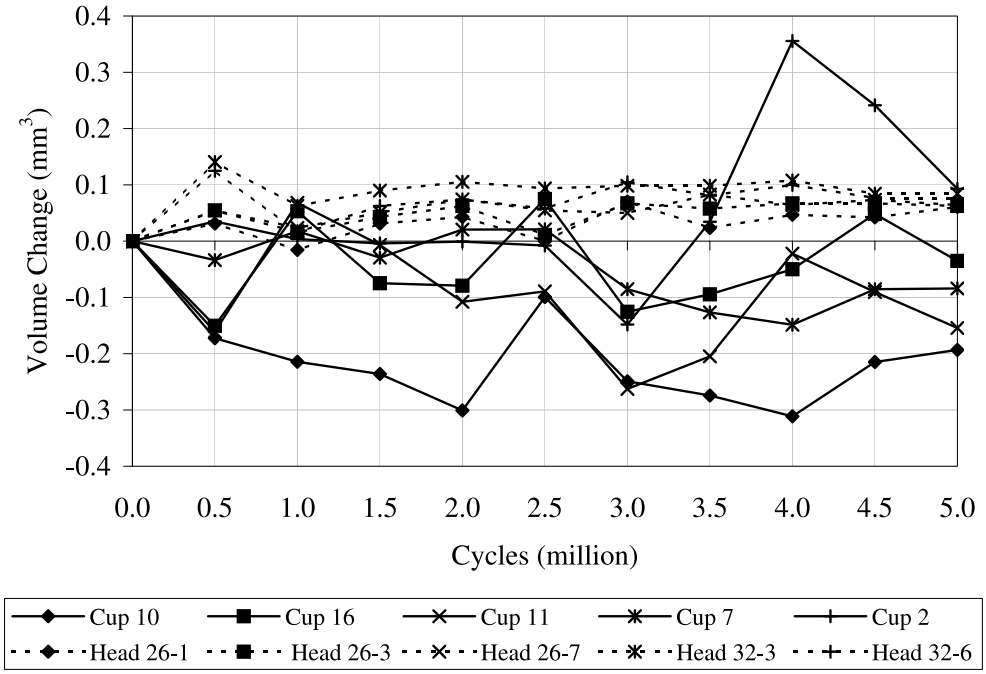

Figure 11.4: *Adjusted volume change of 60 mm ZTA:CoCrMo test under standard wear testing.*

Individual wear rates were calculated for each head and cup, between 0.5-5 million cycles and 1-5 million cycles which are shown in Tables 11.2 and 11.3. A negative wear rate represented a gain in volume and a positive wear rate represented a volume loss. Changing the initial number of cycles for which steady state wear begins, and changing the control used to take account of environmental factors, had a considerable effect on the wear rate of some of the components. For example, head 32-3 changed from a positive wear rate of 0.003 mm^3/mc to a volume gain of -0.005 mm^3/mc by changing from the loaded soak to the soak control between 0.5-5 million cycles. The r^2 values are given to provide an indication of the proportion

of variability accounted for by the regression line, a low r^2 suggesting that the wear rate cannot accurately be predicted by the regression coefficient given.

Average steady state wear rates for the heads and cups were calculated from 1-5 million cycles and are given in Table 11.4.

	Loaded Soak Control				Soak Control			
Cup	0.5-5mc	r^2	1-5mc	r^2	0.5-5mc	r^2	1-5mc	r^2
2	-0.048	0.260	-0.062	0.315	-0.050	0.242	-0.054	0.215
7	0.028	0.473	0.035	0.613	0.026	0.290	0.043	0.598
10	0.008	0.034	0.002	0.001	0.006	0.029	0.009	0.056
11	0.019	0.088	0.036	0.235	0.017	0.053	0.044	0.290
16	-0.011	0.043	0.003	0.004	-0.013	0.056	0.011	0.063

Table 11.2: *Individual 60 mm CoCrMo cup wear rates under standard wear conditions(ZTA test) adjusting with load soak and soak controls.*

	Loaded Soak Control				Soak Control			
Head	0.5-5mc (mm^3/mc)	r^2	1-5mc (mm^3/mc)	r^2	0.5-5mc (mm^3/mc)	r^2	1-5mc (mm^3/mc)	r^2
26-1	-0.009	0.288	-0.012	0.375	-0.017	0.397	-0.009	0.174
26-3	-0.007	0.266	-0.011	0.416	-0.015	0.298	-0.007	0.085
26-7	-0.006	0.329	-0.008	0.381	-0.014	0.235	-0.042	0.031
32-3	0.003	0.065	-0.003	0.0712	-0.005	0.070	0.001	0.004
32-6	-0.003	0.023	-0.012	0.398	-0.011	0.487	-0.008	0.314

Table 11.3: *Individual 60 mm ZTA wear rates under standard wear conditions, adjusting with load soak and soak controls.*

		Head (mm^3/mc)	Cup (mm^3/mc)
Loaded Soak Control	0.5-5mc	-0.0045 ±0.0042	-0.0007 ±0.0181
	1-5mc	-0.0091 ±0.0042	0.0029 ±0.0235
Soak Control	0.5-5mc	-0.0126 ±0.0061	-0.0027 ±0.0282
	1-5mc	-0.0054 ±0.0062	0.0105 ±0.0238

Table 11.4: *Steady state wear rates for the 60 mm ZTA:CoCrMo components.*

A volume loss was measured for the cups between 1-5 million cycles when the results were adjusted with both the loaded soak and soak control. All other measurements including heads, recorded a small volume gain.

Overall wear rates from 0-5 million cycles were calculated (using the loaded control) as -0.009 ± 0.0043 mm^3/million cycles for the heads (volume gain) and 0.0061 ± 0.0359 mm^3/million cycles (volume loss) for the cups.

Running in wear rates were not determined due to the unexpected volume gain experienced after taking account of the control specimen.

11.2 Friction Testing

Friction tests were carried out on 2 unworn samples which resulted in unexpectedly high friction factors which resulted in damage to the metallic cups such as abrasive and adhesive wear. An increase in friction factor was found when the two highest viscosities of fluid were used as the lubricant. The results are shown in Figures 11.5 and 11.6.

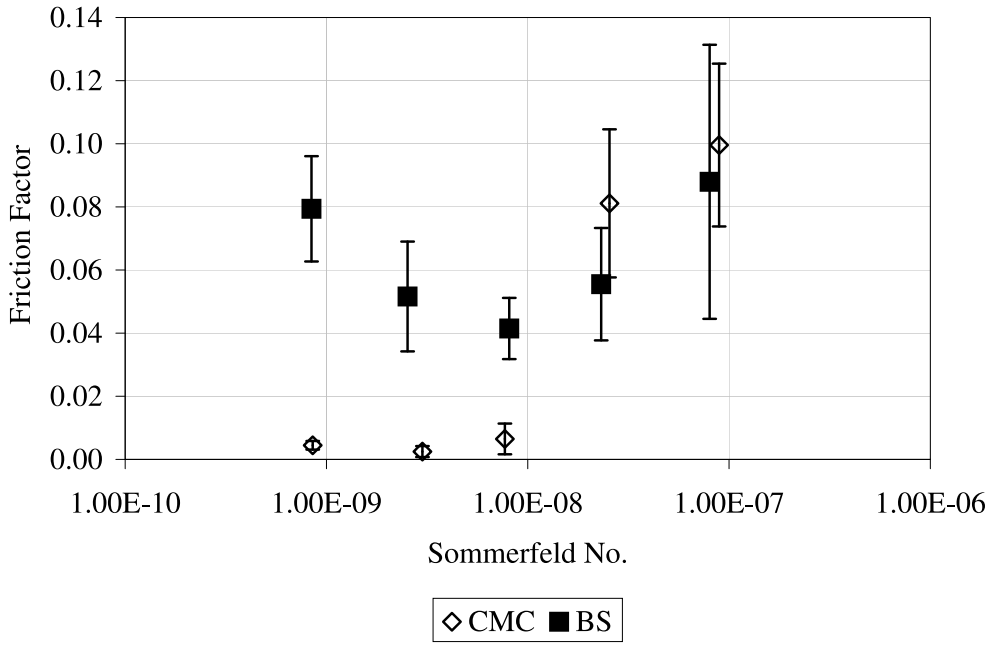

Figure 11.5: *Stribeck Plot of unworn 60 mm ZTA test components using lubricants of both water based and bovine serum based lubricants (head 26-1:cup 10.*

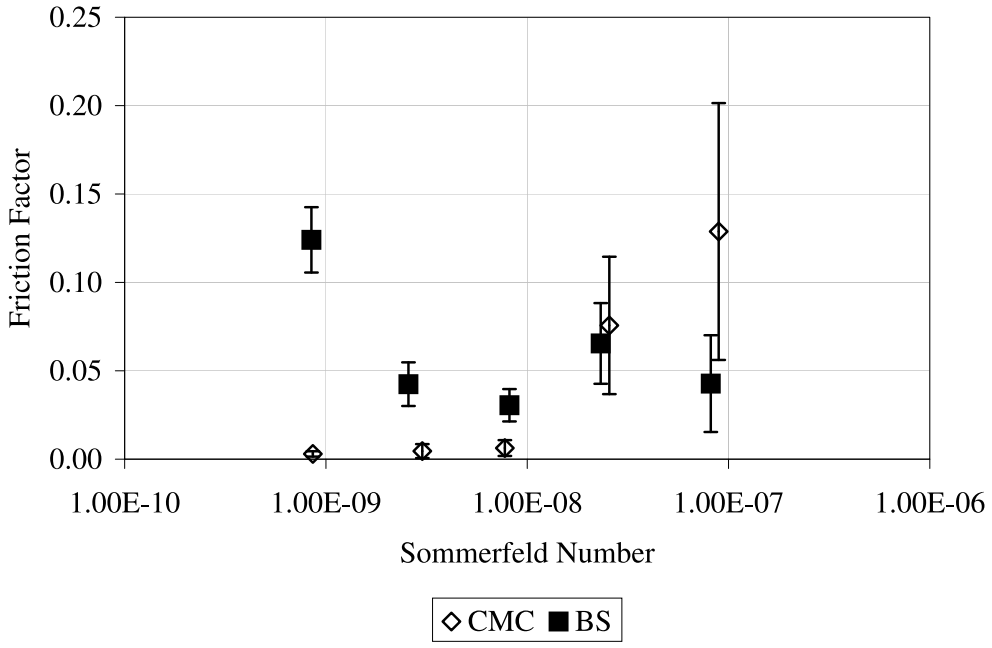

Figure 11.6: *Stribeck Plot of unworn 60 mm ZTA test components using lubricants of both water based and bovine serum based lubricants (head 32-6:cup 2).*

The three lowest viscosities of lubricant showed lower friction factors for the water based lubricants compared with the bovine serum based lubricants. The two highest viscosity lubricants showed similar friction factors for both the CMC based lubricants and the bovine serum based lubricants. Visual inspection of the ceramic heads after the two highest viscosity fluids revealed significant metal transfer from the cup to the ceramic head, and a rectangular 'dry' area within the metal cup. It was therefore concluded that the large diameter and low swing radius may have prevented fluid being drawn into the pole, resulting in dry rubbing, and therefore higher friction.

Table 11.5 shows the change in rms roughness of friction tested head and cup before and after testing. A comparison of the rms roughness of cup 2 and cup 10 before and after testing, using a Mann-Whitney U test due to the non normality of the data (Cup 2- Shapiro-Wilk (20) = 0.740, p $\leq$0.001 and Cup 10 Shapiro-Wilk (20) = 0.879 = p $\leq$0.001) showed that the means for cup 10 were significantly different whereas cup two did not show a significant difference (Cup 2- Mann-Whitney U (20) = 0.5, p$\leq$0.001 and Cup 10 - Mann-Whitney U (20) = 0.000, p$\leq$0.00). The head rms roughnesses did not change as a result of friction testing.

	0mc	After Friction	0.5mc	2.5mc
Cup 2	0.009 ($\pm$ 0.001)	0.020 ($\pm$ 0.009)	0.028 ($\pm$ 0.001)	0.013 ($\pm$ 0.001)
Cup 10	0.007 ($\pm$ 0.002)	0.016 ($\pm$ 0.003)	0.019 ($\pm$ 0.007)	0.018 ($\pm$ 0.001)
Head 26-2	0.010 ($\pm$ 0.001)	0.010 ($\pm$ 0.001)	0.011 ($\pm$ 0.002)	0.010 ($\pm$ 0.001)
Head 32-6	0.017 ($\pm$ 0.012)	0.018 ($\pm$ 0.006)	0.019 ($\pm$ 0.012)	0.011 ($\pm$ 0.005)

Table 11.5: *RMS roughness of the 60 mm ZTA:CoCr over 5 million cycles.*

Figure 11.7 shows images of cup 10 before and after friction testing, where dry rubbing caused large areas of matrix material to be removed resulting in deep holes.

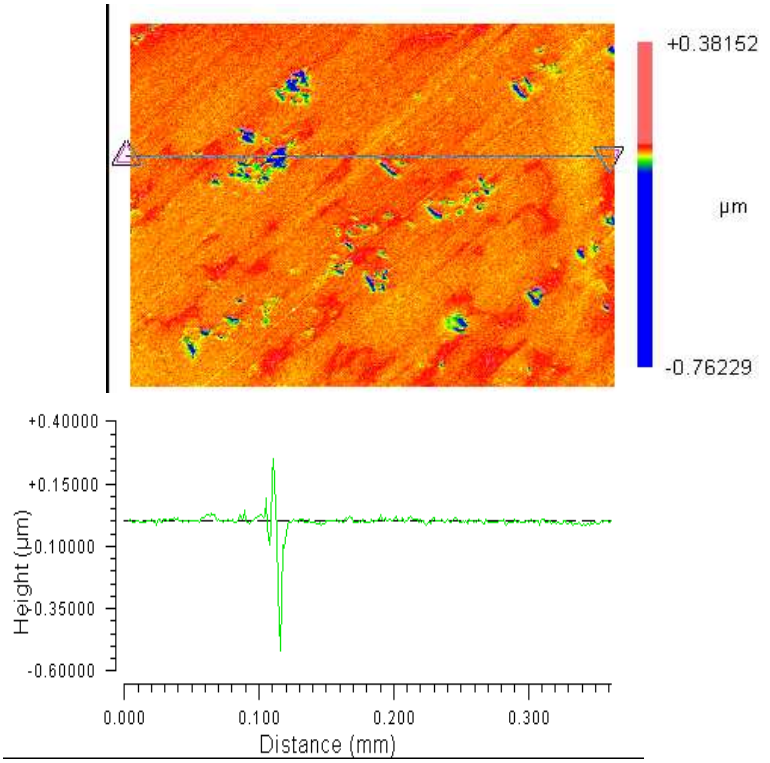

Figure 11.7: *Zygo image showing the line profile of damage caused by friction testing (cup 10).*

A new unworn component was friction tested, and the results of this were compared against two original components tested after 5 million cycles of wear. Figure 11.8 shows the results of the unworn joint, compared with bearing couples (head 32-6 cup 2 and head 26-1 cup 10) after 5 million cycles. These tests were carried out by a 4th year project student, Emma Tonks under the cosupervision of the author for the practical work.

Very little difference was seen between the unworn joint and the two joints worn to 5 million cycles. The initially high friction factors found for the two highest viscosities of water based CMC fluids were found to decrease after 5 million cycles of wear. Except for these two viscosities, all friction factors were less than 0.03 with a curve indicative of fluid film lubrication.

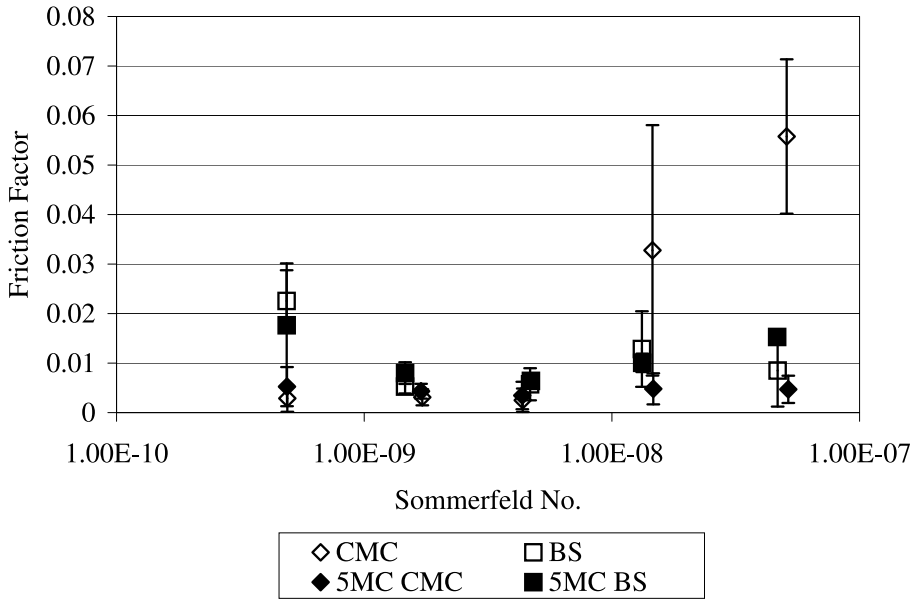

(a) Head 32-6 Cup 2

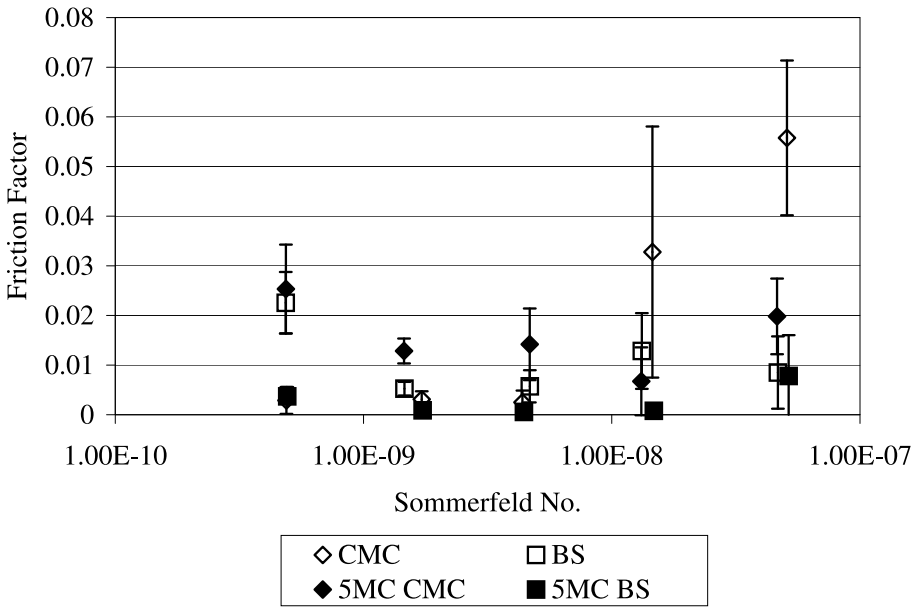

(b) Head 26-1 Cup 10

Figure 11.8: *Friction results of two joints after 5 million cycles of standard walking cycle wear testing, compared with an unworn component.*

Cycles (millions)	Head Rms (μm)	Cup Rms (μm)	H min (μm)	λ	Friction factors CMC*/BS**
0	0.011	0.010	0.187	>3	0.003/0.023
0.5	0.012	0.018	0.187	>3	-
1	0.011	0.014	0.187	>3	-
2.5	0.010	0.012	0.187	>3	

* CMC η=0.001 Pa s^{-1}, **BS η=0.0013 Pa s^{-1}

Table 11.6: *Theoretical minimum film thickness and lambda values for 60 mm diameter ZTA heads against CoCrMo cups.*

Calculations showed the ratio of minimum film thickness to equivalent roughness to be greater than 3 for all measurements up to 2.5 million cycles suggesting the joints should be operating in full fluid film lubrication.

11.3 Surface Analysis

11.3.1 Non Contacting Interferometry

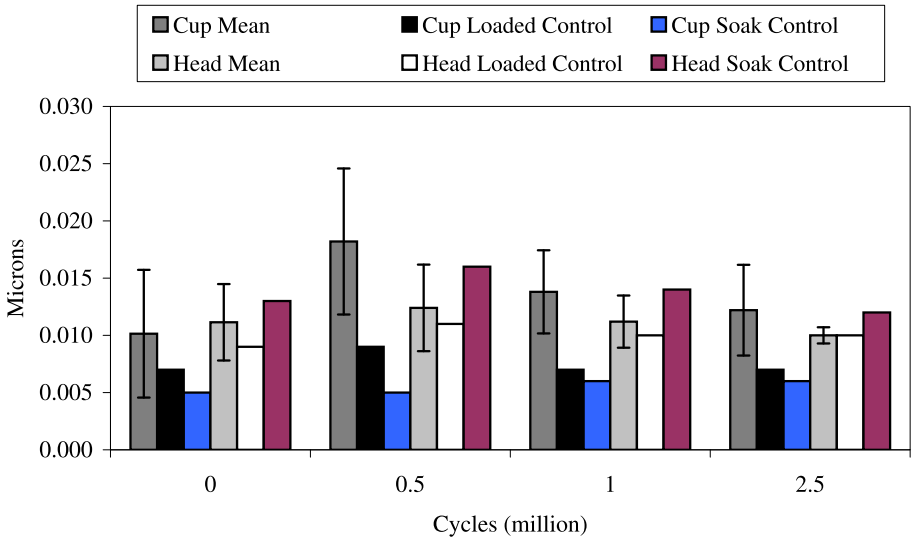

Figure 11.9: *RMS roughness of the 60 mm ZTA components under standard walking cycle wear testing.*

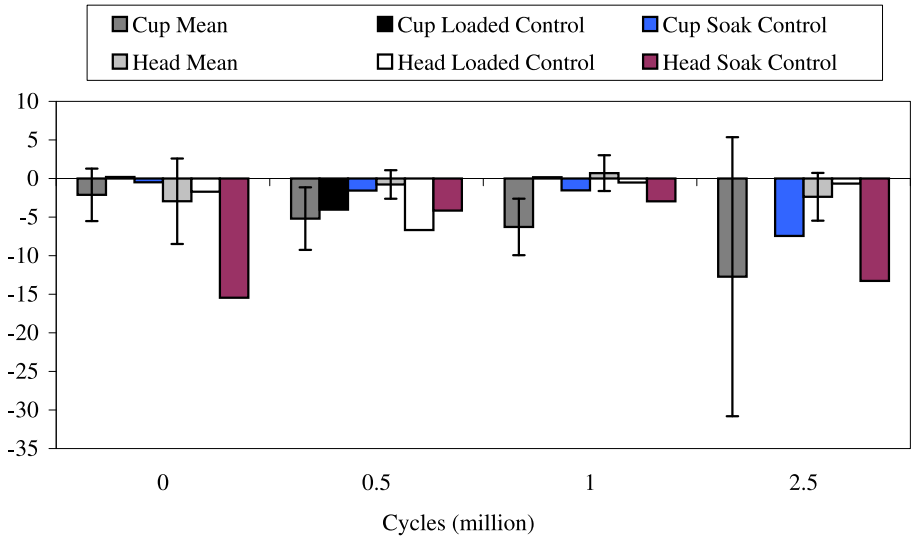

Figure 11.10: *Skewness data for 60 mm ZTA components under standard walking cycle wear testing.*

RMS roughness and skewness values were measured at 0.5, 1.0, and 2.5 million cycles. The unworn ceramic heads and metal cups had similar roughness values at

0.010 μm and 0.011 μm respectively. The roughness did not change much over the entire test. A small increase in mean cup roughness was found with an increase to 0.18 μm by 0.5 million cycles, followed by a decreased after 2.5 million cycles to a value of 0.012 μm. Unfortunately roughness measurements were not available at 5 million cycles. The loaded soak control followed a similar trend to the active stations, however had a consistently lower roughness (loaded soak, initial roughness was 0.07 μm which increased to 0.09 μm by 0.5 million cycles and returned to 0.07 μm by 2.5 million cycles). The head mean head roughness remained similar to the unworn values up to 2.5 million cycles. The head soak control showed the largest rms roughness (0.013 μm) due to holes in the unworn surface (see Figure 11.16(c)). Head 32-6 also had a damaged unworn surface (rms roughness = 0.017 μm, Figure 11.16(e)). The roughness of these two heads remained high compared with the other heads although a slight decrease in roughness was seen for head 32-6 (active station 5) by 2.5 million cycles (0.011 μm).

The skewness values of the components were measured at the same intervals as the rms roughness. A larger standard deviation was found for the skewness of the cup at 2.5 million cycles compared with the previous measurements. The mean head skewness (active stations) fluctuated around zero up to 2.5 million cycles, with consistently lower values compared with the cups. The head soak control measured a high skewness initially due to the damage and grain removal on the pole of the head as previously noted. The skewness of this sample remained higher than the mean value, although it fluctuated as a result of taking the measurements in different positions on the head.

11.3.2 Surface imaging

Analysis of the unworn metal cups revealed that the majority of cups had a relatively smooth surface topography, in which the carbides were only just protruding from the matrix material. Raised areas of matrix material were present around the carbides. Cup 16 and cup 2 were the exceptions in which the carbides were slightly more obvious. Figure 11.11 contrasts the relatively smooth surface of cup 11 (Figure 11.11(a)) found for the majority of the cups and the raised carbides of

cup 16 (Figure 11.11(b)) (also seen for cup 2). This may have been due to the more undulating nature of the matrix which disguised the carbides within the structure.

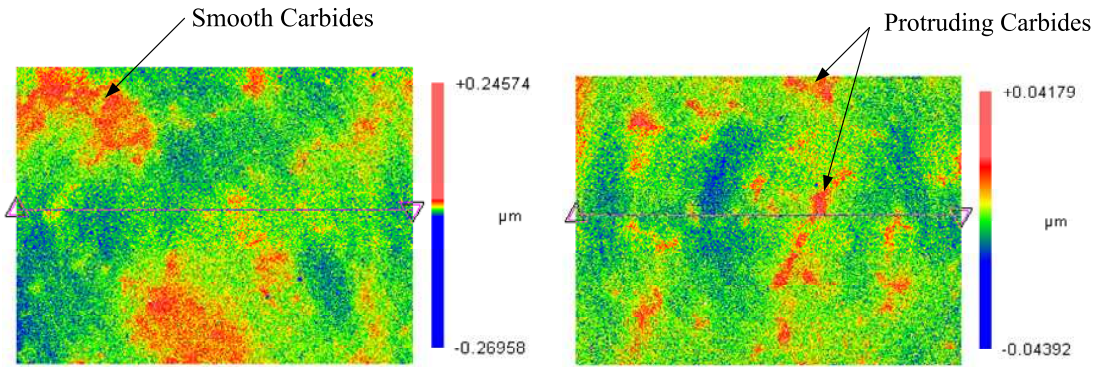

(a) Smooth carbides with raised matrix ***(b) Raised carbides protruding from the matrix***

Figure 11.11: *Zygo images of unworn surface of the 60 mm as-cast CoCrMo cups (from ZTA test) showing the difference in carbides and matrix structure.*

Small holes, thought to be pitting, generally $< 1\mu$m were noticeable on the unworn surfaces. Occasional larger holes of a few microns were found. These were circular in shape and did not appear to be holes left from removed carbides.

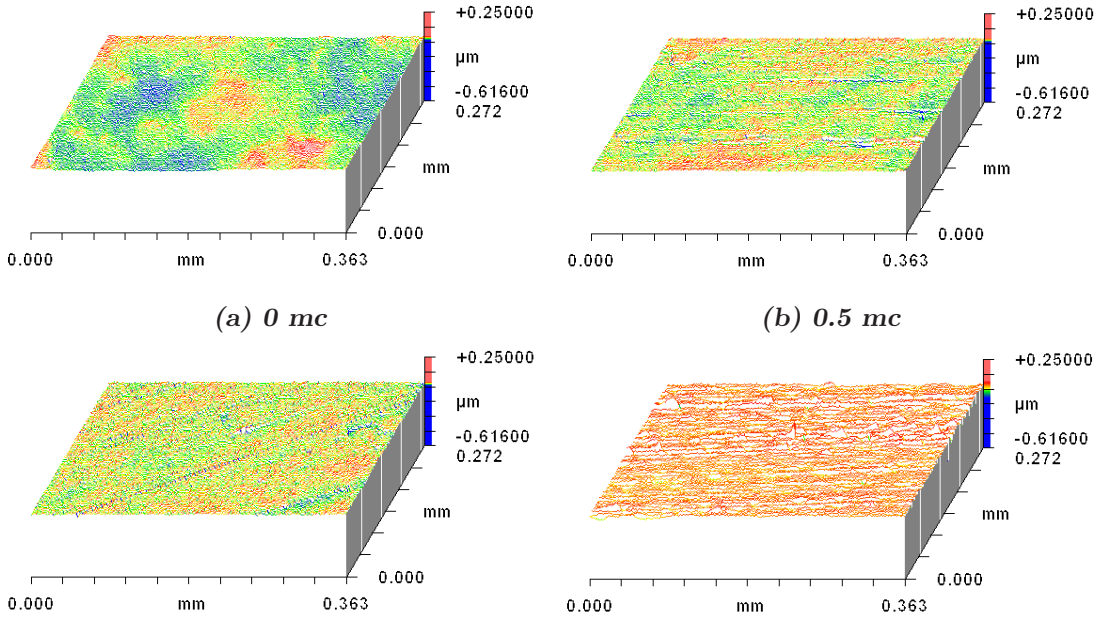

(a) 0 mc ***(b) 0.5 mc***

(c) 1.0 mc ***(d) 2.5 mc***

Figure 11.12: *Zygo images of a typical 60 mm metallic cup up until 2.5 million cycles*

Figure 11.12 shows the progression of cup 7 throughout wear testing. All micrographs are presented on the same scale for comparison, however the detailed changes in the topography were therefore lost as the changes in topography are extremely small.

After 0.5 million cycles the metallic surfaces were abrasively scratched and small holes (pits), were evident. Generally the pits were <1 μm deep. Scratches were generally in the direction of motion (i.e. flexion/extension plane) with discontinuous and continuous scratches. Figure 11.13(b) shows a line profile of Figure 11.13(a), with scratches around 0.3 μm.

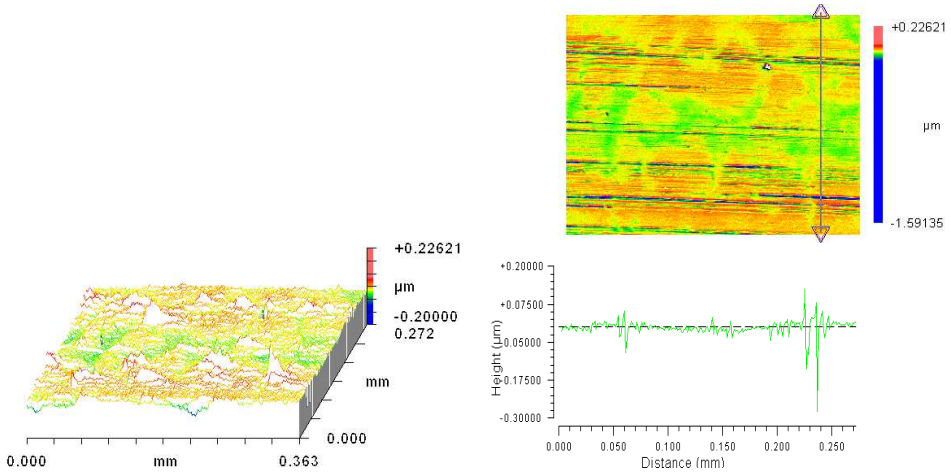

(a) 0.5 mc *(b) 0.5 mc*

Figure 11.13: *Zygo Images of a 60 mm cup showing an oblique plot and the corresponding line profile after 0.5 million cycles of standard wear*

The dominant features on the surfaces of the cups after 2.5 million cycles were the same as those found after 0.5 million cycles. Scratches and pits were found in the wear patch. The pits were present in both the wear patch and the unworn surfaces. By 2.5 million cycles the carbides were found to be either smooth, or slightly below the surface of the matrix. This was most noticeable in cup 16 which had the protruding carbides on the unworn surface. This is shown in Figure 11.14.

The surface topography of the wear patch within all cups was very heterogeneous with the same cup showing badly worn areas and also smooth areas. Figure 11.15 shows the difference in topography found within the wear patch of cup 2.

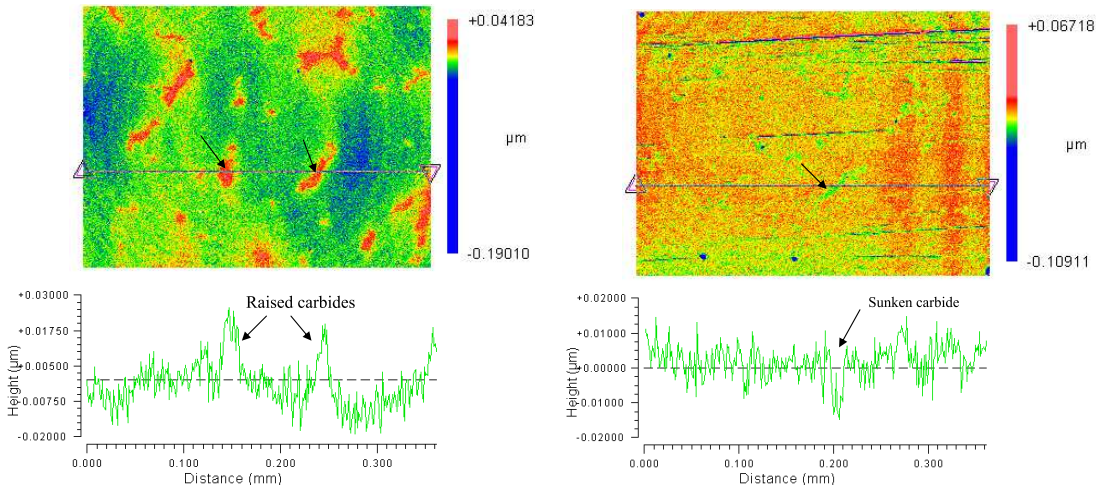

(a) Initial raised carbides of cup 16 ***(b) Sunken carbides of cup 16 after 2.5 million cycles of wear***

Figure 11.14: *Zygo images of cup 16, initially and after 2.5 million cycles of wear showing the initial raised carbides which were sunken after 2.5 million cycles.*

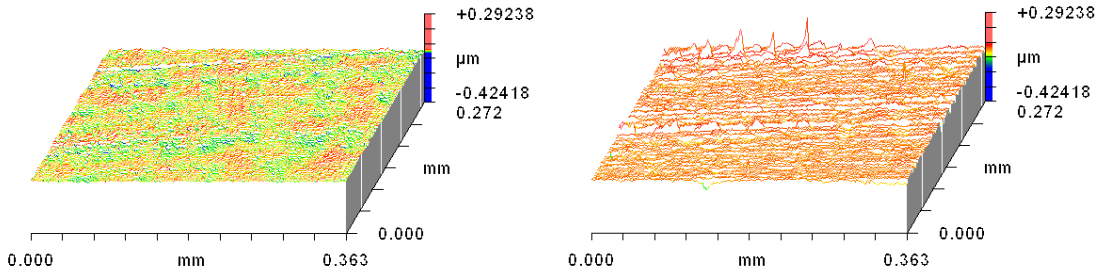

(a) 2.5 mc - rms roughness = 0.007 μm ***(b) 2.5 mc - rms roughness = 0.027 μm***

Figure 11.15: *Zygo images of a 60 mm as-cast CoCrMo cup highlighting smooth and scratched images from the wear patch of cup 2.*

Initial measurements were taken on the pole of the ceramic heads and at approximately 33 degrees to the horizontal. No difference was seen between the two locations on the majority of the heads. However head 32-5 and 32-6 showed considerable damage on the pole of the head with clusters of grains removed from random positions on the pole (see Figure11.16).

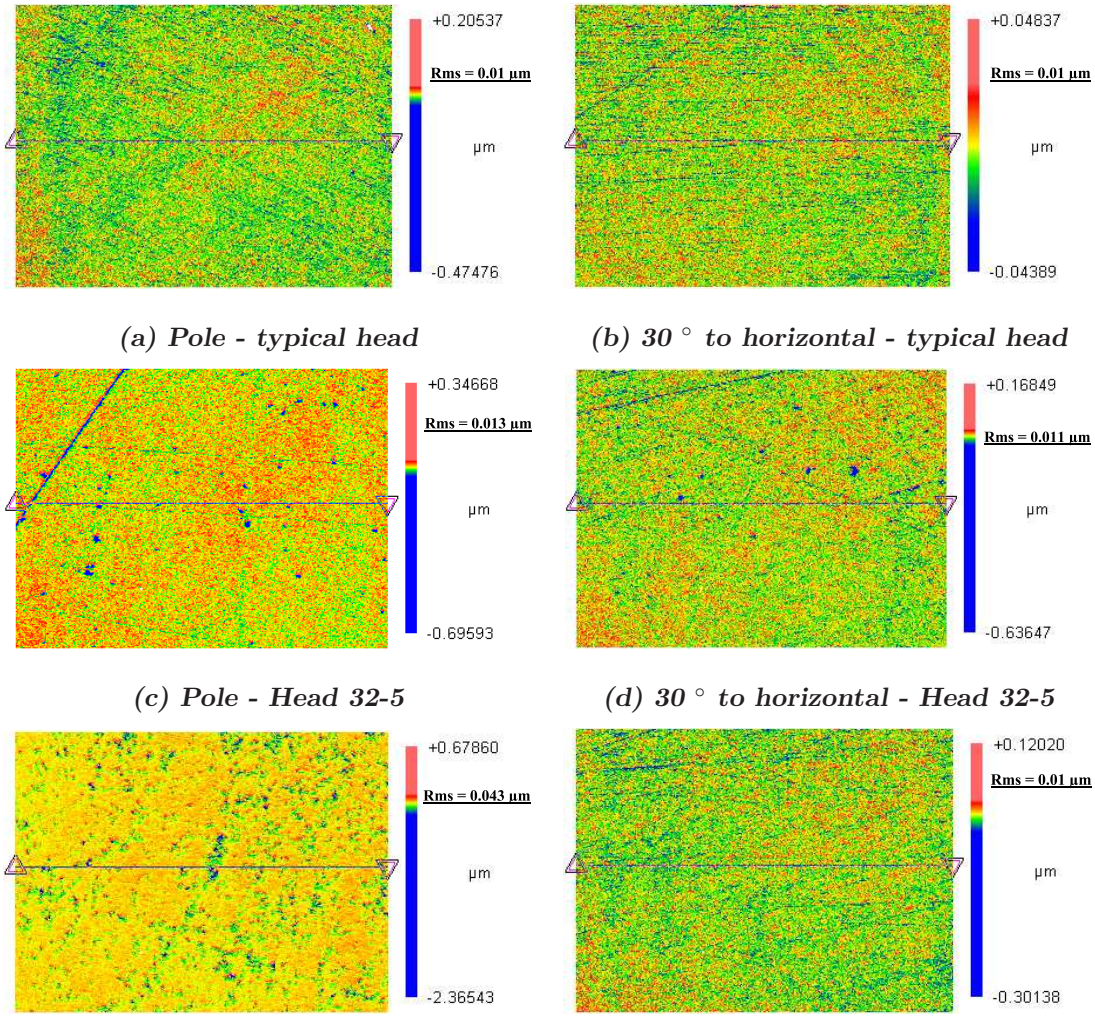

(a) Pole - typical head

(b) 30 ° to horizontal - typical head

(c) Pole - Head 32-5

(d) 30 ° to horizontal - Head 32-5

(e) Pole - Head 32-6

(f) 30 ° to horizontal - Head 32-6

Figure 11.16: *Zygo images of unworn 60 mm ceramic head at different locations on the head.*

The ceramic heads were not affected by wear in the simulator, and kept relatively constant rms roughness and skewness.

11.3.3 Optical Microscopy

Optical micrographs revealed initial surface topography which was similar to the 38 mm metal cup samples shown in previous chapters. Contrasting carbides could be seen within the matrix. Initial images revealed small amounts of pitting over the metal surface which is shown in Figure 11.17. Friction testing led to significant damage to the surfaces of cups 2 and 10, which appeared to have undergone adhesive wear resulting in removal of large portions of the matrix. This however did not appear to affect the wear rates of these two components.

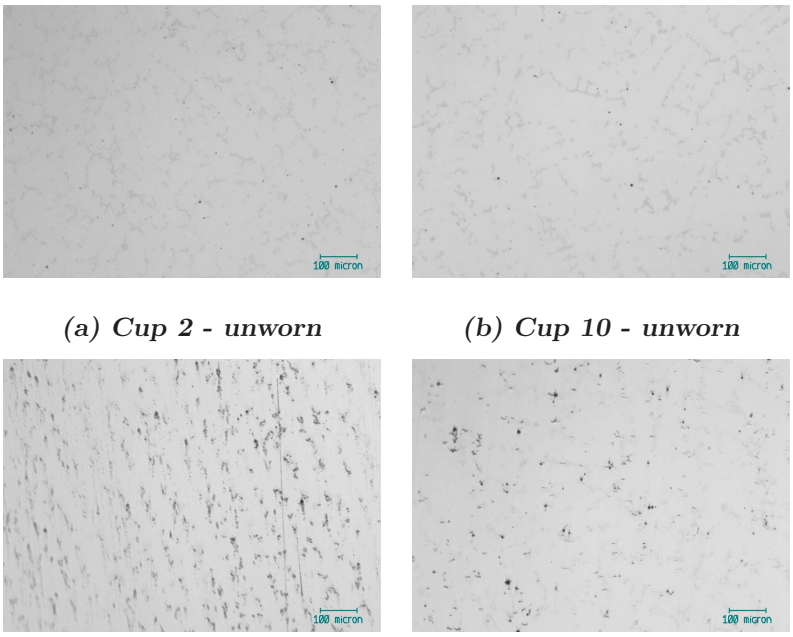

(a) Cup 2 - unworn ***(b) Cup 10 - unworn***

(c) Cup 2 - after friction testing ***(d) Cup 10 - after friction testing***

Figure 11.17: *Optical images of the 60 mm unworn as-cast CoCrMo cups (ZTA test) showing pitting and adhesive damage as a result of friction testing.*

Wear resulted in abrasive scratches in the wear patch of the cups, and pitting was also evident. Cup 11 revealed many abrasive scratches in areas of the cup, however other areas appeared relatively unchanged from the unworn surfaces. These features and the contrasting areas of cup 11 are shown in Figure 11.18.

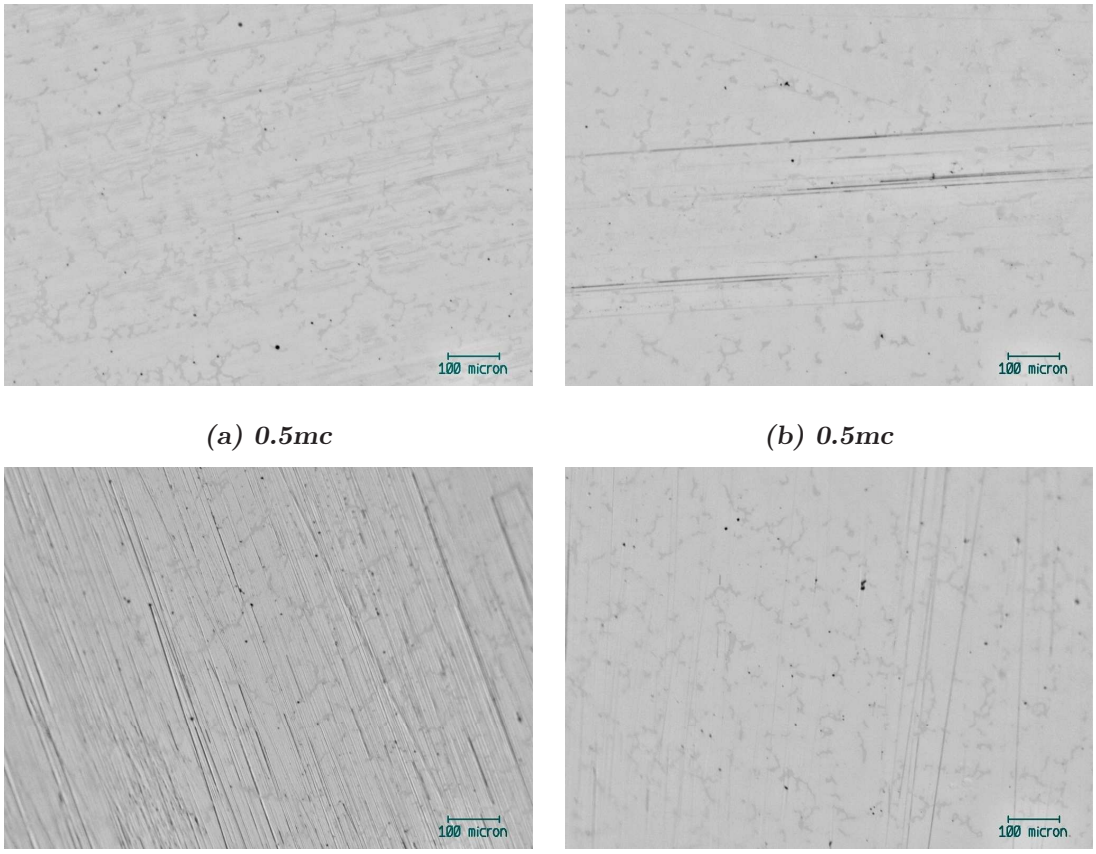

(a) 0.5mc ***(b) 0.5mc***

(c) 0.5mc ***(d) 0.5mc***

Figure 11.18: *Optical images taken of the 60 mm as-cast CoCrMo cups (ZTA test) after 0.5 million cycles. The dominant features of each sub figure are; (a) smooth un-featured surface, (b) abrasive wear, (c) abrasive wear, (d) smooth un-featured*

After 2.5 million cycles of wear the surfaces appeared more damaged with all cups (except the control) showing areas of 'comet tail' wear resulting from adhesive wear. Pitting was evident on many of the surfaces and darkened regions of matrix material surrounded by lighter regions around the carbides (see Figure 11.19).

(a) 2.5mc

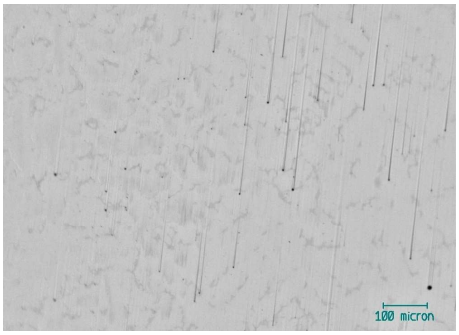

(b) 2.5mc

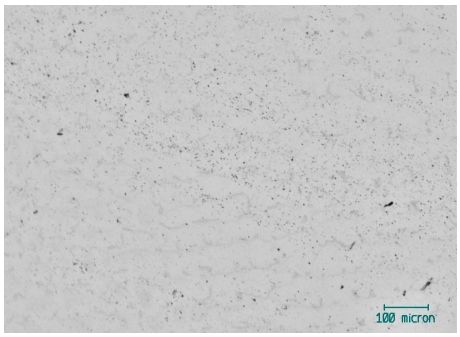

(c) 2.5mc

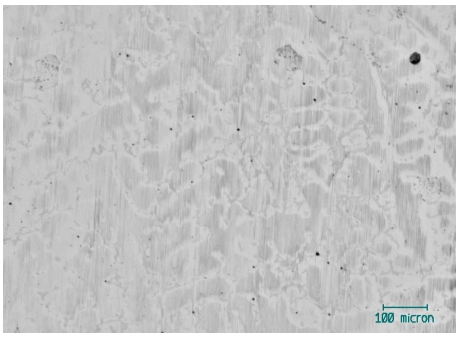

(d) 2.5mc

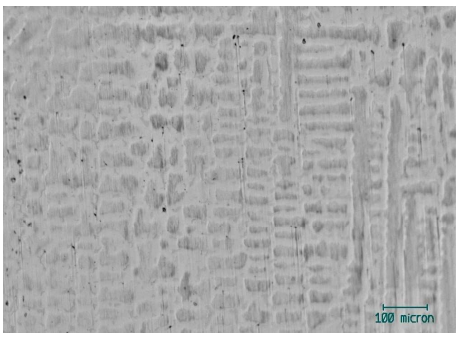

(e) 2.5mc

Figure 11.19: *Optical images of the as-cast CoCrMo cups (ZTA test) after 2.5 million cycles, (a) abrasive and adhesive wear, (b) adhesive wear and 'comet tails', (c) pitting, (d) & (e) transfer/metal particles.*

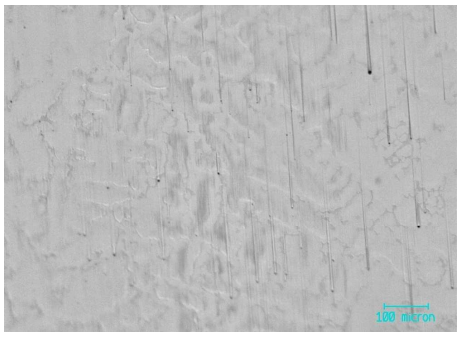

(a) 5mc

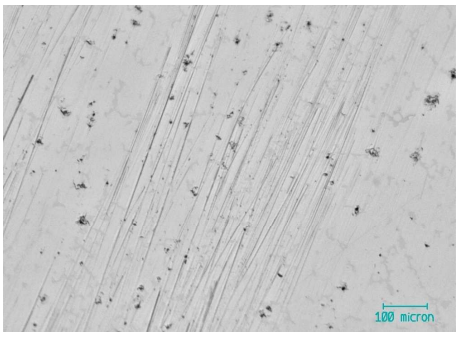

(b) 5mc

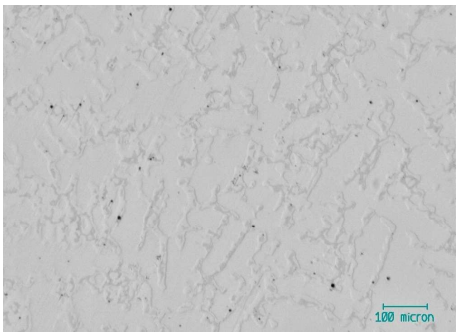

(c) 5mc

Figure 11.20: *Optical images taken of the as-cast CoCrMo cups (ZTA test) after 5.0 million cycles, (a) adhesive wear and 'comet tails', (b) pitting and abrasive wear, (c) smooth un-featured surface*

The surface topography of the cups after 5 million cycles (see Figure 11.20) was similar to that found after 2.5. Abrasive scratching and worn away or carbide shaped holes were evident. Areas of little damage was evident(Figure 11.20(c)). Although cup 10 showed the lowest steady state wear rate, similar wear was apparent on the surface compared with the other cups.

11.3.4 AFM Analysis

With the exception of head 32-5 and 32-6, the heads revealed randomly orientated polishing scratches the deepest of which were approximately 15 nm deep. Grains were not visible on any of the heads. Figure 11.21 compares the unworn surfaces of the heads.

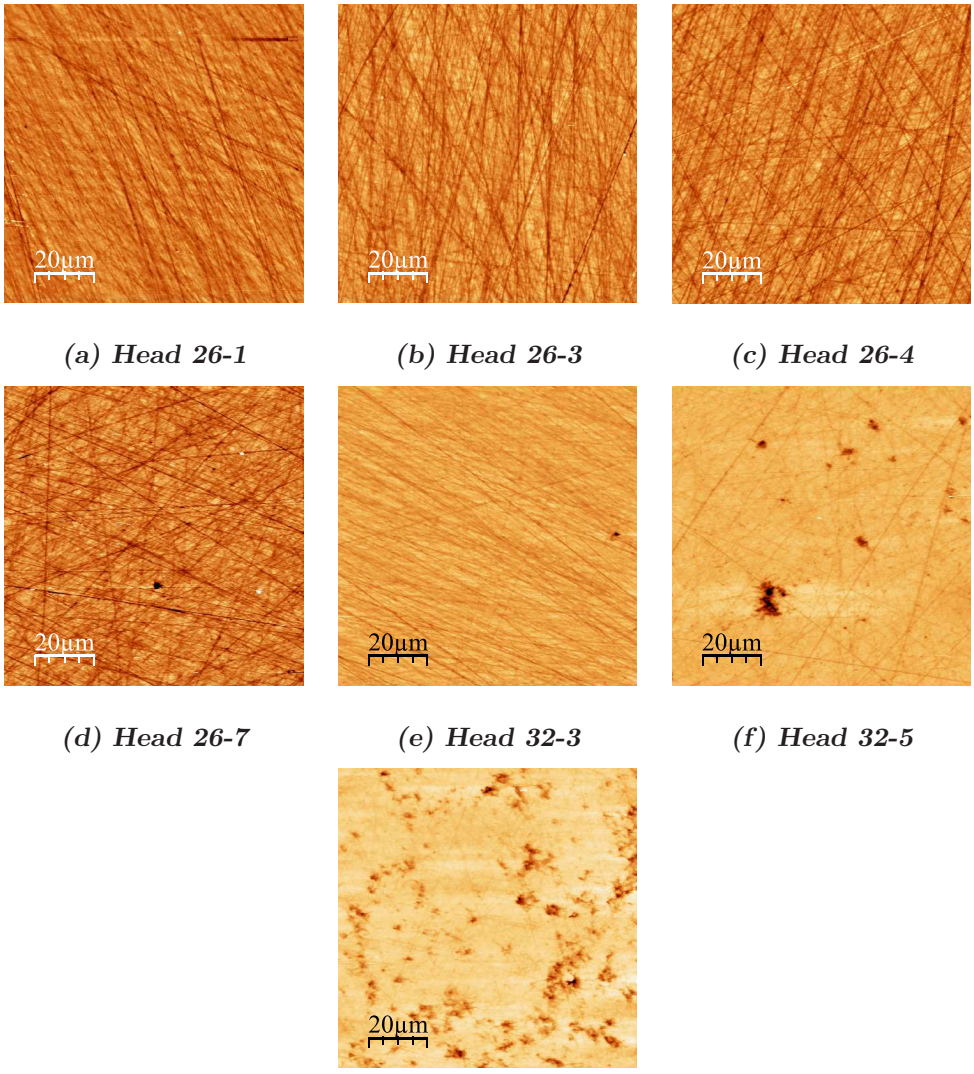

(a) Head 26-1 *(b) Head 26-3* *(c) Head 26-4*

(d) Head 26-7 *(e) Head 32-3* *(f) Head 32-5*

(g) Head 32-6

Figure 11.21: *AFM micrographs of unworn 60 mm ZTA heads.*

Interestingly after 0.5 million cycles, grains became visible on the majority of the poles of the active heads, with the exception of head 26-1. However, by 2.5 million cycles grain removal was clearly visible on the poles of all active stations. Figure 11.22 shows the progression of head 32-3 which is typical of the majority of the active stations, and head 26-1 which took until 2.5 million cycles of wear before grains were visible. Line profiles can be seen in Figure 11.23 which show the removed grains to be approximately 20-40 nm deep. As the grains became more evident, the polishing scratches became less obvious. The topography of head 32-6 and 32-5, which were damaged unworn surfaces, did not change as wear progressed (see Figure 11.24).

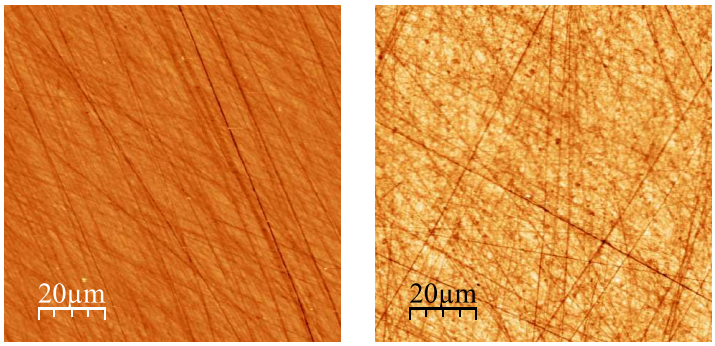

(a) Head 26-1 - 0.5mc *(b) Head 32-3 - 0.5mc*

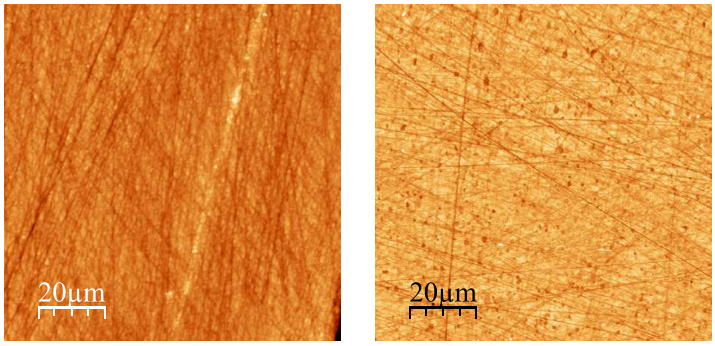

(c) Head 26-1 - 1mc *(d) Head 32-3 - 1mc*

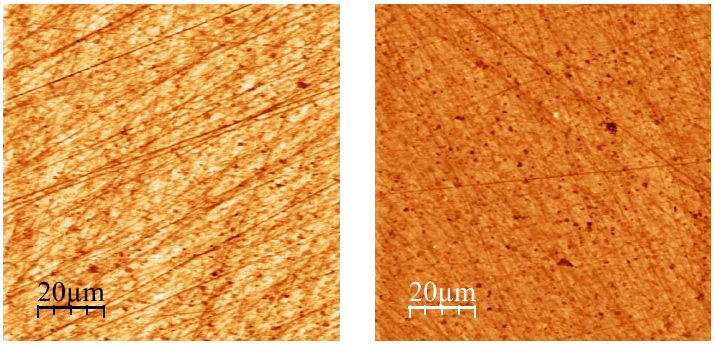

(e) Head 26-1 - 2.5mc *(f) Head 32-3 - 2.5mc*

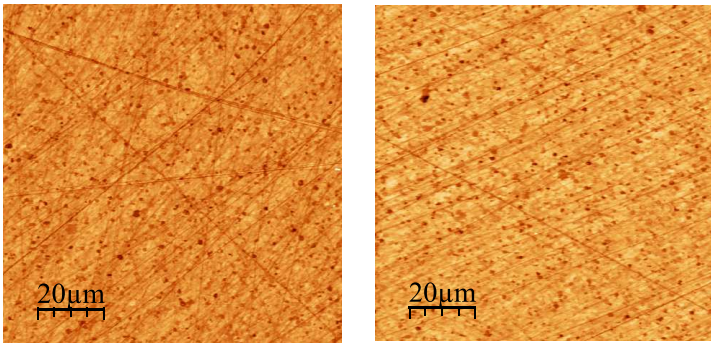

(g) Head 26-1 - 5.0mc *(h) Head 32-3 - 5.0mc*

Figure 11.22: *AFM micrographs of worn 60 mm ZTA heads at 0.5, 1, 2.5 and 5 million cycles.*

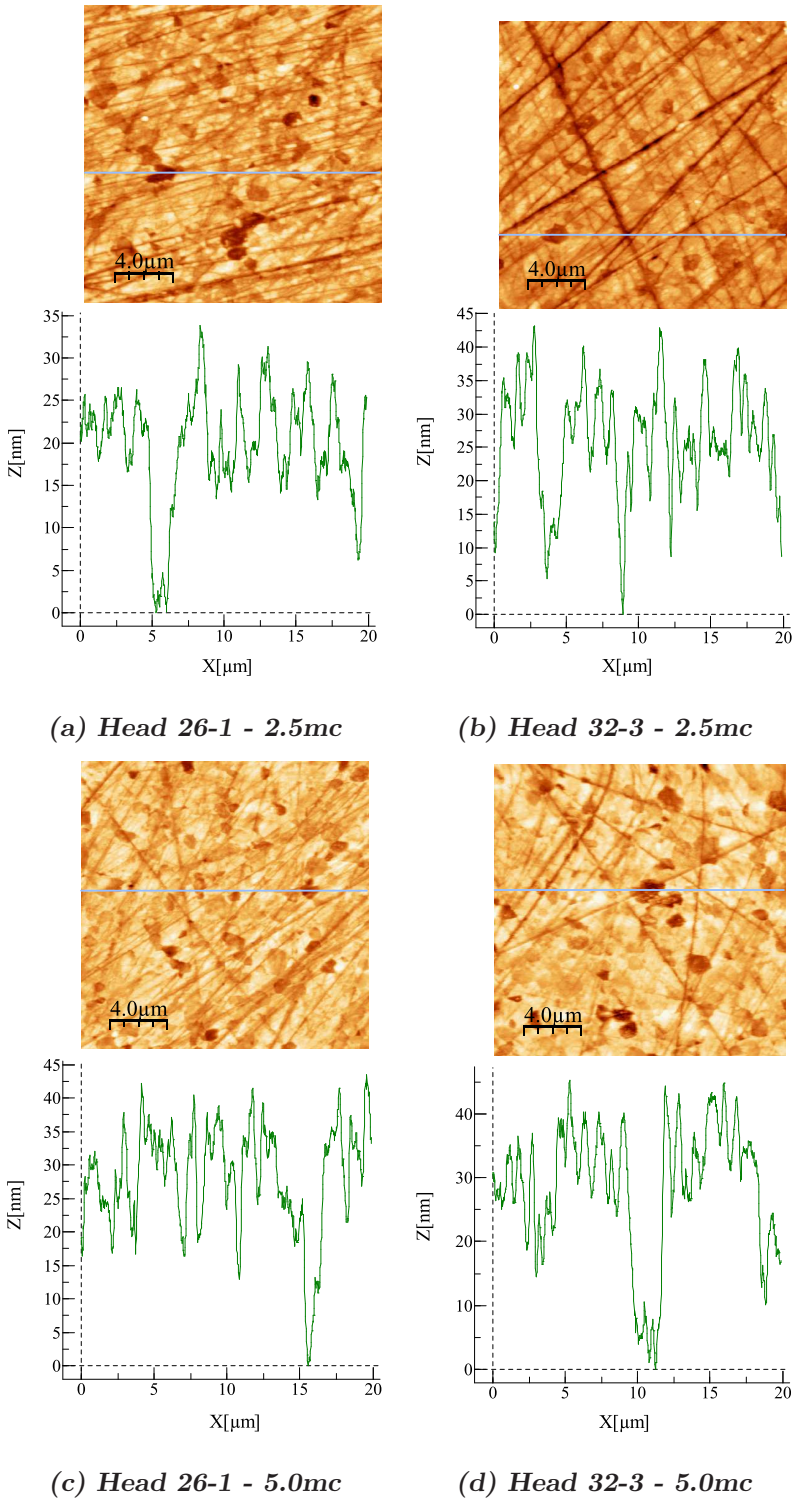

(a) Head 26-1 - 2.5mc *(b) Head 32-3 - 2.5mc*

(c) Head 26-1 - 5.0mc *(d) Head 32-3 - 5.0mc*

Figure 11.23: *AFM line profiles of 60mm heads 26-1 and 32-3 after 2.5 and 5.0 million cycles of wear.*

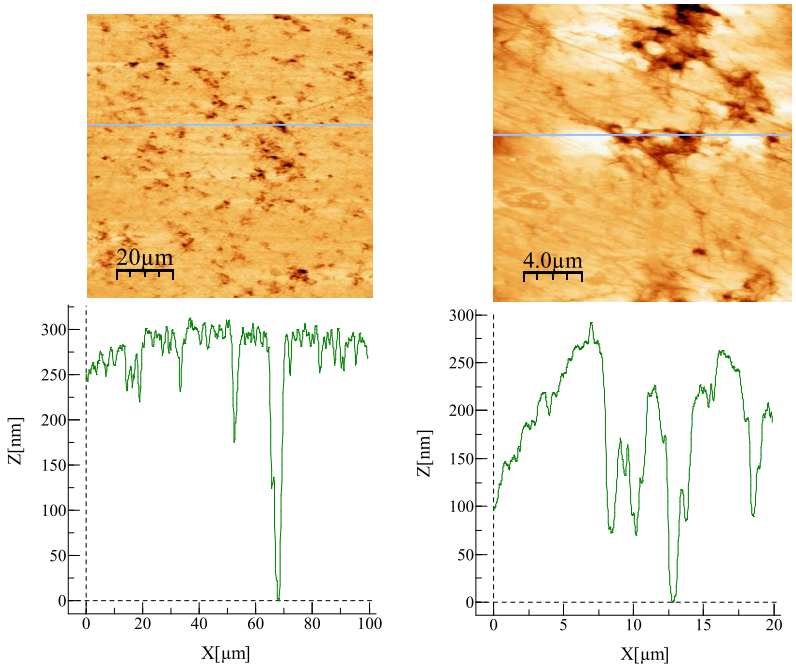

(a) Head 26-1 - 5mc *(b) Head 32-3 - 5mc*

Figure 11.24: *AFM line profiles of 60 mm head 32-6 after 5 million cycles of wear.*

11.4 Protein Deposition

As with previous joints, a white deposit was found on each head and cup after 0.5 million cycles of wear. The deposit was stained with a non permanent ink. Figure 11.25 shows head 26-3 and corresponding cup 16 at various stages throughout testing. The clear area on the pole of the head and in the bottom of the cup are the wear areas where intimate contact has occurred. This has either prevented deposition in these areas, or the deposition is worn off as quickly as it is deposited. No significant difference in deposit was evident at different wear intervals.

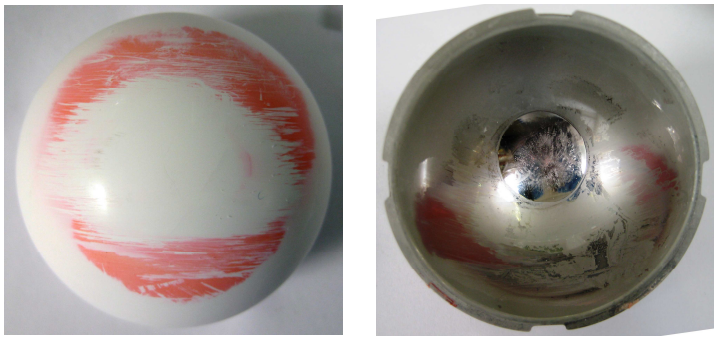

(a) 0.5mc *(b) 0.5mc*

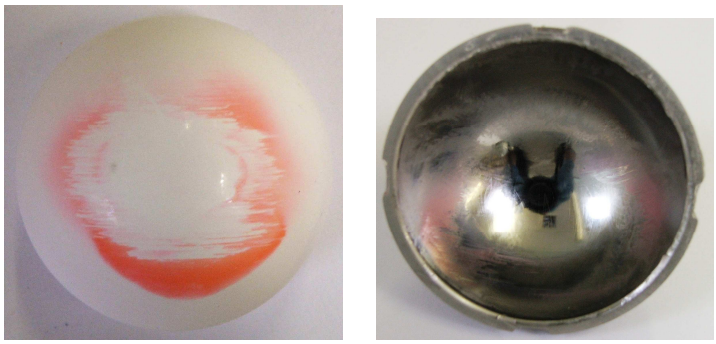

(c) 1.0mc *(d) 1.0mc*

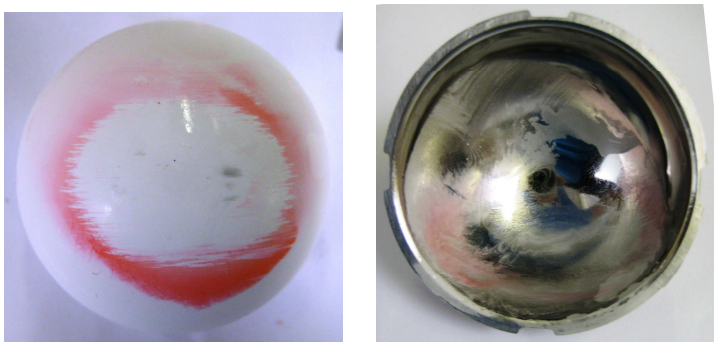

(e) 2.5mc *(f) 2.5mc*

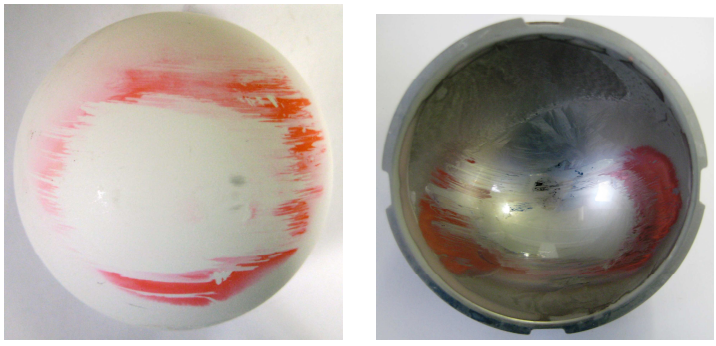

(g) 5.0mc *(h) 5.0mc*

Figure 11.25: *Digital images showing the stained deposit at 0.5, 1, 2.5 and 5 million cycles.*

Figure 11.26 shows more detailed imaged of the deposit at the edge of the wear track. Abrasive scratches are evident, showing asperity contact was occurring, however the underlying ceramic and metal surface appear undamaged.

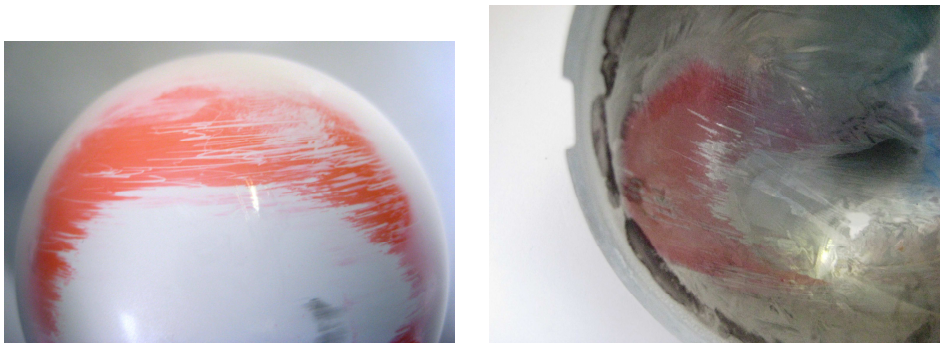

(a) Head 26-1 - 2.5mc ***(b) Head 32-3 - 2.5mc***

Figure 11.26: *Digital images showing detailed areas of the stained deposit on the ceramic head and metal cup.*

Chapter 12

Discussion

Ceramic on metal total hip replacements supplied by Biomet UK, were investigated to understand the wear, friction and surface topography changes caused during *in vitro* wear simulation. Wear was determined gravimetrically and various surface analytical techniques were used to monitor the changes to the surfaces throughout the wear test. Friction was measured to determine the lubricating mechanism occurring between the different joint combinations, as indicated by Stribeck Plots. The optimum result of friction testing would be to have a material combination that exhibited full fluid film lubrication which would be an indication that the joint may therefore exhibit lower wear.

The effect of femoral head diameter and material combinations were investigated under standard, microseparation and third body wear testing. The results showed low wear rates for all ceramic on metal combinations of material and size, and relatively low wear under the severe wear testing conditions. In the majority of cases, the wear rates of the ceramic heads were so low that the gravimetric method was not suitable for measuring the small differences in volume change which occurred as a result of wear testing. It was considered that the detection limits of the technique had been reached therefore further techniques were required which detected small changes in the surface topography, to determine whether wear had taken place.

The knowledge surrounding ceramic on metal prostheses is growing rapidly, and the majority of work to date has revealed a positive outcome for ceramic on metal combinations. Joint diameters from 28-54 mm [1–9] have been investigated re-

sulting in steady state wear rates (under standard conditions) in the range 0.01-0.1 mm^3/million cycles. A range of diametrical clearances, types of simulator and lubricants have been used, all of which result in similar wear rates. All steady state wear rates under standard conditions within this thesis were found within the range of results published in the literature.

Opinions are divided as to whether a biphasic wear pattern is observed for CoM combinations. Firkins *et al.* [1] presented the first simulator study regarding CoM pairings, and did not find a 'running-in' (RI) phase. Smith *et al.* [3] reported a biphasic wear rate only for the larger diameter (28 mm rather than 22 mm) prostheses, and suggested that the running in phase was faster in the CoM pairing than the MoM replacements. It was proposed that this was due to the replacement of the metallic head with a ceramic component which introduced an initially smoother material which was not likely to undergo a running in phase, and accelerated polishing of the metallic cup by the smoother harder ceramic component. However, Ishida *et al* [2] described a biphasic wear pattern for 38 mm and 32 mm CoM joints tested in an orbital simulator to 3.5 million cycles using α-calf serum as the lubricant. Within this thesis, running in was evident for some tests, but not found in others. Within a particular test, the number of cycles after which steady state was reached also varied between stations. Table 12.1 compares the average wear rates for all tests carried out within this thesis. Negligible wear was seen for all heads with the exception of the heads after third body wear tests. The wear of the 60 mm standard wear tested cups was also considered to be negligible.

Test	Size (mm)		Cycles	Heads (mm^3/million cycles)	Cycles	Cups (mm^3/million cycles)
Alumina Std	38	RI	0-0.5mc	negligible wear (0.0572 ±-0.555)	0-0.5	1.04 ±0.293
		SS	0.5-5mc	negligible wear (-0.003 ±0.008)	0.5-5	0.021 ±0.004
ZTA Std	38	RI			0-0.5	0.634 ±0.737
		RI			0-1.0	0.373 ±0.108
		SS	1-6mc	negligible wear (0.0031 ±0.0012)	0.5-6	0.016 ±0.003
		SS			1.0-6	0.028 ±0.007
		SS			1.0-6 (all cups)	0.023 ±0.005
ZTA Std	60	SS	0.5-5	negligible wear (-0.0045 ±0.0042)	0.5-5	negligible wear (-0.0007 ±0.0181)
		SS			1.0-5	negligible wear (0.0029 ±0.0235)
Alumina MXS	38	RI			0-1	3.04 ±0.673
		SS	0-5mc	negligible wear (-0.0016 ±0.0045)	1-5	1.35 ±0.154
ZTA MXS	38	RI	0-2mc	negligible wear(0.0003 ±0.003)	0-2	3.82 ±0.614
		SS	2-5mc	negligible wear(-0.002 ±0.0037)	2-5	0.623 ±0.252
Alumina 3rd Body	38	Particles	2mc	0.019 ±0.027	2mc	1.272 ± 0.254
		No particles	1mc	0.066 ±0.070	1.5mc	0.127 ±0.102
ZTA 3rd Body	38	Particles	2mc	0.064 ±0.005	2mc	3.402 ±0.485
		No particles	1.5mc	0.006 ±0.007	1.5mc	0.249 ±0.181

Table 12.1: *Wear rates for all tests.*

Friction factors for ceramic on metal implants showed similar trends to ceramic on ceramic implants previously tested. Water based lubricants gave lower friction factors than bovine serum based lubricants for the majority of tests. The shape of the curves indicated that the joints were operating close to fluid film lubrication as a decrease in friction factor was found with increasing Sommerfeld number, with a minimum reached before the highest viscosity fluids (see theory section). The friction factors for 25% bovine serum and distilled water, together with the range of friction factors is shown in Table 12.2.

Test	Dimensions (mm)	Cycles (millions)	Friction Factor 25% BS	Range	Friction Factor Distilled water	Range
Alumina STD	38	0	0.023	0.019-0.035	0.011	0.0039-0.035
		5	0.052	0.018-0.052	0.017	0.0027-0.017
ZTA STD	38	0	0.049	0.022-0.049	0.001	0.001-0.006
		5	0.045	0.022-0.045	0.008	0.001-0.008
ZTA STD	60	0	0.023	0.005-0.023	0.003	0.002-0.06
		5	0.018	0.006-0.018	0.005	0.003-0.005
Alumina MXS	38	0	0.067	0.018-0.067	0.023	0.001-0.023
		5	0.018	0.010-0.18	0.002	0.001-0.002
ZTA MXS	38	0	0.039	0.020-0.039	0.013	0.002-0.004
		5	0.034	0.002-0.034	0.004	0.003-0.031
Alumina 3rd Body	38	Particles	0.024	0.006-0.024	0.002	0.0002-0.003
ZTA 3rd Body	38	Particles	0.073	0.021-0.073	0.048	0.010-0.048

Table 12.2: *Friction factors for all tests.*

It has been hypothesized that the proteins which adsorb onto the surface of the bearings may be responsible for the change in lubrication regime between material combinations, in addition to the surface topography of the bearing contact. Scholes and Unsworth [93] investigated the effect of proteins on the friction and lubrication of hip joints. They compared MoP, MoM, and CoC prosthetic hips, lubricated in different viscosities of CMC fluids, and bovine serum with the addition of CMC. Their results showed that for MoM, bovine serum produced the lowest friction factors between 0.09 and 0.15, whilst the CMC fluids produced friction factors between 0.2 and 0.3. Conversely the CoC components showed friction factors less than a hundredth (0.001-0.006) of the values given by MoM pairings when proteins are absent. When proteins were present the friction factors were found to be between 0.02 and 0.06. Their reasoning for the low friction factor for the CoC joint result was that when protein was absent, a λ value of >3 was found which allowed full fluid film lubrication, and so the friction in the joint was due to shearing of the lubricant film only. When proteins were introduced into the lubricant, they adsorbed onto the surface introducing a molecule which is greater in size than the fluid film thickness. The proteins on the surface were sheared in addition to the proteins within the lubricant film. At present, to the authors' knowledge, there is no published data which quantifies the size of the protein layer which adsorbs to the surface during simulator testing which uses bovine serum as a lubricant. However, it can be hypothesized that the adsorbed proteins create a greater friction factor than when the friction is solely caused by shearing of the CMC lubricant film. In addition adsorption of proteins onto the surface may act to alter the surface properties, reducing the hydrophilic nature of the ceramic surfaces, therefore reducing the effectiveness of the lubrication. By contrast, the MoM joints were found to have lower friction factors when the proteins were present. The interactions between asperities was a mixture of metal against metal and protein against protein which lowered the friction produced (compared with metal against metal contact alone).

The wear of the metallic cups increased considerably when modifications to the simulator resulted in medial lateral displacement of the head. An increase was also found during 3rd body testing. Microseparation testing resulted in edge contact

and a flattened lip on the edge of the softer metallic cup and an area of wear on the ceramic head, thought to be due to impact with the cup. Third body wear testing resulted in wearing of the matrix material through severe abrasive wear. Third body testing also had an effect on the ceramic heads, which was not seen with standard and microseparation testing. The ZTA head wear rate increased significantly due to grain removal from the pole. The alumina heads did not increase in wear rate compared with standard tests, even thought considerable grain removal was evident from the AFM analysis.

12.1 Alumina:CoCrMo Alloy (38mm) Standard Wear Testing

A set of six alumina heads were articulated against CoCrMo acetabular cups to 5 million cycles under standard wear conditions. The wear of these components was very low, with running in and steady state wear rates of 1.04 $\pm$0.293 mm^3/million cycles and 0.021 $\pm$0.004 mm^3/million cycles respectively. The wear of the ceramic heads was too small to be detected using the gravimetric method; however a change in surface topography was noticed indicating that some wear had occurred. A change in root mean squared roughness of the heads was not observed, however a change in skewness was noticed. Grain pull out, and a change in the orientation and regularity of the scratches was found on the head during ESEM and AFM analysis, indicating wear had occurred, albeit an extremely small amount. The wear that did occur was important as the grains may have acted as third body wear particles accelerating wear of the metallic cups.

A white deposit was noticed on both the ceramic head and metallic cup. Digital images were taken of the cups, in which deposit can be seen in the superior part of all cups, with the exception of the control, where no deposition was found. The wear patch can clearly be seen in the centre, where contact has occurred and no deposit was situated. Scratches were evident especially on the edge of the deposit showing that abrasive wear was occurring; however these scratches were not noticeable on the underlying ceramic or metallic surface. The area with no deposition on the cup,

corresponded to the area on the head, and was therefore expected to be the wear patch.

The wear patch on the cups showed carbides which were worn smooth, partially or fully pulled out. These often had corresponding abrasive scratches which were continuous through both the matrix and carbides, showing that the scratches were as a result of material of similar or greater hardness than the carbides. It could be concluded that third body particles were therefore either removed by carbides or alumina grains from the femoral heads.

The peak to valley (pv) value of the cups was greatest at 2 million cycles. This may be due to carbide pull-out during the initial stages of the wear testing during the running in stages before wear of the matrix had occurred. A small decrease between 3 and 5 million cycles was likely to be caused by polishing of the metal cup by the smooth harder ceramic head. Conversely the ceramic heads were found to have their greatest pv value at 5 million cycles, possibly due to grain-pull out in the wear track. As polishing is less likely to occur on the ceramics, the holes left by pulled out grains would remain at their original depth, therefore resulting in a large pv value. However it must be noted that small defects on the surface can lead to artificially large pv values; pv is not an average of the surface, but the largest distance between the highest and lowest points within the examination area. A low surface roughness with a large pv can indicate an individual feature on the head, rather than the large pv value representing the dominant surface feature. The skewness values (skw) were as expected with initially both head and cup showing a skw value close to zero, indicating that the surface is equally as likely to have asperities above and below the mean line. However as the test progressed the skw values for the metallic cups became more negative, indicating deep troughs compared with shallow peaks. This is consistent with the proposal that carbides are pulled out of the surface during wear testing and abrasive scratches occurred. The ceramic heads produced low skw values throughout testing until 5 million cycles, where the worn heads became largely negatively skewed. This is consistent with the increase in pv, and the observation of some grain pull out, causing an increased change of the surface topography generally below the mean line. The standard deviation of

the skw of the worn heads at 5 million cycles is large, and some heads had positive skewness possibly due to the small amounts of deposit left on the surface after cleaning, which were not visible by eye.

The present study observed material transfer (thought to be metallic matrix material) onto the ceramic heads, however currently no analysis of the elemental composition has been undertaken. It is thought that the deposition revealed in the current study is not composed of calcium phosphate, due to the addition of EDTA to the bovine serum which acts to bind the calcium in solution, therefore preventing deposition of calcium onto the surfaces. Thus deposition is likely to be predominantly due to albumin and α, β and γ globulins. Scholes [76] reported on the deposition of protein on MoM, MoP and CoC material combination which was analysed using SDS PAGE technique [76]. However the analysis was carried out on the deposition which occurred during soaking in bovine serum for 24 hours, not on the deposition caused during wear simulation. Therefore the composition of the two depositions may differ. In previous studies Firkins *et al.* [1] reported that surface analysis showed no signs of wear or changes in surface roughness after testing, however metal transfer (<20nm thick) and calcium phosphate deposits were found at the edge of the contact area. It was concluded that as this was not in the wear track, it had no effect on the wear of the bearing surfaces. Energy Dispersive X-ray analysis confirmed that it was CoCr alloy with an elemental composition similar to that of the main matrix however it was found that it did not appear to accelerate the wear of the metal cups.

Friction was used to indicate the lubrication regime which was prevalent in the joints under investigation. The alumina components worn to 5 million cycles showed low friction factors below 0.052 with a curve shape indicating that the joints were likely to be operating close to full fluid film lubrication. The joint showed a decrease in friction factor from 0.052 $\pm$0.007 when proteins were present, to 0.017 $\pm$0.017 in the absence of protein.

12.2 ZTA:CoCrMo Alloy (38mm) Standard Wear Testing

The steady state wear rates of the ZTA heads against CoCrMo alloy cups, worn under standard walking cycle conditions, were 0.016 ±0.003 mm^3/million cycles and 0.028 ±0.007 mm^3/million cycles for group 1 and 2 respectively. This was found to be similar to some published results [1, 156] though Ishida *et al.* [2] found greater values than these. A biphasic wear rate was found in the present work with running in and steady state wear rates which were found to have statistically different wear rates at a 95% confidence level. The number of cycles by which steady state wear was established varied between couples, however all bearings were under steady state wear by 1 million cycles. Previous studies of ceramic on metal replacements have found running in to be complete by 1.5 million cycles [156] and 0.5 million cycles [6] and have also concluded that ceramic on metal replacements are not free from the running in phenomenon. Surface topography analysis of the samples revealed extremely low surface roughness; the metal cups always having a lower surface roughness compared with the ceramic heads. The surface roughness of the ceramic heads did not significantly change during testing, and as shown by the AFM images little damage or change to the surface topography occurred. Grains were only occasionally visible on the majority of heads, with occasional grain removal. An exception to this was head 1 (paired with cup #11) which had removed material and troughs on the unworn surface, and was found to have a significantly different wear rate (0.044 mm^3/million cycles) from the remaining 4 couples up to 6 million cycles of wear testing. The root mean square surface roughness of the metallic cups remained similar throughout the test. Limited abrasive scratching and pitting of the surface was seen in both the profilometer images and optical micrographs. Line profiles showed small pits on the surfaces, possibly due to adhesive wear or corrosion of the metallic component. The smooth hard surfaces of the ceramic are likely to have polished the metal surfaces resulting in a smooth, albeit worn surface. The carbides which were clearly visible within the matrix of the unworn metal surfaces had been worn smooth or removed, however the majority of matrix material

appeared relatively unchanged. The lack of grain removal from the ceramic head and limited holes from carbide and matrix removal from the cups are major factors for the limited abrasive scratches found in the metallic cups. The ability of ZrO_2 particles to undergo a phase transformation from the metastable tetragonal phase to the monoclinic phase increased the fracture toughness of the alumina, resulting in reduced grain removal or further evidence of wear in the ZTA components. This reduction in ceramic particles may be the reason why less damage is seen on the metallic cups, due to the reduction in third body wear. The low wear and damage to the components suggest that zirconia toughened alumina material combination is appropriate for hybrid hip replacements.

Low friction factors were found when testing the 38 mm ZTA against CoCrMo, both initially and after 5 million cycles of wear. The friction factors together with the shape of the Stribeck plot suggested that the joints were operating close to full fluid film lubrication, where the lubricant film separates the bearing surfaces and limited asperity contact occurs. Theoretical calculations using the Hamrock and Dowson minimum film thickness equation [157] resulted in $\lambda > 3$ for both the initial and final root mean square roughness values, again indicating the joints were operating in full fluid film lubrication. This differs from the alumina tests previously mentioned in which initial calculations (of unworn surfaces) revealed values closer to $\lambda = 3$ suggesting the joints were operating closer to the mixed lubrication in parts of the walking cycle where some asperity contact is likely to occur. This may therefore support the explanation of why the higher running-in wear rates were found for the alumina tests compared with the ZTA tests. The greater roughness of the unworn cups for the alumina test suggest asperity contact would occur in the initial states of wear testing compared with ZTA tests where the joints appeared to be operating in full fluid film lubrication for the majority of the test. The final surface roughness for the alumina resulted in $\lambda > 3$ suggesting limited asperity contact resulting in a lower steady state wear rate. The low friction factors found for the ZTA bearings was supported by the limited wear seen on both the metallic and ceramic components. The presence of proteins in the lubricant increased the friction factor from approximately 0.004 in deionised water to 0.047 when 25% bovine serum

is used as a lubricant (mean of the unworn and final friction factor). The highly hydrophilic nature of ZTA resulted in a extremely wettable surface which helped to entrain the lubricant into the joint forming a fluid film. The presence of proteins within the lubricant introduced large molecules with higher shear forces than water alone which acted to increase the friction factors between the joints. A comparison of the friction results found by Brockett *et al.* [5] using 28mm Biolox delta femoral heads against CoCrMo alloy cups shows very similar results to the present study when lubricated in 25% bovine serum as shown in Table 12.3.

Study	Dimensions	Head	Cup	Lubricant	Protein content	Mean Friction Factor	Head Ra (μm)	Cup Ra (μ)
Brockett *et al.* [5]	28mm	ZTA	CoCrMo	25% BS	15.46 g/L	0.05±0.010	0.003	0.009
Brockett *et al.* [5]	28mm	ZTA	CoCrMo	Water	0 g/L	≈0.018	0.003	0.009
Current Study Worn	38mm (5 mc)	ZTA	CoCrMo	25% BS	18.75 g/L	0.05 ±0.001	0.008	0.005
Current Study Worn	38mm (5 mc)	ZTA	CoCrMo	Distilled Water	0 g/L	0.001±0.006	0.007	0.006

Table 12.3: *Friction results for ZTA 38 mm joints compared with literature.*

A slight difference in friction factors was seen when distilled water was used as the lubricant, as a friction factor less than one tenth of the 28 mm joint was found for the 38 mm bearings.

A white deposit, thought to be protein, was found on all bearing surfaces (except the control) during each 0.5 million cycles wear period as evident in Figure 7.24. Increases in temperature resulting in denaturing of proteins in the lubricant have been found to occur between bearing surfaces resulting in precipitation of the serum proteins and adsorption onto the surfaces [94, 96, 99, 100]. Albumin, an abundant protein in both synovial fluid and bovine serum, has been reported to adsorb to surfaces in both the native and unfolded form depending on the conditions and materials involved [96]. Hypotheses have suggested that tribological processes such as friction and wear can result in adsorption of albumin to certain bearing surfaces[27] some suggesting that unfolding of the secondary structure reveals more of the hydrophobic contact area of the albumin resulting in a compact layer deposited onto the surface increasing the friction compared with native albumin which has a better 3D structure [100]. The majority of the work has concentrated on the deposition of protein onto hydrophobic polymer surfaces, however there are cases in the literature of albumin being adsorbed to metallic and ceramic bearing materials. Interestingly the results differ with some authors suggesting that albumin does not adsorb on surfaces of an alumina on alumina pin on disc tribometer test [99] where other cases have shown albumin to adsorb to both metallic and ceramic surfaces, adsorbing to the metallic one to a greater extent than ceramic [97]. In the current study, deposition was found on all ZTA components (except the control, see Figure 7.24) in the area surrounding the pole, and has previously been reported on alumina femoral heads in the same laboratory ([7]). If an increase in temperature due to friction can lead to unfolding of the proteins and adsorption onto the bearing surfaces, protein adsorption is likely to occur in regions where the temperatures are greatest [99]. It is expected in hip replacements this region is the area where the head and cup fit together in close contact. However, adsorbed molecules will only remain on the surfaces in regions where physical contact and motion does not occur. This may provide an explanation of why deposition is not found in the circular contact region,

but is found in the region surrounding the wear patch where temperatures are high but physical contact has not occurred. The deposition is likely to protect the pole the bearing surface against wear by acting as a boundary lubricant which if thick enough can break through the fluid film and interaction of the protein layers may occur. Previous studies have noticed white deposits on the components after wear and friction, [96, 99, 115] and discussed the concerns that it may protect the surface from wear. Fine scratches can be seen in the deposition at the edge of the contact area showing that either third body, abrasive wear or a combination of both types of wear has occurred. Metal staining which occurred in the contact area was found to change as the test progressed and metal was transferred back to the metallic cup or worn away resulting in metal particle and ion release. It is hypothesised that the larger scratches in the deposition, which are too large for third body particulate wear or abrasive scratches, are due to taking the components out of the simulator and are not caused during wear simulation.

12.3 ZTA:CoCrMo alloy(60 mm) Standard Wear Testing

Very low wear was found for the larger diameter ZTA:CoCrMo components over 5 million cycles of standard wear testing. Unexpectedly the control component lost the greatest volume in the first 0.5 million cycles compared with the active stations. Therefore when the control component was used to adjust the results, an apparent increase in volume for all active stations would have occurred. As a result of this the control station was only used to adjust the results between 0.5-5 million cycles and the unadjusted data was used between 0-0.5 million cycles. The steady state wear rate of the metallic cups between 0.5-5 million cycles was found to be -0.0007 $\pm$0.0181 mm^3/mc (volume gain) and between 1-5 million cycles was found to be 0.0029 $\pm$ 0.0235 mm^3/mc (volume loss). These results highlight the difference in wear rates depending on the number of cycles used in the calculation, showing comparison between studies of different number of cycles may be difficult. In this case, the wear rates determined are so small with r^2 values of 0.00012 and 0.0015

and non significant regression lines respectively, that the wear is considered to be negligible.

Friction testing revealed interesting results with an unexpected rise in friction factors for the highest two viscosities of water based lubricants. From previous tests using ceramic on metal components, lower friction factors were expected for the water based lubricants compared with the bovine serum based lubricants. Theory suggested that $\lambda \approx 12$, therefore the components should operate well within fluid film lubrication. The ceramic heads had small metal transfer smudges at the edge of the wear track which may be signs of poor lubrication and adhesive wear occurring as a result of the large diameter. When the direction of motion changes, the lubricant film may be disrupted and asperity contact may occur. After removing the components from the friction simulator, a dry area was seen in the centre of the wear patch. It was therefore hypothesised that the larger diameter and a low swing angle may be the reason for the higher results as the swing may not be great enough to entrain the fluid into the centre of the joint. High suction was found between the components as a result of squeeze film which may have lifted the cup out of the carriage during testing. As a result the mechanism used to hold the cups into the simulator was modified and the tests repeated with a different unworn joint. This resulted in a reduced friction factor however the shape of the curve was similar. The friction factor for the greatest viscosity of water based lubricant was 0.056 which was higher than expected from previous experience. For comparison, the unworn joint was compared against data for 2 different worn joint, of which all the tests were carried out on the same simulator under identical conditions. Similar results were found for all lubricants for the unworn and worn joint, except the two highest viscosities of water based lubricant which reduced considerably after wear testing. After 5 million cycles, the Stribeck plots indicated full fluid film lubrication with the highest friction factors at the greatest and lowest viscosities.

Even though low wear rates were found the surface topography analysis showed removed grains on the ceramic heads and abrasive scratching on the metallic cups. Only small changes in rms roughness were found for the metallic cups which increased from an initial value of 0.10 μm to 0.18 μm by 0.5 million cycles. This was

thought to be due to an increase by 2.5 million cycles, the rms roughness returned to a lower value of 0.12 μm however, the appearance of the surfaces remained similar throughout the test. An increase in skewness was found with number of cycles due to abrasive scratches, pitting and possibly carbide removal.

The rms roughness of the ceramic heads did not change significantly with number of cycles. The head soak control rms roughness was consistently higher than the active stations due to damage on the unworn surfaces. Head 32-6 (active station) was also found to have a damaged unworn surface which with an initial rms roughness nearly twice that of the other components. Interestingly the roughness of head 32-6 was found to decrease from 0.017 μm to 0.011 μm by 2.5 million cycles. The increased initial roughness of head 32-6 did not have any effect on the wear rate of that head which was found to have an individual steady state wear rate of -0.012 mm^3/mc (volume gain) which although was the highest individual wear rate, it was similar to two other, non damaged active stations (head 26-1 and 26-3).

The optical micrographs revealed unworn surfaces similar to those seen in previous tests however the surfaces appeared extremely smooth and the contrast of the carbides within the matrix material was difficult to identify. After 0.5 million cycles, abrasive scratches were visible in the direction of flexion/extension. Although frequent, many of the scratches were shallow and short. Pits were clearly visible in the metal surface, some of which had corresponding comet tail scratches. These were thought to be as a result of adhesive wear, in which pulled out sections of the matrix or carbide act as third body wear particles, or become attached to the opposing ceramic surface for a short time, acting as an abrasive surface until it is released into the lubricant. A heterogeneous topography was found within the wear patch of each individual cup, some areas being significantly scratched and some showing a surface similar to that of the unworn samples. After 2.5 and 5 million cycles, scratches, both from abrasive and adhesive wear were evident, however darkened areas were also found. These areas, called 'smudging', revealed a pattern on the surface. These areas were thought to be troughs where metal particles have collected and subsequently become embedded into the surface, therefore highlighting the topography of the surface. Areas which were almost unchanged from the unworn surface, except

for a lower contrast between the carbides and the matrix material were also found. As no corresponding abrasive scratches were evident, it is likely that the carbides were worn smooth due to the harder ceramic counterpart, resulting in very small nanometer size particles. This may be as a result of small parts breaking of the porous carbide structure and may suggest the majority of abrasive wear on the cups from the alumina test were due to alumina fractured or removed grains.

AFM analysis of the majority of the unworn ceramic heads revealed polishing scratches which became less evident as the test progressed. Head 32-5 and 32-6 were damaged and revealed clusters of removed grains (in addition to the polishing scratches) which were significant enough to increase the roughness of the surfaces compared with the active stations. By 2.5 million cycles, grain removal was visible on the pole of all active stations. Grains appeared as small irregular polygon shaped shallow holes on the surface of the ceramic. As the grains increased, the polishing scratches became move evident. The removed grains were found to be approximately 30-40 nm deep. The depth of each individual hole was not consistent suggesting that each hole maybe as a result of fractured grains, or removal of whole grains. The depth of the holes found on the initially 'damaged' heads were much deeper, in the hundreds of nanometre range.

Deposition was found on all active stations surrounding the pole of the heads and within the superior lateral region of the cup. A circular clear patch was visible on the top of the ceramic heads where contact had occurred, and prevented deposition onto the surface. Scratches were seen on the edge of the deposit which showed abrasive wear was occurring, however the abrasive particle did not appear to scratch the underlying ceramic material as regular parallel scratches were not seen on the head under AFM imaging.

12.4 Alumina:CoCrMo Alloy (38mm) Microseparation Wear Testing

Research in the early 2000's led to the development of microseparation simulators which included medial lateral displacement of the head with respect to the cup

in order to create edge contact. The aim was to achieve 'stripe wear', an area of increased wear on the side of the head. The modifications to the simulator within this thesis resulted in edge contact and an area of wear thought to be similar to 'stripe wear' found on retrieved replacements.

An increased wear rate was seen for the components under microseparation conditions, compared with standard testing, with running in and steady state wear rates of 3.04 $\pm$0.673 mm^3/mc and 1.35 $\pm$0.154 mm^3/mc respectively. The head volume change fluctuated around zero as the measuring technique was not sensitive enough even to detect wear from a more severe wear test. Medial lateral displacement resulted in a flattened lip forming at the edge of the metallic cup resulting from head relocation. This lip was found to increase in width and breadth with number of cycles. The metal transfer seen at approximately 33 ^{o} to the horizontal on the lateral side of the head was thought to be as a result of dislocation of the head rather than head impact, due to the location of the metal transfer and stripe wear.

Friction tests before and after microseparation were not expected to differ from those of the standard test as friction was tested at the pole of the head and did not involve the edge contact region. The head was not separated during friction testing and the wear on the pole and within the cup was not severe enough to result in an increase in friction. The results showed a small drop in friction factors for the bovine serum based lubricants after wear testing, however the water based fluids before and after testing were similar. All water based lubricants gave lower friction factors than bovine serum based lubricants as the bovine serum introduced proteins which require a higher shear force for sliding to occur compared with water based lubricants.

The rms roughness of the metal cups increased as a result of abrasive and adhesive wear within the wear patch. Interruptions in the fluid film due to impact of the head and cup led to increased adhesive wear as a result of increased intimate contact between the bearing surfaces. Larger abrasive scratches were seen possibly as a result of matrix or carbide removal which subsequently acted as third body or two body abrasive wear. SEM images showed porous carbides located within the matrix material with carbide removal. These hard ceramic particles may have acted

as the abrasive wear particles leading to increased wear. Wispy abrasive scratches were seen in both the optical and SEM images providing evidence for third body particle wear. The carbides within the wear patch had either been worn smooth or removed, which was shown by the decreased contrast between the carbides and matrix material in the optical images. This could also be seen in the SEM images which showed the porous carbides situated at a similar level to the matrix material. Carbides outside the wear patch were clearly distinguishable from the matrix material under optical microscopy as the height difference between matrix and carbides were greater. This was supported by line profiles from the non contacting profilometer. Optical micrographs showed plastic deformation of the matrix material possibly as a result impact of the head upon relocation. This was found towards the edge of the wear patch and may be as a result of a poor lubricating film at the point where the direction of motion changed. Areas of metal transfer, or metal particles embedded into the matrix were seen on the edge of the flattened lip. This darker region was found to highlight the carbides or the holes where the carbides once were on the edge of, and within the flattened lip. On some cups, a second or third lip was found to form on top of the first lip. This may be as a result of the cup moving within the holder which is made from UHMWPE, resulting in a slight change in the position of the cup in relation to the head. This would mean that edge contact does not occur at the same location every cycle.

AFM analysis showed grain removal on the pole of the head, with areas of metal transfer found at approximately 33 degrees to the horizontal. These metal layers were nanometres thick and did not significantly change the roughness of the surface. The area of metal transfer did show a positive skewness whereas the pole and stripe regions showed negative skewness due to removed grains. As with the standard test, the holes left from the grains were shallow and only tens of nanometres deep. Deposition was found on the head after each 0.5 million cycle wear period and was not present in areas where edge contact had occurred.

12.5 ZTA:CoCrMo Alloy (38mm) Microseparation Wear Testing

Microseparation testing was also carried out on ZTA:CoCrMo components similar to those tested under standard wear testing. An increased wear rate was found for the cups compared with standard testing, with a running in and steady state wear rate of 3.28 $\pm$0.614 mm^3/mc and 0.623 $\pm$0.252 mm^3/mc respectively. The head volume change fluctuated around zero for the entire test as with the standard test. The load soak and soak control components showed a similar trend and magnitude of fluctuations as the active stations, indicating that external factors during the weighing process had a greater effect on the volume changes than the wear testing itself. The softer metallic counterpart was found to wear the most due to impact with the harder ceramic components. The control cup lost significantly less mass compared with the active stations. Medial lateral displacement led to a flattened lip forming on the superior lateral edge of the cup. Throughout testing the lip was roughly measured to monitor changes as the test progressed. Generally the width and breadth of the lip increased with number of cycles. A second and occasionally third lip was found to develop on top of the first lip but this did not lead to noticeable differences in wear rate between components. It is thought that the majority of the increase in wear compared with the standard tests, was due to the wear of the edge of the cup, rather than within the wear patch, although the wear patch may have also contributed to the increased wear. The difference in wear rate between running in and steady state may therefore be due to age hardening of the material on the flattened lip, and an increased area of impact as the test progressed. As repeated impact occurred, fatigue mechanisms may have resulted in material fracture and removal. Initially plastic deformation of the lip may be relatively easy due to the small area and high pressure. However as the area reached a plateau, the pressure decreases and the wear becomes steady. As the wear continues and the impact area increases, the head becomes easier to relocate into the cup and the wear rate remains stable.

Friction testing revealed low friction factors both before and after wear testing.

Similar trends were found for water based lubricants on the unworn and worn sample with the exception of the highest viscosity which gave over twice the friction factor after wear testing. The unworn tests produced higher friction factors for bovine serum lubricants compared with the water based lubricants, as was expected, with a trend indicative of full fluid film lubrication. However after wear testing, the bovine serum and water based lubricants showed friction factors in a similar range, however the trend was a decreasing friction factor with increasing Sommerfeld number which is more indicative of mixed lubrication. Two components were tested and the trend was similar for both pairs. This may be due to the wear of the components resulting in more asperity contact and a mixed lubrication regime.

Experience gained from previous microseparation tests allowed the surface topography to be monitored in three areas of interest. The three areas were;

- pole-the area in line with the direction of force and where the main wear occurs once the head has relocated into the cup during the stance phase of the walking cycle,
- metal stripe region - resulting from dislocation of the head from the cup,
- stripe region - resulting from edge contact with the cup.

Surface topography data was recorded using the non contacting profilometer for both the head and cups up to 1 million cycles. After this the AFM was used to record rms and skewness data for the ceramic heads only. Measurements on the unworn metallic cups surfaces revealed a difference in carbide topography between cups. Three cups showed relatively smooth carbides, and three cups showed carbides which stuck out of the surface further. This was also noticeable in the optical images where the contrast between carbides and matrix highlighted the height difference between features. The difference in carbide position was less significant by 0.5 million cycles. The running in wear rates of the cups with protruding carbides showed the extremes of wear rate for all active stations, therefore the carbide position did not appear to have an effect.

The active cup skewness values had a large standard deviation initially due to protruding carbides which were found in some, but not all cups. The mean

skewness became slightly more negative as abrasive scratches and pitting became more evident. The optical images revealed areas of pitting with comet tails showing adhesive wear was occurring. Wispy scratches were also evident showing third body wear has occurred, along with parallel scratches in the flexion/extension direction. Areas of little obvious wear were also evident. Images were taken after 0.5 million cycles in which areas where metal particles appear to be agglomerated with the deposition and stick to the surface. The lip region, where edge contact occurred shows areas similar to that found within the wear patch. Areas of limited damage and adhesive wear were evident. A region of transfer was found on the edge of the lip, possibly due to metal particles embedded into the softer matrix, or within the deposition along the edge of the lip.

AFM analysis of the heads revealed random polishing scratches on the unworn samples with occasional deeper scratches in the 20 nm range. By 0.5 million cycles a few shallow grains were noticeable on the pole as a result of polishing. The removed grains appeared as small dark spots on the AFM image which were shown to be holes when line profiles of the surface were taken. Metal transfer found at approximately 33 degrees to the horizontal, was thought to be as a result of dislocation of the head from the cup. Line profiles showed the metal to be tens of nanometres thick which may have acted to protect the underlying ceramic surface from wear as no damage or grain removal was found on the underlying ceramic surface. After 5 million cycles a region was found, where occasional grain removal was evident. This was considered to be the 'stripe wear' region where relocation of the head occurred resulting in removal of grains. Again these appeared as small irregularly shaped dots on the AFM images. Within this region the polishing scratches seen on the initial images were less evident, as seen where grain removal occurred on the pole. The 'stripe wear' region was not obvious by eye, therefore defining the boundaries was difficult. Further observations of the deposition on the head revealed an area on the posterior lateral side in which no deposition was located. A straight edge was found, which highlighted an approximate area of grain removal.

12.6 'Stripe' Wear Under Microseparation Conditions

'Stripe' wear patterns were found under microseparation testing for both 38 mm alumina and ZTA tests reported on within this thesis. Two 'stripe' regions were identified, one as a result of dislocation of the head at the beginning of the swing phase (metal transfer region) and one as a result of impact with the rim of the cup (stripe wear region). A flattened lip was also established on the rim of the metallic cup. As a result of the ceramic on metal material combination, the wear of the ceramic head was unmeasurable using the gravimetric method. The 'stripe' area was not visible by eye and therefore accurate measuring of the position and size was difficult. It was however established that an area with higher wear, through grain removal, were apparent on the inferior lateral section of the head.

The available literature regarding microeparation wear scars does not appear to have established a clear conclusion for the position or size of wear scar. A report by Williams in 2008 [7] reported no wear scars on the ceramic head from a ceramic on metal component, with only a narrow scar on the rim of the metallic cup. This differs from the current study, where two areas of contact were established on the head. This may be due to differences in the methods used to produce microseparation in the *in vitro* simulators. Retrieval studies are not available for ceramic on metal combinations however the work can be compared to retrieval studies of ceramic on ceramic implants which have shown significantly different retrieval wear pattern results.

Several authors have presented *in vitro* results for ceramic on ceramic components [158–160] which have shown a single stripe on one side, half way up the head and a corresponding mark on the rim of the cup. A more recent report [161] showed two wear scars at 0.1 million cycles, the larger found at $+75^o$ to $+90^o$ and the second narrower stripe at $+45^o$ to $+60^o$. However these were found to have coalesced by 5 million cycles forming a single wear scar with a width of around 44 mm. From the images presented within the paper, the position of the scars were similar to the metal transfer found within the current study however as with many studies it is

difficult to establish the exact anatomical position of the wear. The 'stripe' wear found on the ceramic heads within this thesis were narrower and closer to the pole. The wear scar on the rim of the cups for the ceramic on ceramic test [161] subtended between 10-90^o with the largest found to be 180^o. This again was similar to that found within the current study. The scars for the ceramic on ceramic components [161] were found to extend deeper into the cup by 5 million cycles showing a similar pattern to the flattened lip on the metallic cups within this study.

Comparisons between *in vitro* results and retrieval implants have shown *in vitro* simulators to produce narrower scars compared with retrieved implants, however considerably variation was also found with the retrievals [118]. Biolox heads were reported to show two wear scars, one of which was thought to be due to microseparation, whilst the second was as a result of neck-socket impingement. An Osteal retrieved component revealed only one stripe scar which was much larger and thought to be soley due to edge impact. However, the severity of the wear was considered to be less than that found for the Biolox heads. A further report which analysed three retrieved ceramic on ceramic implants showed three heads to give significantly different results. One head show no wear scars, one showed a narrow wear scar and the third showed a broad stripe scar on the medial, anterior and lateral sides of the head, which covered 180^o [124]. The ceramic inlays also showed considerable variation with one inlay showing wear through 360^o whilst the other cup showed a narrow scar only on the lateral side of the rim which was similar to that found on the metallic cups within this thesis. The mechanism of microseparation proposed by other researchers and presented within this thesis, are unlikely to produce wear through 360^o on the cup. It is therefore suggested that some of the scars found on retrieval implants are produced via a different mechanism to that used within this thesis.

The largest ceramic on ceramic retrieval study focusing on stripe wear was by Walter in 2004 [125] in which 11 heads and 2 liners were reported to show stripe wear. All head scars were found to be retroverted (defined as the scar sloping from anterolateral to posteromedial) and the stability of the joint was found to effect the the severity and position of the scar. The stripe wear image showed a similar

position to those produced within this thesis on both the head and cup. However Walters study suggested that the scars analysed on the 9 stable components could not be causing during normal walking gait and may have been caused when the hip is flexed such as rising from a chair or climbing a high step. The variation in results found within the literature clearly show that further research is required before a conclusion can be drawn as to the mechanism and motion responsible for the wear found *in vivo*. The current work provides further evidence that a mechanism can be achieved which produces similar wear scars and wear rates, however if these truly replicate the wear found *in vivo* is yet to be established.

12.7 Third Body Wear Testing (38 mm)

Third body testing was conducted using 0.5 g of <1 μm particles in the lubricant. ESEM was used to image the alumina particles. Each individual particle was round in morphology and less than 1 μm in diameter. However particles tended to agglomerate into the diameters tens of microns which are larger than the fluid films predicted using minimum film thickness theory, therefore the agglomerated particles may find it difficult to fit between the bearing surfaces. Standard walking cycle wear testing was carried out for 2 million cycles with particles in the lubricant, followed by a recovery period where only clean lubricant was used, stage 1 and 2 respectively. Higher wear rates were found for the particle tests compared with the standard tests. The cups from the ZTA test gave the highest wear rate, 3.402 $\pm$0.485 mm^3/million cycles compared with 1.272 $\pm$0.245 mm^3/million cycles for the cups from the alumina test. The higher wear rate for the cups may be as a result of higher wear rate found for the ZTA head (0.046 $\pm$0.0.005 mm^3/million cycles, ZTA heads, compared with 0.019 $\pm$0.0.027 mm^3/million cycles for the alumina heads), resulting in more ceramic particles for third body wear. These higher wear rates are as a result of significant differences on the pole of the ceramic heads after particle testing. The alumina heads showed randomly shaped holes with abrasive wear tails originating from the holes in the direction of motion. The holes were hundreds of nanometres deep. The ZTA heads showed a greater number of randomly distributed holes over

the surface, thought to be primarily caused by removal of ZrO_2 particles, which were distributed throughout the alumina matrix in the ZTA structure as shown in Figure 5.1. Abrasive comet tails were not seen. The holes within the ZTA heads appeared to be tens of nanometres deep, which were shallower than those found in the alumina head. The holes in the alumina test appeared to be one removed grain as the holes had one depth, whereas the holes from the ZTA test showed two or more peaks within in each hole which could indicate more than one smaller grain had been removed. This feature is supported by the hypothesis that within the ZTA structure, the wear is caused by removed ZrO_2 particles removed from within the alumina matrix. The surface topography did not change during stage 2 when clean lubricant was used. The topography of the surfaces where clean lubricant was used throughout did not change from that seen during standard walking cycle testing. The rms roughness of the ceramic heads did not change even though grain removal was evident.

The surface topography of the cups changed when particles were included within the lubricant. Third body particles had resulted in areas of many parallel scratches within the wear patch, however areas of less regularly distributed scratches were also seen. Dark areas were observed, possibly as a result of metal particles which became embedded into the matrix resulting in a contrasting feature under the optical microscope. Protein and metal agglomerates may also be an explanation for the darkened areas. The topography of the cups from the alumina and ZTA test did not differ considerably, with no obvious increase in wear seen for the cups from the ZTA test compared with the alumina test even though the wear rates suggested there should be. The results of the optical microscope from the clean lubricant stations were the same as found during standard wear testing.

Images from the non contacting profilometer revealed an interesting feature on the metallic cups during third body testing. After standard testing, carbide shaped holes were found in surface within the matrix. However after 2 million cycles of particle testing, the carbides were found to protrude from the surface compared with the matrix material. Following a period of testing with clean lubricant, carbide shaped holes were again left within the matrix. This was evident on all active

stations, for both the alumina and ZTA test. During standard testing, wear occurs as a result removing or wearing the carbides smooth, in addition to wearing of the softer matrix. However, during third body testing wear was due removal of the softer matrix material in which the carbides sit. The additional alumina particles were small enough to fit between the carbides and wear the matrix, leaving the carbides intact. As a result of this, it may be hypothesised that the as-cast structure would be preferable if third body particles were present as the carbides act to protect the surfaces and reduce the wear compared with a heat treated metallic structure where the carbon are dissolved within the matrix.

Friction tests were carried out after third body particle testing. The results of the ZTA test were similar to those found after 5 million cycles of standard wear testing showing friction factors less than 0.1 and a curve indicative of full fluid film lubrication. The alumina test showed similar friction factors for the water based lubricants. The friction factors for the bovine serum based lubricants were slightly lower after particle testing, however a similar shaped curve was observed. Again the low friction factors and shape of the curve were indicative of full fluid film lubrication. However it must be noted that the friction tests were carried out with clean lubricant only, therefore this would not represent the friction factors observed during third body particle testing.

12.8 Material Comparison

Pure alumina, and zirconia toughened alumina ceramic heads were paired against as-cast CoCrMo cups. The conditions for the two tests were identical. The diameter of joints used was 38mm and 25% bovine serum as the lubricant. Under standard wear conditions, the steady state wear rate of the metallic cups for the alumina and ZTA tests were very similar at 0.021 $\pm$0.004 mm^3/million cycles and 0.023 $\pm$0.005 mm^3/million cycles respectively. This showed that under standard conditions both ceramics performed well against CoCrMo alloy cups. For both tests, the ceramic head volume change was found to fluctuate around zero, and as the wear was so small, the limits of detection of the gravimetric technique were reached.

The head control stations for both materials, were found to follow the same trends as the active stations, showing that environmental techniques during the weighing process were having a greater effect on the mass than wear during simulation. However, the alumina test clearly showed removed grains and a change in the polishing scratches after 5 million cycles of wear, showing wear had occurred, albeit small. In contrast, the ZTA heads showed only very occasional removed grains and was not as significant as the grain removal on the alumina heads.

However, the running in wear rate of the metallic cups from the tests differed. The alumina test gave a running in wear rate of 1.04 $\pm$0.293 mm^3/million cycles compared with 0.634 $\pm$0.737 mm^3/million cycles and 0.373 $\pm$0.108 mm^3/million cycles for the groups of components from the ZTA test. The alumina test had over twice the running in of the ZTA test, which may be as a result of the higher rms roughness of the unworn metallic cups from the alumina test compared with the ZTA test. The cups from the alumina test had an average rms roughness of 0.023 μm which reduced to 0.017 μm by 5 million cycles. The cups from the ZTA test had an initial rms roughness of 0.007 μm which changed to 0.009 μm by 5 million cycles. These changes are considered negligible in terms of roughness changes, however these slightly lower roughness values may be an explanation for the lower running in wear rate of the cups from the ZTA test compared with the alumina test.

A considerable difference in cup topography was found between the two tests. The carbides had become worn smooth or flattened in both tests shown by the lower contrast between the matrix and carbides under the optical microscope. The cups from the alumina test showed extensive abrasive scratching whereas the cups from the ZTA test had little abrasive scratching. The reason for the difference in abrasive wear may be down to the difference in grain removal from the ceramics. The alumina head had considerably more grains removed, which may have then acted as third body abrasive particles. In contrast the ZTA head had only very occasional grain removal, therefore limiting the amount of wear occurring.

The Stribeck plots of the 38 mm Alumina test and 38 mm ZTA test were similar. With the exception of one point (lowest viscosity of bovine serum based lubricant after 5 million cycles in the ZTA test), all results showed friction factors less than

0.06. Water based lubricants gave lower friction factors than bovine serum based lubricants for all tests, similar to that found for ceramic on ceramic tests reported in the literature [33]. The shape of the curve, a decreasing friction factor with increasing Sommerfeld number, indicated the joints were working close to full fluid film lubrication during parts of the walking cycles, however as the topography results showed, some asperity contact and wear was occurring.

12.9 Dimetral Size Comparison

To investigate the effect of size, 38 mm and 60 mm components, were compared under identical standard wear conditions. The heads were made from ZTA and paired with as-cast CoCrMo alloy. The wear rates of the heads were negligible as the volume changes fluctuated around zero. During steady state wear, the control station volume change fluctuated to the same trend and magnitude as active stations again showing that the gravimetric technique was not reliable enough to monitor such small changes in mass. The steady state wear rate of the 38 mm test was found to be 0.024 $\pm$0.005 mm^3/million cycles (1-6 mc) compared with 0.003 $\pm$0.0235 mm^3/million cycles for the 60 mm test (1-5 mc). The negligible wear for the 60 mm test is likely to be due to the higher entraining velocity as a result of the increased diameter which creates a thicker fluid film between the bearing surfaces resulting in full fluid film lubrication. Theoretical calculations predict λ ratio well above 3, firmly suggesting the joints should work in full fluid film lubrication.

Although negligible wear was recorded for the 60 mm ceramic heads, grain fracture and removal on the pole of the head was seen. This was noticed on some heads by 0.5 million cycles of wear, and on all active station heads after 2.5 million cycles. Line profiles of small irregular dark areas on the AFM images showed shallow holes which were tens of nanometres deep which are thought to be ZrO_2 particles removed from within the alumina matrix. A decrease in polishing scratches was found as the holes became more obvious. However, in contrast the identical ZTA heads which were 38 mm showed only very occasional grain removal. The metallic cups corresponding to the 60 mm test showed some abrasive scratching along with adhesive

wear and associated comet tails. Areas where little change in surface topography were also noticed. Darkened areas which highlighted the general topography of the surface were also noticed, thought to be due to small metal or ceramic particles which become embedded into the softer matrix in the troughs between the carbides or within abrasive wear tracks.

The friction results of the two diameters were found to be similar. Generally the water based lubricants gave lower friction factors than the bovine serum based lubricants. Due to the low surface roughness's of the two bearing surfaces, friction was solely caused by shearing of the lubricant rather than as a result of asperity contact. When bovine serum was introduced, the large proteins between the bearing surfaces increase the friction, as the shear force to slide the proteins over one another was larger than water molecules alone. An exception to this was the results from the unworn sample of the 60 mm when tested with the highest viscosities of water based lubricant, which showed the highest friction factors. This was thought to be due to the larger diameter joint and dry rubbing on the pole. The majority of friction factors for both joints were less than 0.06 and showed a curve shape indicating full fluid film lubrication.

12.10 Testing Conditions

As both the alumina and ZTA tests showed very little wear under standard conditions, two types of severe wear testing were carried out to investigate what effect this would have on the material combinations. Microseparation was introduced which resulted in edge contact between the head and cup. In addition, alumina particles were added to the lubricant to encourage third body wear and see what effect this has on the material surfaces, especially the ceramic heads.

12.10.1 Alumina:CoCrMo

Standard, microseparation and third body testing was carried out on 38 mm diameter joints. The wear rate of the cups in shown in Table 12.4.

Standard wear testing gave the lowest wear rate both for running in and steady

Test	CUP Running in wear rate mm^3/mc	CUP Steady state wear rate mm^3/mc
Standard	1.04 ±0.293	0.021 ±0.004
Microseparation	3.04 ±0.673	1.35 ±0.154
Third Body		1.27 ±0.245

Table 12.4: *Wear rates for the three tests for the Alumina tests.*

state wear. During microseparation testing the steady state wear rate were at least 64 times that of standard wear tests. The steady state wear rates during microseparation testing was similar to that found during third body testing although different mechanisms of wear were responsible for this volume change. Microseparation testing resulted in a flattened lip on the superior lateral edge of the cup. Third body testing resulted in significant abrasive wear which resulted in considerable amounts of wear in both matrix and through carbide removal.

Third body testing resulted in a greater proportion of grain removal from the alumina head than microseparation testing which resulted in only shallower polygonal removed grains. AFM imaging showed grain removal hundreds of nanometres deep from the third body testing, with corresponding comet tail abrasive scratches. This was thought to be caused primarily by an adhesive wear mechanism between the additional alumina particles and removed grains. The flexion/extension direction was obvious from the direction of the abrasive scratches from the removed grains. Microseparation resulted in shallow grain removal due to fracture and partial removal of the grains on the pole and within the stripe wear region. However despite the difference in topography the wear rates of the heads in both tests were negligible.

12.10.2 ZTA:CoCrMo

The wear rates of the cups from the ZTA tests under the three wear conditions is shown in Table 12.5.

The wear rate of the cups from the ZTA test was considerably higher under severe wear testing compared with standard wear testing. The running in wear rate

Test	CUP Running in wear rate mm^3/mc	CUP Steady state wear rate mm^3/mc
Standard	0.405 ±0.102	0.023 ±0.005
Microseparation	3.82 ±0.614	0.623 ±0.252
Third Body		3.402 ±0.485

Table 12.5: *Wear rates for the three tests for the ZTA test.*

of the microseparation test was over 9 times greater than that seen for the standard wear test. The steady state wear rate was significantly higher (approximately 27 times greater) for the microseparation test, and even greater (147 times greater) for the third body test compared with standard wear testing. This is likely to be partly linked with the amount of grain pull out seen on the ceramic counterpart. Only very occasional grains were removed from the pole of the ZTA heads for the standard wear test, therefore limiting the amount of third body wear occurring and abrasive scratching. Microseparation testing resulted in slightly more grain removal on the pole and within a small stripe wear section on the posterior which is indicated in the increased wear rate. The microseparation test also results in a flattened lip and increased wear as a result of edge contact and head relocation. The increased wear of the cups found for the third body tests was due to third body abrasive particles which wore the softer matrix material and removed carbides. In addition to the particles within the lubricant, extensive grain pull out was seen for the ZTA heads under third body testing. AFM images revealed many shallow holes on the pole of the heads which were tens of nanometres deep. Comet tails were not seen on the ZTA heads as was seen for the alumina heads. This may be because the holes in the ZTA heads were mostly from removed ZrO_2 particles which were softer than the surrounding alumina matrix therefore did not result in abrasive comet tails.

As with the cups from the alumina test, the cups from the ZTA test showed significant damage from the severe testing. Microseparation testing led to significant abrasive and adhesive wear compared with the standard tests which showed little damage to the metal cups. Third body testing resulted in significant areas of extreme abrasive scratching with parallel scratches in the direction of motion. Darkened areas

were seen throughout the wear patch which are thought to be due to metal or carbide particles which are embedded within the softer matrix. The flattened lip showed areas of little damage in terms of abrasive or adhesive scratching however areas were seen where abrasive scratches were found as a result of the head relocating into the cup. Darkened areas were seen on the edge of the lip which again may be metal particles or an agglomerate of metal and protein deposition.

12.11 Deposition

Deposition was found on all components after each 0.5 million cycle period. The deposition was a creamy white colour, and could be stained using non permanent ink. The deposition was thought to be protein which has denatured and precipitated from the solution as a result of heating or mechanical damage and adsorbed to the surface. The deposit was found on both the metal and ceramic counterparts around the wear patch. Deposit was not found directly on the pole as it was prevented from adsorbing to the surfaces, or the mechanical action of asperity contact removed the deposition as it adsorbed. A greater amount of deposition was found on the ZTA heads compared with the alumina heads, possibly due to differences in thermal conductivity. The ZTA heads under microseparation conditions showed less deposition than found for the standard test. This is thought to be due to a decrease in temperature of the lubricant around the pole as during head and cup separation the lubricant can circulate between the components, thus decreasing the temperature of the lubricant and preventing denaturing of the molecules in the lubricant. The modified motion is likely to prevent deposition by allowing the deposit to move away from the bearing surfaces. The alumina heads from the third body test showed less deposition compared with the ZTA heads. The stations with particles included into the lubricant showed less deposition than the stations with clean lubricant on both the alumina and ZTA test as a result of the alumina particles which act to removed the deposition by third body wear mechanisms.

The greater amount of deposition found on the ZTA surfaces may explain why less wear was found under standard conditions, as the deposition acted to protect

the surfaces from wear. However during 3rd body particle testing, the deposition was unable to adhere to the surfaces and therefore wear of the ZTA components occurred. This may suggest that under standard conditions the ZTA components withstand wear well partly due to the protective deposition on the surfaces, however if the conditions do not allow the deposition to form, and wear of the actual material surfaces occur, ZTA does not resist wear and a more severe wear rate is found.

12.12 Comparing wear rate with the literature

Figures 12.1,12.2,12.4 and 12.3 compare the wear rates calculated from the tests within this thesis, with wear rates found in the literature. Table 12.6 provides the references for the data within the Figures. All wear rates are for the steady state period of wear. The current study results are highlighted in pink.

Figure	Number	Reference	Figure	Number	Reference
12.1	1	Liao 2008	12.2	1	Williams 2004 [137]
	2	Ishida 2008 [2]		2	Liao 2008 [156]
	3	Current work		3	Smith 2001 [162]
	4	Williams 2007 [163]		4	Ishida 2008 [2]
	5	Firkins 2001 [1]		5	Essner 2005 [117]
	6	Barnes 2008 [9]		6	Bowsher 2004 [164]
				7	Barnes 2008 [9]
				8	Current work [165]
				9	Oonishi 2004 [165]
				10	Clarke 2000 [115]
				11	Stewart 2001 [135]
				12	Williams 2007 [163]
12.4	1	Stewart 2001 [135]	12.3	1	Stewart 2001 [135]
	2	Butterfield [166]		2	Butterfield [166]
	3	Stewart 2003 [158]		3	Stewart 2003 [158]
	4	Williams 2007 [163]		4	Williams 2007 [163]
	5	Current work		5	Current work
	6	Williams 2004 [137]		6	Williams 2004 [137]

Table 12.6: *Literature references for comparison graphs*

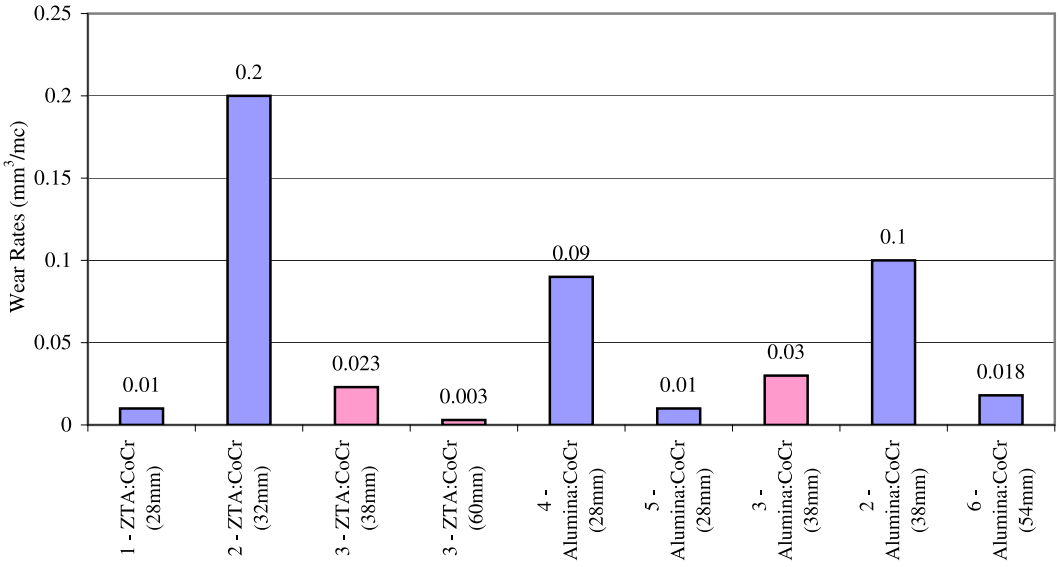

Figure 12.1: *Comparison of wear rates with the literature - Ceramic on metal standard wear conditions (current work in pink).*

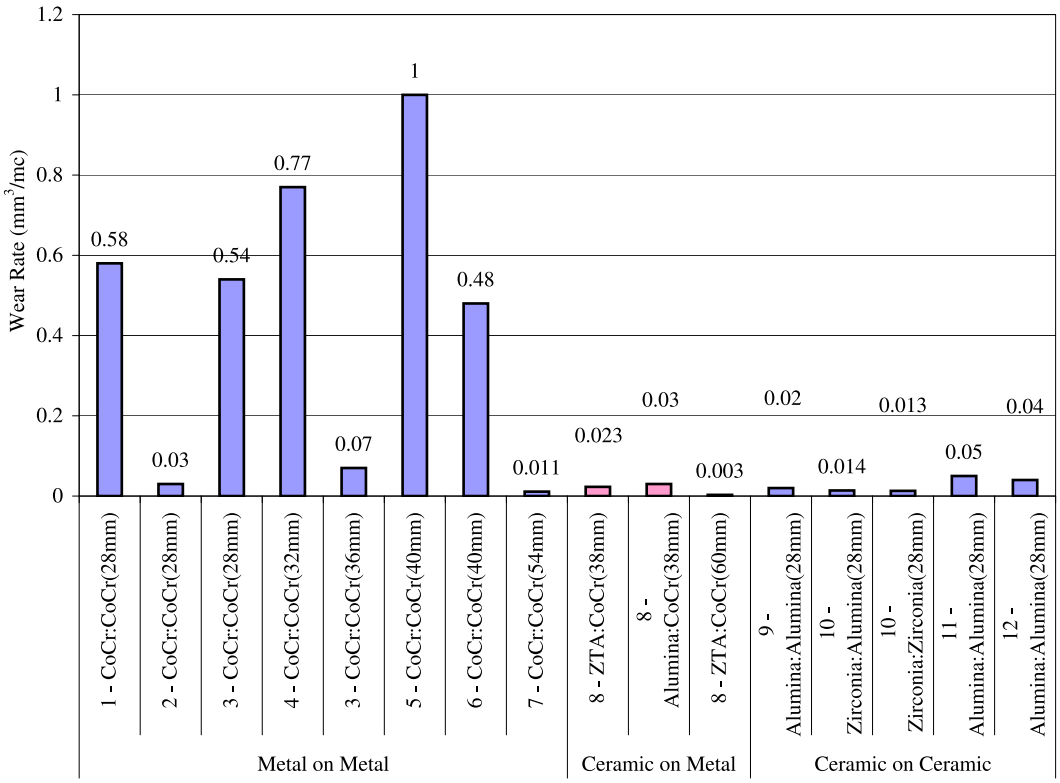

Figure 12.2: *Comparison of wear rates with the literature - Ceramic on metal with metal on metal and ceramic on ceramic under standard wear conditions (current work in pink).*

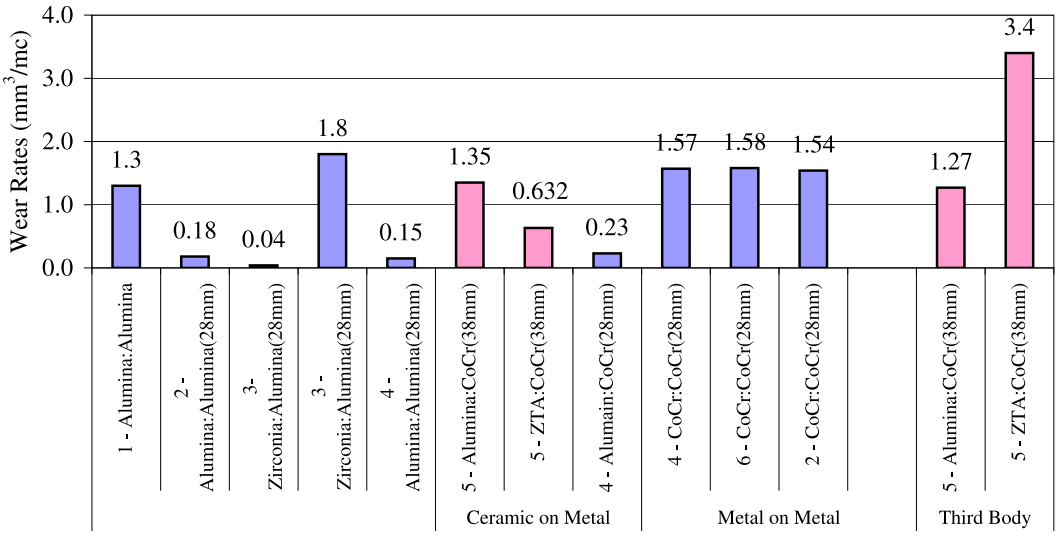

Figure 12.3: *Comparison of wear rates with the literature - Third body wear (current work in pink).*

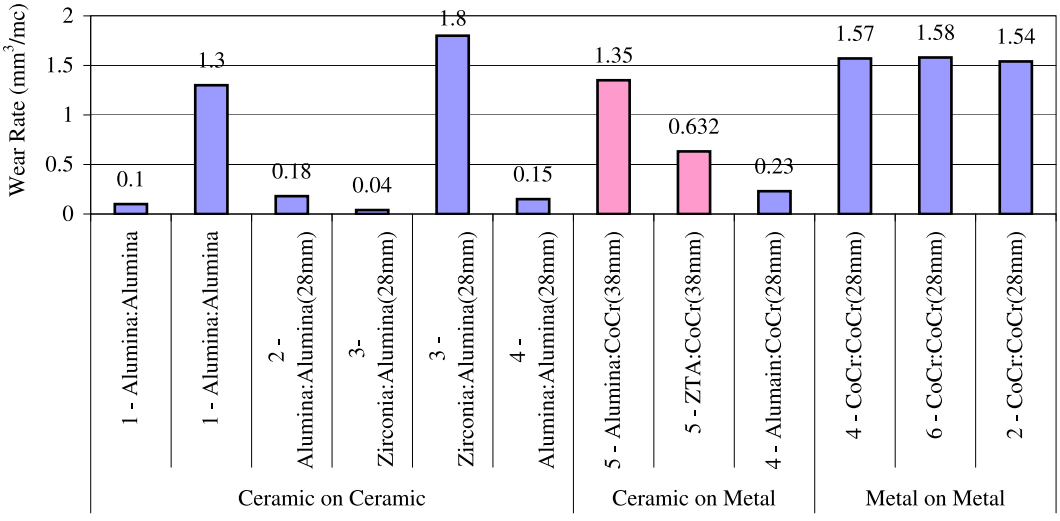

Figure 12.4: *Comparison of wear rates with the literature - Microseparation wear conditions (current work in pink).*

Figure 12.1 shows that the wear rates from other laboratories for ceramic on metal components, produced under standard wear conditions, were similar to those found here. The lowest wear of the all components, was found for the 60 mm cups which may be as a result of the improved lubrication due to the large diameter which theoretically suggests full fluid film lubrication should prevail.

Figure 12.2 compares the results of the ceramic on metal (CoM) tests carried out within this thesis, with the wear rates of metal on metal (MoM) and ceramic on ceramic (CoC) joints in the literature. As would be expected, the wear rates of the CoM combinations were significantly less than MoM combinations in which both the head and cup components wore. The higher wear is likely to be due to a combination of the softer material, the poorer surface roughness value, and the greater possibility of adhesive wear between similar materials. CoC combinations were found to show comparable wear to the CoM combinations. CoC combinations showed low wear due to the more hydrophilic nature of ceramics, the lower surface roughness and the greater hardness which resists wear. However, if the lubricant film was disrupted and wear was to occur, the resultant ceramic particles act to accelerate the wear due to adhesive and abrasive mechanisms which lead to further fractured and removed grains. This hypothesis is supported by the results seen for the third body tests (shown in Figure 12.3), which show an increase in wear for the ceramics head shown by considerable grain removal. Within the CoM combinations the ceramic counterpart is protected by the sacrificial metal cup which wears instead of the ceramic head therefore only minimal ceramic grains are produced.

The results of the microseparation tests, shown in Figure 12.4, were found to be greater than the other published data for a ceramic on metal combination tested under similar wear conditions, however was found to be similar to data published for ceramic on ceramic and slightly less than those found for metal on metal replacements. These results support the hypothesis that having one harder ceramic counterpart reduces the wear compared to fully metal joints, however the brittle nature of fully ceramic combinations may result in high wear due to grain fracture and removal. The wear rates for the current study are for the metal cups alone, as the wear rates for the ceramic heads were undetectable using the gravimetric method.

The addition of alumina particles within the lubricant of the third body tests resulted in a considerable increase in wear rate of the cups for both the alumina and ZTA tests as shown in Figure 12.3. The third body wear of the cups from the alumina test was comparable to that found for microseparation tests, however the ZTA test cups showed considerably more wear, which was supported by the dramatic increase in grain removal on the pole of the ceramic head which was likely to be due removal of the ZrO_2 particles embedded within the alumina matrix. These therefore act as further third body particles, adding to the wear of the metallic cup.

12.13 Limitations of the study

Any experimental study will have limitations and constraints and these are considered here to assist in assessing the relevance of the overall work.

12.13.1 Hip Simulators

Hip simulators are used to simulate, as closely as possible, the conditions present within the body during walking and act as pre-clinical validation of biomaterials used for orthopaedic implants. They also provide a means to test different tribological factors such as surface roughness and radial clearance, under a controlled environment. However experiments are expensive and extremely time consuming as a 5 million cycle test can take 6 months. For this reason simple pin-on-plate or pin-on-disc machines are often used to initially screen material combinations in a time and cost effective manner. A 5 million cycle pin on plate test takes approximately 3 months, and the cost of the components and consumables such as bovine serum are considerably reduced. Pin on plate tests have shown wear factors comparable to clinical results if both translation and rotation motion are included [167].

Several variations of hip simulator exist in different laboratories around the world. These slightly differ from each other in parameters such as the loading pattern, motion, number of stations, cup position, lubricant volume and temperature control. Current simulators include;

- HUT-4 simulator [168] - a 12 station anatomical hip simulator with abduction-adduction and flexion-extension motion of 46° and 12° respectively. A double peak loading cycle between 0.4 kN and 2.0 kN was used.

- Shore western commercial simulator, USA, [169] - a 12 station inverted cup position simulator with the cup located at 23° to the horizontal. The simulator produced biaxial rocking motion of ± 22.5° with a sinusoidal loading profile and a peak magnitude of approximately 2.0 kN at a frequency of 1 Hz.

- ProSim commercial simulator, UK, [170]. - a five or ten station hip joint simulator with two independently controlled axes of rotation and variable axes

of loading. The cups were anatomically mounted at an angle of 35° to the horizontal. Flexion-extension motion was applied through +30° and -15° and internal-external rotation through ±10°. A twin peak loading profile with a maximum of 3 kN and minimum of 0.1 kN [170] was used.

- Durham Mark II, custom-made machine, UK, [144] - which had two axes of rotation and a load vector which oscillated with the angle of swing of the femoral component. The cup was anatomically positioned at 33° to the horizontal. The loading profile was variable but in this application a square wave with a maximum and minimum of 2.5 kN and 0.3 kN respectively was used [144].

The multi-station devices provided greater flexibility and allowed more components to be tested at one time, providing greater confidence in the results. The development of wear simulators indicated that the motions could be varied and physiologically relevant results could still be obtained, providing correct wear vectors and conditions were used. However, there is still much debate over the level of sophistication required to achieve clinically relevant results, such as the use of more complicated systems which include microseparation.

12.13.2 Simulator Development

Early simulators were designed to incorporate the motions and loading found *in vivo*. The joints were subjected to [171]:

- Flexion-extension,
- Abduction-adduction, and
- Pelvic rotation.

In addition three mutually perpendicular loads were applied, namely,

- the vertical load,
- the anterior-posterior axis load, and
- the medial-lateral load.

The articulation and loading patterns were variable in amplitude, shape and frequency and the machines could be set up to simulate the physiological conditions imposed on the hip. However the capital and running costs of such a complicated simulator restricted the number of stations and therefore the significance of the results.

Human gait studies [172] have shown that the loading and rotation occurred simultaneously along three axes. Barbour *et al.* [173]compared the wear path of a physiological three axis of motion to simplified motion using two axis of motion (flexion-extension and internal-external rotation). During the simplified test the motions were set to 180° and 90° out of phase, and the wear patterns investigated. The motion was applied as smooth sinusoidal cycles with flexion-extension applied to the femoral component with amplitudes of +30° and -15° and internal-external rotation applied to the cup through an amplitude of ±10°. The wear pattern on the femoral head was investigated and it was found that the physiological wear pattern differed to the simplified motion only by a 'figure of eight' loop which occurred at the extreme point of flexion. This however, occurred during the low friction low load point in the cycle, and the motion when the friction forces were greatest showed that the simple biaxial wear patterns were similar to physiological conditions [173]. Wear testing results showed that although the physiological simulator, using three axes of load and motion, provided the most accurate conditions, similar wear rates were found from simplified simulators which incorporate one axis of load and two axes of rotation. From this it was concluded that the wear mechanisms would be similar for both motions and therefore to save money and complexity of the simulator a simplified loading and motion pattern could be used.

Further studies using the Durham simulators [25] showed that a square wave loading pattern showed no significant difference in wear rates for ceramic and metal femoral heads against polymer cups compared with a double peak loading profile. However simplification from two axes of rotation to one axis gave unrepresentative wear rates. It was shown that simplified square wave loading with two axes of motion (flexion-extension and internal-external rotation), set 90° out of phase, produced the correct traction vectors and comparable wear rates to more physiologically compli-

cated designed simulators thus providing evidence for the use of the simulator used within this study.

Wear rates are regularly published from different research laboratories around the world, however it can be difficult for direct comparisons to be made between results. Recently 'microseparation' simulators have been developed, where researchers have used a number of different techniques to achieve similar wear patterns to those obtained clinically in ceramic on ceramic replacements particularly. The first 'microseparation' wear simulators were developed at Leeds university and used 'separation springs' to push the cup horizontally relative to the head [174]. The cup was positioned anatomically at 45 ° to the horizontal and a swing phase load of 50 N was implemented. Following this, researchers at Loma Linda University in California [161] developed a 12 station hip simulator set in the anatomical position, with an inclination angle of 50 ° to the horizontal. A physiological loading pattern of 0.2-2 kN was imposed.

The current study achieved microseparation motion through the use of a displacement block, to push the head medio-laterally relative to the cup, and was assembled with a cup inclination angle of 33 ° to the horizontal. The loading cycle was set with a minimum and maximum of 0 N and 2500 N respectively. The results from all three simulators claim to produce wear patterns similar to those found *in vivo* however differences in wear rate were observed. It is likely that the differences in the inclination angle, the loading pattern and the separation mechanisms may have produced different wear scars and wear rates, and therefore a multi-laboratory test may be required to validate the use of different simulators. As discussed in Section 3.7, the original fluoroscopy work by Komistek and Dennis [21–24, 127] was controversial, with a number of researchers questioning the validity of the results and the methods used. It has been suggested that the stripe wear scars on [125] retrieved components could not have developed through normal walking gait, and therefore must have occurred during stair climbing or when the hip was flexed greater that 90°. From the literature it does not appear that a consensus has been reached as to how the stripe wear patterns develop, and therefore the current wear simulators only attempt to simulate the conditions thought to be found *in vivo*. They do however, provide a

more severe impact test allowing differentiation between components which under standard walking conditions show negligible wear. Further fluoroscopy and retrieval analysis may be required before it is established how stripe wear develops in vivo.

12.14 Multi-laboratory testing

In order to establish the differences in wear rates attributed to different wear simulators, a multi-laboratory analysis was carried out using standard wear testing conditions and identical components in various laboratories around the world. The study, reported by Clarke *et al.* [175] investigated PTFE components, which were tested in different simulators using lubricants with varying protein contents. Each laboratory was asked to use their own protocols to test identical 32 mm CoCr heads against PTFE cups. The lubricant protein concentrations ranged from 17-69 mg/ml. The results showed that the protein content had the greatest influence on the wear rate with a general trend for increased wear with increasing protein content, however this was not consistent with some anomalies found. Differences in wear rate were also found for the different types of serum used with alpha calf serum producing significantly lower wear rates than bovine calf serum. The albumin/globulin ratio was also thought to be important. The authors noted that a higher gamma-globulin concentration was often found in patients with infections, tumors and various related problems of the immune system and therefore the ratio of albumin/globulin could be an important factor with higher ratios producing less wear [175]. The serum chamber volume was also found to have a significant effect on the wear rates of PTFE with higher wear found for a higher volume of serum used. The smallest serum volume (35 ml) showed the lowest wear, which was thought to be as a result of a greater amount of protein degradation (due to the greater risk of thermal-degradation) which protected the components from wear. They also noted that it may not be sensible to heat the serum as it could cause protein degradation and in fact the serum should be cooled to reduce these effects [175]. In addition the position of the cup was found to affect the wear rates. Inverted cups produced more consistent results than anatomical cups, and the inverted cups showed a 40%

increase in wear rate. This may also have been as a result of debris falling under gravity into the anatomically positioned cup.

Their conclusions showed that the best conditions for *in vitro* wear testing was a low protein content lubricant, with a chamber volume greater than 200 ml and an inverted cup position. They also concluded that the concentration and nature of the serum proteins were the dominant factors affecting the wear rate, and that although the volume of serum and cup orientation had a significant effect on the wear, they were less important. Factors which increased the temperature such as the motion frequency were also thought to be of significance to the wear rates, and therefore these factors needed to be considered during simulator set-up.

The interesting results of this study indicated that factors other than the wear simulator have a significant effect on the wear rates found and it may be more important to control the temperature and protein content than the mechanics of the wear simulators, so that comparable wear rates are produced. In addition *in vitro* simulators are run continuously, simulating conditions not often found *in vivo*. The thermal impact of running the simulators continuously may result in non clinically relevant results due to thermal degradation of the proteins. It has also been suggested that *in vivo* the components experience many different conditions in addition to normal walking, such as running, jumping, tripping. Although these conditions have been considered by some researchers, it is not common practice for them to be included. However, then the question may be, how many of each condition would you expect an average person, with a hip replacement, to undertake and how do we arrive at a standard 'severe' protocol?

12.14.1 Minimum film thickness calculations

The research paper presented by Hamrock and Dowson [38] in 1978 presented a minimum film thickness equation for contacting surfaces. A simple ball on plate configuration was modelled and the fluids were assumed to be isoviscous and the bearing materials were linear elastic. In addition for hard on hard bearing components, the bearing surfaces were assumed to be semi-infinite. For a hip configuration the ellipticity factor is 1, therefore the equation reduces to:

$$\frac{h_{min}}{R_x} = 2.80\left(U^{0.65}W^{-0.21}\right) \tag{12.1}$$

This form of the equation has been used by many researchers [39][176][177] to estimate theoretically the lubrication regime under which the components were operating. A ratio of the minimum film thickness to the combined roughness provided a parameter, λ, which if greater than 3 suggested the components were working within full fluid film lubrication where the surfaces were separated and asperity contact did not occur. However, the λ value assumes that an accurate prediction of surface roughness can be determined. It has been suggested that protein deposition may adsorb onto the articulating surface during testing and alter the roughness, therefore the real lubrication regimes may be worse than theoretically predicted. For the current work, the combined roughness was an average value of 100 points in the area considered to be the wear patch (10 per head and cup, 5 active stations). It is likely that larger scratches and peaks would be present on the surface, which give local areas of significantly greater roughness than that suggested by the mean value. Therefore even if theoretically λ was ¿3, areas of asperity contact and wear may occur.

The real lubrication mechanism is extremely complex, therefore the simplifications used to calculate theoretical values may not provide accurate predictions of the lubrication regime. The value of λ >3 indicating full fluid film lubrication comes from the rule of thumb that at 3 standard deviations away from the mean, there is a 99% confidence that the asperities will not touch. However contact will still occur for 1% of asperities. In addition, the film thickness equations predict film thicknesses under steady conditions and cannot predict values during stopping and starting, and therefore even if theoretically fluid film lubrication should hold, wear can occur during asperity contact at stopping and starting. The λ ratio provides an indication of the lubrication regime, under ideal conditions, however experimental results are also required to support the hypothesis.

12.14.2 Sample size

Often a major limitation of *in vitro* wear simulators is the small samples size and the fact that the samples are not, strictly, independent measurements. All of the components experience the same loading and motion, and therefore the results of each station are likely to be related. Such small sample sizes often violate assumptions of many statistical analyses and therefore non parametric or exact statistics must be used. Small samples increase the standard error of the means, therefore to achieve statistical significance large effects must be present. Ideally a greater number of samples would be tested and the tests repeated so that a true average wear rate could be determined. However due to cost and time restrictions this is often not possible. Recently a 100 station pin-on-disc machine was developed which allowed different materials and conditions to be tested simultaneously. The standard deviation of wear rates were found to be 4 % of the mean value and therefore this was considered to be a lower value than those produced by other commercial 6-station pin-on-disc devices [178]. However although this is possible for simple screening devices, a 100 station anatomical wear simulator would not be viable.

To generate wear rates, linear regression analysis was used. The results of the current tests often gave wear rates with low r^2 values which indicated that the proportion of data accounted for by the regression equation was low, and in fact a linear trend may not be the most suitable. A greater number of samples may help establish if a linear trend was the best fit for the data, and may improve the confidence in the wear rate.

12.15 Clinical and Scientific Relevance

Orthopaedic implant manufacturers endeavour to design a replacement hip which can last the patient's lifetime and fulfil the needs of the ever younger patients. The economic impacts of requiring a secondary replacement place great strain on the NHS and therefore there is a great demand for a life-long implant. Researchers work to develop implants with better performance, fewer revisions and significant savings in terms of the cost of the component and implantation.

The rationale behind the use of ceramic on metal replacements, as tested within this study, are often quoted as reducing the number of metal ions and particles found within the body whilst reducing the chances of ceramic fracture by introducing a softer metal component. Early concerns regarding ceramic component fracture have been greatly diminished as a result of improved manufacturing techniques and the introduction of composite ceramic materials. Alumina matrix composites such as zirconia toughened alumina (ZTA) have provided low wear rates giving surgeons confidence in using ceramics as implant materials. The suppression of crack tip growth in ZTA components greatly increases the fracture toughness of the material, therefore reducing the number of failures as a result of fracture of the ceramic [179]. Advantages of ceramics such as the low wear, good wettability, low friction and low incidences of osteolysis, are well known and have resulted in ceramics emerging as highly desirable materials for use in hip replacements.

There is limited clinical data to support the use of ceramic on metal hip replacements. An early clinical trial [163] monitoring the metal ion levels of devices showed that although the mean ion levels of COM were similar to COC and COP and lower than MOM bearings, no significant differences were found between components. A large variation in the change in metal ion levels was observed for the COM and MOM bearings which was said to be caused by two outliers. When the outliers were removed, the mean difference in metal ion levels for both COM and MOM bearings were reduced however at a 95% significance level there was no difference between COM and MOM. The outliers were found to have either higher implantation angles or an unusually high degree of anteversion, which may have been the cause of the higher ion levels in those two cases. The relatively short follow-up times (6 months)

and the small numbers of patients (31 patients) mean that further research is required before a conclusion can be made to whether COM bearings reduce the ion levels in patients.

As discussed in Section 3.4.2, recent reports have shown an incidence of pseudotumours or benign masses [15, 17, 107, 109, 110] in some metal on metal devices. The masses are often asymptomatic however they are locally destructive and as a result revision operations are required in a high proportion of patients. Reports show that the outcome of revision surgery following a pseudotumour is poor. The use of the term pseudotumour has become controversial as the mass of cells is not found to have properties found in carcinogenic tumors and therefore the term can be misleading. As a result of this orthopaedic device manufacturers are becoming increasingly concerned as to the use of metal devices.

In August 2010, DePuy, a major orthopaedic implant manufacturer recalled all of their ASR^{TM}XL Acetabular System and DePuy ASR^{TM} Hip Resurfacing Platform products as a result of data which showed that more people than expected who received these implants experienced pain and other symptoms which lead to a revision. Data showed that after 5 years, 12% of people with a resurfacing device and 13% of patients with a total hip replacement needed revision surgery. The results, from the National Joint Registry of England and Wales showed that the risk was greatest in head sizes below 50 mm and among female patients [180]. This recall may have detrimental effects on all metal on metal products for all manufacturers as it casts considerable doubt over the use of metal on metal implants and possibly the use of ceramic on metal replacements. These concerns may lead orthopeadic surgerons to choose alterative bearings such as ceramic on ceramic or ceramic on polyethylene in favour of devices containing metal components. This may therefore impact on the use of ceramic on metal devices, as surgeons may take the view that any increase in metal ions, as a result of a hip replacement, is not acceptable.

The gold standard of hip replacements, a metal head against a polyethylene cup, is often the primary choice of hip replacement for surgeons implanting into older patients. Due to the reduced activity, and possibly shorter residual life span of older patients, the problems of polymer particle induced osteolysis are often outweighed

by the improved mobility and quality of life of elderly patients. To the authors knowledge there are no reports of metal induced tumors or pseudo-tumors from metal on polyethylene devices as the significant wear is found on the polyethylene component and wear of the metal is negligible. Low wearing implants are required for younger, more active patients, therefore it is likely that bearing combinations which do not have the associated problems of osteolysis should be chosen. As a result of this, metal on metal resurfacings are often the choice of implant for younger patients with good bone quality, as they preserve bone mass in case a second replacement is needed. However the recent concerns with metal implants have led to concerns amongst the orthopaedic community that the metal particles and ions produced may be detrimental to health. Alternatively, ceramic on ceramic components have been offered for younger patients due to the reports of low wear and friction. Although concerns with ceramic fracture have deterred some orthopaedic surgeons from using ceramics, they may provide a solution to the problem of metal ions, especially in patients who have shown hypersensitivity to metal.

12.15.1 Future Development

As an alternative to standard UHMWPE, advances in polymer technology have led to the introduction of cross-linked and vitamin E infused cross-linked polyethylene (e-poly or E1). Clinical results of cross-linked ultra high molecular weight polyethylene (XLPE)(Marathon, Depuy, Warsaw, Ind) have shown promising results in patients younger than 50 years old with no radiographic evidence of osteoylsis or revision [181]. E-poly is a cross-linked polyethylene which was introduced to combat the problems with residual free radicals in the polyethylene. Vitamin E is an antioxidant which is diffused into the surface of the UHMWPE, where it reacts with the free radicals, reducing embrittlement. Results have shown that a concentration of vitamin E as low as 0.05% are effective in protecting the UHMWPE from oxidation even under extreme conditions [182] and producing approximately ten times less wear [183]. Biomet claims that E1^{TM} acetabular liners show a 99% reduction in wear compared with clinically proven AcCom liners [184]. With the problems associated with metal particles, highly cross linked and vitamin E infused

polyethylenes articulating against ceramic components, may provide an alternative bearing materials.

The problems of bone loss as a result of stress shielding are likely to cause developments of new materials which more accurately match the elastic modulus of bone in order to prevent bone re-modelling. The high elastic modulus of ceramics can result in significant bone loss around the implant which can lead to loosening of the implant. However, the excellent tribological properties such as the hydrophilic smooth surfaces that can be manufactured, make it a highly desirable surface. As a result of this, materials such as Oxinium [185] have been developed. Oxinium is a niobium alloy of zirconium which encompasses a metallic alloy core with a ceramic surface, incorporating the advantageous properties of both metals and ceramics. The metal core provides excellent fracture toughness whilst the ceramic surface provides low wear and friction. The ceramic surface which can be made micrometers thick, is not a coating, but an enhanced part of the metal substrate, therefore cannot chip off or become damaged. The manufacturers claim that an Oxinium on XLPE provides an advanced bearing system without compromise, reducing the chance of fracture, chipping (compared with coatings) and squeaking [185] which has been reported with some ceramic components. Further advantages may be the reduction in metal allergies as Oxinium has no detectable nickel content and yields a reduced quantity of metal ions. Studies at two years have reported no detectable wear between a 32 mm oxinium head and XLPE [186]. In addition, polymers such as carbon fibre reinforced PEEK have been introduced to match the elastic properties of bone and prevent stress shielding. Early results show relatively low wear when tested *in vitro* [187], which provides an indication that CFR-PEEK may be a suitable material for future use.

Chapter 13

Conclusion

The standard walking cycle wear testing of all ceramic on metal components tested, produced low wear rates, similar to comparable results presented in the literature. The introduction of microseparation wear testing led to an increase in wear for the CoCrMo alloy cups, tested against both the alumina and zirconia toughened alumina. In both the standard and microseparation wear tests, the head wear rates were undetectable using the gravimetric method. Surface analysis including non contacting profilometry, optical microscopy, atomic force microscopy revealed wear of the ceramic components through grain pull out and a decrease in original polishing marks. An area of stripe wear, at approximately 33 ^{o} to the horizontal, was found in both material tests and was thought to be as a result of edge contact between the head and cup. A corresponding flattened lip was found on the rim of the cup which led to an increased wear rate. Third body wear tests saw an increase in wear rate of the CoCrMo alloy cups corresponding to both ceramic materials, however interestingly an increase in wear was also observed for the ZTA head when alumina particles were added to the lubricant. In all cases, low friction factors were found when the components were tested in the Durham Friction simulator with the majority of Stribeck plots showing joints to be operating close to full fluid film lubrication during the stance phase of the walking cycle. Both water based and bovine serum based CMC fluids were used as the lubricant for all tests, which revealed a similar trend to that found for ceramic on ceramic replacements. Water based CMC fluids showed lower friction factors than bovine serum based fluids in all

cases, indicating the lubrication regime for ceramic on metal implants to be close to full fluid film lubrication. A comparison of 38 mm components under all conditions, and different diametral sizes of the same material, are given below.

13.1 38 mm alumina versus zirconia toughened alumina

Under standard wear conditions:

- Running in wear rates of the cups was greater for the alumina test compared with the ZTA test
  (1.04 $\pm$0.293 mm^3/million cycles and 0.634 $\pm$0.737 mm^3/million cycles respectively)
- Alumina and ZTA tests showed similar cup steady state wear rates
  (0.021 $\pm$0.004 mm^3/million cycles and 0.023 $\pm$0.005 mm^3/million cycles respectively).
- Wear rates of the heads was unmeasurable using the gravimetric method.
- Considerable grain pull out was observed on the alumina heads after 5 million cycles, however only very occasional removed grains was observed on the ZTA heads, which showed a similar topography to those of the unworn components.
- Friction tests showed all components to be working close to full fluid film lubrication.

Under the more severe microseparation test:

- Cup running in wear rates were similar for both the alumina and ZTA tests (3.04 $\pm$0.673 mm^3/million cycles and 3.82 $\pm$0.614 mm^3/million cycles respectively)
- The cup steady state wear rate for the alumina test was twice that of the ZTA test (1.35 $\pm$0.154 mm^3/million cycles and 0.623 $\pm$0.252 mm^3/million cycles respectively).

- Grain pull out was observed on both ceramic materials after testing under microseparation conditions, on both the pole and stripe wear region.
- Metal transfer was found at approximately 33^0 to the horizontal thought to be as a result of dislocation of the head
- The flattened lip was formed when the load increased and edge impact occurred.
- The friction of these components was unchanged from the standard tests.

13.2 Third body tests

- Dramatic increases in steady state wear rate for the cups (3.402 $\pm$0.485 mm^3/million cycles and 1.27 $\pm$0.245 mm^3/million cycles for ZTA and Alumina tests respectively).
- An increase in wear rate was also observed for the ZTA heads which showed a wear rate of 0.046 $\pm$0.005 mm^3/million cycles which was over twice that found for the alumina heads (0.019 $\pm$0.027 mm^3/million cycles).
- The metal cups from both tests showed significant wear of the softer matrix material surrounding the carbides with parallel third body or two-body abrasive scratches.
- The ceramic heads revealed considerable grain removal compared with standard testing. The alumina heads showed deep holes with corresponding comet tails indicating an abrasive wear mechanism. In contrast the ZTA heads showed a great proportion of shallow removed grains, with no corresponding abrasive scratches, suggesting a wear mechanism where the particles fall out rather than being adhesively pull out of the surface. It was hypothesised that the holes were left by the zicronia particles which sit within the alumina matrix and are removed during wear with third body particles.
- Friction test results were not considerably different to the results after standard or microsepartion testing.

13.3 38 mm and 60 mm zirconia toughened alumina

Two diameters of ZTA joints were tested under similar standard walking cycle conditions. The results showed:

- The wear of the ceramic heads was negligible for both diameters.
- Grain pull out was observed on the 60 mm joints which was absent on the 38 mm components.
- The cup steady state wear rate was 8 times less for the 60 mm joint (0.003 ± 0.0235 mm^3/million cycles) compared with the 38 mm joints (0.024 ± 0.005 mm^3/million cycles). However, a greater amount of scratching was present on the 60 mm metallic cups seen in the form of pitting, adhesive and abrasive wear.
- Friction testing showed both diameters to be working close to full fluid film lubrication, although the two highest viscosity Sommerfeld numbers of water based CMC fluid friction factors were higher than was expected. The reason for this was not established.

13.4 Future work

The work carried out within this thesis has substantially increased the knowledge in the field of large, ceramic on metal hip replacements, specifically those of large diameter. It has sparked several areas of interest in which work could be continued. This includes:

- Further standard wear simulation on 60 mm joints to confirm or not the low wear rates found during this test. As the tests were the first to be undertaken, further testing would help confirm and support the wear rates found within this thesis.

- Modifications to the microseparation simulator to allow accurate measuring and control of the displacements. This may decrease the variation in wear rates found between stations and allow the true displacements to be monitored. It may also allow different degrees of separation to be monitored to see what effect that has on the wear of the components.

- Particle and ion analysis of the serum used during wear testing. Serum from each test was collected and frozen in the hope that it may be analysed for particle size and morphology. Ion analysis may also be carried out using techniques such as inductively coupled plasma mass spectrometry, to compare with the wear rates found. The technique may eliminate the fluctuations found by the gravimetric method.

- Clinical reports have shown that the cup is occasionally implanted with the incorrect inclination angle, therefore *in vitro* testing with various cup inclination angles would be interesting and may help in understanding clinical wear rates.

- Further third body testing using different sizes and particle morphology may provide results to see if these factors effect the wear rates of both the head and cup.

References

[1] P. J. Firkins, J. L. Tipper, E. Ingham, M. H. Stone, R. Farrar, and J. Fisher. A novel low wearing differential hardness ceramic-on-metal hip joint prosthesis. *Journal of Biomechanics*, 34:1291–1298, 2001.

[2] T. Ishida, I. C. Clarke, T. Sorimachi, H. Shirasu, T. Shishido, and K. Yamamoto. Ceramic-on-metal vs. metal-on-metal bearings in hip simulator studies. In *54th Annual Meeting of the Orthopaedic Research Society*, page Poster 1915, San Francisco, 2008.

[3] S. L. Smith, A. A. J. Goldsmith, and D. Dowson. Lubrication and wear of zirconia-on-metal total hip replacements. *Tribology Series*, 40:377–386, 2002.

[4] C. Brown, S. Williams, J. L. Tipper, J. Fisher, and E. Ingham. Characterisation of wear particles produced by metal on metal and ceramic on metal hip prostheses under standard and microseparation simulation. *Journal of Materials Science-Materials in Medicine*, 18(5):819–827, 2007.

[5] C. Brockett, S. Williams, J. Zhongmin, G. Isaac, and J. Fisher. Friction of total hip replacements. *Journal of Biomedical Materials Research Part B:Applied Biomaterials*, 81B:508–515, 2007.

[6] H. Haider, J. N. Weisenburger, M. G. Maylor, D. W. Schroeder, R. E. Croson, and K. L. Garvin. Bearing diameter, radial clearance and their effect on wear in ceramic-on-metal total hip replacements. In *54th Annual Meeting of the Orthopaedic Research Society*, volume Poster 1792, San Francisco, 2008.

[7] S. Williams, C. Brockett, G. Isaac, and J. Fisher. A comparison of ceramic-on-metal and metal-on-ceramic hip replacements under severe test conditions.

In *54th Meeting of the Orthopeadic Research Society*, volume Poster 1914, San Francisco, 2008.

[8] B. S. Bal, A. Khandkar, R. Lakshminarayanan, I. Clarke, A. A. Hoffman, and M. N. Rahaman. Fabrication and testing of silicon nitride bearings in total hip arthroplasty: Winner of the 2007 "hap" paul award. *The Journal of Arthroplasty*, 24(1):110–116, 2009.

[9] C. L. Barnes, D. DeBoer, R. S. Corpe, S. Nambu, M. Carroll, and I. Timmerman. Wear performance of large-diameter differential-hardness hip bearings. *The Journal of Arthroplasty*, 23(6, Supplement 1):56–60, 2008.

[10] L. D. Dorr, K. R. Hilton, Z. Wan, G. D. Markovich, and R. Bloebaum. Modern metal on metal articulations for total hip replacements. *Clinical Orthopaedics and Related Research*, 333:108–117, 1996.

[11] L. D. Dorr, Z. Wan, and D. B. Longjohn. Total hip arthroplasty with use ofthe metasul metal on metal articulation : Four to severn year results. *The Journal of Bone and Joint Surgery*, 82-A(6):789–798, 2000.

[12] J. Tipper, E. Ingham, Z. Jin, and J. Fisher. (iv) the science of metal-on-metal articulation. *Current Orthopeadics*, 19:280–287, 2005.

[13] J. H. Dumbleton and M. Manley. Metal on metal total hip replacement: What does the literature say. *The Journal of Arthroplasty*, 20(2):174–188, 2005.

[14] J. J. Jacobs, N. J. Hallab, A. K. Skipor, and R. M. Urban. Metal degradation products: a cause for concern in metal-metal bearings. *Clinical Orthopaedics and Related Research*, 417:139–147, 2003.

[15] P. Campbell, A. Shimmin, L. Walter, and M. Solomon. Metal sensitivity as a cause of groin pain in metal-on-metal hip resurfacing. *The Journal of Arthroplasty*, 23(7):1080–1085, 2008.

[16] M. Huber, G. Reinisch, G. Trettenhahn, and K. Zweymuller. Presence of corrosion products and hypersensitivity associated rections in periprosthetic

tissue after asceptic loosening of total hip replacements with bearings surfaces. *Acta Biomaterialia*, 5:172–180, 2009.

[17] H. Pandit, S. Glyn-Jones, P. McLardy-Smith, R. Gundle, D. Whitwell, C. L. M. Gibbons, S. Ostlere, N. Athanasou, H. S. Gill, and D. W. Murray. Pseudotumours associated with metal-on-metal hip resurfacings. *The Journal of Bone and Joint Surgery*, 90-B(7):847–851, 2008.

[18] J. W. Greene, A. L. Malkani, F. R. Kolisek, N. M. Jessup, and D. L. Baker. Ceramic-on-ceramic total hip arthroplasty. *The Journal of Arthroplasty*, 24(6, Supplement 1):15–18, 2009.

[19] L. M. Jazrawi, E. Bogner, C. J. Della Valle, F. S. Chen, K. I. Pak, S. A. Stuchin, V. H. Frankel, and P. E. Di Cesare. Wear rates of ceramic-on-ceramic bearing surfaces in total hip implants: A 12-year follow-up study. *The Journal of Arthroplasty*, 14(7):781–787, 1999.

[20] B.-W. Min, K.-S. Song, C.-H. Kang, K.-C. Bae, Y.-Y. Won, and K.-Y. Lee. Delayed fracture of a ceramic insert with modern ceramic total hip replacement. *The Journal of Arthroplasty*, 22(1):136–139, 2007.

[21] R. Komistek, D. Dennis, J. A. Ochoa, B. D. Haas, and C. Hammill. In vivo comparison of hip separation after metal-on-metal or metal-on-polyethylene total hip arthroplasty. *Journal of Bone and Joint Surgery*, 84-A(10):1836–1841, 2002.

[22] D. Dennis, R. Komistek, O. J., E. Northcut, and C. MHammill. In vivo determination of hip joint separation in subjects having either a metal-on-metal or metal-on-polyethylene tka. In *46th Annual meeting, Orthopaedic Research Society*, volume 25, Orlando, Florida, 2000.

[23] D. Dennis, R. Komistek, E. Northcut, J. Ochoa, and C. Hammill. In vivo determination of hip joint separation in subjects having either a metal-on-metal or metal-on-polyethylene total hip arthroplasty. *47th Annual Meeting Orthopaedic Research Society*, 26, 2001.

[24] D. Dennis, R. Komistek, E. Northcut, J. Ochoa, and A. Ritchie. "in vivo" determination of hip joint separation and the forces generated due to impact loading conditions. *Journal of Biomechanics*, 34:623–629, 2001.

[25] S. L. Smith and A. Unsworth. Simplified motion and loading compared to physiological motion and loading in a hip joint simulator. *ImechE*, 214 - Part H:233–238, 2000.

[26] U. Hansen, S. Masouros, and A. A. Amis. Material properties of biological tissues related to joint surgery. *Current Orthopaedics*, 20(1):16–22, 2006.

[27] B. H. Thomas, J. C. Fryman, K. Liu, and J. Mason. Hydrophilic-hydrophobic hydrogels for cartilage replacement. *Journal of the Mechanical Behaviour of Biomedical Materials*, 2:588–595, 2009.

[28] R. L. Drake, W. Vogl, and A. W. M. Mitchell. *Grays Anatomy for Students*. Churchill Livingstone, UK, 2005.

[29] NHS. Osteoarthritis- nhs choises, your health, your choices. *http://www.nhs.uk/Conditions/Osteoarthritis/Pages/Introduction.aspx*, date accessed: 28th April 2010.

[30] E. Rabinowicz. *Friction and wear of materials*. Wiley-Interscience, 2 edition, 2005.

[31] A. R. Lansdown and A. L. Price. Materials to resist wear : a guide to their selection and use. *Journal of Tribology*, 109(2):379–380, 1987.

[32] B. J. Roberts, A. Unsworth, and N. Mian. Modes of lubrication in human hip joints. *Annals of the Rheumatic Diseases*, 41:217–224, 1982.

[33] S. Scholes and A. Unsworth. Comparison of friction and lubrication of different hip prostheses. *ImechE*, 214-Part H(1):49–57, 2000.

[34] S. C. Scholes, A. Unsworth, R. M. Hall, and R. Scott. The effects of material combination and lubricant on the friction of total hip prostheses. *Wear*, 241(2):209–213, 2000.

[35] V. Saikko, T. Ahlroos, O. Calonius, and J. Keranen. Wear simulation of total hip prostheses with polyethylene against cocr, alumina and diamond-like carbon. *Biomaterials*, 22(12):1507–1514, 2001.

[36] Y. S. Liao, D. McNulty, and M. Hanes. Wear rate and surface morphology of uhmwpe cups are affected by the serum lubricant concentration in a hip simulation test. *Wear*, 255(7-12):1051–1056, 2003.

[37] A. Unsworth, D. Dowson, and V. Wright. The frictional behaviour of human synovial joints - part i natural joints. *Journal of Lubrication Technology - Transactions of the Asme*, 97(3):369–376, 1975.

[38] B. J. Hamrock and D. Dowson. Elastohydrodynamic lubrication of elliptical contacts for materials of low elastic modulus. i- fully flooded conjunction. *Journal of Lubrication Technology*, 100:236–245, 1978.

[39] Z. M. Jin, D. Dowson, and J. Fisher. Analysis of fluid film lubrication in artificial hip joint replacement with surfaes of high elastic modulus. *Proceedings of the I MECH E Part H Journal of Engineering in Medicine*, 211 (H3):247–256, 1997.

[40] M. Jagatia and Z. M. Jin. Elastohydrodynamic lubrication analysis of metal-on-metal hip prostheses under steady state entraining motion. *Proceedings of the Institution of Mechanical Engineers Part H-Journal of Engineering in Medicine*, 215(H6):531–541, 2001.

[41] D. Dowson. Tribological principles in metal-on-metal hip joint design. *Proceedings of the Institution of Mechanical Engineers, Part H: Journal of Engineering in Medicine*, 220(2):161–171, 2006.

[42] M. A. MacConaill. The function of intra-articular fibro cartilgagee, with special reference to the knee and inferior radio-ulnar joints. *Journal of Anatomy*, 66:210–227, 1932.

[43] P. J. Prendergast and T. C. Lee. Walking on water: The biomechan-

ics of michael a. macconaill (1902-1987). *Irish Journal of Medical Science*, 175(3):69–75, 2006.

[44] A. Unsworth, D. Dowson, and V. Wright. Some new evidence on human joint lubrication. *Annals of the Rheumatic Diseases*, 34(4):277–285, 1975.

[45] C. W. McCutchen. The frictional properties of animal joints. *Wear*, 5:1–17, 1962.

[46] T. Little, M. Freeman, and A. Swanson. Experiments on friction in the human hip joint. *Lubrication and Wear in Joints*, page 110, 1969.

[47] L. Dintenfass. Lubrication in synovial joints: A theoretical analysis: A rheological approach to the problems of joint movements and joint lubrication. *The Journal of Bone and Joint Surgery*, 45A:1241–1256, 1963.

[48] P. S. Walker, D. Dowson, M. D. Longfield, and R. J. Wright. "boosted lubrication" in synotival joints by fluid entrapment and enrichment. *Annals of the Rheumatic Diseases*, 27:512, 1968.

[49] C. H. Barnett and A. F. Cobbold. Lubrication within living joints. *Journal of Bone and Joint Surgery*, 44B(3):662–674, 1962.

[50] F. C. Linn and E. L. Radin. Lubrication of animal joints. iii. the effect of certain chemical alterations of the cartilage and lubricant. *Arthtitis and Rheumatism*, 11(5):674–682, 1968.

[51] E. L. Radin and I. L. Paul. A consolidated concept of joint lubrication. *The Journal of Bone and Joint Surgery*, 54A(3):607–616, 1972.

[52] J. F. Archard. Contact and rubbing of flat surfaces. *Journal of Applied Physics*, 24:981–988, 1953.

[53] K. Miyoshi. Fundamental considerations in adhesion, friction and wear for ceramic – metal contacts. *Wear*, 141(1):35–44, 1990.

[54] G. W. Stachowiak and A. W. Batchelor. *Engineering Tribology (third edition)*. Elsevier Butterworth-Heinemann, Oxford, 2005.

[55] I. M. Hutchings. *Tribology :friction and wear of engineering materials.* Metallurgy and materials science series. Edward Arnold, london, 1992.

[56] B. Bhushan. *Modern Tribology Handbook*, volume v. 1. Principles of tribology of *Mechanics and Materials Science Series.* CRC Press, London, 2001.

[57] J. A. Williams. *Engineering Tribology.* Oxford University Press, Oxford, 1994.

[58] J. Black. *Orthopeadic Biomaterials in Research and Practise.* Churchill Livingstone Inc., New York, 1988.

[59] B. D. Ratner, A. S. Hoffman, F. J. Schoen, and J. E. Lemons. *Biomaterials Science - An Introduction to Materials in Medicine.* Academic Press, San Diego, 1996.

[60] J. J. Jacobs, J. L. Gilbert, and R. M. Urban. Current concepts review: Corroion of metal orthopeadic implants. *The Journal of Bone and Joint Surgery*, 80-A(2):268–282, 1998.

[61] Swedish Hip Arthroplasty Register. The swedish hip arthroplasty register annual report 2006. *http://www.jru.orthop.gu.se/*, date accessed: 23rd September 2010.

[62] National Joints Register. Njr stats online. *http://www.njr.org.uk*, date accessed: 15th May 2010.

[63] Census 2001. Key statistics in health areas in england and wales. *http://www.statistics.gov.uk/downloads/census2001/KS_health_part_1_revisedDec03.pdf*, date accessed: 28th April 2010.

[64] A. Unsworth. Recent developments in the tribology of artificial joints. *Tribology International*, 28(7):485–495, 1995.

[65] J. Charnley. Arthroplasty of the hip - a new operation. *The lancet*, pages 1129–1132, 1961.

[66] J. Charnley. An artificial bearing in the hip joint: implications in biological lubrication. *Federation proceedings*, 25(3):1079–1081, 1966.

[67] J. Charnley, A. Kamangar, and M. D. Longfield. The optimum size of prosthetic heads in relation to the wear of plastic sockets in total replacement of the hip. *Med. and Biol. Engng*, 7:31–39, 1969.

[68] J. Charnley. The long term results of low-friction arthroplasty of the hip as a primary intervention. *Journal of Bone and Joint Surgery*, 54B:61–76, 1972.

[69] J. Charnley and Z. Cupic. The nine and ten year results of the low-friction arthroplasty of the hip. *Clinical Orthopaedics and Related Research*, 95:9–25, 1973.

[70] M. M. Mullins, W. Norbury, J. K. Dowell, and M. Heywood-waddington. Thirty-year results of a prospective study of charnley total hip arthroplasty by the posterior approach. *The Journal of Arthroplasty*, 22(6):833–839, 2007.

[71] P. S. Walker and B. L. Gold. The tribology (friction, lubrication and wear) of all-metal artificial hip joints. *Wear*, 17(4):285–299, 1971.

[72] F. Higuchi, A. Inoue, and M. Smelitsch. Metal-on-metal cocrmo mckee-farrar total hip arthroplasty: Charateristics from a long-term follow-up study. *Arch Orthop Trauma Surg*, 116:121–124, 1997.

[73] M. T. Clarke, C. Darrah, T. D. Stewart, E. Ingham, J. Fisher, and J. F. Nolan. Long-term clinical, radiological and histopathpological follow-up of a well-fixed mckee-farrar metal-on-metal total hip arthroplasty. *The Journal of Arthroplasty*, 20(4):542–546, 2005.

[74] F. P. Patterson and C. S. Brown. The mckee-farrar total hip replacement: Preliminary results and complications of 368 operations performed in five general hospitals. *The Journal of Bone and Joint Surgery*, 54-A(2):257–275, 1972.

[75] R. Poss, G. W. Brick, R. J. Wright, D. W. Roberts, and C. B. Sledge. The effects of modern cementing techniques on the longevity of total hip arthroplasty. *Orthopedic Clinics of North America*, 19(3):591–598, 1988.

[76] S. C. Scholes. The tribology of hard bearing surfaces for use in hip protheses. *Durham University*, Ph.D., 1999.

[77] B. M. Wroblewski. Wear of the high-density polyethylene socke in total hip arthroplasty and its role in endosteal cavitation. *Proceedings of the Institution of Mechanical Engineers Part H-Journal of Engineering in Medicine*, 211:109–118, 1997.

[78] W. H. Harris. Osteolysis and particle disease in hip replacement - a review. *Acta Orthopaedica Scandinavica*, 65(1):113–123, 1994.

[79] E. A. Balazs. *Disorders of the knee*. The physical properties of synovial fluid and the special role of hyaluronic acid. T.B. Lippincott Company, Philadelphia, 1974.

[80] H. Fam, J. T. Bryant, and M. Kontopoulou. Rheological properties of synovial fluids. *Biorheology*, 44:59–74, 2007.

[81] H.-W. Fang, M.-L. Shih, J.-H. Zhao, H.-T. Huang, H.-Y. Lin, H.-L. Liu, C.-H. Chang, C.-B. Yang, and H.-C. Liu. Association of polyethylene friction and thermal unfolding of interfacial albumin molecules. *Applied Surface Science*, 253:6896–6904, 2007.

[82] R. J. A. Bigsby, D. D. Auger, Z. M. Jin, D. Dowson, C. S. Hardaker, and J. Fisher. A comparative tribological study of the wear of composite cushion cups in a physiological hip joint simulator. *Journal of Biomechanics*, 31(4):363–369, 1998.

[83] A. A. J. Goldsmith, D. Dowson, G. H. Isaac, and J. G. Lancaster. A comparative joint simulator study of the wear of metal-on-metal and alternative material comvinations in hip replacements. *Proceedings of the I MECH E*, 214-Part H:39–47, 2000.

[84] S. Affatato, G. Bersaglia, M. Rocchi, P. Taddei, C. Fagnano, and A. Toni. Wear behaviour of cross-linked polyethylene assessed in vitro under severe conditions. *Biomaterials*, 26(16):3259–3267, 2005.

[85] D. Dowson, C. Hardaker, M. Flett, and G. H. Isaac. A hip joint simulator study

of the performance of metal-on-metal joints: Part i: The role of materials. *The Journal of Arthroplasty*, 19(8, Supplement 1):118–123, 2004.

[86] S. Affatato, C. Mazzega-Fabbro, V. Sergo, and M. Viceconti. Is ceramic-on-ceramic squeaking phenomenon reprodicible in vitro? a long-term sinulator study under severe conditions. *Journal of Biomedical Materials Research Part B:Applied Biomaterials*, 91B:264–271, 2009.

[87] S. Williams, D. Jalali-Vahid, C. Brockett, Z. Jin, M. H. Stone, E. Ingham, and J. Fisher. Effect of swing phase load on metal-on-metal hip lubrication, friction and wear. *Journal of Biomechanics*, 39(12):2274–2281, 2006.

[88] Y. S. Liao, P. D. Benya, and H. A. McKellop. Effect of protein lubrication on the wear properties of materials for prosthetic joints. *Journal of Biomedical Materials Research (Applied Biomaterials)*, 48:465–473, 1999.

[89] N. E. Bishop, F. Waldow, and M. M. Morlock. Friction moments of large metal on metal hip joint bearings and other modern designs. *Medical Engineering & Physics*, 30(8):1057–1064, 2008.

[90] International Standard ISO 14242-2. Implants for surgery-wear of total hip-joint prostheses. part 2: Methods of measurement. 2000.

[91] A. Wang, A. Essner, C. Stark, and J. H. Dumbleton. Comparison of the size and morphology of uhmwpe wear debris produced by a hip joint simulator under serum and water lubricated conditions. *Biomaterials*, 17(9):865–871, 1996.

[92] J. Bell, J. Tipper, E. Ingham, M. Stone, and J. Fisher. The influence of phosphlipid concentration in protein-containing lubricants on the wear of ultra-high molecular weight polyethylene in artificial hip joints. *Proceedings of the Institution of Mechanical Engineers Part H-Journal of Engineering in Medicine*, 215:259–263, 2001.

[93] S. Scholes and A. Unsworth. The effects of proteins on the friction and lubri-

cation of artificial joints. *Proceedings of the I MECH E*, 220-Part H:687–693, 2006.

[94] Z. Lu and H. A. McKellop. Frictional heating of bearing materials tested in a hip joint wear simulator. *Proceedings of the I MECH E*, Part H(211):101–108, 1997.

[95] N. Shaklai, R. L. Garlick, and H. F. Bunn. Nonenzymaic glycosylation of human serum albumin alters its conformation and function. *The Journal of Biolofical Chemistry*, 259(6):3812–3817, 1984.

[96] M. P. Heuberger, M. R. Widmer, E. Zobeley, R. Glockshuber, and N. D. Spencer. Protein-mediated boundary lubrication in arthroplasty. *Biomaterials*, 26(10):1165–1173, 2005.

[97] A. P. Serro, M. P. Gispert, M. C. L. Martins, P. Brogurira, R. Colaco, and B. Saramago. Adsorption of albumin on prosthetic materials:implication for tribological behaviour. *Journal of Biomedical Materials Research*, 78A:581–589, 2006.

[98] M. P. Gispert, A. P. Serro, R. Colaco, and B. Saramago. Friction and wear mechanisms in hip prosthesis: Comparison of joint materials behaviour in several lubricants. *Wear*, 260:149–158, 2006.

[99] H. Mishina and M. Kojima. Changes in human serum albumin on arthroplasty frictional surfaces. *Wear*, 265(5-6):655–663, 2008.

[100] C.-B. Yang, H.-W. Fang, H.-L. Liu, C.-H. Chang, M.-C. Hsieh, W.-M. Lee, and H.-T. Huang. Frictional characteristics of the tribological unfolding albumin for polyethylene and cartilage. *Chemical Physics Letters*, 431(4-6):380–384, 2006.

[101] M. Roba, M. Naka, E. Gautier, N. D. Spencer, and R. Crockett. The adsorption and lubrication behaviour of synovial fluid proteins and glycoproteins on the bearing-surface materials of hip replacements. *Biomaterials*, 30:2072–2078, 2009.

[102] K. A. De Smet, C. Pattyn, and R. Verdonk. Early results of primary birmingham hip resurfaceing using a hybride metal on metal couple. *Hip International*, 12(2):158–162, 2002.

[103] D. Dowson, C. Hardaker, M. Flett, and G. Isaac. A hip joint simulator study of the performance of metal on metal joints, part ii:design. *The Journal of Arthroplasty*, 19(8 Suppl. 3):124–130, 2004.

[104] M. A. L. Hernandez-Rodriguez, R. D. Mercado-Solis, A. J. Perez-Unzueta, D. I. Martinez-Delgado, and M. Cantu-Sifuentes. Wear of cast metal-metal pairs for total replacement hip prostheses. *Wear*, 259(7-12):958–963, 2005.

[105] S. C. Scholes, S. M. Green, and A. Unsworth. The wear of metal on metal total hip prostheses measured in a hip simulator. *Proceedings of the I MECH E Part H Journal of Engineering in Medicine*, 215:523–530, 2001.

[106] K. R. St. John, L. D. Zardiackas, and R. A. Poggie. Wear evaluation of cobalt chromium alloy for use in a metal-on-metal hip prosthesis. *Journal of Biomaterials Research Part B: Applied Biomaterials*, 68B:1–14, 2004.

[107] A. P. Davies, H. G. Willert, P. A. Campbell, I. D. Learmonth, and C. P. Case. An unusual lymphocytic perivascular infiltration in tissues around contemporary metal-on-metal joint replacements. *The Journal of Bone and Joint Surgery*, 87-A(1):18–27, 2005.

[108] R. M. Urban, J. J. Jacobs, M. J. Tomlinson, J. Gavrilovic, J. Black, and M. Peoc'h. Dissemination of wear particles to the liver, spleen, and abdominal lymph nodes of patients with hip or knee replacement. *The Journal of Bone and Joint Surgery*, 82-A(4):457–, 2000.

[109] G. Grammatopolous, H. Pandit, Y.-M. Kwon, R. Gundle, P. McLardy-Smith, D. J. Beard, D. W. Murray, and H. S. Gill. Hip resurfacings revised for inflammatory pseudotumour have a poor outcome. *Journal of Bone and Joint Surgery*, 91-B:1019–1024, 2009.

[110] D. R. Boardman, F. R. Middleton, and T. G. Kavanagh. A benign psoas mass following metal-on-metal resurfacing of the hip. *The Journal of Bone and Joint Surgery*, 88-B(3):402–404, 2006.

[111] H. G. Willert, G. H. Buchhorn, A. Fayyazi, and C. Lohnmann. Vascular changtes and lymphocyte aggregations in aseptic loosening of all-metal hip joint replacements. In *Sixth World Biomaterials Congress*, Kamuela, HI, 2000.

[112] M. Boehler, K. Knahr, H. Plenk, A. Walter, M. Salzer, and V. Schreiber. Long-term results of uncemented alumina acetabular implants. *Journal of Bone and Joint Surgery*, 76-B(1):53–59, 1994.

[113] J. E. Nevelos, E. Ingham, C. Doyle, J. Fisher, and A. B. Nevelos. Analysis of retrieved alumina ceramic components from mittelmeier total hip prosthesis. *Biomaterials*, 20:1833–1840, 1999.

[114] P. Bizot and L. Sedel. Alumina bearings in hip replacement: Theoretical and practical aspects. *Operative Techniques in Orthopeadics*, 11(4):263–269, 2001.

[115] I. C. Clarke, V. Good, P. Williams, D. Schroeder, L. Asnissian, A. Stark, H. Oonishi, J. Schuldies, and G. Gustafson. Ultra-low wear rates for rigid-on-rigid bearings in total hip replacements. *ImechE*, 214 - Part H:331–347, 2000.

[116] S. L. Smith and A. Unsworth. An in vivo wear study of alumina-alumina total hip prostheses. *ImechE*, 215 - Part H(5):443–446, 2001.

[117] A. Essner, K. Sutton, and A. Wang. Hip simulator wear comparison of metal-on-metal, ceramic-on-ceramic and crosslinked uhmwpe bearings. *Wear*, 259:992–995, 2005.

[118] T. Shishido, K. Yamamoto, I. C. Clarke, T. Masaoka, M. Manaka, and T. Tateiwa. Comparison of the results of a simulator study and retrieval implants in ceramic tha. *Key Engineering Materials*, 309-311:1277–1280, 2006.

[119] C. G. Figueiredo-Pina, Y. Yan, A. Neville, and J. Fisher. Understanding the differences between the wear of metal on metal and ceramic on metal total hip replacements. *ImechE*, 222 Part H:285–296, 2008.

[120] Y. Yan, A. Neville, D. Dowson, S. Williams, and J. Fisher. Tribo-corrosion analysis of wear and metal ion release interactions from metal-on-metal and ceramic-on-metal contacts for the application in artificial hip prostheses. *ImechE*, 222-Part J(Special Issue Paper):483–492, 2008.

[121] A. Unsworth. Tribology of artificial hip joints. *Proceedings of the I MECH E*, Part J 220(8):711–718, 2006.

[122] F. Hinrichs and P. Griss. Retrieved wear couple ceramic-on-metal: Case study. In *Proceedings 6th International Biolox Symposium*, George Thieme Verlag, Stuttgart, 2001.

[123] J. R. Valenti, J. D. Rio, and S. Ammillo. Catastrophic wear in a metal-on-ceramic total hip arthroplasty. *The Journal of Arthroplasty*, 22(6):920–922, 2007.

[124] T. Yamamoto, M. Saito, M. Ueno, T. Hananouchi, Y. Tokugawa, and K. Yonenobu. Wear analysis of retrieved ceramic-on-ceramic articulations in total hip arthroplasty: Femoral head makes contact with the rim of the socket outside of the bearing surface. *Journal of Biomaterials Research Part B: Applied Biomaterials*, 73B:301–307, 2005.

[125] W. L. Walter, G. M. Insley, W. K. Walter, and M. A. Tuke. Edge loading in third generation alumina ceramic-on-ceramic bearings - stripe wear. *The Journal of Arthroplasty*, 19(4):402–413, 2004.

[126] M. Manaka, I. C. Clarke, K. Yamamoto, T. Shishido, A. Gustafson, and A. Imakiire. Stripe wear rates in alumina thr - comparison of microseparation simulator study with retrieved implants. *Journal of Biomaterials Research Part B: Applied Biomaterials*, 69B:149–157, 2004.

[127] D. Dennis, R. Komistek, J. Ochoa, E. Northcut, and C. Hammill. In vivo determination of femoral head loci pathways during gait in subjects having a metal on metal or metal on polyethylene tha. In *47th Annual Meeting Orthopaedic Research Society*, volume 0168, San Francisco, California, 2001.

[128] A. V. Lombardi, T. H. Mallory, D. A. Dennis, R. D. Komistek, R. A. Fada, and E. J. Northcut. An in vivo determination of total hip arthroplasty pistoning during activity. *The Journal of Arthroplasty*, 15(6):702–709, 2000.

[129] R. W. Mann. Letter to the editor. *The Journal of Arthroplasty*, 16(8):1084–1085, 2001.

[130] B. Derbyshire, M. L. Porter, D. Howard, L. Kenney, and C. Nester. Letter to the editor. *The Journal of Arthroplasty*, 16(8):1085–1086, 2001.

[131] J. Fisher. Letter to the editor - reply. *The Journal of Arthroplasty*, 16(8):1086–1087, 2001.

[132] R. D. Komistek. Letter to the editor- reply. *The Journal of Arthroplasty*, 16(8):1087–1091, 2001.

[133] W. A. Hodge, R. S. Fijan, K. L. Carlson, R. G. Burgess, W. H. Harris, and R. W. Mann. Contact pressures in the human hip joint measured in vivo. *Proc Natl Acad Sci USA*, 83(9):2879–2883, 1986.

[134] J. Nevelos, E. Ingham, C. Doyle, R. Streicher, A. Nevelos, W. Walter, and J. Fisher. Microseparation of the centers of alumina-alumina artificial hip joints during simulator testing produces clinically relevant wear rates and patterns. *The Journal of Arthroplasty*, 15(6):793–795, 2000.

[135] T. D. Stewart, J. Tipper, R. Streicher, E. Ingham, and J. Fisher. Long-term wear of hiped alumina on alumina bearings for thr under microseparation conditions. *Journal of Materials Science: Materials in Medcine*, 12:1053–1056, 2001.

[136] M. Akagi, T. Nonaka, F. Nishisaka, S. Mori, K. Fukuda, and C. Hamanishi. Late dissociation of an alumina-on-alumina bearing modular acetabular component. *The Journal of Arthroplasty*, 19(5):647–651, 2004.

[137] S. Williams, T. D. Stewart, E. Ingham, M. H. Stone, and J. Fisher. Metal-on-metal bearing wear with different swing phase loads. *Journal of Materials Research Part B: Applied Biomaterials*, 70B:233–239, 2004.

[138] S. Williams, M. Butterfield, T. D. Stewart, E. Ingham, M. Stone, and J. Fisher. Wear and deformation of ceramic-on-polyethylene total hip replacements with joint laxity and swing phase microseparation. *ImechE*, 217-Part H:147–153, 2003.

[139] K. Kubo, I. C. Clarke, T. Sorimachi, P. A. Williams, T. K. Donaldson, and K. Yamamoto. Aggressive 3rd-body wear challenge to highly crosslinked polyethylene: A hip simulator model. *Wear*, 267:734–742, 2009.

[140] C. R. Bragdon, M. Jasty, O. K. Muratoglu, and W. H. Harris. Third-body wear testing of a highly cross-linked acetabular liner: The effect of large femoral head size in the presence of particulate poly(methyl-methacrylate) debris. *The Journal of Arthroplasty*, 20(3):379–385, 2005.

[141] A. Wang and A. Essner. Three-body wear of uhmwpe acetabular cups by pmma particles against cocr, alumina and zirconia heads in a hip joint simulator. *Wear*, 250(1-12):212–216, 2001.

[142] L. Que and L. D. Timmie Topoleski. Third-body wear of cobalt-chromium-molybdenum implant alloys initiated by bone and poly(methyl methacrylate) particles. *Journal of Biomaterials Research Part A*, 50:322–330, 2000.

[143] K. D. Mimnaugh, J. Q. Yao, M. P. Laurent, R. Crowninshield, J. J. Mason, and C. Blanchard. The effect of entrapped bone particles on the surface morphology and wear of polyethylene. *The Journal of Arthroplasty*, 24(2):303–309, 2009.

[144] S. L. Smith and A. Unsworth. A five-station hip joint simulator. *ImechE*, 215-Part H:61–64, 2001.

[145] J. O'Kelly, A. Unsworth, D. Dowson, B. Jobbins, and V. Wright. Pendulum and simulator studies of friction in hip joints. In *The Biological Engineering Society*, volume Evaluation of Artificial Joints, pages 19–29, London, 1977.

[146] J. O'Kelly, A. Unsworth, D. Dowson, A. Hall, and V. Wright. A study of the role of synovial fluid and its constituents in the friction and lubrication of human hip joints. *ImechE - Engineering in Medicine*, 7(2), 1978.

[147] A. Unsworth, M. J. Pearcy, E. F. T. White, and G. White. Frictional properties of artificial hip joints. *Engineering in Medicine*, 17(3), 1988.

[148] A. Unsworth. The effect of lubrication in hip joint prostheses. *Phys. Med. Biol.*, 23(2):253–268, 1978.

[149] A. Unsworth, M. J. Pearcy, E. F. T. White, and G. White. Soft layer lubrication of artificial hip joints. *Proceedings of the Institution of Mechanical Engineers Part H-Journal of Engineering in Medicine*, pages 715–724, 1987.

[150] P. E. Sinnett-Jones, J. A. Wharton, and W. R.J.K. Micro-abrasion-corrosion of a cocrmo alloy in simulated artificial hip joint environments. *Wear*, 259:898–909, 2005.

[151] C. Valero Vidal and A. Igual Munoz. Effect of thermal treatment and applied potential on the electrochemical behaviour of cocrmo biomedical alloy. *Electrochimica Acta*, 54(6):1798–1809, 2009.

[152] C. Morillo, Y. Sawae, and T. Murakami. Effect of bovine serum constituents on the surface of the tribological pair alumina/alumina nanocomposites for total hip replacement. *Tribology International*, 43(5-6):1158–1162, 2010.

[153] D. Casellas, M. M. Nagl, L. Llanes, and M. Anglada. Fracture toughness of alumina and zta ceramics: microstructural coarsening effects. *Journal of Materials Processing Technology*, 143-144:148–152, 2003.

[154] International Standard ISO14242-1. Implant for surgery-wear of total hip-joint prostheses- part 1: Loading and displacement parameters for wear-testing machines and corresponding environmental conditions for test. (First edition 2002-03-01), 2002.

[155] K. Vassiliou. Tribological studies of modern orthopeadic biomaterial combinations. *University of Durham*, PhD, 2005.

[156] Y.-S. Liao. Comparison of metal ion release in the serum lubricants from multiple hip simulation studies using bearings of metal-on-metal, metal-on-poly and ceramic-on-metal. In *8th World Biomaterials Congress*, Amsterdam RAI, The Netherlands, 2008.

[157] B. J. Hamrock and D. Dowson. Isothermal elastohydrodynamic lubrication of point contacts: Part iii- fully flooded results. *Transaction of the ASME. J. Lubric. Technology*, 100:236–245, 1977.

[158] T. D. Stewart, J. L. Tipper, G. M. Insley, R. M. Streicher, E. Ingham, and J. Fisher. Severe wear and fracture of zirconia heads against alumina inserts in hip simulator studies with microseparation. *The Journal of Arthroplasty*, 18(6):726–734, 2003.

[159] M. M. Mak, A. A. Besong, Z. M. Jin, and J. Fisher. Effect of microseparation on contact mechanics in ceramic-on-ceramic hip joint replacements. *ImechE*, 216-Part H:403–408, 2002.

[160] G. M. Insley, T. D. Stewart, J. E. Nevelos, J. Fisher, and R. M. Streicher. *Wear of ceramic-on-ceramic hip prostheses under microseparation simulation conditions*. Friction, Lubrication and Wear of Artificial Joints. Professional Engineering Publishing, Suffolk, 2002.

[161] I. C. Clarke, D. D. Green, P. A. Williams, K. Kubo, G. Pezzotti, A. Lombardi, A. Turnbull, and T. K. Donaldson. Hip-simulator wear studies of an alumina-matrix composite (amc) ceramic compared to retrieval studies of amc balls with 1-7 years follow-up. *Wear*, 267:702–709, 2009.

[162] S. L. Smith, D. Dowson, and A. A. J. Goldsmith. The effect of femoral head diameter upon lubrication and wear of metal-on-metal total hip replacements. *ImechE*, 215(2):161–170, 2001.

[163] S. Williams, A. Schepers, G. Isaac, C. Hardaker, E. Ingham, D. Van Der Jagt, A. Breckon, and J. Fisher. Ceramic-on-metal hip arthroplasties; a comparative in vitro and in vivo study. *Clinical Orthopaedics and Related Research; The 2007 Otto Aufranc Award*, 465:23–32, 2007.

[164] J. G. Bowsher, J. Nevelos, J. Pickard, and J. C. Shelton. Do heat treatments influence the wear of large diameter metal-on-metal hip joints. an in vitro study under normal and adverse gait conditions. In *49th Annual Meeting of the Orthopeadic Research Society*, page Poster 1398, New Orleans, Louisiana, 2003.

[165] H. Oonishi, I. C. Clarke, V. Good, H. Amino, and M. Ueno. Alumina hip joints characterised by run-in wear and steady state wear to 14 million cycles in hip-simulator model. *Journal of Biomedical Materials Research*, 70A:523–532, 2004.

[166] M. Butterfield, T. D. Stewart, S. Williams, E. Ingham, M. Stone, and J. Fisher. Wear of metal-metal and ceramic-ceramic hip prosthesis with swing phase microseparation. In *48th Annual Meeting of the Orthopeadic Research Society*, page Poster 0128, Dalas, 2002.

[167] S. Scholes. Pin on plate studies on the effect of rotation on the wear of metal on metal samples. *Journal of Material Science:Materials in Medicine*, 12:299–303, 2001.

[168] V. Saikko. A 12-station anatomic hip joint simulator. *Proc Instn Mech Engers*, Part H(219):437–448, 2005.

[169] S. Affatato, M. Testoni, G. L. Cacciari, and A. Toni. Mixed oxides prosthetic ceramic ball heads. part 1: effect of the zro2 fraction on the wear of ceramic on polyethylene joints. *Biomaterials*, 20(10):971–975, 1999.

[170] P. S. M. Barbour, M. H. Stone, and J. Fisher. A hip joint sinulator study using new and physiologically scratches femoral heads with ultra-high molecular weight polyethylene acetabular cups. *Proc Instn Mech Engers*, Part H(214):569–576, 2000.

[171] D. Dowson and B. Jobbins. Design and development of a versatile hip joint simulator and preliminary assessment of wear and creep in charnley total replacement hip joints. *Engineering in Medicine*, 17(3):111–117, 1988.

[172] J. P. Paul. Forces transmitted by joints in the human body. *ImechE*, 181:8–15, 1967.

[173] P. S. M. Barbour, M. H. Stone, and J. Fisher. A hip joint simulator study using simplified loading and motion cycles generating physiological wear paths and rates. *ImechE*, 213(Part H):455–467, 1999.

[174] T. D. Stewart, J. L. Tipper, G. M. Insley, R. M. Streicher, E. Ingham, and J. Fisher. Long-term wear of ceramic matrix composite materials for hip prostheses under severe swing phase microseparation. *Journal of Biomedical Materials Research Part B:Applied Biomaterials*, 66B:567–573, 2003.

[175] I. C. Clarke, F. W. Chan, A. Essner, V. Good, C. Kaddick, R. Lappalainen, M. Laurent, H. Mckellop, W. McGarry, D. Schroeder, M. Selenius, M. C. Shen, M. Ueno, A. Wang, and J. Yao. Multi-laboratory simulator studies on effects of serum proteins on ptfe cup wear. *Wear*, 250:188–198, 2001.

[176] Z. M. Jin, M. Stone, E. Ingham, and J. Fisher. (v) biotribology. *Current Orthopaedics*, 20(1):32–40, 2006.

[177] L. Mattei, F. Di Puccio, B. Piccigallo, and E. Ciulli. Lubrication and wear modelling of artificial hip joints: A review. *Tribology International*, In Press, Corrected Proof.

[178] V. Saikko. Performance analysis of an orthopaedic biomaterial 100-station wear test system. *Proc Instn Mech Engers*, Part C(224):697–701, 2010.

[179] A. H. De Aza, J. Chevalier, G. Fantozzi, M. Schehl, and R. Torrecillas. Crack growth resistance of alumina, zirconia and zirconia toughened alumina ceramics for joint prostheses. *Biomaterials*, 23(3):937–945, 2002.

[180] Depuy Inc. Asr hip system recall health care professional information. *http://www.depuy.com/corporate-information/depuy-divisions/depuy-orthopaedics-inc/surgeonasr*, date accessed: 19th September 2010.

[181] Y.-H. Kim, Y. Choi, and J.-S. Kim. Cementless total hip arthroplasty with alumina-on-highly cross-linked polyethylene bearing in young patients with femoral head osteonecrosis. *The Journal of Arthroplasty*, In Press, Corrected Proof.

[182] R. Lerf, D. Zurbrgg, and D. Delfosse. Use of vitamin e to protect cross-linked uhmwpe from oxidation. *Biomaterials*, 31(13):3643–3648.

[183] E. Oral, S. D. Christensen, A. S. Malhi, K. K. Wannomae, and O. K. Muratoglu. Wear resistance and mechanical properties of highly cross-linked, ultrahigh-molecular weight polyethylene doped with vitamin e. *The Journal of Arthroplasty*, 21(4):580–591, 2006.

[184] Biomet Uk Healthcare Ltd. E1 with exceed abt. *http://www.biomet.co.uk/medhome-uk/hip/hips-primary/epoly-exceed*, date accessed: 19th September 2010.

[185] Smith and Nephew. Oxinium - oxidizes zirconium. *http://global.smith-nephew.com/us/OXINIUM_HIP_IMPLANTS_9113.htm*, date accessed: 19th September 2010.

[186] P. M. Lewis, C. A. Moore, M. Olsen, E. H. Schemitsch, and J. P. Waddell. Comparison of mid-term clinical outcomes after primary total hip arthroplasty with oxinium vs cobalt chrome femoral heads. *Orthopedics*, 31(12):109–112, 2008.

[187] S. Scholes, I. A. Inman, A. Unsworth, and E. Jones. Tribological assessment of a flexible carbon-fibre-reinforced poly(ether-ether-ketone) acetabular cup

articulating against an alumina femoral head. *Proc Instn Mech Engers*, Part H(222):273–283, 2007.

Appendix A

Washing Protocol

- Run for the ultrasonic bath for 5 minutes on degas.
- Rinse components in tap water and gently clean with a brush to remove any serum residue
- Rinse with de-ionised water.
- Put the component into the holding tray and place into the ultrasonic bath (remember to tip the heads up to release the air pocket)
- Sonicate for 10 minutes in deionized water.
- Remove from bath and rinse with deionised water.
- Sonicate for 10 minutes in a mixture of ultrasonic cleaning detergent (neutrocon) in deionized water at a weak concentration (1-2 squirts).
- Remove and rinse thoroughly in deionized water.
- Sonicate for 10 minutes in deionized water.
- Remove and rinse in deionized water.

(If necessary to stop, now is a good point)

- Soinicate for a further 3 minutes in deionized water.
- Dry with lint free paper

- Rinse all surfaces in isopropanol
- Dry with lint free paper
- Dry with a jet of filtered inert gas
- Vacuum oven dry for 30 minutes
- Weigh each component to get 3 consecutive results to 0.1mg

The final washing, drying and weighing must be carried out with 90 minutes.